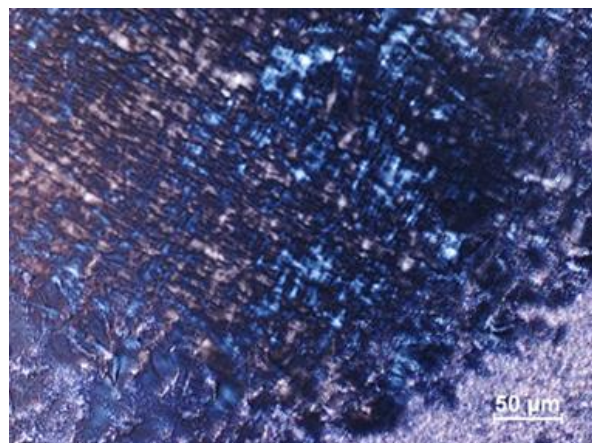
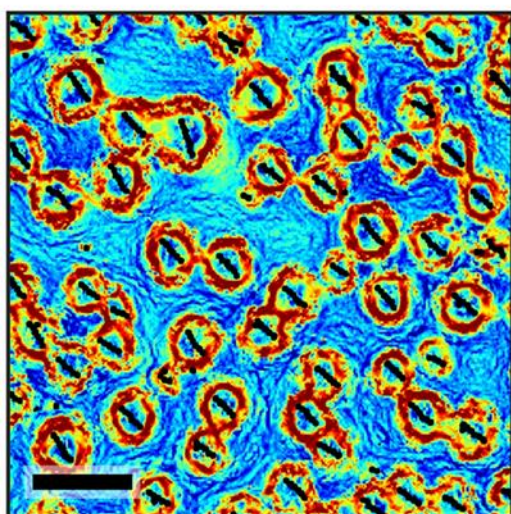
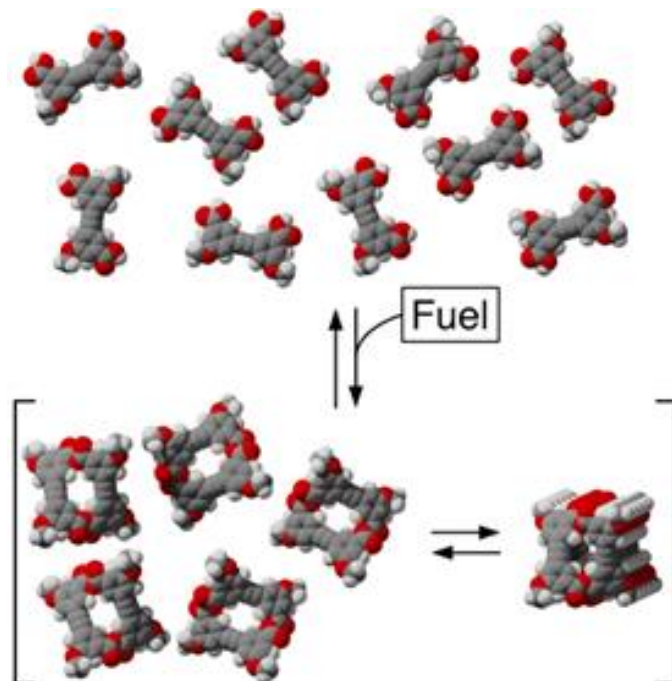
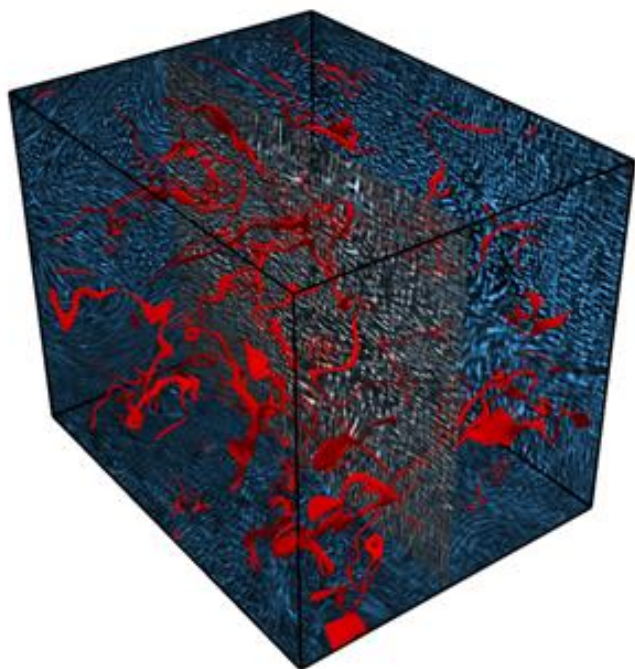


# Biomolecular Materials Principal Investigators' Meeting

Virtual Meeting, August 3-5, 2021

*Program and Abstracts*



U.S. DEPARTMENT OF  
**ENERGY**

Office of  
Science

**Office of Basic Energy Sciences**  
**Materials Sciences and Engineering Division**

## On the Cover

- Top Left: Light sheet microscopy image of a 3D active liquid crystal with single filament resolution formed from kinesin molecular motors and microtubules suspended in a nematic liquid crystal made from colloidal rods. Motor proteins consume chemical energy to walk along protein microtubules generating microscopic-scale forces. These forces produced a dynamic network of motile topological defects shown in red that continuously combine with other defects and stream throughout the sample.  
*Zvonimir Dogic, University of California, Santa Barbara*
- Top Right: A carbodiimide fuel causes difunctional molecules to temporarily assemble into macrocycles, instead of forming polymers chains. The macrocycles are favored in part because they can undergo further assembly into aggregates, and in part because they are favored by entropy. Application of these principles to related systems, like cage structures, should greatly increase the structural space that can be explored in chemically fueled assembly.  
*Christopher Hartley, Miami University*
- Bottom Left: Experimental snapshot of a hydrodynamic vorticity field induced by a swarm of synchronized spinning particles in a liquid-like state under influence of a rotational magnetic field. The activity of spinning self-assembled particles produces flows that cause neighboring spinning particles to self-organize into lattice-like structures. The dynamic spinner lattices are reconfigurable, capable of self-healing behavior and transport of embedded inert cargo particles that can be remotely tuned by the parameters of the external excitation field. The ability to manipulate active colloidal structures is crucial for the development of directed transport at the micro-scale and progress of self-assembled micro-robotics. Scale bar is 1 mm.  
*Alexey Snezhko, Argonne National Laboratory*
- Bottom Right: Birefringence in optical microscope from liquid crystal phase in a concentrated rigid peptide-based rod solution in water. Computationally designed peptide bundles can be precisely linked to form extremely rigid polymer chains that are much stiffer than other known polymers. These new design methods allow the desired size, shape, and display of the chemical groups in the customizable peptide building blocks (bundlemers) that are linked through designed “click” covalent interactions between bundle termini to produce a huge array of polymers. Linking identical bundlemers together in different ways allows fine tuning of polymer stiffness and properties.  
*Darrin Pochan, University of Delaware and Jeffery Saven, University of Pennsylvania*

---

This document was produced under contract number DE-SC0014664 between the U.S. Department of Energy and Oak Ridge Associated Universities.

The research grants and contracts described in this document are supported by the U.S. DOE Office of Science, Office of Basic Energy Sciences, Materials Sciences and Engineering Division.

## Foreword

This volume comprises the scientific content of the presentations made at the 2021 Biomolecular Materials Principal Investigators' Meeting, sponsored by the Materials Sciences and Engineering (MSE) division in the Office of Basic Energy Sciences (BES) of the U.S. Department of Energy (DOE). The meeting's focus is on the fundamental science supported by the Biomolecular Material Core Research Area (CRA) to create materials and multiscale systems that exhibit well-coordinated resiliency, functionality and information content approaching that of biological materials but capable of functioning under harsher, non-biological environments. The meeting took place August 3–5, 2021 as a virtual event conducted entirely over the internet. The use of virtual meetings rather than the traditional in-person gatherings is due to the COVID-19 pandemic.

This is one of a series of Principal Investigators' Meetings organized regularly by BES. The purpose of the meeting is to bring together all the Principal Investigators with currently active projects in the Biomolecular Materials program for the multiple purposes of raising awareness among PIs of the overall program content and of each other's research, encouraging exchange of ideas, promoting collaboration and stimulating innovation. The meeting also provides an opportunity for the Program Managers and MSE/BES management to get a comprehensive overview of the program on a periodic basis, which provides opportunities to identify program needs and potential new research directions.

Biomolecular Materials research activity seeks fundamental knowledge needed for co-design and scalable synthesis of materials for clean energy and quantum information science that coherently manage and self-regulate multiple complex and simultaneous functions and tolerate abuse. An area of emphasis is understanding and controlling assembly mechanisms to seamlessly integrate capabilities developed over one length scale across multiple length scales as the material is constructed. Another important objective is research to develop predictive models and AI/ML for data-driven science that accelerate materials discovery and support fundamental science to direct clean, energy efficient scalable synthesis with real-time adaptive control.

I would like to thank the meeting attendees for their active participation and for sharing their ideas and new research results, which will bring fresh insights for the continued development of this field and its value to DOE as has been the case at past BES Principal Investigators' Meetings. Sincere thanks also go to Teresa Crockett of BES/MSE and Linda Severs and her colleagues at the Oak Ridge Institute for Science and Education (ORISE) for their excellent work providing all the logistical support for the meeting.

Mike Markowitz  
Team Lead, MSE Materials Discovery, Design and Synthesis  
Program Manager, Biomolecular Materials  
Materials Sciences and Engineering Division  
Office of Basic Energy Sciences  
U.S. Department of Energy



## Table of Contents

<b>Foreword</b> .....	i
<b>Agenda</b> .....	vii
 <b>Laboratory Projects</b>	
<i>Computationally Driven Design and Synthesis for Electron Transfer Materials based on Nonnatural Polymers</i>	
<b>Marcel D. Baer</b> .....	3
 <i>Bioinspired Metamaterials</i>	
<b>Surya Mallapragada, Andrew Hillier, Marit Nilsen-Hamilton, Tanya Prozorov, Alex Travesset, David Vaknin, and Wenjie Wang</b> .....	4
 <i>Precision Synthesis and Assembly of Ionic and Liquid Crystalline Polymers</i>	
<b>Paul Nealey, Juan de Pablo, and Matthew Tirrell</b> .....	10
 <i>Design, Synthesis, and Assembly of Biomimetic Materials with Novel Functionality</i>	
<b>Aleksandr Noy, Anthony van Burren, James J. De Yoreo, Chun-Long Chen, and Marcel Baer</b> .....	19
 <i>Adaptive Interfacial Assemblies Towards Structuring Liquids</i>	
<b>Thomas P. Russell, Paul D. Ashby, Phillip Geissler, Brett A. Helms, and Alex Zettl</b> .....	25
 <i>Dynamics of Active Self-Assembled Materials</i>	
<b>Alexey Snezhko, Andrey Sokolov, and Andreas Glatz</b> .....	31
 <b>University Grant Projects</b>	
<i>Bioinspired Active Transport and Energy Transduction using Liquid Crystals Beyond Equilibrium</i>	
<b>Nicholas L. Abbott and Juan J. de Pablo</b> .....	39
 <i>Biomimetic Self-Growing Modular Materials with Encoded Morphologies and Deformabilities</i>	
<b>Joanna Aizenberg and Anna C. Balazs</b> .....	43
 <i>Self-Assembled Adaptive Materials via 3D Printed Active Programmable Building Blocks</i>	
<b>Igor S. Aronson and Ayusman Sen</b> .....	48

<i>Principles of De Novo Protein Nanomaterial Assembly in 1, 2 and 3 Dimensions</i> <b>David Baker and Jim De Yoreo</b> .....	52
<i>Controlling Physical and Chemical Dynamics of Heterogeneous Networks Constructed from Soft Macromolecular Building Blocks</i> <b>Anna C. Balazs, Krzysztof Matyjaszewski, and Tomasz Kowalewski</b> .....	56
<i>Bio-inspired Shape-Morphing and Self-Propelled Active Sheets</i> <b>Anna C. Balazs</b> .....	61
<i>Self-Assembly and Self-Replication of Novel Materials from Particles with Specific Recognition</i> <b>Paul M. Chaikin, David Pine, Nadrian C. Seeman, and Marcus Weck</b> .....	66
<i>Design Principles of Biomolecular Metamaterials</i> <b>Jong Hyun Choi</b> .....	72
<i>Energy-Efficient Self-Organization and Swarm Behavior in Active Matter</i> <b>Jerome Delhommelle, Paul Chaikin, and Stefano Sacanna</b> .....	76
<i>Porin-Inspired Ionomers with sub-nm Gated Ion Channels for High Ion Conductivity and Selectivity</i> <b>Shudipto Konika Dishari</b> .....	81
<i>Microtubule-Based Three-Dimensional Active Matter</i> <b>Zvonimir Dogic</b> .....	86
<i>Reactive, Functional Droplets in Bio-inspired Materials and Smart Interfaces</i> <b>Todd Emrick</b> .....	90
<i>Early Formation Stages and Pathway Complexity in Functional Bio-Hybrid Nanomaterials</i> <b>Lara A. Estroff and Ulrich Wiesner</b> .....	94
<i>Programmable Dynamic Self-Assembly of DNA Nanostructures</i> <b>Elisa Franco and Rebecca Schulman</b> .....	100
<i>Bioinspired Design of Multifunctional Dynamic Materials</i> <b>Zhibin Guan</b> .....	105
<i>Propulsion of Synthetic Protocells and Coacervates Driven by Biochemical Catalysis</i> <b>Daniel A. Hammer, Daeyeon Lee, and Matthew C. Good</b> .....	109
<i>Chemically Fueled Dissipative Assembly of Complex Molecular Architectures</i> <b>C. Scott Hartley and Dominik Konkolewicz</b> .....	114

<i>Controlling Lattice Organization, Assembly Pathways and Defects in Self-Assembled DNA-Based Nanomaterials</i> <b>Sanat K. Kumar and Oleg Gang</b> .....	119
<i>Command of Active and Responsive Elastomers by Topological Defects and Patterns</i> <b>Oleg D. Lavrentovich</b> .....	126
<i>Understanding Functional Dynamics on the Nanoscale through an Integrated Experimental–Computational Framework</i> <b>Erik Luijten and Qian Chen</b> .....	131
<i>Bio-mimetic Material Design Based on Principles of Disorder</i> <b>Sidney R. Nagel and Andrea J. Liu</b> .....	135
<i>Electrostatic Driven Self-Assembly Design of Functional Nanostructures</i> <b>Monica Olvera de la Cruz and Michael J. Bedzyk</b> .....	140
<i>Active Noise to Control and Direct Self-Assembly</i> <b>J�r�mie Palacci</b> .....	146
<i>Nanomaterial Construction through Peptide Computational Design and Hierarchical Solution Assembly</i> <b>Darrin Pochan, Jeffery G. Saven, and Chris Kloxin</b> .....	148
<i>New Principles of Self-Organization Created through the Interplay of DNA Condensates, Microtubules, and Motors</i> <b>Paul W.K. Rothmund</b> .....	152
<i>Polyelectrolyte-Mediated Shape Transitions and Assembly in Microtubules and Tubulin Oligomers</i> <b>C. R. Safinya, Y. Li, and K. Ewert</b> .....	157
<i>Tension- and Curvature- Controlled Fluid-Solid Domain Patterning in Single Lamellae</i> <b>Maria M. Santore and Gregory M. Grason</b> .....	162
<i>Controlling Exciton Dynamics with DNA Origami for Quantum Information Science</i> <b>Gabriela S. Schlau-Cohen, Mark Bathe, and Adam Willard</b> .....	167
<i>What Are the Principles Controlling Biomimetic Heteropolymer Secondary Structure?</i> <b>Michael R. Shirts</b> .....	172
<i>Bio-inspired Polymer Membranes for Resilience of Electrochemical Energy Devices</i> <b>Meredith N. Silberstein</b> .....	176
<i>Biomimetic Strategies for Defect Annealing in Colloidal Crystallization</i> <b>Michael J. Solomon and Sharon C. Glotzer</b> .....	180

<i>Materials Exhibiting Biomimetic Carbon Fixation and Self Repair: Theory and Experiment</i> <b>Michael S. Strano</b> .....	185
<i>Supramolecular Dynamics in Self-Assembling Materials</i> <b>Samuel I. Stupp</b> .....	190
<i>Protein Self-Assembly by Rational Chemical Design</i> <b>F. Akif Tezcan</b> .....	195
<i>Designing Adaptive Information Processing Materials using Nonequilibrium Forcing</i> <b>Suriyanarayanan Vaikuntanathan</b> .....	200
<i>Reciprocal Energy Exchange in Hierarchical DNA Origami-Nanoparticle Composites</i> <b>Jessica Winter, Carlos Castro, Michael Poirier, and Ezekiel Johnston-Halperin</b> .....	203
<i>DNA-Tile Caged NPs toward Materials Agnostic Surface Modification</i> <b>Jessica Winter, Carlos Castro, Michael Poirier, and Ezekiel Johnston-Halperin</b> .....	207
<i>Biomimetic Light Harvesting Complexes Based on Self-Assembled Dye-DNA Nanostructures</i> <b>Hao Yan, Neal Woodbury, and Su Lin</b> .....	211
<i>Steering the Pathways of Hierarchical Self-Assembly at Solid Surfaces</i> <b>Tao Ye, Yonggang Ke, and Gaurav Arya</b> .....	216
<b>Author Index</b> .....	223
<b>Participant List</b> .....	227

# 2021 DOE BES Biomolecular Materials Virtual Principal Investigators' Meeting

Meeting Chair: **Michael Markowitz**, Program Manager, DOE/BES

**All times are Eastern Time**

## Day 1 - Tuesday, August 3, 2021

10:45 – 11:00 **Zoom Log in**

11:00 – 11:15 Welcome and Materials Sciences and Engineering Division Update  
**Andrew Schwartz**, Acting Division Director, *MSED, DOE-BES*

11:15 – 11:30 Introductory Remarks from **Mike Markowitz**,  
Team Lead, *BES Materials Discovery, Design and Synthesis*,  
Program Manager, *BES Biomolecular Materials*

### Session 1 Dissipative Assembly

11:30 – 11:45 **Zvonimir Dogic**, University of California, Santa Barbara  
*Microtubule-Based Three Dimensional Active Matter*

11:45 – 12:00 **Paul Rothemund**, California Institute of Technology  
*New Principles of Self-Organization Created through the Interplay of DNA Condensates, Microtubules, and Motors*

12:00 – 12:15 **Christopher Hartley**, Miami University  
*Chemically Fueled Dissipative Assembly of Complex Molecular Architectures*

12:15 – 12:30 **Alexey Snezhko**, Argonne National Laboratory  
*Dynamics of Active Self-Assembled Materials*

12:30 – 12:45 **Suriyanarayanan Vaikuntanathan**, University of Chicago  
*Designing Adaptive Information Processing Materials using Nonequilibrium Forcing*

12:45 – 1:45 **BREAKOUT**

### Session 2 Controlling Self-Assembly Pathways

1:45 – 2:00 **Darrin Pochan**, University of Delaware and **Jeffery Saven**, University of Pennsylvania  
*Nanomaterial Construction through Peptide Computational Design and Hierarchical Solution Assembly*

- 2:00 – 2:15 **David Baker**, University of Washington  
*Principles of De Novo Protein Nanomaterial Assembly in 1, 2 and 3 Dimensions: Investigation of Design Principles for Synthetic Light Harvesting and Conductive Protein Assemblies*
- 2:15 – 2:30 **Lara Estroff**, Cornell University  
*Early Formation Stages and Pathway Complexity in Functional Bio- Hybrid Nanomaterials*
- 2:30 – 2:45 **F. Akif Tezcan**, University of California, San Diego  
*Protein Self-Assembly by Rational Chemical Design*
- 2:45 – 3:45 **BREAKOUT**

### **Session 3 Controlling Light Interactions**

- 3:45 – 4:00 **Michael Solomon**, University of Michigan  
*Biomimetic Strategies for Defect Annealing in Colloidal Crystallization*
- 4:00 – 4:15 **Surya Mallapragada**, Ames Laboratory  
*Bioinspired Materials*
- 4:15 – 4:30 **Gabriela Schlau-Cohen**, Massachusetts Institute of Technology  
*Controlling Exciton Dynamics with DNA Origami for Quantum Information Science*
- 4:30 – 4:45 **Hao Yan**, Arizona State University  
*Biomimetic Light Harvesting Complexes Based on Self-Assembled Dye-DNA Nanostructures*
- 4:45 – 5:45 **BREAKOUT**
- 5:45 **Adjourn Day 1**

## **Day 2 - Wednesday, August 4, 2021**

- 10:45 – 10:55 **Zoom Log In**
- 10:55 – 11:00 **Welcome to Day 2 (BES Staff)**

### **Session 4 Bioinspired Design**

- 11:00 – 11:15 **Anna Balazs**, University of Pittsburgh  
*Bio-inspired Shape-Morphing and Self-Propelled Active Sheets*
- 11:15 – 11:30 **J r mie Palacci**, University of California, San Diego  
*Active Noise to Control and Direct Self-Assembly*

- 11:30 – 11:45 **Andrea Liu**, University of Pennsylvania and **Sidney Nagel**, University of Chicago  
*Bio-mimetic Material Design Based on Principles of Disorder*
- 11:45 – 12:00 **Aleksandr Noy**, Lawrence Livermore National Laboratory and **James De Yoreo**, Pacific Northwest National Laboratory  
*Design, Synthesis, and Assembly of Biomimetic Materials with Novel Functionality*
- 12:00 – 12:15 **Shudipto Dishari**, University of Nebraska-Lincoln  
*Porin-Inspired Ionomers with sub-nm Gated Ion Channels for High Ion Conductivity and Selectivity*
- 12:15 – 1:15 **BREAKOUT**

### Session 5 Active Matter from Different Building Blocks

- 1:15 – 1:30 **Jerome Delhommelle**, University of North Dakota and **Stefano Sacanna**, New York University  
*Energy-Efficient Self-Organization and Swarm Behavior in Active Matter*
- 1:30 – 1:45 **Erik Luijten**, Northwestern University and **Qian Chen**, University of Illinois, Urbana Champaign  
*Understanding Functional Dynamics on the Nanoscale through an Integrated Experimental-Computational Framework*
- 1:45 – 2:00 **Igor Aronson**, Pennsylvania State University  
*Self-Assembled Adaptive Materials via 3D Printed Active Programmable Building Blocks*
- 2:00 – 2:15 **Oleg Lavrentovich**, Kent State University  
*Command of Active and Responsive Elastomers by Topological Defects and Patterns*
- 2:15 – 2:30 **Daniel Hammer**, University of Pennsylvania  
*Propulsion of Synthetic Protocells and Coacervates Driven by Biochemical Catalysis*
- 2:30 – 3:30 **BREAKOUT**

### Session 6 Macromolecular Assembly

- 3:30 – 3:45 **Todd Emrick**, University of Massachusetts-Amherst  
*Reactive, Functional Droplets in Bio-inspired Materials and Smart Interfaces*
- 3:45 – 4:00 **Matthew Tirrell**, Argonne National Laboratory  
*Precision Synthesis and Assembly of Ionic and Liquid Crystalline Polymers*
- 4:00 – 4:15 **Zhibin Guan**, University of California, Irvine  
*Bioinspired Design of Multifunctional Dynamic Materials*

- 4:15 – 4:30 **Meredith Silberstein**, Cornell University  
*Bio-inspired Polymer Membranes for Resilience of Electrochemical Energy Devices*
- 4:30 – 4:45 **Michael Shirts**, University of Colorado  
*What Are the Principles Controlling Biomimetic Heteropolymer Secondary Structure?*
- 4:45 – 5:45 **BREAKOUT**
- 5:45 **Adjourn Day 2**

## Day 3 - Thursday, August 5, 2021

- 10:45 – 10:55 **Zoom Log In**
- 10:55 – 11:00 **Welcome to Day 3: (BES Staff)**

### Session 7 Programmable Assembly

- 11:00 – 11:15 **Paul Chaikin**, New York University  
*Self-Assembly and Self-Replication of Novel Materials from Particles with Specific Recognition*
- 11:15 – 11:30 **Tao Ye**, University of California, Merced, **Yonggang Ke**, Emory University and **Gaurav Arya**, Duke University  
*Conformationally-Steered Hierarchical Self-Assembly at Solid Surfaces*
- 11:30 – 11:45 **Sanat Kumar**, Columbia University  
*Controlling Lattice Organization, Assembly Pathways and Defects in Self-Assembled DNA-Based Nanomaterials*
- 11:45 – 12:00 **Elisa Franco**, University of California, Los Angeles and **Rebecca Schulman**, Johns Hopkins University  
*Programmable Dynamic Self-Assembly of DNA Nanostructures*
- 12:00 – 12:15 **Jessica Winter**, The Ohio State University  
*Reciprocal Energy Exchange in Hierarchical DNA Origami-Nanoparticle Composites*
- 12:15 – 1:15 **BREAKOUT**

### Session 8 Dynamics and Assembly

- 1:15 – 1:30 **Maria Santore**, University of Massachusetts-Amherst  
*Tension- and Curvature- Controlled Fluid-Solid Domain Patterning in Single Lamellae*
- 1:30 – 1:45 **Samuel Stupp**, Northwestern University  
*Supramolecular Dynamics in Self-Assembling Materials*

- 1:45 – 2:00 **Thomas Russell**, Lawrence Berkeley National Laboratory  
*Adaptive Interfacial Assemblies Towards Structuring Liquids*
- 2:00 – 2:15 **Joanna Aizenberg**, Harvard University  
*Biomimetic Self-Growing Modular Materials with Encoded Morphologies and Deformabilities*
- 2:15 – 2:30 **Monica Olvera de la Cruz**, Northwestern University  
*Electrostatics and Elasticity in Self-Assembled Nanostructures*
- 2:30 – 3:30 **BREAKOUT**

### **Session 9 Pathways for Targeted Assembly and Function**

- 3:30 – 3:45 **Nicholas Abbott**, Cornell University  
*Bioinspired Active Transport and Energy Transduction Using Liquid Crystals Beyond Equilibrium*
- 3:45 – 4:00 **Michael Strano**, Massachusetts Institute of Technology  
*Materials Exhibiting Biomimetic Carbon Fixation and Self-Repair: Theory and Experiment*
- 4:00 – 4:15 **Cyrus Safinya**, University of California, Santa Barbara  
*Miniaturized Hybrid Materials Inspired by Nature: Polyelectrolyte-Mediated Shape Transitions and Assembly in Microtubules and Tubulin Oligomers*
- 4:15 – 4:30 **Jong Hyun Choi**, Purdue University  
*Design Principles of Biomolecular Metamaterials*
- 4:30 – 5:30 **BREAKOUT**
- 5:30 – 5:45 **Closing Remarks - Mike Markowitz, BES**
- 5:45 **Adjourn Pls Meeting**



# ***LABORATORY PROJECTS***



# Computationally Driven Design and Synthesis for Electron Transfer Materials based on Nonnatural Polymers

Marcel D. Baer, Pacific Northwest National Laboratory

## Program Scope

Developing new materials that exhibit control over electron transfer processes is necessary to address challenges in energy production and storage. Nature provides a blueprint for achieving this control through use of protein machinery evolved from archaic modules of small proteins that carry out coupled oxidation and reduction — or redox — reactions. Electrons are transferred from one module to the next within this machinery, with each module containing one or more redox centers. Control is achieved by the sequence of redox centers whose potentials are defined by the local environment within the protein. However, efforts to harness the complex functionality of Nature's modular material design for energy technologies must address the challenge of operating under harsh non-biological conditions. Recent synthetic advances now enable design and synthesis of nanostructured materials from nonnatural, sequence-defined polymers (i.e., peptoids<sup>1</sup> and triazine-based polymers<sup>2</sup>) that mimic proteins but exhibit high stability in such conditions. The purpose of this research is to develop the understanding of structure and function required to incorporate redox centers that mimic the electron transfer function of natural proteins.

## Future Plans

The focus will be on computational design of individual macromolecular units containing four iron ions and four sulfide ions placed at the vertices of a cubane-type cluster, whose redox potentials are tunable through their local environment. Methods ranging from quantum to molecular mechanics and coarse grain simulations will be used to (1) predict the minimal sequence that can bind redox clusters with tunable reduction potentials by identifying the positions and types of coordinating side chains and their optimal spacings within the sequence, leading to a stable configuration of the cluster and its immediate macromolecular environment, (2) elucidate the conformational stability—and the factors that control it—of secondary structural elements for nonnatural, sequence-defined polymers, and (3) develop computational designs of biomimetic units containing redox clusters and secondary structural elements that will allow for higher length-scale organization toward multi-unit ET chains.

## References

1. Sun, J.; Zuckermann, R. N., Peptoid polymers: a highly designable bioinspired material. *ACS Nano* **2013**, 7 (6), 4715-32.
2. Grate, J. W.; Mo, K. F.; Daily, M. D., Triazine-Based Sequence-Defined Polymers with Side-Chain Diversity and Backbone-Backbone Interaction Motifs. *Angew. Chem Int Ed Engl* **2016**, 55 (12), 3925-30.

## Bioinspired Metamaterials

**PIs:** Surya Mallapragada, Andrew Hillier, Marit Nilsen-Hamilton, Tanya Prozorov, Alex Traveset, David Vaknin, and Wenjie Wang, Ames Laboratory

**Mailing Address:** Division of Materials Sci. and Eng., Ames Laboratory, Ames, IA 50011

### Program Scope

The Bioinspired Metamaterials FWP at the Ames Laboratory focuses on developing fundamental bioinspired approaches leading to novel fabrication techniques for creating self-assembled mesoscale 2D and 3D structures that can serve as functional metamaterials. We are developing bioinspired, bottom up synthesis approaches as alternatives to top-down lithography, using macromolecular templates for metallization to create nanoresonators and to enable their higher-level 2D and 3D mesoscale organization and alignment. To achieve this, we are investigating mechanistic questions related to dynamic and tunable fabrication of these controlled nanostructures and their hierarchical assemblies. Our interdisciplinary collaborative and integrated approach combines experiment and theory, with built-in feedback. This bottom-up approach for functional materials design aligns well with DOE's priorities laid out in the Synthesis Science workshop report for the synthesis of complex nanostructures and multi-scale assemblies, and directly addresses the *DOE's Grand Challenge*, to orchestrate atomic and electronic constituents to control material properties.

### Recent Progress

The two main goals of the project are: 1) creation of individual metallic nanoresonators such as split-ring resonators (SRR), and other meta-atoms using bottom-up approaches, 2) development of polymer functionalization-based approaches for self-assembled 2D and 3D mesoscale superstructures of these nanoresonators to create optical metamaterials. Synthesis and fabrication approaches have been accompanied by development and use of synchrotron X-ray scattering, and scanning transmission electron microscopy (STEM) techniques to characterize meta-atoms and their assemblies. The experimental approaches have been closely coupled with theoretical efforts, such as predicting the impact of disorder on optical properties, predicting 2D and 3D assemblies and developing a general formalism for phase diagram of functionalized nanostructures.

**Goal 1 - Creation of Individual Meta-atoms:** We developed DNA-origami methods to create desired meta-atom templates and methods to selectively metallize the nanostructured templates to create individual nanoresonator structures. With the unparalleled direct nanoscale visualization capabilities afforded by the liquid phase STEM imaging *in situ*, we are able to probe the fundamental mechanisms of meta-atom metallization. We predicted optical responses of these metallized nanoresonators, showed that the optical resonances are robust even in the presence of roughness and surface defects, and measured optical scattering from individual nanoresonators.

*Meta-Atom Template Formation and Metallization:* Efforts focused on developing DNA-origami templates to create precisely defined meta-atoms with specific shapes, which were then metallized to serve as nanoresonators possessing both electric and magnetic resonant signatures. Geometric origami shapes created, included triangles and various gapped or ring-like structures, including

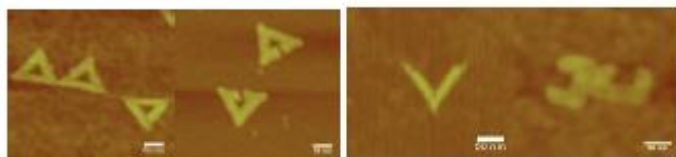


**Fig. 1** DNA origami templates of meta-atom shapes

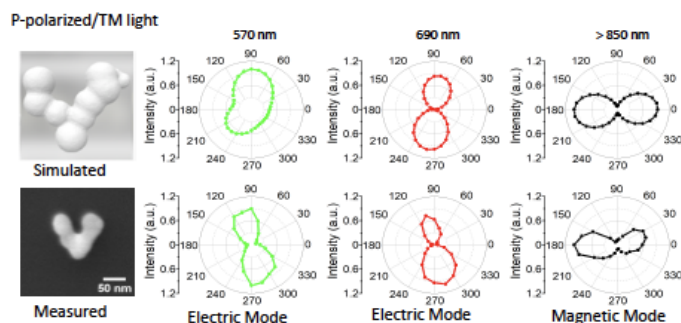


**Fig. 2** Simulated (top) and experimentally measured (bottom) scattering signals from v-shaped meta-atoms (mimicking split ring resonators) providing evidence of electric and magnetic resonance modes

gapped-triangles, V, C and U shapes (**Fig. 1**). We showed that DNA origami triangles could be successfully imaged in detail without the negative staining using HAADF-STEM to further enable the ongoing spatio-chemical analysis of seeding and metallization processes.

We developed methods for metallization of these DNA templates via site-specific metal seeding of silver nanoparticles followed by electroless deposition of gold<sup>2</sup>. We were able to observe early stages of seeding and growth of DNA-templated nanostructures in the liquid phase directly and investigate mechanism of meta-atom growth *in situ*.

**Predicting Meta-Atom Optical Properties:**

The optical responses of these metallized structures were evaluated through a

detailed optical modeling study using the shape, morphology and composition of example metallized DNA origami structures as deduced by electron and atomic force microscopy. A custom dark-field scattering instrument was assembled to perform single-particle scattering measurements to collect orientation and polarization-depending resonance signatures from metal nanostructures from the visible to the near-infrared regime. Detailed information about the various resonance modes of these objects could be readily obtained to map optical signatures as a function of various input field polarization, sample shape and orientation. The role of surface morphology on the optical resonance modes showed both electric and magnetic resonances in v-shaped split rings (**Fig. 2**). We have developed disorder models to allow realistic electromagnetic modeling of meta-atoms grown from metallized DNA-templates and numerically demonstrated robust resonant optical response and strong tolerance against surface disorder and structural defects.

**Goal 2 - 2D and 3D assembly of Nanostructures into Mesoscale Superstructures:** Metallic superstructures (e.g., nanospheres, as well as asymmetric and larger structures such as nanorods, nanotriangles and nanooctahedra), made of gold or silver, are ideal model systems for metamaterials assembly relevant to our research goals. We have developed 2D and 3D bottom-up strategies using synthetic polymer functionalization to assemble these model nanostructures at the aqueous surface and in the bulk respectively, and these studies are pivotal to understanding and controlling the assembly of the metallized DNA origami meta-atoms. The resultant superlattice structures are characterized by surface sensitive X-ray scattering methods at the DOE Advanced Photon Source in addition to in-house facilities. Theory has been advanced by developing both analytical and coarse-grained models. From this combined experimental and theoretical approach, we have successfully determined the parameters that govern the assembly of meta-atoms into 2D and 3D superlattices and demonstrated fine control of the lattice spacing.

**Tunable nanoparticle assemblies:** Inspired by strategies to assemble structures through DNA-hybridization, we have developed interpolymer complexation (IPC) assembly methods where two

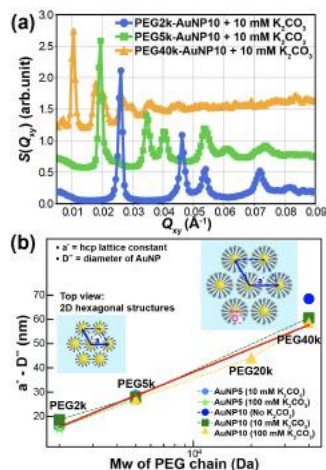


**Fig. 3** (a) fcc AuNP superlattices with long-range order mediated by salt. (b) Tunable lattice spacings of AuNPs controlled by PEG chain length

synthetic polymers chains undergo hydrogen bonding, similar to the DNA base-pairing interactions. In this case, we use poly(ethylene glycol) (PEG) as a grafting polymer on the AuNPs and hydrogen bond acceptor and loose poly(acrylic acid) (PAA) as the donor of the IPC pair. The hydrogen bonds are pH tunable and PEG-AuNPs crystallize into *fcc* superlattices with long-range order. We have also use PEG functionalization and salt to create assemblies with long-range order. We showed that the lattice constant and crystal quality can be tuned by polymer concentration, suspension pH, and the length of polymer chains (**Fig. 3**). We further developed a coarse-grained computational model for PEG-PAA IPC (**Fig. 4**) to predict the structure/dynamics of the *fcc* superlattice. Our theoretical results describe a scenario where assembly by hydrogen bonding is subsequently strengthened by van der Waals forces between the complexed coronas, leading to robust assembled structures in between the ones obtained through

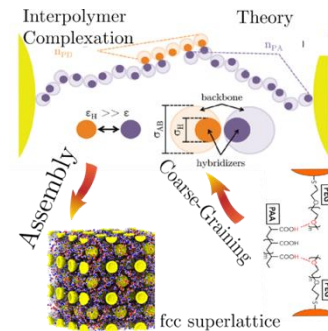


**Fig. 4.** Coarse grained MD simulations for IPC superlattice assemblies

solvent evaporation and those from DNA assembly, that remains intact outside the solution, unlike superlattices assembled using DNA hybridization.

**Isotropic/anisotropic nanostructure 2D and 3D assembly:** To achieve our ultimate goal of assembling SRRs and other meta-atoms, we expanded our strategies to more diverse nanostructure geometries and larger sizes. We have successfully extended our strategies to the assembly of gold nanorods (AuNRs) into 2D films at the vapor/liquid interface using nanorods capped with PEG, and assembly is induced by changes in ionic strength. PEG-AuNRs in aqueous suspensions migrate to the vapor/liquid interface in the presence of salt, forming a uniform monolayer with planar-to-surface orientation. Furthermore, the 2D assembled PEG grafted AuNRs exhibit short-range order into rectangular symmetry with side-by-side and tail-to-tail nearest-neighbor packing. Theoretical modeling has enabled the quantification of the effect of PEG chain length and salt concentration and its impact on the 2D assembly on aqueous surfaces. Both assembly strategies, i.e., either changing aqueous solvent by salts or IPC-linker polymers (PAA for grafted-PEG), induce 3D ordered assembly of nanorods only above a threshold temperature. The PEG-AuNRs form hexagonal columnar phases. The quality *and* stability of the superstructures increase with temperature (**Fig. 5**), with tunable lattice constants based on the interplay between electrostatic and hydrophobic effects.

Other anisotropic nanostructured building units, such as model triangular- and octahedral-shaped gold nanostructures were synthesized in our lab. We then grafted them with PEG (referred to as PEG-AuNTs and PEG-AuNOh, respectively), and investigated their assembly into complex structures (**Fig. 6**). The assembly strategies involving salts, IPC, and temperature show versatility in packing modes specific to these nanostructures' geometry. Our results show that PEG-AuNTs

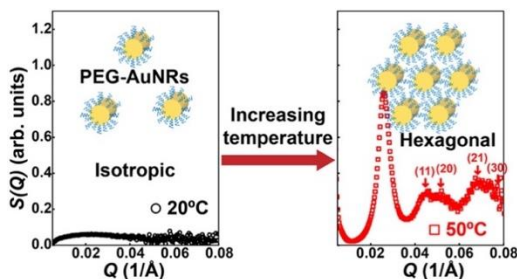


**Fig. 5.** Effect of temperature on 3D assembly of AuNR using IPC linkers

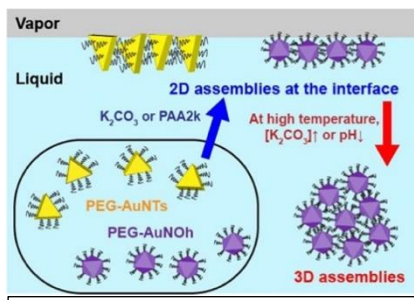


**Fig. 6.** Schematic of 2D assembly of AuNTs and AuNOh structures at the air-water interface

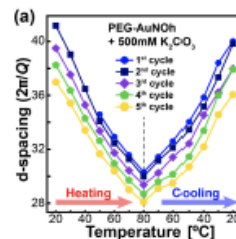


**Fig. 7** Lattice constants of AuNOh assemblies can be reversibly tuned by temperature

and PEG-AuNOh populate the vapor/suspension interface, with some degree of orientation with respect to the liquid surface. The resulting assemblies can be tuned by the regulating electrolyte and pH levels of the suspensions. Similar suspension manipulations induce 3D assemblies revealed with small-angle X-ray scattering. In addition, raising the temperature from 20 to above 50°C induces and even improves the ordering of the assemblies and can be used to tune lattice spacing as well (**Fig. 7**). We have developed and utilized advanced microscopy techniques for investigating assemblies of nanostructures to complement the X-ray scattering studies. We are also developing a computational software package for the X-ray data so that the structural insights from the data can be rapidly and efficiently extracted.

In summary, during the current cycle, we have developed DNA origami metallization strategies to create uniform meta-atoms and measured their optical responses. We have developed versatile avenues for the assembly of model metallic nanostructures into ordered superstructures in 2D and 3D using synthetic polymeric ligands in aqueous solutions. The superlattices are robust and the lattice constant is controllable with temperature and other parameters. We have advanced theory, an integral part of this effort, to predict these structures. These achievements using model systems validate powerful approaches for assembling meta-atoms.

## Future Plans

Our plans for the next phase of the project are focused on creating metallized DNA origami-based meta-atoms that can serve as functional nanoresonators; and bioinspired approaches to assemble them into 2D and 3D self-assembled arrays that demonstrate the existence of the desired resonances characteristic for functional metamaterials. We anticipate enhancing optical properties and implementing new electromagnetic functionality by creating new individual articulating meta-atoms enabling dynamic tunable responses, or nonlinear metamaterials exhibiting new physical behavior. We will continue to develop and use advanced characterization techniques to provide insights that enable improved control of DNA meta-atom template metallization. 2D and 3D assembly of these meta-atoms to create functional metamaterials is exceedingly challenging as it requires an exquisite understanding of complex molecular interactions to enable fundamental advances towards our ability to form *robust and highly stable* superstructures of these meta-atoms. We will couple synthetic methods with the insights gained by theory and through development and use of X-ray scattering (utilizing the DOE synchrotron facilities) and liquid phase TEM, to create and investigate hierarchical assemblies of meta-atoms that demonstrate the desired resonance characteristics.

## Publications (\* indicates journals with impact factor >6)

1. H.J. Kim, W. Wang, H. Zhang, F. Guillame, B. Ocko, A. Travesset, S.K. Mallapragada and D. Vaknin, “Effect of Polymer Chain Length on Superlattice Assembly of Functionalized Gold Nanoparticles”, *Langmuir* (submitted).
2. Islam, M. M., Hossen, M.M., Koschny, T. and Hillier, A.C., “ Shape and Orientation-Dependent Scattering of Isolated Gold Nanostructures Using Polarized Dark-Field Microscopy”, *J. Phys. Chem. C*, **125** (21), 11478-88 (2021). [10.1021/acs.jpcc.1c03671](https://doi.org/10.1021/acs.jpcc.1c03671).
3. \*S. Minier, H.J. Kim, J. Zaugg, S.K. Mallapragada, D. Vaknin, W. Wang, “Poly(N-isopropylacrylamide)-grafted gold nanoparticles at the vapor/water interface,” *J. Colloid Interfac. Sci.*, **585**, 312-319 (2021). <https://doi.org/10.1016/j.jcis.2020.11.080>
4. A. Londoño-Calderon, W. Wang, J.J. Lawrence, W. Bu, D. Vaknin, T. Prozorov, “Salt-induced liquid-liquid phase separation and interfacial crystal formation in poly(N-isopropylacrylamide)-capped gold nanoparticles,” *J. Phys. Chem. C*, **125**(9), 5349–5362 (2021). <https://doi.org/10.1021/acs.jpcc.0c11307>
5. \*H.J. Kim, W. Wang, S.K. Mallapragada, D. Vaknin, “The Effects of temperature on the assembly of gold nanoparticle by interpolymer complexation,” *J. Phys. Chem. Lett.*, **12**, 1461-1467 (2021). <https://doi.org/10.1021/acs.jpcclett.0c03749>
6. \*H.J. Kim, W. Wang, A. Travesset, S.K. Mallapragada, D. Vaknin, “Temperature-induced tunable assembly of columnar phases of nanorods,” *ACS Nano*, **14**(5), 6007-6012 (2020). <https://doi.org/10.1021/acsnano.0c01540>
7. M. Pham, A. Travesset, “Ligand structure and adsorption free energy of nanocrystals on solid substrates,” *J. Chem. Phys.*, **153**, 204701 (2020). <https://doi.org/10.1063/5.0030529>
8. H.J. Kim, M.M. Hossen, A.C. Hillier, D. Vaknin, S.K. Mallapragada, W. Wang, “Interfacial and bulk assembly of anisotropic gold nanostructures: Implications for photonics and plasmonics,” *ACS Appl. Nano Materials*, **3**(8), 8216-8223 (2020). <https://doi.org/10.1021/acsanm.0c01643>
9. \*N. Shen, M. Hossen, A.C. Hillier, T. Koschny, C.M. Soukoulis, “Robustness of optical response for self-assembled plasmonic metamaterials with morphological disorder and surface roughness,” *Adv. Opt. Mater.*, **8**, 1901794 (2020). <https://doi.org/10.1002/adom.201901794>
10. W. Wang, H.J. Kim, W. Bu, S. Mallapragada, D. Vaknin, “Unusual effect of iodine ions on the self-assembly of poly(ethylene glycol)-capped gold nanoparticles,” *Langmuir*, **36**(1), 311-317 (2020). <https://doi.org/10.1021/acs.langmuir.9b02966>
11. \*S. Ren, Y. Sun, F. Zhang, A. Travesset, C.-Z. Wang, K.-M. Ho, “Phase diagram and structure map of binary nanoparticle superlattices from a Lennard-Jones model,” *ACS Nano*, **14**(6), 6795-6802 (2020). <https://doi.org/10.1021/acsnano.0c00250>
12. \*Londoño-Calderon, M.M. Hossen, P.E. Palo, L. Bendickson, S. Vergara, M. Nilsen-Hamilton, A. C. Hillier, and T. Prozorov, Imaging of Unstained DNA Origami Triangles with Electron Microscopy. *Small Methods* **3**, 1900393, 1900391-1900310 (2019) doi:<https://doi.org/10.1002/smt.201900393>. The paper was featured on the Inside Front Cover of the Volume 3(12).
13. N. Horst, S. Nayak, W. Wang, S. Mallapragada, D. Vaknin, A. Travesset, “Superlattice assembly by interpolymer complexation,” *Soft Matter*, **15**(47), 9690-9699 (2019). <https://doi.org/10.1039/C9SM01659G>

14. S. Murthy, W.J. Wang, S.D. Sommerfeld, D. Vaknin, J. Kohn, "Temperature-activated PEG surface segregation controls the protein repellency of polymers," *Langmuir*, **35**(30), 9769-9776 (2019). <https://doi.org/10.1021/acs.langmuir.9b00702>
15. H.J. Kim, Wenjie Wang, W. Bu, M.M. Hossen, A. Londono-Calderon, A.C. Hillier, T. Prozorov, S. Mallapragada, D. Vaknin, "Salt mediated self-assembly of poly(ethylene glycol)-functionalized gold nanorods," *Sci. Rep.*, **9**(1), 20349 (2019). <https://doi.org/10.1038/s41598-019-56730-2>

## FWP PRJ1000089 Precision synthesis and assembly of ionic and liquid crystalline polymers

**Paul Nealey (PI), Materials Science Division, Argonne National Laboratory**  
**Juan de Pablo (co-PI), Materials Science Division, Argonne National Laboratory**  
**Matthew Tirrell (co-PI), Materials Science Division, Argonne National Laboratory**

### Program Scope

Molecular self-assembly is arguably the most promising strategy for imparting structure and function to materials at the molecular, meso-, and macro-scale and for developing high-performance soft and biomolecular materials for energy related applications. The challenge is to encode information into the building blocks of materials systems through precision synthesis, thereby introducing specific and controllable intra- and intermolecular interactions to drive assembly with hierarchical structure. A key aspect of our functional self-assembling materials design is avoiding or overcoming undesirable states through pathway engineering. Defects and disorder can be mitigated or controlled, for example, by relying on external fields or templates to direct assembly (in conjunction with self-assembly), leading to a better understanding of fundamental behavior. We note that the basic tenets of molecular self-assembly and directed self-assembly are derived from biology, but that synthetic organic material scientists have not yet systematically deployed the full range of molecular interactions used in biology to create functional soft materials, nor are they limited to the toolsets of biology resulting from evolution. Our activities are organized into three interrelated thrusts of increasing complexity, from the self-assembly of sequence-specific homopolymers in solution in Thrust 1: “Physics and materials science of hetero-charged polymers from A to Z (Polyampholytes to Polyzwitterions),” to the directed self-assembly and intrinsic ion-conducting properties of (A-block-(B-random-C)) architectures in Thrust 2: “Fundamental investigation of physical and electrochemical properties of block copolymer electrolytes,” to the most complex materials incorporating liquid crystallinity and charge in fully three-dimensional assemblies in Thrust 3: “Directed self-assembly of blue phase liquid crystals- fundamentals and functionality.” The themes that connect our activities include manipulating sequence, charges, and liquid crystallinity to control structure and achieve function, and cross-cutting synthetic strategies, characterization techniques, and theoretical and computational methods.

### Recent Progress

*Physics and materials science of hetero-charged polymers.* Work on hetero-charged polymers has concentrated on expanding the range of zwitterionic polymers that can be studied, with the ultimate goal of determining quantitatively how this class of polymers interacts with water, which is likely the key to their unique properties of biocompatibility and anti-biofouling. We are specifically exploring polyether backbones, incorporating poly(allyl glycidyl ether) (PAGE), which give us a pendant side chain that can be

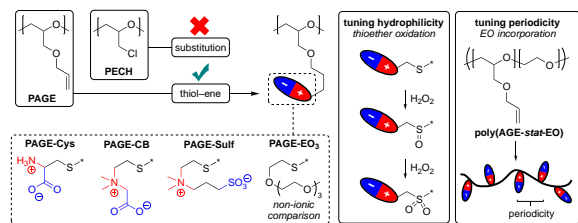


**Figure 1.** High throughput synthesis of a library of zwitterionic polymers.

functionalized in a variety of ways (see Figure 1). These polymers, and other zwitterionic polymers, can be made in soluble or grafted brush form, the latter providing a unique experimental platform to examine the conformational aspects of these polymers under different solution conditions.<sup>1</sup>

*Ion Transport Behavior in Ethylene Oxide (EO)-Based Block Copolymer Electrolytes (BCEs).* Many fundamental aspects of the ionic transport behavior in salt-blended BCEs are still not fully understood. Recent experiments have shown differences on the dependence of ionic conductivity on salt concentration between polystyrene-*b*-poly(ethylene oxide) (SEO)-LiTFSI BCEs and PEO-LiTFSI homopolymers, but no clear description of the actual changes in terms of ionic solvation properties had been given. Through experimental and simulation methods, we showed that these differences can be explained by changes in ionic solvation, association, and distribution at the molecular level. Comparison of conductivities as function of  $r = [\text{Li}]/[\text{EO}]$  showed similar behavior for both systems up to the maximum in conductivity at a concentration of  $r = 1/12$ , where about half of the available solvation sites in the system are filled (see Figure 2a). Above this regime, the conductivity of the homopolymer drops while conductivity of the BCEs remains constant up to  $r = 1/4$ . Vibrational spectroscopy measurements and atomistic MD simulations showed that in the second regime, no additional EO units in BCEs participate in cation coordination but instead clusters or partial clusters of ions segregate to the interfacial mixing layer, keeping the solvated ion concentration close to the optimal value for maximum conductivity in the conducting BCE domains as shown in Figure 2b.<sup>2</sup>

*Ion Transport Behavior in Ethylene Oxide-Based Side-chain Polymer Electrolytes.* Incorporation of EO side-chain units to polymers is a common strategy to impart and improve – through lowering of the glass transition temperature ( $T_g$ ) – their ionic conductivity, but low  $T_g$  alone is not necessarily a good predictor of this property. We synthesized a series of EO side-chain polymers and used impedance and vibrational spectroscopies, as well as atomistic MD simulations to understand how chain architecture, polymer composition and side-chain length affect ion solvation, ionic conductivity and segmental dynamics of these electrolytes at the molecular level. We observed that the ionic conductivity varies by an order of magnitude in poly[(oligo(ethylene oxide)) methyl ether methacrylate] (POEM) materials of different side-chain lengths, and that this effect is not well explained by differences in  $T_g$  or ionic dissociation (see Figure

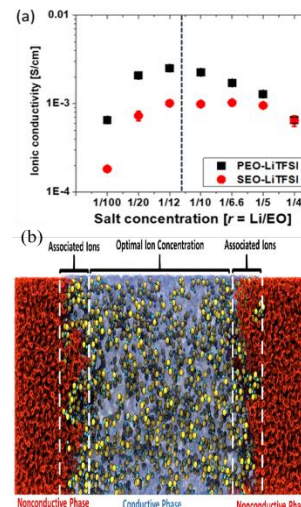


**Figure 2.** (a) Salt concentration dependence of  $\text{Li}^+$  conductivity in PEO and SEO at 100 C; (b)  $\text{Li}^+$  distribution in SEO at  $r = 0.2$ .

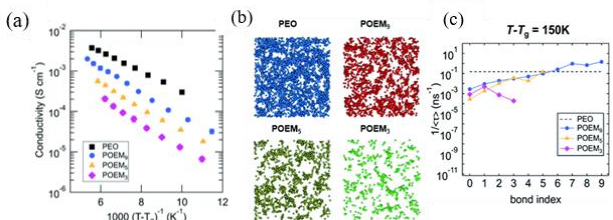


**Figure 3.** (a) Experimental conductivity corrected by  $T_g$ ; (b) visualization of solvation site network in PEO and POEM<sub>x</sub> from MD simulations; (c) inverse mean relaxation time ( $1/\langle\tau\rangle$ ) of bonds along polymer chains.  $1/\langle\tau\rangle$  serves here as an indicator of local segmental.

3a). By introducing solvation site edge density, solvation site connectivity and local relaxation times of EO segments as additional metrics to the analysis, we were able to fully capture the transport behavior in side-chain polyethers (see Figure 3b and 3c), and most importantly, to identify local segmental mobility of EO side chains to be the most critical parameter in determining ion conductivity rather than overall ether oxygen content.<sup>3,4</sup>

*Correlation Length in the Directed Self-Assembly of Blue Phase Liquid Crystals (BPLCs).* The correlation length dictates the length-scale over which templated order can be maintained. Lithographically defined chemical patterns with alternating homeotropic and planar regions, and with pitches equal to the blue-phase unit cell size, can be used to nucleate and grow single crystals of BPLCs. To determine the correlation length, we patterned alternating regions of chemical patterns to direct the assembly of BPLCs and unpatterned interspatial regions with separation distances from 2 to 20  $\mu\text{m}$ . As shown in Figure 4, if the distance between patterned and unpatterned regions was shorter than the correlation length, single BPLCs extended over both the templating and non-templating regions, whereas for distances greater than the correlation length, a polycrystalline morphology resulted. In a separate set of experiments, the correlation length was determined from the minimum size of the patterned region to observe directed self-assembly. Both sets of experiments indicate the correlation length to be  $\sim 10 \mu\text{m}$ .

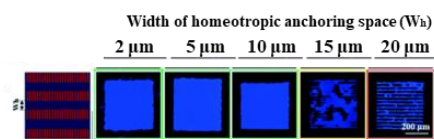


**Figure 4.** Directed self-assembly of BPLC on chemical patterns was used to extract a correlation length.

The experimentally observed correlation length is consistent with our theoretical estimate derived from continuum free energy simulations. Our work demonstrates that blue-phases can serve as model systems to test theories of nucleation and establishes a new strategy to maximize the size of blue-phase single crystals.<sup>5</sup>

*Active Liquid Crystals.* Our efforts about active liquid crystals have established that topological defects can be confined by introducing gradients of activity. In particular, we have studied the dynamical behavior of two defects confined by a sharp gradient of activity that separates an active circular region and a surrounding passive nematic material. Using continuum simulations, we have explained how the interplay between energy injection into the system, hydrodynamic interactions, and frictional forces governs the dynamics of topological self-propelling defects. Our findings have been rationalized in terms of a phase diagram for the dynamical response of defects in terms of activity and frictional damping strength. Different regions of the underlying phase diagram correspond to distinct dynamical modes, namely immobile defects, steady rotation of defects, bouncing defects, bouncing-cruising defects, dancing defects, and multiple defects with irregular dynamics. These dynamic states raise the prospect of generating synchronized defect arrays for microfluidic applications.<sup>6</sup>

## Future Plans

For synthesis and self-assembly of heterocharged polymers, our efforts in the next year will produce systematic variations in polyzwitterionic structures leading to a database of information

on polymer configurational properties in different solution conditions that can be mined to ascertain the dominant, controlling, structural features of their hydration and interactions with water. Tools to be applied are SAXS, light scattering, IR spectroscopy, and surface forces measurement. For ion conducting BCEs, we will: 1) elucidate the role that intermixing of conducting and nonconducting components plays on ionic mobility by comparing the ionic conductivity of polymer blends and block copolymers of differing interaction strength; 2) extend to side-chain polyether-based BCE our previous hypothesis on  $\chi$  being the main factor dictating the ionic conductivity rather than  $T_g$  differences at the domain interface; 3) understand the ion transport mechanism in polyether-polycarbonate copolymers, where multiple solvation site forming moieties may compete. In our research on 3D liquid crystals, we will: 1) use single crystalline blue phase gels to prepare isoporous membranes by washing out the non-polymerizable mesogens; 2) render the assemblies conductive by refilling washed out blue-phases gels with electrolytes to probe the influence of lattice orientation and grain boundaries on ion-transport; and 3) use sequential infiltration synthesis on washed out gels to prepare inorganic membranes templated by the disclination network of blue-phases. In our inter FWP research with the Snezhko group active liquid crystal design, we will seek to validate the predictions of our active liquid crystal design simulations in experiments. An important new direction will be to combine and integrate different active region designs, with the goal of creating active systems that can perform logic operations.

## References

1. Dinic, J.; Marciel, A. B.; **Tirrell, M. V.** Polyampholyte Physics: Liquid-Liquid Phase Separation and Biological Condensates. *Curr. Opin. Colloid Interface Sci.* **2021**, 101457.
2. Sharon, D.; Bennington, P.; Webb, M. A.; Deng, C.; **de Pablo, J. J.**; Patel, S. N.; **Nealey, P. F.** Molecular Level Differences in Ionic Solvation and Transport Behavior in Ethylene Oxide-Based Homopolymer and Block Copolymer Electrolytes. *J. Am. Chem. Soc.* **2021**, *143*, 3180–3190.
3. Deng, C.; Webb, M. A.; Bennington, P.; Sharon, D.; **Nealey, P. F.**; Patel, S. N.; **de Pablo, J. J.** Role of Molecular Architecture on Ion Transport in Ethylene Oxide-Based Polymer Electrolytes. *Macromolecules* **2021**, *54*, 2266–2276.
4. Bennington, P.; Deng, C.; Sharon, D.; Webb, M. A.; **de Pablo, J. J.**; **Nealey, P. F.**; Patel, S. N. Role of Solvation Site Segmental Dynamics on Ion Transport in Ethylene-Oxide Based Side-Chain Polymer Electrolytes. *J. Mater. Chem. A* **2021**, *9*, 9937–9951.
5. Li, X.; Martínez-González, J. A.; Guzmán, O.; Ma, X.; Park, K.; Zhou, C.; Kambe, Y.; Jin, H. M.; Dolan, J. A.; **Nealey, P. F.**; **de Pablo, J. J.** Sculpted Grain Boundaries in Soft Crystals. *Science Advances* **2019**, *5*, eaax9112
6. Mozaffari, A.; Zhang, R.; Atzin, N.; **de Pablo, J. J.** Defect Spirograph: Dynamical Behavior of Defects in Spatially Patterned Active Nematics. *Phys. Rev. Lett.* **2021**, *126*, 227801.

**Publications** (Reverse chronological order since October 1, 2018)

### Primary

1. Zhang, R.; Mozaffari, A.; **de Pablo, J. J.** Autonomous Materials Systems from Active Liquid Crystals. *Nature Reviews Materials* **2021**, 1–17. <https://doi.org/10.1038/s41578-020-00272-x>.
2. Sharon, D.; Bennington, P.; Webb, M. A.; Deng, C.; **de Pablo, J. J.**; Patel, S. N.; **Nealey, P. F.** Molecular Level Differences in Ionic Solvation and Transport Behavior in Ethylene Oxide-Based Homopolymer and Block Copolymer Electrolytes. *J. Am. Chem. Soc.* **2021**, *143*, 3180–3190. <https://doi.org/10.1021/jacs.0c12538>.
3. Rumyantsev, A. M.; Jackson, N. E.; Johner, A.; **de Pablo, J. J.** Scaling Theory of Neutral Sequence-Specific Polyampholytes. *Macromolecules* **2021**, *54*, 3232–3246. <https://doi.org/10.1021/acs.macromol.0c02515>.
4. Rumyantsev, A. M.; Jackson, N. E.; **de Pablo, J. J.** Polyelectrolyte Complex Coacervates: Recent Developments and New Frontiers. *Annu. Rev. Condens. Matter Phys.* **2021**, *12*, 155–176. <https://doi.org/10.1146/annurev-conmatphys-042020-113457>.
5. Mozaffari, A.; Zhang, R.; Atzin, N.; **de Pablo, J. J.** Defect Spirograph: Dynamical Behavior of Defects in Spatially Patterned Active Nematics. *Phys. Rev. Lett.* **2021**, *126*, 227801. <https://doi.org/10.1103/PhysRevLett.126.227801>.
6. Huang, H.-H.; Ma, Z.; Strzalka, J.; Ren, Y.; Lin, K.-F.; Wang, L.; Zhou, H.; Jiang, Z.; Chen, W. Mild Water Intake Orients Crystal Formation Imparting High Tolerance on Unencapsulated Halide Perovskite Solar Cells. *Cell Reports Physical Science* **2021**, *2*, 100395. <https://doi.org/10.1016/j.xcrp.2021.100395>.
7. Dolan, J. A.; Cai, H.; Delalande, L.; Li, X.; Martinson, A. B. F.; **de Pablo, J. J.**; López, D.; Nealey, P. F. Broadband Liquid Crystal Tunable Metasurfaces in the Visible: Liquid Crystal Inhomogeneities Across the Metasurface Parameter Space. *ACS Photonics* **2021**, *8*, 567–575. <https://doi.org/10.1021/acsp Photonics.0c01599>.
8. Dinic, J.; Marciel, A. B.; **Tirrell, M. V.** Polyampholyte Physics: Liquid-Liquid Phase Separation and Biological Condensates. *Current Opinion in Colloid & Interface Science* **2021**, 101457. <https://doi.org/10.1016/j.cocis.2021.101457>.
9. Deng, C.; Webb, M. A.; Bennington, P.; Sharon, D.; **Nealey, P. F.**; Patel, S. N.; **de Pablo, J. J.** Role of Molecular Architecture on Ion Transport in Ethylene Oxide-Based Polymer Electrolytes. *Macromolecules* **2021**, *54*, 2266–2276. <https://doi.org/10.1021/acs.macromol.0c02424>.
10. Cohen, A. E.; Jackson, N. E.; **de Pablo, J. J.** Anisotropic Coarse-Grained Model for Conjugated Polymers: Investigations into Solution Morphologies. *Macromolecules* **2021**, *54*, 3780–3789. <https://doi.org/10.1021/acs.macromol.1c00302>.
11. Bennington, P.; Deng, C.; Sharon, D.; Webb, M. A.; **de Pablo, J. J.**; **Nealey, P. F.**; Patel, S. N. Role of Solvation Site Segmental Dynamics on Ion Transport in Ethylene-Oxide Based Side-Chain Polymer Electrolytes. *J. Mater. Chem. A* **2021**, *9*, 9937–9951. <https://doi.org/10.1039/D1TA00899D>.
12. Webb, M. A.; Jackson, N. E.; Gil, P. S.; **de Pablo, J. J.** Targeted Sequence Design within the Coarse-Grained Polymer Genome. *Sci. Adv.* **2020**, *6*, eabc6216. <https://doi.org/10.1126/sciadv.abc6216>.

13. Bezik, C. T.; **de Pablo, J. J.** Formation, Stability, and Annihilation of the Stitched Morphology in Block Copolymer Thin Films. *Macromolecules* **2020**, *53*, 10446–10456. <https://doi.org/10.1021/acs.macromol.0c01777>.
14. Yu, J.; Mao, J.; Nagao, M.; Bu, W.; Lin, B.; Hong, K.; Jiang, Z.; Liu, Y.; Qian, S.; **Tirrell, M.**; Chen, W. Structure and Dynamics of Lipid Membranes Interacting with Antivirulence End-Phosphorylated Polyethylene Glycol Block Copolymers. *Soft Matter* **2020**, *16*, 983–989. <https://doi.org/10.1039/C9SM01642B>.
15. Yu, B.; Rauscher, P. M.; Jackson, N. E.; Rumyantsev, A. M.; **de Pablo, J. J.** Crossover from Rouse to Reptation Dynamics in Salt-Free Polyelectrolyte Complex Coacervates. *ACS Macro Lett.* **2020**, *9*, 1318–1324. <https://doi.org/10.1021/acsmacrolett.0c00522>.
16. Sharon, D.; Bennington, P.; Patel, S. N.; **Nealey, P. F.** Stabilizing Dendritic Electrodeposition by Limiting Spatial Dimensions in Nanostructured Electrolytes. *ACS Energy Lett.* **2020**, *5*, 2889–2896. <https://doi.org/10.1021/acsenerylett.0c01543>.
17. Sharon, D.; Bennington, P.; Dolejsi, M.; Webb, M. A.; Dong, B. X.; **de Pablo, J. J.**; **Nealey, P. F.**; Patel, S. N. Intrinsic Ion Transport Properties of Block Copolymer Electrolytes. *ACS Nano* **2020**, *14*, 8902–8914. <https://doi.org/10.1021/acsnano.0c03713>.
18. Sadati, M.; Martinez-Gonzalez, J. A.; Zhou, Y.; Qazvini, N. T.; Kurtenbach, K.; Li, X.; Bokusoglu, E.; Zhang, R.; Abbott, N. L.; Hernandez-Ortiz, J. P.; **de Pablo, J. J.** Prolate and Oblate Chiral Liquid Crystal Spheroids. *Science Advances* **2020**, *6*, eaba6728. <https://doi.org/10.1126/sciadv.aba6728>.
19. Rumyantsev, A. M.; **de Pablo, J. J.** Microphase Separation in Polyelectrolyte Blends: Weak Segregation Theory and Relation to Nuclear “Pasta.” *Macromolecules* **2020**, *53*, 1281–1292. <https://doi.org/10.1021/acs.macromol.9b02466>.
20. Ren, J.; Segal-Peretz, T.; Zhou, C.; Craig, G. S. W.; **Nealey, P. F.** Three-Dimensional Superlattice Engineering with Block Copolymer Epitaxy. *Science Advances* **2020**, *6*, eaaz0002. <https://doi.org/10.1126/sciadv.aaz0002>.
21. Rauscher, P. M.; Rowan, S. J.; **de Pablo, J. J.** Hydrodynamic Interactions in Topologically Linked Ring Polymers. *Phys. Rev. E* **2020**, *102*, 032502. <https://doi.org/10.1103/PhysRevE.102.032502>.
22. Qiao, Y.; Zhou, H.; Jiang, Z.; He, Q.; Gan, S.; Wang, H.; Wen, S.; **de Pablo, J. J.**; Liu, Y.; **Tirrell, M. V.**; Chen, W. An in Situ Shearing X-Ray Measurement System for Exploring Structures and Dynamics at the Solid–Liquid Interface. *Review of Scientific Instruments* **2020**, *91*, 013908. <https://doi.org/10.1063/1.5129819>.
23. Palacio-Betancur, V.; Armas-Pérez, J. C.; Villada-Gil, S.; Abbott, N. L.; Hernández-Ortiz, J. P.; **de Pablo, J. J.** Cuboidal Liquid Crystal Phases under Multiaxial Geometrical Frustration. *Soft Matter* **2020**, *16*, 870–880. <https://doi.org/10.1039/C9SM02021G>.
24. Menéndez, C. A.; Byléhn, F.; Perez-Lemus, G. R.; Alvarado, W.; **de Pablo, J. J.** Molecular Characterization of Ebselen Binding Activity to SARS-CoV-2 Main Protease. *Science Advances* **2020**, *6*, eabd0345. <https://doi.org/10.1126/sciadv.abd0345>.
25. Jin, H. M.; Li, X.; Dolan, J. A.; Kline, R. J.; Martínez-González, J. A.; Ren, J.; Zhou, C.; **de Pablo, J. J.**; **Nealey, P. F.** Soft Crystal Martensites: An in Situ Resonant Soft x-Ray Scattering Study of a Liquid Crystal Martensitic Transformation. *Science Advances* **2020**, *6*, eaay5986. <https://doi.org/10.1126/sciadv.aay5986>.
26. Jackson, N. E.; Bowen, A. S.; **de Pablo, J. J.** Efficient Multiscale Optoelectronic Prediction for Conjugated Polymers. *Macromolecules* **2020**, *53*, 482–490. <https://doi.org/10.1021/acs.macromol.9b02020>.

27. Li, X.; Martínez-González, J. A.; Guzmán, O.; Ma, X.; Park, K.; Zhou, C.; Kambe, Y.; Jin, H. M.; Dolan, J. A.; **Nealey, P. F.**; **de Pablo, J. J.** Sculpted Grain Boundaries in Soft Crystals. *Science Advances* **2019**, *5*, eaax9112. <https://doi.org/10.1126/sciadv.aax9112>.
28. Zhou, Y.; Senyuk, B.; Zhang, R.; Smalyukh, I. I.; **de Pablo, J. J.** Degenerate Conic Anchoring and Colloidal Elastic Dipole-Hexadecapole Transformations. *Nat Commun* **2019**, *10*, 1000. <https://doi.org/10.1038/s41467-019-08645-9>.
29. Xu, X.; Mastropietro, D.; Ruths, M.; **Tirrell, M.**; Yu, J. Ion-Specific Effects of Divalent Ions on the Structure of Polyelectrolyte Brushes. *Langmuir* **2019**, *35*, 15564–15572. <https://doi.org/10.1021/acs.langmuir.9b01984>.
30. Webb, M. A.; Delannoy, J.-Y.; **de Pablo, J. J.** Graph-Based Approach to Systematic Molecular Coarse-Graining. *J. Chem. Theory Comput.* **2019**, *15*, 1199–1208. <https://doi.org/10.1021/acs.jctc.8b00920>.
31. Wang, X.; Zhou, Y.; Kim, Y.-K.; Tsuei, M.; Yang, Y.; **de Pablo, J. J.**; Abbott, N. L. Thermally Reconfigurable Janus Droplets with Nematic Liquid Crystalline and Isotropic Perfluorocarbon Oil Compartments. *Soft Matter* **2019**, *15*, 2580–2590. <https://doi.org/10.1039/C8SM02600A>.
32. Rumyantsev, A. M.; Jackson, N. E.; Yu, B.; Ting, J. M.; Chen, W.; **Tirrell, M. V.**; **de Pablo, J. J.** Controlling Complex Coacervation via Random Polyelectrolyte Sequences. *ACS Macro Lett.* **2019**, *8*, 1296–1302. <https://doi.org/10.1021/acsmacrolett.9b00494>.
33. Rumyantsev, A. M.; **de Pablo, J. J.** Liquid Crystalline and Isotropic Coacervates of Semiflexible Polyanions and Flexible Polycations. *Macromolecules* **2019**, *52*, 5140–5156. <https://doi.org/10.1021/acs.macromol.9b00797>.
34. Qu, J.; Zhao, Q.; Zhou, J.; Lai, H.; Liu, T.; Li, D.; Chen, W.; Xie, Z.; He, F. Multiple Fused Ring-Based Near-Infrared Nonfullerene Acceptors with an Interpenetrated Charge-Transfer Network. *Chem. Mater.* **2019**, *31*, 1664–1671. <https://doi.org/10.1021/acs.chemmater.8b05047>.
35. Molina, J.; **Pablo, J. J. de**; Hernández-Ortiz, J. P. Structure and Proton Conduction in Sulfonated Poly(Ether Ether Ketone) Semi-Permeable Membranes: A Multi-Scale Computational Approach. *Phys. Chem. Chem. Phys.* **2019**, *21*, 9362–9375. <https://doi.org/10.1039/C9CP00598F>.
36. Li, X.; Martínez-González, J. A.; Park, K.; Yu, C.; Zhou, Y.; **de Pablo, J. J.**; **Nealey, P. F.** Perfection in Nucleation and Growth of Blue-Phase Single Crystals: Small Free-Energy Required to Self-Assemble at Specific Lattice Orientation. *ACS Appl. Mater. Interfaces* **2019**, *11*, 9487–9495. <https://doi.org/10.1021/acsami.8b18078>.
37. Li, J.; Deng, T.-S.; Liu, X.; Dolan, J. A.; Scherer, N. F.; **Nealey, P. F.** Hierarchical Assembly of Plasmonic Nanoparticle Heterodimer Arrays with Tunable Sub-5 Nm Nanogaps. *Nano Lett.* **2019**, *19*, 4314–4320. <https://doi.org/10.1021/acs.nanolett.9b00792>.
38. Kambe, Y.; Arges, C. G.; Czaplewski, D. A.; Dolejsi, M.; Krishnan, S.; Stoykovich, M. P.; **de Pablo, J. J.**; **Nealey, P. F.** Role of Defects in Ion Transport in Block Copolymer Electrolytes. *Nano Lett.* **2019**, *19*, 4684–4691. <https://doi.org/10.1021/acs.nanolett.9b01758>.
39. Jackson, N. E.; Bowen, A. S.; Antony, L. W.; Webb, M. A.; Vishwanath, V.; **de Pablo, J. J.** Electronic Structure at Coarse-Grained Resolutions from Supervised Machine Learning. *Science Advances* **2019**, *5*, eaav1190. <https://doi.org/10.1126/sciadv.aav1190>.
40. Jackson, N. E.; Webb, M. A.; **de Pablo, J. J.** Recent Advances in Machine Learning towards Multiscale Soft Materials Design. *Current Opinion in Chemical Engineering* **2019**, *23*, 106–114. <https://doi.org/10.1016/j.coche.2019.03.005>.

41. Ediger, M. D.; **de Pablo, J. J.**; Yu, L. Anisotropic Vapor-Deposited Glasses: Hybrid Organic Solids. *Acc. Chem. Res.* **2019**, *52*, 407–414. <https://doi.org/10.1021/acs.accounts.8b00513>.
42. Dong, B. X.; Bennington, P.; Kambe, Y.; Sharon, D.; Dolejsi, M.; Strzalka, J.; Burnett, V. F.; **Nealey, P. F.**; Patel, S. N. Nanothin Film Conductivity Measurements Reveal Interfacial Influence on Ion Transport in Polymer Electrolytes. *Mol. Syst. Des. Eng.* **2019**, *4*, 597–608. <https://doi.org/10.1039/C9ME00011A>.
43. Doise, J.; Bezik, C.; Hori, M.; **de Pablo, J. J.**; Gronheid, R. Influence of Homopolymer Addition in Templated Assembly of Cylindrical Block Copolymers. *ACS Nano* **2019**, *13*, 4073–4082. <https://doi.org/10.1021/acsnano.8b08382>.
44. Colón, Y. J.; Guo, A. Z.; Antony, L. W.; Hoffmann, K. Q.; **de Pablo, J. J.** Free Energy of Metal–Organic Framework Self-Assembly. *J. Chem. Phys.* **2019**, *150*, 104502. <https://doi.org/10.1063/1.5063588>.
45. Arges, C. G.; Li, K.; Zhang, L.; Kambe, Y.; Wu, G.-P.; Lwoya, B.; Albert, J. N. L.; **Nealey, P. F.**; Kumar, R. Ionic Conductivity and Counterion Condensation in Nanoconfined Polycation and Polyanion Brushes Prepared from Block Copolymer Templates. *Mol. Syst. Des. Eng.* **2019**, *4*, 365–378. <https://doi.org/10.1039/C8ME00081F>.
46. Sharon, D.; Bennington, P.; Liu, C.; Kambe, Y.; Dong, B. X.; Burnett, V. F.; Dolejsi, M.; Grocke, G.; Patel, S. N.; **Nealey, P. F.** Interrogation of Electrochemical Properties of Polymer Electrolyte Thin Films with Interdigitated Electrodes. *J. Electrochem. Soc.* **2018**, *165*, H1028–H1039. <https://doi.org/10.1149/2.0291816jes>.
47. Sevgen, E.; Dolejsi, M.; **Nealey, P. F.**; Hubbell, J. A.; **de Pablo, J. J.** Nanocrystalline Oligo(Ethylene Sulfide)-*b*-Poly(Ethylene Glycol) Micelles: Structure and Stability. *Macromolecules* **2018**, *51*, 9538–9546. <https://doi.org/10.1021/acs.macromol.8b01812>.
48. Qiu, Y.; Antony, L. W.; Torkelson, J. M.; **de Pablo, J. J.**; Ediger, M. D. Tenfold Increase in the Photostability of an Azobenzene Guest in Vapor-Deposited Glass Mixtures. *J. Chem. Phys.* **2018**, *149*, 204503. <https://doi.org/10.1063/1.5052003>.
49. Lueckheide, M.; Viereg, J. R.; Bologna, A. J.; Leon, L.; **Tirrell, M. V.** Structure–Property Relationships of Oligonucleotide Polyelectrolyte Complex Micelles. *Nano Lett.* **2018**, *18*, 7111–7117. <https://doi.org/10.1021/acs.nanolett.8b03132>.
50. Liu, Z.; Gao, Y.; Dong, J.; Yang, M.; Liu, M.; Zhang, Y.; Wen, J.; Ma, H.; Gao, X.; Chen, W.; Shao, M. Chlorinated Wide-Bandgap Donor Polymer Enabling Annealing Free Nonfullerene Solar Cells with the Efficiency of 11.5%. *J. Phys. Chem. Lett.* **2018**, *9*, 6955–6962. <https://doi.org/10.1021/acs.jpcclett.8b03247>.
51. Bowen, A. S.; Jackson, N. E.; Reid, D. R.; **de Pablo, J. J.** Structural Correlations and Percolation in Twisted Perylene Diimides Using a Simple Anisotropic Coarse-Grained Model. *J. Chem. Theory Comput.* **2018**, *14*, 6495–6504. <https://doi.org/10.1021/acs.jctc.8b00742>.

## Collaborative Publications

1. Yanagimachi, T.; Li, X.; **Nealey, P. F.**; Kurihara, K. Surface Anchoring of Nematic Liquid Crystal on Swollen Polymer Brush Studied by Surface Forces Measurement. *Advances in Colloid and Interface Science* **2019**, *272*, 101997. <https://doi.org/10.1016/j.cis.2019.101997>.
2. Fukami, M.; Yale, C. G.; Andrich, P.; Liu, X.; Heremans, F. J.; **Nealey, P. F.**; Awschalom, D. D. All-Optical Cryogenic Thermometry Based on Nitrogen-Vacancy Centers in Nanodiamonds. *Phys. Rev. Applied* **2019**, *12*, 014042. <https://doi.org/10.1103/PhysRevApplied.12.014042>.

3. Bagchi, K.; Jackson, N. E.; Gujral, A.; Huang, C.; Toney, M. F.; Yu, L.; **de Pablo, J. J.**; Ediger, M. D. Origin of Anisotropic Molecular Packing in Vapor-Deposited Alq<sub>3</sub> Glasses. *J. Phys. Chem. Lett.* **2019**, *10*, 164–170. <https://doi.org/10.1021/acs.jpcllett.8b03582>.
4. Liu, L.; Chen, H.; Chen, W.; He, F. From Binary to Quaternary: High-Tolerance of Multi-Acceptors Enables Development of Efficient Polymer Solar Cells. *J. Mater. Chem. A* **2019**, *7*, 7815–7822. <https://doi.org/10.1039/C9TA00948E>.
5. Chen, H.; Qu, J.; Liu, L.; Chen, W.; He, F. Carrier Dynamics and Morphology Regulated by 1,8-Diiodooctane in Chlorinated Nonfullerene Polymer Solar Cells. *J. Phys. Chem. Lett.* **2019**, *10*, 936–942. <https://doi.org/10.1021/acs.jpcllett.9b00063>.
6. Hsieh, H.-C.; Hsiow, C.-Y.; Su, Y.-A.; Liu, Y.-C.; Chen, W.; Chiu, W.-Y.; Shih, Y.-C.; Lin, K.-F.; Wang, L. Two-Dimensional Polythiophene Homopolymer as Promising Hole Transport Material for High-Performance Perovskite Solar Cells. *Journal of Power Sources* **2019**, *426*, 55–60. <https://doi.org/10.1016/j.jpowsour.2019.04.008>.
7. Wang, J.-Y.; Chen, W.; Nagao, M.; Shelat, P.; Hammer, B. A. G.; Tietjen, G. T.; Cao, K. D.; Henderson, J. M.; He, L.; Lin, B.; Akgun, B.; Meron, M.; Qian, S.; Ward, S.; Marks, J. D.; Emrick, T.; Lee, K. Y. C. Tailoring Biomimetic Phosphorylcholine-Containing Block Copolymers as Membrane-Targeting Cellular Rescue Agents. *Biomacromolecules* **2019**, *20*, 3385–3391. <https://doi.org/10.1021/acs.biomac.9b00621>.
8. Sokolov, A.; Mozaffari, A.; Zhang, R.; **de Pablo, J. J.**; Snezhko, A. Emergence of Radial Tree of Bend Stripes in Active Nematics. *Phys. Rev. X* **2019**, *9*, 031014. <https://doi.org/10.1103/PhysRevX.9.031014>.

## Design, Synthesis, and Assembly of Biomimetic Materials with Novel Functionality

Aleksandr Noy, Anthony van Burren (LLNL), James J. De Yoreo, Chun-Long Chen, Marcel Baer (PNNL)

### Program Scope

The overarching goal of this project is to develop synthetic self-assembling systems that mimic the hierarchical nature of biological membranes and carry out high-level functions based on a predictive understanding of both assembly and function. In particular, we seek to create fully synthetic self-assembling biomimetic structures that mimic the environment, versatility, and functionality of cell membranes based on a predictive understanding of: (a) the link between macromolecular sequence and organization, (b) controls on assembly and ordering, (c) incorporation of artificial functional channel units such as carbon nanotube porins (CNTPs), and (d) mechanisms that underpin fast and selective transport through these materials. Our approach integrates synthesis of defined sequence peptoid polymers, in situ atomic-level characterization of molecular structure and interactions, assembly dynamics and interfacial structure, molecular simulations of structure and assembly, and measurements of ionic and molecular transport through tailored carbon nanotube porin channels. Taken together, these advances build a foundation for design of functional materials based on an understanding of the link between sequence, assembly, and function to result in a new generation of biomimetic membranes with rationally-tunable pore size and chemical selectivity for applications in a wide range of energy systems.

### Recent Progress

#### Artificial peptoid-based membrane matrices: Membrane-mimetic 2D nanosheets with responsive behavior and high photostability.

Inspired by turn-on fluorescent  $H_2S$  probes, we designed and synthesized  $H_2S$ -responsive peptoid nanosheets where we used 3,5-dinitrophenol (NDP)-modified 1,8-naphthalimide (NI) as the  $H_2S$  responsive probes that were added to lipid-like peptoids (LLPs). (**Fig. 1**)<sup>1</sup> NDP-NI

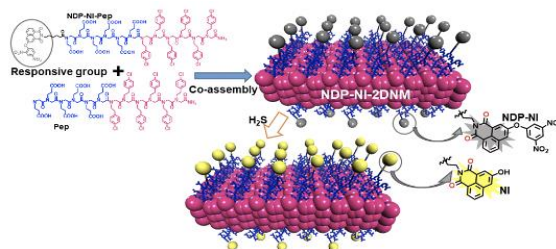


**Figure 1.** Self-assembly of  $H_2S$  responsive nanosheets. responds to  $H_2S$  with high specificity as a result of  $H_2S$ -induced thiolysis of dinitrophenyl ether. AFM imaging showed that co-assembly of NDP-NI-Pep and Pep at the molar ratio of 2:8 leads to the formation of uniform nanosheets with straight edges. X-ray diffraction data indicated that NDP-NI-containing 2D nanomembranes (2DNMs) were highly crystalline and exhibited a similar framework structure to nanomembranes without NDP-NI. Thus, we believe that  $H_2S$  responsive NDP-NI probes were precisely displayed and pointed outward at both polar surfaces of 2DNMs, while the hydrophobic  $N_4$ -Cipe domains formed the core of 2DNMs. After NDP-NI reacted with  $H_2S$  to become fluorescent NI, the sheet framework structure remained fully intact. These results demonstrate our capabilities to control peptoid assembly to synthesize responsive nanosheets.

By taking advantage of the high crystallinity of 2DNMs and their high programmability, we also demonstrated how tuning of the density and long-range ordering of dansyl dyes within 2DNMs allowed us to achieve high quantum yield and superior photostability for these nanostructures. These highly bright and photostable 2DNMs offer new opportunities for development of photoactive materials for photocatalysis, photovoltaic, and imaging applications.<sup>2</sup>

**Atomic level characterization and simulation: Structure of copolymer-lipid vesicles.** We have explored the morphological dependence of adding carbon nanotubes to copolymer (PB-PEO)–lipid (DPOC) vesicle-bilayers with *in situ* SAXS/WAXS and course-grained MD.<sup>3</sup> The presence of CNTs in hybrid copolymer–lipid vesicles increases the bilayer thickness and enhances ordering and density within the hydrophobic region. MD results indicate that the dioleoyl interactions change the most, suggesting a preferred affinity of CNT to dioleoyl (**Fig. 2**). We also used in situ

SAXS to probe the assembly of peptoid amphiphiles.<sup>4</sup> These measurements reveal that prior to crystallization the peptoids first assemble into amorphous particles. The data showed diffraction peaks associated with aromatic interactions during the early stages of assembly. These peaks also developed the fastest, with the aromatic domains arranging in a herringbone pattern (**Fig. 2**).

**Mapping and simulating interfacial structure.** In the vicinity of membranes surfaces

and pore openings, solvent fluctuations that drive ion/solute dynamics should differ significantly from those in the bulk liquid. Understanding these differences and how they depend on details of interfacial surface chemistry is central to our ability to design and tune transport properties of synthetic membranes. To understand the relationship between surface chemistry and ion/solute dynamics in terms of water’s interfacial molecular structure, we combined MD simulations with a recently developed AFM-based capability—fast force mapping (FFM)—that maps the 3D distribution of water near an interface at near-atomic resolution (**Fig. 3**) by using the relationship between the force gradient seen by an oscillating AFM tip and the local water density.<sup>5</sup> In our other projects, we have successfully applied this method to multiple crystalline surfaces and compared the results with a range of simulation techniques to understand the role of tip size and chemistry.<sup>5</sup> For LLP membranes, our simulations predict distinct hydration layers with variations in water

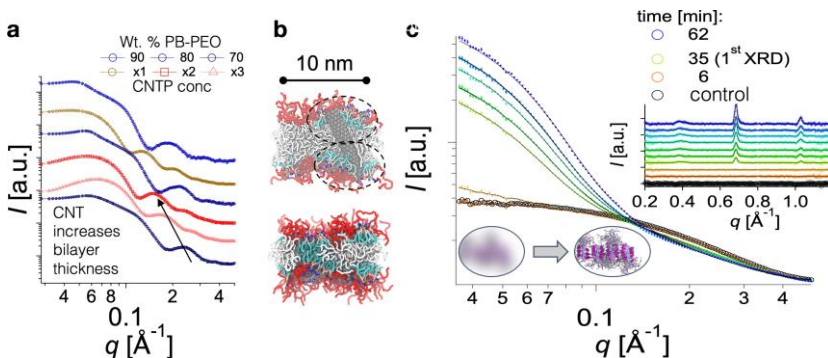


**Figure 2. SAXS reveals atomic level structure of self-assembled membranes.** **a.** SAXS data obtained from hybrid copolymer/lipid vesicles at varying copolymer loadings (blue) with copolymer/lipid/CNTP vesicles with similar copolymer loadings (red-brown). **b.** Coarse-grain MD showing preferential interactions of dioleoyl moieties with the CNT (dashed circles) and leads to slightly thicker bilayers observed by SAXS. **c.** Time-resolved SAXS and WAXS (inset) showing signal increasing during the course of peptoid assembly/crystallization.

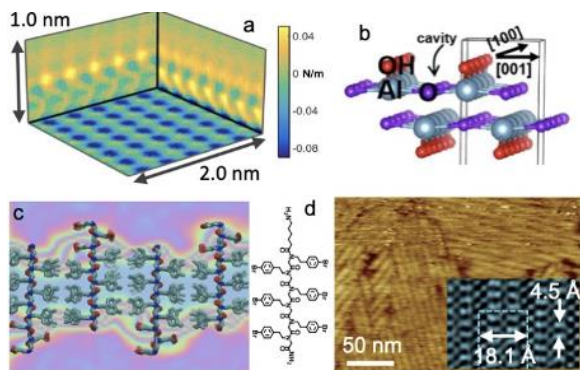


**Figure 3.** We have implemented 3D FFM of water structure illustrated by orthogonal cuts of an FFM map on (a) AIOOH.<sup>106</sup> The complex structure arises from corrugations of OH and cavity sites (b). MD simulations (c) predict alternating hydrophilic ridges (pink) and hydrophobic troughs (yellow) on LLP membranes. Short LLP (d) seen here by AFM and cryoTEM are our first targets.

lipid membrane covering the surface of a Si nanoribbon pH sensor (Fig. 4) protect that surface from long-term biological fouling, while still allowing fast unimpeded proton transport to the sensor. We have demonstrated stable long-term pH sensing with these devices in a range of highly-fouling environments, such as bovine plasma, serum albumin solution, and even milk.

**Understanding thermodynamic and kinetic controls on matrix and protein assembly: Self-assembly of proteins on solid surfaces.** Recognizing that biological systems utilize organization of proteins to create functional structures, we used in situ AFM to investigate assembly of both natural proteins on surfaces engineered to guide assembly<sup>6</sup> and synthetic proteins designed *de novo* to assemble into 1D and 2D structures.<sup>7</sup> We found that assembly of bacterial surface layer (S-layer) proteins on a mica undergoes a two-step nucleation process involving a metastable intermediate is followed by a growth phase.<sup>8</sup> From analysis of the assembly dynamics, we developed a quantitative model that accounts for nucleation, growth and structural rearrangements across s-to-hr and nm-to-m scales. With this model in hand, we investigated a bottom-up approach to directing S-layer assembly by exploiting non-specific interactions on block copolymer (BCP) films. We showed that the chemical heterogeneity of BCP films indeed directs assembly, with adsorption and self-assembly confined to the hydrophobic block and the S-layer domains aligned to the BCP domains (Fig. 5). The assembly dynamics were followed by AFM under continuous flow conditions, enabling determination of rate constants. The

density both normal to the surface and laterally across peptoid rows. The first hydration layer lies close ( $<0.4\text{nm}$ ) to hydrophilic rows and is interrupted in the vicinity of hydrophobic rows (Fig. 3c). We are currently working to compare the predictions obtained to date on highly-ordered peptoid membranes assembled from short LLPs in which the row-by-row structure is clear (Fig. 3d).

**Integration and properties of biomimetic CNTP membrane: CNTP membranes control access to biosensor surfaces.** We showed that CNTP-based membrane materials could be integrated with the silicon nanoribbon biosensors to control access of specific analytes to the sensor surface. Specifically, we demonstrated that CNTPs incorporated into the

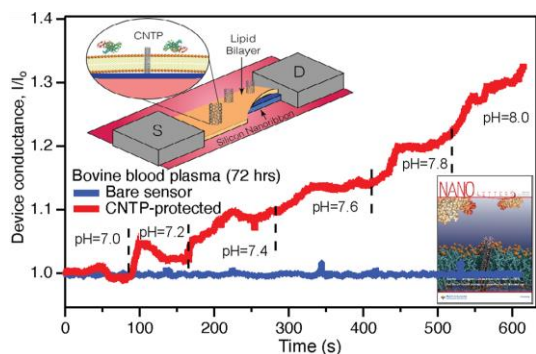


**Figure 4.** Si nanoribbon pH sensors protected by a membrane with CNTP pores. Only the sensors protected by a CNTP membrane show pH response after being exposed to bovine blood plasma for 3 days.

pattern of alternating, chemically distinct nanoscale domains drastically increased the assembly rates compared to non-patterned chemically homogeneous substrates, highlighting the role of confinement within the hydrophobic block.

## Future Plans

Our future plans center on continuing to design, synthesize, and characterize versatile and tunable components for biomimetic membrane assemblies that combine lipid, polymer, and peptoid matrix materials. In a significant step forward, we also plan to incorporate de-novo designed protein pores into these membrane assemblies. We also plan to characterize assembly process, atomic level structure, and transport properties of these membranes and ultimately to determine the physico-chemical principles and structure-function relationships that control structure and transport properties in these assemblies. Our final goal will be to achieve highly-efficient transport and strong tunable molecular selectivity in these biomolecular materials.

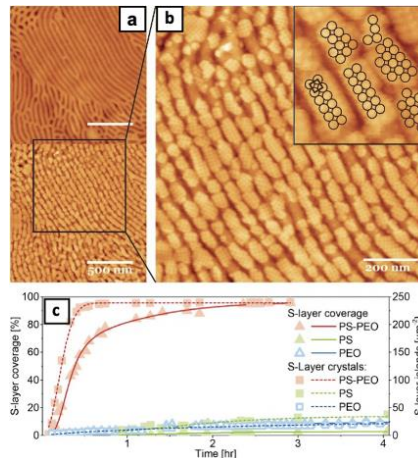


**Figure 5. Even non-specific interactions enable control of protein assembly on surfaces**, as demonstrated for S-layers on BCPs, where **a** and **b** show before and after assembly and **c** shows that confinement to hydrophobic block dramatically increases rates of coverage and nucleation.

## References

- 1 Wang, M. *et al.* Peptoid-Based Programmable 2D Nanomaterial Sensor for Selective and Sensitive Detection of H<sub>2</sub>S in Live Cells. *ACS Applied Bio Materials* **3**, 6039-6048, doi:10.1021/acsabm.0c00657 (2020).
- 2 Song, Y. *et al.* Highly Bright and Photostable Two-Dimensional Nanomaterials Assembled from Sequence-Defined Peptoids. *ACS Materials Letters* **3**, 420-427, doi:10.1021/acsmaterialslett.1c00110 (2021).
- 3 Hammons, J. A. *et al.* Decoupling copolymer, lipid and carbon nanotube interactions in hybrid, biomimetic vesicles. *Nanoscale* **12**, 6545-6555 (2020).
- 4 Hammons, J. A. *et al.* Early-Stage Aggregation and Crystalline Interactions of Peptoid Nanomembranes. *The Journal of Physical Chemistry Letters* **12**, 6126-6133, doi:10.1021/acs.jpcclett.1c01033 (2021).
- 5 Nakouzi, E. *et al.* Moving beyond the Solvent-Tip Approximation to Determine Site-Specific Variations of Interfacial Water Structure through 3D Force Microscopy. *J. Phys. Chem. C* **125**, 1282-1291, doi:10.1021/acs.jpcc.0c07901 (2021).
- 6 Stel, B. *et al.* Contrasting chemistry of block copolymer films controls the dynamics of protein self-assembly at the nanoscale. *ACS Nano* **13**, 4018-4027 (2019).
- 7 Ben-Sasson, A. J. *et al.* Design of biologically active binary protein 2D materials. *Nature* **589**, 468-473 (2021).
- 8 Stel, B., Cometto, F., Rad, B., De Yoreo, J. J. & Lingenfelder, M. Dynamically resolved self-assembly of S-layer proteins on solid surfaces. *Chem. Commun. (Cambridge, U. K.)* **54**, 10264-10267 (2018).

## Project publications

- Hammons, J. ; Baer, M.; Jian, T.; Lee, J.; Weiss, T.; De Yoreo, J.; Noy, A.; Chen, C.-L.; van Buuren, A. (2021) Early-Stage Aggregation and Crystalline Interactions of Peptoid Nanomembranes. *Journal of Physical Chemistry Letters*. 12, 6126-6133.
- Song, Y.; Wang, M.; Akkineni, S.; Yang, W.; Hettige, J. J.; Jin, H.; Liao, Z.; Mu, P.; Yan, F.; Baer, M.; De Yoreo, J. J.; Du, D.; Lin, Y.; Chen, C.-L., (2021) Highly Bright and Photostable Two-Dimensional Nanomaterials Assembled from Sequence-Defined Peptoids. *ACS Materials Letters*. 21 (4), 420-427.
- Ma, Z.; Wang, S.; Kim, M.; Liu, K.; Chen, C.-L., Pan, W. Transfer learning of memory kernels for transferable coarse-graining of polymer dynamics. **Soft Matter** 2021, 17, 5864-5877.
- Wang, M.; Song, Y.; Zhang, S.; Zhang, X.; Cai, X.; Lin, Y., De Yoreo, J. J.; Chen, C.-L. Programmable two-dimensional nanocrystals assembled from POSS-containing peptoids as efficient artificial light-harvesting systems. **Science Advances** 2021, 7, eabg1448.
- Cai, X.; Wang, M.; Mu, P.; Jian, T.; Liu, D.; Ding, S.; Luo, Y.; Du, D.; Song, Y.; Chen, C.-L.; Lin, Y. Sequence-Defined Nanotubes Assembled from IR780-Conjugated Peptoids for Chemophototherapy of Malignant Glioma. **Research**, 2021, 9861384.
- Cai, B.; Li, Z.; Chen, C.-L., Programming Amphiphilic Peptoid Oligomers for Hierarchical Assembly and Inorganic Crystallization. *Acc. Chem. Res.* **2021**. 54, 1, 81-91. (**Journal Cover**)
- Hammons J. A., Ingolfsson H. I., Lee J. R. I., Carpenter T. S., Sanborn J., Tunuguntla T., Yao Y. C., Weiss T. M., Noy A., and Van Buuren T. (2020) Decoupling copolymer, lipid and carbon nanotube interactions in hybrid, biomimetic vesicles. *Nanoscale* 12, (11) 6545-6555. DOI. 10.1039/c9nr09973e
- Wang M., Song Y., Mu P., Cai X., Lin Y., and Chen C.-L. (2020) Peptoid-based programmable 2D nanomaterial sensor for selective and sensitive detection of H<sub>2</sub>S in live cells. *ACS Applied Bio Materials* 3, (9) 6039-6048. DOI. 10.1021/acsabm.0c00657
- Sullivan K., Zhang Y. L., Lopez J., Lowe M., and Noy A. (2020) Carbon nanotube porin diffusion in mixed composition supported lipid bilayers. *Scientific Reports* 10, (1) 8. DOI. 10.1038/s41598-020-68059-2
- Noy A. and Wanunu M. (2020) A new type of artificial water channels. *Nature Nanotechnology* 15, (1) 9-10. DOI. 10.1038/s41565-019-0617-5
- Jiao F., Wu X. P., Jian T. Y., Zhang S., Jin H. B., He P. G., Chen C. L., and De Yoreo J. J. (2019) Hierarchical assembly of peptoid-based cylindrical micelles exhibiting efficient resonance energy transfer in aqueous solution. *Angewandte Chemie-International Edition* 58, (35) 12223-12230. DOI. 10.1002/anie.201904598
- Jin H. B., Jian T. Y., Ding Y. H., Chen Y. L., Mu P., Wang L., and Chen C. L. (2019) Solid-phase synthesis of three-armed star-shaped peptoids and their hierarchical self-assembly. *Biopolymers* 110, (4) 7. DOI. 10.1002/bip.23258
- Hemmatian Z., Tunuguntla R. H., Noy A., and Rolandi M. (2019) Electronic control of H<sup>+</sup> current in a bioprotonic device with carbon nanotube porins. *PLOS One* 14, (2) 9. DOI. 10.1371/journal.pone.0212197
- Chen Z. B., Johnson M. C., Chen J. J., Bick M. J., Boyken S. E., Lin B. H., De Yoreo J. J., Kollman J. M., Baker D., and DiMaio F. (2019) Self-assembling 2D arrays with de Novo protein building blocks. *Journal of the American Chemical Society* 141, (22) 8891-8895. DOI. 10.1021/jacs.9b01978

Chen X., Zhang H. N., Tunuguntla R. H., and Noy A. (2019) Silicon Nanoribbon pH Sensors Protected by a Barrier Membrane with Carbon Nanotube Porins. *Nano Letters* 19, (2) 629-634. DOI. 10.1021/acs.nanolett.8b02898

Zhang S., Chen J. J., Liu J. L., Pyles H., Baker D., Chen C. L., and De Yoreo J. J. (2020) Engineering biomolecular self-assembly at solid-liquid interfaces. *Advanced Materials*, Article ID# 1905784. DOI. 10.1002/adma.201905784

Ben-Sasson A. J., Watson J. L., Sheffler W., Johnson M. C., Bittleston A., Somasundaram L., Decarreau J., Jiao F., Chen J. J., Mela I., Drabek A. A., Jarrett S. M., Blacklow S. C., Kaminski C. F., Hura G. L., De Yoreo J. J., Kollman J. M., Ruohola-Baker H., Derivery E., and Baker D. (2021) Design of biologically active binary protein 2D materials. *Nature*, In press. DOI. 10.1038/s41586-020-03120-8

O'Callahan B. T., Park K.-D., Novikova I. V., Jian T., Chen C.-L., Muller E. A., El-Khoury P. Z., Raschke M. B., and Lea A. S. (2020) In liquid infrared scattering scanning near-field optical microscopy for chemical and biological nanoimaging. *Nano Letters*, In Press. DOI. 10.1021/acs.nanolett.0c01291.

Yao Y. C., Taqieddin A., Alibakhshi M. A., Wanunu M., Aluru N. R., and Noy A. (2019) Strong Electroosmotic Coupling Dominates Ion Conductance of 1.5 nm Diameter Carbon Nanotube Porins. *ACS Nano* 13, (11) 12851-12859. DOI. 10.1021/acsnano.9b05118

Tuladhar A., Chase Z. A., Baer M. D., Legg B. A., Tao J. H., Zhang S., Winkelmann A. D., Wang Z. M., Mundy C. J., De Yoreo J. J., and Wang H. F. (2019) Direct observation of the orientational anisotropy of buried hydroxyl groups inside muscovite mica. *Journal of the American Chemical Society* 141, (5) 2135-2142. DOI. 10.1021/jacs.8b12483

Stel B., Gunkel I., Gu X., Russell T. P., De Yoreo J. J., and Lingenfelder M. (2019) Contrasting chemistry of block copolymer films controls the dynamics of protein self-assembly at the nanoscale. *ACS Nano* 13, (4) 4018-4027. DOI. 10.1021/acsnano.8b08013

Luo Y. N., Song Y., Wang M. M., Jian T. Y., Ding S. C., Mu P., Liao Z. H., Shi Q. R., Cai X. L., Jin H. B., Du D., Dong W. J., Chen C. L., and Lin Y. H. (2019) Bioinspired peptoid nanotubes for targeted tumor cell imaging and chemo-photodynamic therapy (Journal Cover). *Small* 15, (43) Article ID# 1902485. DOI. 10.1002/smll.201902485 .

Denton J. K., Kelleher P. J., Johnson M. A., Baer M. D., Kathmann S. M., Mundy C. J., Rudd B. A. W., Allen H. C., Choi T. H., and Jordan K. D. (2019) Molecular-level origin of the carboxylate head group response to divalent metal ion complexation at the air-water interface. *Proc. Natl. Acad. Sci. USA* 116, (30) 14874-14880. DOI. 10.1073/pnas.1818600116

## **Adaptive Interfacial Assemblies Towards Structuring Liquids**

**Thomas P. Russell, Materials Sciences Division, LBNL, Berkeley, CA and Polymer Science and Engineering Dept., University of Massachusetts Amherst, Amherst, MA**

**Paul Ashby, Molecular Foundry, Lawrence Berkeley National Laboratory, Berkeley, CA**

**Phillip Geissler, Chemistry Department, University of California Berkeley, Berkeley, CA and Materials Sciences Division, LBNL, Berkeley, CA**

**Brett Helms, Molecular Foundry, LBNL, Berkeley, CA**

**Alex Zettl, Physics Department, University of California Berkeley, Berkeley, CA and Materials Sciences Division, LBNL, Berkeley, CA**

### **Program Scope**

This FWP advances a new concept in materials based on the interfacial formation, assembly and jamming of nanoparticle surfactants (NPSs). Materials are usually classified as solids or liquids, based on their structural stability, dynamic response and rheological properties. However, if we learn to manipulate the interfacial packing of the NPSs using external triggers, a new class of materials will emerge that synergistically combines the desirable characteristics of fluids—rapid transport of energy carriers, conformability to arbitrary shapes, and controlled dissipation of mechanical energy—with the structural stability of a solid. Structured liquids will have spatial and temporal characteristics of solids and liquids spanning from the nanoscopic to macroscopic length scales, over many orders of magnitude in time. The FWP addresses the translation of control over individual nanoparticle chemistries, and their assembly and dynamics at interfaces, to translate events on the nanoscopic to the macroscopic level. We quantify the interfacial assemblies of NP-surfactants, their dynamics, and their response to external stimuli. Dynamic covalent bonding chemistries and inclusion of active materials are developed to impart responsiveness and adaptability to the assemblies, so as to produce all-liquid, energy-relevant systems that can be re-structured. Revolutionary design strategies will emerge for directing flow of mechanical, electrical or optical energy in materials or systems. Fundamental challenges are faced in tailoring NPS chemistry, assembly and dynamics to affect controlled macroscopic changes in structure.

### **Recent Progress**

**Direct Observation of Nanoparticle-Surfactant Assembly and Jamming at the Water-Oil Interface:** To understand the interfacial behavior of NPSs it is necessary to understand the mechanism by which the NPSs attach to the interface and the dependence of this attachment on the area coverage of the interface. Through direct observation with high spatial and temporal, using laser scanning resolution and *in situ* atomic force microscopy, the early-stage attachment was found to be diffusion limited and with increasing areal density. When the local areal density of the NPSs assembled at the interface increases and there is insufficient free space to accommodate

the entry of a new NP, the assembled NPs do require rearrangement. Time-dependent *in situ* AFM images of the interface with co-assembled 100- and 300-nm NPSs are shown in Fig. 2B at time  $t_0$  and  $t_0 + 5$  min. At  $t_0$ , there is a very dense layer of NPSs assembled on the interface (both 100 and 300 nm), and fluctuations in the areal density are evident along with regions of closest packed structure. There is no bare interface with sufficient area to accommodate the entry of a new 300-nm NP to the assembly. After a 5-min time period, a 300-nm NP (circled in white) does attach to the interface, accompanied by several 100-nm NPs that disappear from view (labeled by faded red circles in Fig. 1C) and two 100-nm NPs that markedly change their positions (indicated by the arrows in Fig. 1C). These results show that a cooperative structural change of the NPSs assembled at the interface is required to accommodate the attachment of additional NPs from the bulk phase at these high packing densities as has been previously modeled using Monte Carlo simulations (1). In addition to the 100-nm NPs that laterally shifted their positions, several are no longer detectable. The unprecedented detail provided by *in situ* AFM revealed the highly non-equilibrium nature of the assembly.

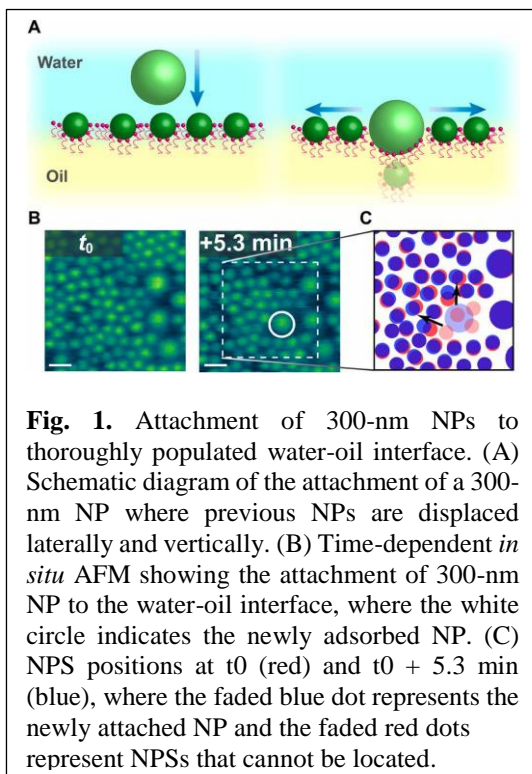


**Fig. 1.** Attachment of 300-nm NPs to thoroughly populated water-oil interface. (A) Schematic diagram of the attachment of a 300-nm NP where previous NP are displaced laterally and vertically. (B) Time-dependent *in situ* AFM showing the attachment of 300-nm NP to the water-oil interface, where the white circle indicates the newly adsorbed NP. (C) NPS positions at  $t_0$  (red) and  $t_0 + 5.3$  min (blue), where the faded blue dot represents the newly attached NP and the faded red dots represent NPSs that cannot be located.

**Spontaneous Emulsification Induced by Nanoparticle Surfactants:** Unlike conventional emulsions, microemulsions form spontaneously, have a monodisperse droplet size that can be controlled by adjusting surfactant concentration, and are stable. To make microemulsions, judicious choice of surfactant molecule must be made, which significantly limits their potential use. NPSs, on the other hand, are a promising alternative because the surface chemistry needed to make them bind to a liquid-liquid interface is both flexible and understood. A thermodynamic model predicting the conditions in which NPSs drive spontaneous emulsification was derived that quantitatively agreed with experiments.

We measured the IFT of this system using pendant drop tensiometry for different Noria surfactant concentrations to determine the binding strength,  $U$ , and particle radius,  $r$ , as free fitting parameters. A Noria radius of  $r = 0.51$  nm was found, very close to x-ray diffraction results (2), and that the binding strength is  $U = 11$  kBT. The estimated binding energy is four times larger than the prediction of the Pieranski model (3), since all of the carboxy groups on the Noria can interact with PDMS-NH<sub>2</sub>. We extend our model to allow an aqueous volume,  $V$ , to be arranged in  $m \propto 6VD-3$  identical droplets with the diameter  $D$  and total surface area  $A = 6VD-1$  (4). The droplet relaxes to thermodynamically stable state, obtained by minimizing the free energy with respect to the packing fraction,  $\eta$ , and microemulsion droplet diameter,  $D$ .  $\eta$  and  $D$ , as a function of the Noria concentration, showed good agreement with dynamic light scattering measurements of 50  $\mu$ l aqueous droplets [Figure 2c], yielding an increase of up to four orders of magnitude of the oil-water interfacial area [Figure 2D] as the Noria concentration increases.

**Explosive Spontaneous Emulsification:** Interfacial phenomena are ubiquitous in nature and play a critical role in a plethora of materials engineering<sup>1-3</sup>, chemical reaction<sup>4-7</sup>, and mass transport

processes<sup>8-10</sup> that rely on energy conversion. Interfacial energy can be used to cause motion driven by, for example, capillary forces<sup>11-15</sup>, or it can be converted into an elastic energy causing a structural deformation to generate new interfaces<sup>16-24</sup>. These generally require large forces to overcome interfacial stress. We have uncovered a low-energy route to convert stored potential energy into a kinetic energy. Using an external magnetic field, the areal density of paramagnetic NPSs assembled on the surface of an aqueous droplet emersed in oil can be quenched to a super-saturated state, completely suppressing spontaneous emulsification by the induced magnetic dipolar interactions between the nanoparticles. The interfacial tension, now much less than the equilibrium surface energy, represents a stored potential energy. Upon removal of the field, this stored potential energy is released by an explosive emulsification, manifest in a plume of ferromagnetic liquid microdroplets that burst from the surface of the drop with kinetic energies that depend on the magnetic characteristics of the microdroplets and the parent drop. The transfer of the paramagnetic NPSs to the microdroplets, rapidly reduces the areal density of the NPSs on the parent drop, returning the interfacial tension to the equilibrium value. This highly efficient energy conversion process has the potential of revolutionizing energy storage, micropropulsion systems, e.g., thrusters for nanosatellites, and remotely controlled soft microrobots.

**Structured Liquid Batteries:** Chemical systems may be maintained far from equilibrium by

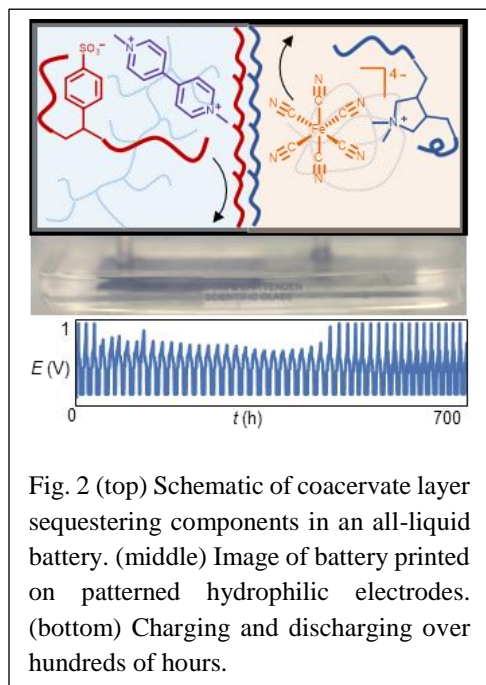


Fig. 2 (top) Schematic of coacervate layer sequestering components in an all-liquid battery. (middle) Image of battery printed on patterned hydrophilic electrodes. (bottom) Charging and discharging over hundreds of hours.

sequestering otherwise reactive species into different microenvironments. Controlling the amount of chemical energy stored in such systems and to utilize it on demand to perform useful work is a challenge. Redox-active molecules compartmentalized in multi-phasic structured liquid devices were charged and discharged to power a load on an external circuit. Here, we harness the interfacial assembly of polyelectrolytes to fabricate structured liquid batteries on hydrophobic substrates with patterned hydrophilic electrodes (**Figure 2**) (5). By controlling the geometry and surface chemistry of the current collectors,(6,7) we can prescribe an interface between aqueous biphasic anolytes and catholytes deposited onto the electrodes (**Figure 2b**). Once the interface is formed, polyanions, e.g., poly(sodium 4-styrene sulfonate), PSS-Na, dissolved in the anolyte form an ionically conductive coacervate membrane with polycations, e.g., polydiallyldimethylammonium chloride, PDADMA-Cl dissolved in the catholyte (5,8). We also leverage ion-

pairing between polyelectrolytes and oppositely-charged charged active materials to mitigate the rate of active-material crossover between phases, allowing most of the theoretical capacity to be accessed as the device is cycled over hundreds of hours (9-11).

### Future Plans

Our recent discoveries have opened intriguing questions on the roles of interparticle interactions, both attractive and repulsive, on the interfacial packing of NPSs. Theoretical descriptions of these non-equilibrium behaviors are being pursued by **Geissler** and **Omar**. These will be complemented by in situ AFM and magnetic AFM studies by **Ashby**, **Zettl** and **Russell** to obtain single-particle resolution images of the distribution of NPSs and mixed NPS system, where the introduction non-

functional NPs into the NPSs, as shown by **Russell** with Fischer (Magnetics Program), mediate interactions and can lead to heterogeneous NPS assemblies. **Helms** will provide chemistries to modify the interactions between the ligands, providing and additional means of manipulating interparticle interactions. In collaboration with staff scientists at the Molecular Foundry and **Zettl**, **Russell** have designed and fabricated a liquid TEM cell to investigate in situ the assembly and jamming of NPSs and mixed NPSs at liquid-liquid interfaces. Droplets stabilized by the NPSs with flow past the electron beam where the spatial location of the beam impingement will define a time scale to map NP trajectories providing detailed insights into the kinetics of diffusion, jamming and solidification. Complemented by *ex situ* AFM studies of **Ashby**, unprecedented details on the NP assemblies will be obtained for computational modeling by **Geissler** and **Omar**. Phase separation of mixed NPSs will lead to droplets with a heterogeneous distribution of NPSs that will be characterized by **Russell**, **Zettl** and **Ashby**. Selective functionalization of the NPSs by **Helms** yields droplets with heterogeneous surface functionalization that, in turn, will be used to generate hierarchical droplet assemblies in 3D. that will be modeled by **Omar** and **Geissler** and extensively characterized by **Russell** and **Ashby**, using atomic force, electron, optical and fluorescence microscopy methods. Encoding the NPs and associated ligands with specific functionality, 3D constructs will self-assemble, spanning orders of magnitude of length scales. **Geisser** and **Omar** have been engaged in theoretical treatments of assemblies that incorporate or encapsulate active matter. **Russell** and **Helms** have been investigating dissipative systems that can be parlayed with theory to generate evolutionary, dissipative systems that can self-tailor their shape in response to external stimuli.

## References

1. K. Schwenke, L. Isa, E. Del Gado, Assembly of Nanoparticles at Liquid Interfaces: Crowding and Ordering. *Langmuir*. **30**, 3069–3074 (2014).
2. R. S. Patil, D. Banerjee, C. M. Simon, J. L. Atwood, and P. K. Thallapally, Chem.:Eur. J. **22**, 12618 (2016).
3. P. Pieranski, Phys. Rev. Lett. **45**, 569 (1980).
4. A. Wang, J. W. Zwanikken, D. M. Kaz, R. McGorty, A. M. Goldfain, W. B. Rogers, V. N. Manoharan, Before the breach: Interactions between colloidal particles and liquid interfaces at nanoscale separations. *Phys. Rev. E*. **100**, 42605 (2019).
5. G. Xie, J. Forth, Y. Chai, P. D. Ashby, B. A. Helms, T. P. Russell, *Chem* **2019**, *5*, 2678–2690.
6. L. Wu, Z. Dong, F. Li, Y. Song, *Langmuir* **2018**, *34*, 639–645.
7. J. M. Scheiger, M. A. Kuzina, M. Eigenbrod, Y. Wu, F. Wang, S. Heißler, S. Hardt, B. Nestler, P. A. Levkin, *Adv. Mater.* **2021**, e2100117.
8. Q. Wang, J. B. Schlenoff, *Macromolecules* **2014**, *47*, 3108–3116.
9. K. W. Knehr, E. Agar, C. R. Dennison, A. R. Kalidindi, E. C. Kumbur, *J. Electrochem. Soc.* **2012**, *159*, A1446;
10. J. grosse Austing, C. Nunes Kirchner, L. Komsiyaska, G. Wittstock, *J. Power Sources* **2016**, *306*, 692–701.
11. R. Darling, K. Gallagher, W. Xie, L. Su, F. Brushett, *J. Electrochem. Soc.* **2015**, *163*, A5029.

## Publications

### Primary Funding from Program

1. X. F. Wu *et al.*, Ferromagnetic liquid droplets with adjustable magnetic properties. *Proceedings of the National Academy of Sciences of the United States of America* **118** (2021).
2. S. Y. Sun, T. Liu, S. W. Shi, T. P. Russell, Nanoparticle surfactants and structured liquids. *Colloid and Polymer Science* **299**, 523-536 (2021).
3. M. Q. Hu, T. P. Russell, Polymers with advanced architectures as emulsifiers for multi-functional emulsions. *Materials Chemistry Frontiers* **5**, 1205-1220 (2021).
4. P. Y. Gu *et al.*, Visualizing Interfacial Jamming Using an Aggregation-Induced-Emission Molecular Reporter. *Angewandte Chemie-International Edition* **60**, 8694-8699 (2021).
5. P. Y. Gu *et al.*, Surfactant-Induced Interfacial Aggregation of Porphyrins for Structuring Color-Tunable Liquids. *Angewandte Chemie-International Edition* **60**, 2871-2876 (2021).
6. G. H. Xie *et al.*, Hanging droplets from liquid surfaces. *Proceedings of the National Academy of Sciences of the United States of America* **117**, 8360-8365 (2020).
7. R. Streubel, X. B. Liu, X. F. Wu, T. P. Russell, Perspective: Ferromagnetic Liquids. *Materials* **13** (2020).
8. J. Hasnain *et al.*, Spontaneous emulsification induced by nanoparticle surfactants. *Journal of Chemical Physics* **153** (2020).
9. P. Y. Gu *et al.*, Conductive Thin Films over Large Areas by Supramolecular Self-Assembly. *Acs Applied Materials & Interfaces* **12**, 54020-54025 (2020).
10. J. Forth *et al.*, "Bijels the Easy Way" in *Bijels: Bicontinuous Particle-Stabilized Emulsions*, P. S. Clegg, Ed. (2020), vol. 10, pp. 211-245.
11. Y. Chai *et al.*, Direct observation of nanoparticle-surfactant assembly and jamming at the water-oil interface. *Science Advances* **6** (2020).
12. A. Toor *et al.*, Mechanical Properties of Solidifying Assemblies of Nanoparticle Surfactants at the Oil-Water Interface. *Langmuir* **35**, 13340-13350 (2019).
13. X. B. Liu *et al.*, Reconfigurable ferromagnetic liquid droplets. *Science* **365**, 264-+ (2019).
14. H. H. Hou *et al.*, Interfacial Activity of Amine-Functionalized Polyhedral Oligomeric Silsesquioxanes (POSS): A Simple Strategy To Structure Liquids. *Angewandte Chemie-International Edition* **58**, 10142-10147 (2019).
15. P. Y. Gu *et al.*, Stabilizing Liquids Using Interfacial Supramolecular Polymerization. *Angewandte Chemie-International Edition* **58**, 12112-12116 (2019).
16. J. Forth *et al.*, Building Reconfigurable Devices Using Complex Liquid-Fluid Interfaces. *Advanced Materials* **31** (2019).
17. W. Q. Feng *et al.*, Harnessing liquid-in-liquid printing and micropatterned substrates to fabricate 3-dimensional all-liquid fluidic devices. *Nature Communications* **10** (2019).
18. J. D. Cain *et al.*, Sculpting Liquids with Two-Dimensional Materials: The Assembly of Ti<sub>3</sub>C<sub>2</sub>T<sub>x</sub> MXene Sheets at Liquid-Liquid Interfaces. *Acs Nano* **13**, 12385-12392 (2019).

### Support cited but not primary

- 1 B. B. Wang, H. Chen, T. Liu, S. W. Shi, T. P. Russell, Host-Guest Molecular Recognition at Liquid-Liquid Interfaces. *Engineering* **7**, 603-614 (2021).
- 2 H. L. Sun *et al.*, Redox-Responsive, Reconfigurable All-Liquid Constructs. *Journal of the American Chemical Society* **143**, 3719-3722 (2021).

3. Q. Q. Yuan *et al.*, Size-Dependent Interfacial Assembly of Graphene Oxide at Water-Oil Interfaces. *Journal of Physical Chemistry B* **124**, 4835-4842 (2020).
4. R. Y. Xu *et al.*, Interfacial Assembly and Jamming of Polyelectrolyte Surfactants: A Simple Route To Print Liquids in Low-Viscosity Solution. *Acs Applied Materials & Interfaces* **12**, 18116-18122 (2020).
- 5.. H. L. Sun, L. S. Li, T. P. Russell, S. W. Shi, Photoresponsive Structured Liquids Enabled by Molecular Recognition at Liquid-Liquid Interfaces. *Journal of the American Chemical Society* **142**, 8591-8595 (2020).
6. B. Q. Qian, S. W. Shi, H. Q. Wang, T. P. Russell, Reconfigurable Liquids Stabilized by DNA Surfactants. *Acs Applied Materials & Interfaces* **12**, 13551-13557 (2020).
7. D. D. Lin *et al.*, Stabilizing Aqueous Three-Dimensional Printed Constructs Using Chitosan-Cellulose Nanocrystal Assemblies. *Acs Applied Materials & Interfaces* **12**, 55426-55433 (2020).
8. Y. F. Jiang, R. Chakroun, P. Y. Gu, A. H. Groschel, T. P. Russell, Soft Polymer Janus Nanoparticles at Liquid-Liquid Interfaces. *Angewandte Chemie-International Edition* **59**, 12751-12755 (2020).
9. X. F. Wu *et al.*, Nanorod-Surfactant Assemblies and Their Interfacial Behavior at Liquid-Liquid Interfaces. *Acs Macro Letters* **8**, 512-518 (2019).
10. S. W. Shi *et al.*, Self-Assembly of MXene-Surfactants at Liquid-Liquid Interfaces: From Structured Liquids to 3D Aerogels. *Angewandte Chemie-International Edition* **58**, 18171-18176 (2019).
11. P. Y. Kim *et al.*, Assessing Pair Interaction Potentials of Nanoparticles on Liquid Interfaces. *Acs Nano* **13**, 3075-3082 (2019).
12. L. S. Li *et al.*, Gated Molecular Diffusion at Liquid-Liquid Interfaces. *Angewandte Chemie-International Edition* 10.1002/anie.202105500.

## **Dynamics of Active Self-Assembled Materials**

**PI: Alexey Snezhko, Co-Investigators: Andrey Sokolov, Andreas Glatz**

**Materials Science Division, Argonne National Laboratory, 9700 South Cass Avenue, Argonne, IL60439**

### **Program Scope**

Self-assembly, a natural tendency of simple building blocks to organize into complex architectures, is a unique opportunity for materials science. The in-depth understanding of self-assembly paves the way for the design of tailored smart materials for emerging energy technologies, such as materials that can self-heal, regulate porosity, strength, or conductivity. Self-assembled out of equilibrium materials pose a significant challenge as they are intrinsically complex, with often hierarchical organization occurring on many nested length and time scales. The program is focused on the fundamental aspects of out-of-equilibrium dynamics and self-assembly of bio-inspired materials.

We explore two complementary systems: driven colloids energized by external fields, and suspensions of active swimmers. The major challenges are: understanding fundamental mechanisms leading to collective behavior and dynamic self-organization from the interactions between unitary building blocks, and designing new active self-assembled materials with tunable structural and transport properties. In the past two years our program yielded discoveries of reconfigurable structures and tunable transport in synchronized active, spinner materials, novel emergent patterns in active chiral fluids realized by a shape-anisotropic rollers with activity-controlled curvatures of trajectories, self-organized multi-vortical states in ensembles of active magnetic rollers, novel dynamic patterns in active liquid crystals. For all these systems we have developed theoretical understanding leading to a better control of the self-assembled structures and dynamics. In the next few years, we will investigate mechanisms controlling collective self-organized states and synchronization phenomena in chiral active ensembles, and explore fundamental mechanisms controlling self-assembled patterns and dynamics of topological defects in active liquid crystals.

### **Recent Progress**

Self-organized multivortex states in flocks of active rollers. Active matter, both synthetic and biological, demonstrates complex spatiotemporal self-organization and the emergence of collective behavior. A coherent rotational motion, the vortex phase, is of great interest because of its ability to orchestrate well-organized motion of self-propelled particles over large distances. However, its generation without geometrical confinement has been a challenge. Flocking magnetic rollers constitute rich and well-controlled experimental realization of active matter. We have demonstrated by experiments and computational modeling that concentrated magnetic rollers are able to self-organize into long-lived multi-vortex states in an unconfined environment.

The reported state is dynamic by nature and exists only while the system actively dissipates energy supplied by the alternating magnetic field. We show that local dynamic spontaneous densifications of rollers trigger the formation of multiple vortices not constrained by any confinement. Both vortex chiralities (clockwise and counterclockwise) are equally probable, with

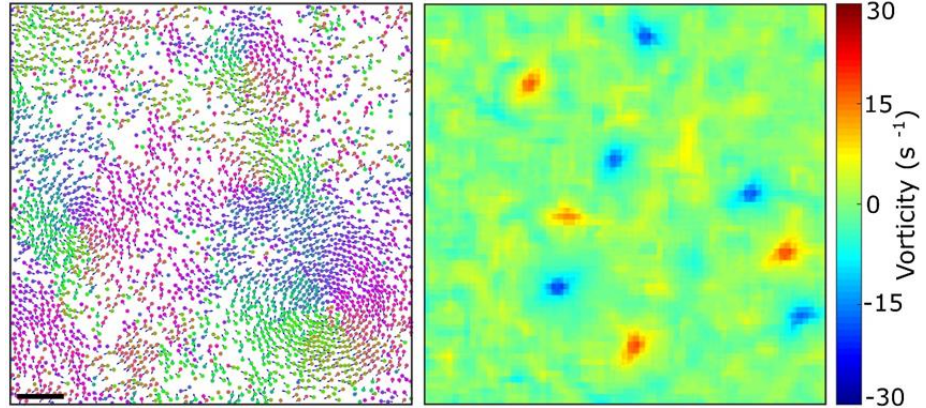


Figure 1. Emergent multi-vortex states in active magnetic roller system. Left panel: experimental snapshot of a magnetic rollers suspension in the state with multiple vortices. Groups of particles with identical color represent flocks moving in the same direction, while rainbow-like patterns visualize spontaneous vortices. The actual direction of motion is indicated by arrows. Scale bar: 3mm. Right panel: vorticity field of the rollers in a self-organized multi-vortex state. Vortices of both chiralities, clockwise (blue) and

typical neighborhood of a reference vortex populated by vortices of opposite chirality (see Fig. 1). While the vortices are stable and preserve their shape for a long time, they constantly exchange roller material with their neighbors. Our studies provide insights into the mechanism for the emergence of coherent collective motion on the macroscale from the coupling between microscale rotation and translation of individual active elements. These results may stimulate design strategies for self-assembled dynamic materials and particulate manipulation at the macroscale.

### Reconfigurable structure and tunable transport in synchronized active spinner materials. An

active spinner fluid is a member of active chiral colloids where rotational activity is not coupled to a self-propulsion. We have demonstrated that ferromagnetic micro-particles suspended at an

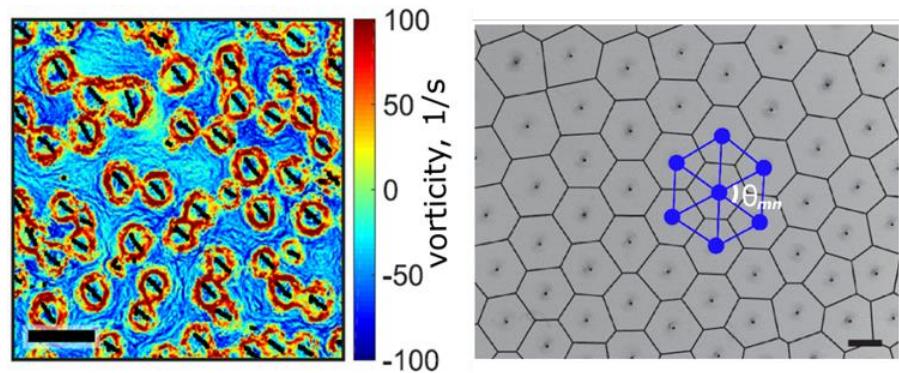


Figure 2. Self-assembled synchronized spinners in active magnetic suspensions. Left panel: experimental snapshot of a hydrodynamic vorticity field induced by a swarm of self-organized synchronized spinner in a liquid-like state. Scale bar is 2 mm; Right panel: dynamic spinner lattice formed by the spinners. Voronoi diagram is overlaid with the observed lattice. The spinners are blurred because of the long exposure time that enabled precise identification of the rotational axes. Scale bar is 1 mm.

air-water interface and energized by an external rotating magnetic field spontaneously form dynamic ensembles of synchronized spinners in

a certain range of the excitation field parameters. The activity in the system originates solely from the rotational motion of the spinners, in contrast to conventional active systems composed of self-propelling units. Each spinner generates strong hydrodynamic flows, and collective interactions of the multiple spinners promote the formation of dynamic lattices, see Fig. 2. On the basis of experiments and simulations, we reveal that collective interactions between spinners give rise to new dynamic phases—spinner liquids and lattices. Self-organized spinner lattices support an active diffusion by means of vigorous self-generated hydrodynamic flows and are capable of self-healing behavior. The transport of inert cargo particles embedded in self-organized active spinner lattices can be remotely controlled and manipulated. Our findings provide insights into the behavior of active spinner materials with reconfigurable structural order and tunable functionalities.

Reconfigurable emergent patterns in active chiral fluids. Active fluids comprised of autonomous spinning units injecting energy and angular momentum at the microscopic level represent a promising platform for active materials design. The variety and complexity of the accessible dynamic states are expected to dramatically increase in the case of chiral active units. We have

used shape anisotropy of colloidal particles (pear-shaped) to introduce chiral rollers with activity-controlled curvatures of their trajectories and spontaneous handedness of their motion. By controlling activity through variations of the energizing static electric field, we revealed a set of emergent reconfigurable dynamic phases: gas of spinners, localized aster-like vortices and rotating polar flocks (see Fig. 3), enabled by the chiral motion of the unitary building blocks (circle rollers). Among the remarkable features of these structures is the ability to develop and manipulate on demand the particles' collective orientational order, polar, or nematic, in response to the activity levels. Control and reversibility of these dynamic states by activity has been

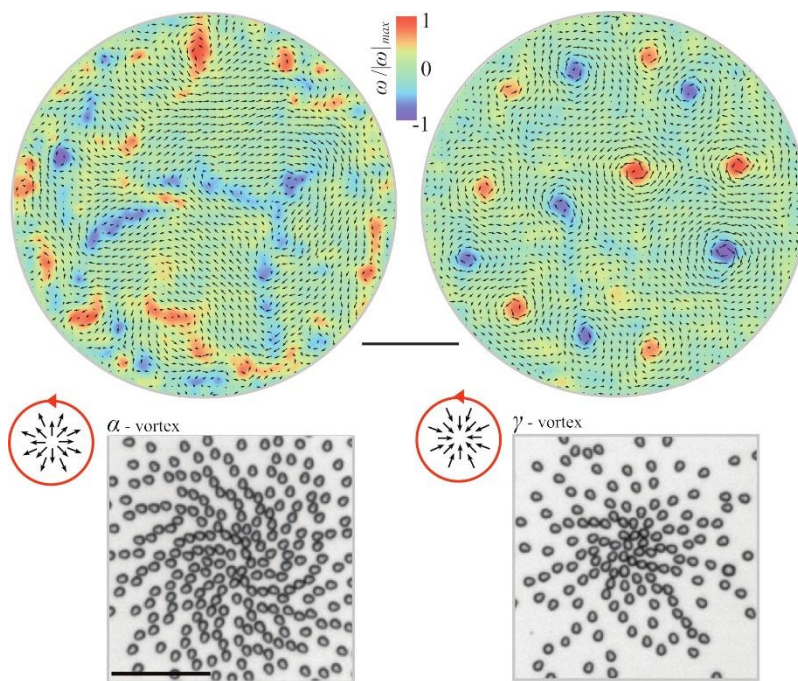


Figure 3. Emergent patterns in active chiral fluid. Top panel: experimental snapshots of a colloidal suspension of pear-shaped particles in the states of rotating flocks (left) and multiple vortices (right). Superimposed velocity (arrows) and vorticity (background color) fields of the chiral rollers are shown. Scale bar: 0.5 mm. Bottom panels: snapshots of novel structured self-organized vortices. Spiral vortex with all particles oriented away (left), and towards (right) the vortex eye. Scale bar is 0.1 mm.

demonstrated. The vortices formed by pear-shaped rollers have a certain characteristic size that depends on the activity and come in two equally probable flavors: CW and CCW. Once formed, dynamic vortices are stable, while energy is provided to the system by the electric field. Arrays of self-organized vortices show tendency toward a 2D antiferromagnetic ordering. Our findings provide insights into the onset of spatial and temporal coherence in a broad class of active chiral systems, both living and synthetic, and hint at design pathways for active materials based on self-organization and reconfigurability.

## **Future Plans**

We plan to continue focusing our research on new approaches to discovery, synthesis and characterization of active colloidal materials. Comprehensive studies of globally correlated polar states in active spinner systems in response to temporal modulation of activity and confinement will be performed. We plan to investigate mechanisms controlling collective self-organized states and synchronization phenomena in two complementary active roller systems: ensembles of Quincke rollers (including chiral rollers) energized by static electric fields, and populations of ferromagnetic rollers energized by a uniaxial alternating magnetic field. We will explore, experimentally and computationally, the behavior of confined active roller liquids in the presence of scatterers. We envision novel dynamic states with controlled lifetime, and patterns with oscillating chirality.

We continue to focus on fundamental mechanisms controlling self-assembled patterns and dynamics of topological defects in active liquid crystals with engineered spatial inhomogeneities based on active-inactive interfaces. We plan to exploit the delicate interplay between activity, elasticity and alignment to generate novel dynamic phases of active liquid crystals and dynamics of topological defects not available through conventional techniques. We have recently demonstrated that an externally induced inhomogeneity in the liquid crystal (LC) director field produced by a micro-vortex in a 2D film of active LC gives rise to a remarkable dynamic pattern consisting of branched, radially elongated bands of high curvature of the director field. We plan to introduce novel acoustically powered active nematic material based on pre-designed spatially distributed actuators.

To advance our understanding of the recently discovered unconfined multi-vortical states in ferromagnetic rollers suspensions we will continue a systematic study of long range self-organized patterns of unbound vortices with and without overlaid external potentials. We envision the onset of stable vortex lattices with square symmetry and antiferromagnetic ordering of the vortex states; however more complex arrangements or even phase separation of the vortices of the same chirality are possible.

## Publications

1. B. Zhang, A. Sokolov, A. Snezhko, “Reconfigurable emergent patterns in active chiral fluids”, *Nature Communications* **11**, 4401 (2020)
2. K. Han, G. Kokot, O. Tovkach, A. Glatz, I. Aranson, A. Snezhko, “Emergence of self-organized multivortex states in flocks of active rollers”, *Proceedings of the National Academy of Sciences* **117**, 9706 (2020)
3. G. Kokot, A. Sokolov, A. Snezhko, “Guided Self-Assembly and Control of Vortices in Ensembles of Active Magnetic Rollers”, *Langmuir* **36**, 6957 (2020)
4. K. Han, G. Kokot, S. Das, R.G. Winkler, G. Gompper, A. Snezhko, “Reconfigurable structure and tunable transport in synchronized active spinner materials”, *Science Advances* **6**, eaaz8535 (2020)
5. A. Sokolov, A. Mozaffari, R. Zhang, J. de Pablo, A. Snezhko, “Emergence of radial tree of bend stripes in active nematics”, *Physical Review X* **9**, 031014 (2019)
6. H. Reinken, D. Nishiguchi, S. Heidenreich, A. Sokolov, M. Bär, S.H.L. Klapp, I. Aranson, “Organizing bacterial vortex lattices by periodic obstacle arrays”, *Communications Physics* **3**, 76 (2020)
7. B. Zhang, H. Karani, P. Vlahovska, A. Snezhko, “Persistence length regulates emergent dynamics in active roller ensembles”, *Soft Matter* **17**, 4818 (2021)
8. M.P. Smylie, K. Kobayashi, T. Takahashi, C. Chaparro, A. Snezhko, W-K Kwok, U. Welp, “Nodeless superconducting gap in the candidate topological superconductor  $\text{Sn}_{1-x}\text{In}_x\text{Te}$  for  $x=0.7$ ”, *Physical Review B* **101**, 094513 (2020)
9. K. Han, A. Snezhko, “Programmable chiral states in flocks of active magnetic rollers”, *Lab on a Chip* **21**, 215 (2021)
10. P. Tierno, A. Snezhko, “Transport and assembly of magnetic surface rotors”, *ChemNanoMat* **7**, 1–14 (2021)
11. B. Zhang, B. Hilton, C. Short, A. Souslov, A. Snezhko, “Oscillatory chiral flows in confined active fluids with obstacles”, *Physical Review Research* **2**, 043225 (2020)



***UNIVERSITY  
GRANT  
PROJECTS***



# Bioinspired Active Transport and Energy Transduction using Liquid Crystals Beyond Equilibrium

Nicholas L. Abbott, Cornell University (Principal Investigator), Juan J. de Pablo, University of Chicago (Co-Investigator)

## Program Scope

Biological systems function out of equilibrium, with structure and dynamics that arise from dissipative processes involving the interplay of advective and diffusive transport. The complex dynamic behaviors found in biology often reflect highly non-linear phenomena that lead to surprisingly localized responses to delocalized fields. In this project, we are exploring an emerging class of dynamic, cooperative phenomena that have recently been observed in liquid crystals (LCs) – solitary waves, or “solitons”, as the basis of new designs of active soft matter for achieving rapid and directed transport processes and new modes of energy transduction. These localized responses have analogies to many other physical and biological phenomena, and have only recently been shown to occur in LCs. Solitons consist of waves of localized orientational perturbations that can travel at high speed and over long distances. They can interact with particles and form a variety of organized, non-equilibrium assemblies, thereby offering exciting opportunities to achieve new forms of active matter. Through closely coupled simulations and experiments, this project is addressing open questions regarding the mechanisms by which solitons form and move, with the long term goal of manipulating them for applications.

## Recent Progress

Solitons form within confined LC systems, yet the role of LC surface interactions on soliton formation and propagation is poorly understood. Over the past year, we have performed experiments and simulations aimed at elucidating the role of surface interactions on LC solitons. We have used two experimental systems in these investigations: polyimide-coated surfaces, and self-assembled monolayers (SAMs) formed from alkanethiols on gold. The former surfaces were used to make contact with prior experimental observations, and the latter class of surfaces were used because they offer a high level of control over surface properties. Significantly, as described below, over the past year, we have obtained the first experimental observations of the formation of solitons using LCs confined by SAMs formed from alkanethiols. We have used SAMs to form patterned orientations of LCs, and used the patterned LCs to reveal new ways to control soliton

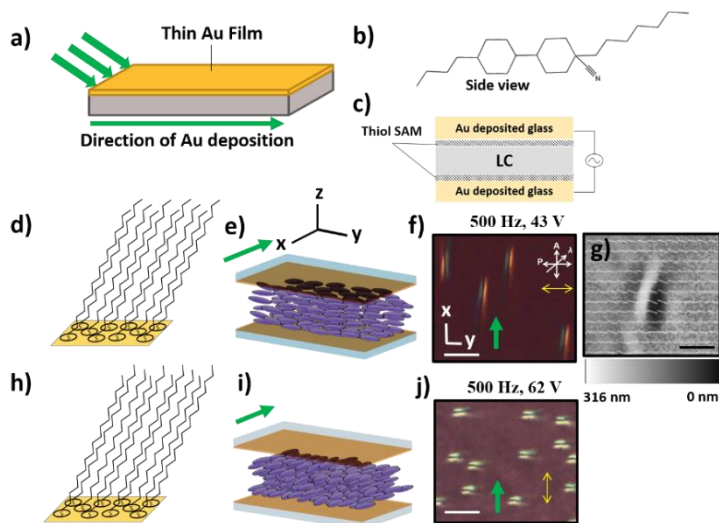


**Figure 1.** a) Schematic showing oblique deposition of gold onto a glass substrate. (b) Molecular structure of the liquid crystal 4'-butyl-4-heptylbicyclohexyl-4-carbonitrile (CCN-47) used. (c) Experimental setup comprising of an optical cell with SAM-coated surfaces. (d, h) Schematic illustrations of (d) C15SH and (h) C16SH SAMs on the gold films. (e, i) Schematic illustrations of LC orientations on (e) C15SH and (i) C16SH SAMs. (f, j) “Bullet” solitons observed using (f) C15SH and (j) C16SH SAMs. Scale bar 50  $\mu\text{m}$ . (g) Polscope image showing the LC orientations within a travelling “bullet” soliton.

motion. Additionally, we have developed a computational framework with which we are now performing simulations of solitons that complement the above-described experiments.

In our first experiments, we demonstrated formation of solitons in LCs aligned on SAMs formed from pentadecanethiol (C15SH) and hexadecanethiol (C16SH) using gold films deposited at an oblique angle of incidence by physical vapor deposition (Figure 1). Past studies have demonstrated that C15SH and C16SH SAMs cause LCs to align in orthogonal directions on gold surfaces (within the plane of the surface). For both C16SH and C15SH SAMs, we observed the formation of soliton “bullets” over specific but distinct (for the two types of SAMs) ranges of applied voltages and frequencies. The directions of motion of the solitons were orthogonal on the two types of SAMs, in both cases corresponding to a direction that was perpendicular to the LC orientation.

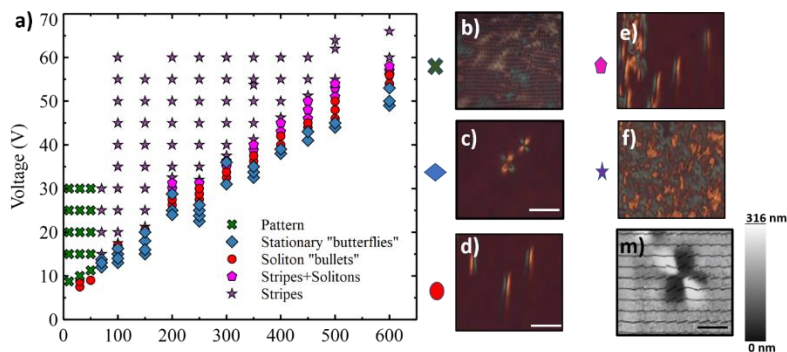


**Figure 2.** a) Phase diagram of dynamic LC director distortions as a function of applied voltage and frequency – b) Low frequency patterns, c) stationary “butterflies”, d) “bullet” solitons, (e) solitons + stripes and (f) stripes. (m) Polscope image showing the azimuthal director profile within a stationary “butterfly”.

To elucidate how electric field strength and frequency affect soliton generation on SAMs formed from alkanethiols, we performed a series of experiments using C15SH SAMs. At low frequencies ( $< 100$  Hz), we observed a periodic pattern to form in bulk LC (Figure 2), similar to electrohydrodynamic convection patterns reported previously in the literature. Beyond 100 Hz, with increasing voltage, we next observed stationary director distortions in the shape of a butterfly (Figure 2c). These “butterfly” shaped structures exhibit a quadrupolar symmetry with four lobes with symmetrical LC director tilts. We observed that the butterfly structures form around small particles or imperfections in the gold surfaces. These observations and the initial results of simulations (see below) suggest that the triggering of solitons is facilitated by local LC distortions at the surface. Upon increasing the voltage at a fixed frequency, we observed the formation of “bullet” solitons. The butterfly structures often serve as sites for the nucleation of these bullet solitons. Both the number and velocity of solitons were found to increase with the applied voltage, until space-filling stripes occupied the LC.

We have also used microcontact printing to generate a range of patterned LC orientations, and begun exploring how the patterning of LCs impacts soliton formation and dynamics. One such example is shown in Figure 3a-g with the patterning of LC twist: Bullet-like solitons initially travel in a horizontal direction, which is perpendicular to the LC alignment in that region (no twist; dark region in Figure 3b-g). When the solitons collide with the twisted domain of LC (green region), they are either (i) reflected from the boundary (soliton within white circle) or (ii) refracted at the boundary and continue to propagate across the twisted LC domain (solitons within red circles). As shown by the results in Figure 3h-j, we have also observed solitons to be refracted across the interface of two twisted LC domains. Ongoing experiments are being performed to unmask the rules that govern these and other new behaviors of solitons that we have observed using patterned LC systems.

To understand the factors that control the formation of solitons observed in our experiments and the key variables that influence their dynamical behavior, we have implemented a theoretical continuum framework based on Landau-de Gennes theory. In particular, the free energy description includes the effects of flexoelectricity. Simulations have been performed using LC anchored in a manner similar to our experiments with the exception of a small patch of homeotropic anchoring in the center of one of the confining surfaces. Through this construct, we have been able to produce a small region of LC having a conical structure. Analogous to experiments, we simulate an electric field along the Z axis, which is perpendicular to the surface. In Figure 4 (left), we show the simulated LC structure at the mid-plane of the LC film. By applying a weak electric field, we can generate the “butterfly” structure seen in experiments. This structure is strongly dependent on surface interactions. The nematic structure has a cross-like feature, with directors tilted in the perpendicular plane. By using the method of Jones matrices, where the incident polarized wave vector propagates along the Z axis, we calculated the optical appearance of the deformation, as seen on the left side of Figure 4. This appearance is similar to the “butterflies” observed in the experiments reported in Figure 2. Figure 4 (Right) shows a simulation with a higher electric field intensity, which breaks the symmetry in the “butterfly” and produces a “bullet”-like structure. After the symmetry breaking, one half of the “butterfly” is static in its initial position, and the other half of the “butterfly” moves perpendicular to the LC orientation direction, consistent with the experimental observations of the propagation of bullet-like solitons from butterflies (Figure 1 and 2).

### Future Plans

As described above, this project is combining simulation and experiment to establish foundational knowledge regarding electrically triggered solitons in LCs. Over the past year, we have been addressing key questions regarding the mechanism of formation of solitons in nematics, with a particular focus on understanding how to create solitons in a predictable and controlled manner in both experiment and simulations. We have also obtained exciting preliminary results showing how patterned orientations of

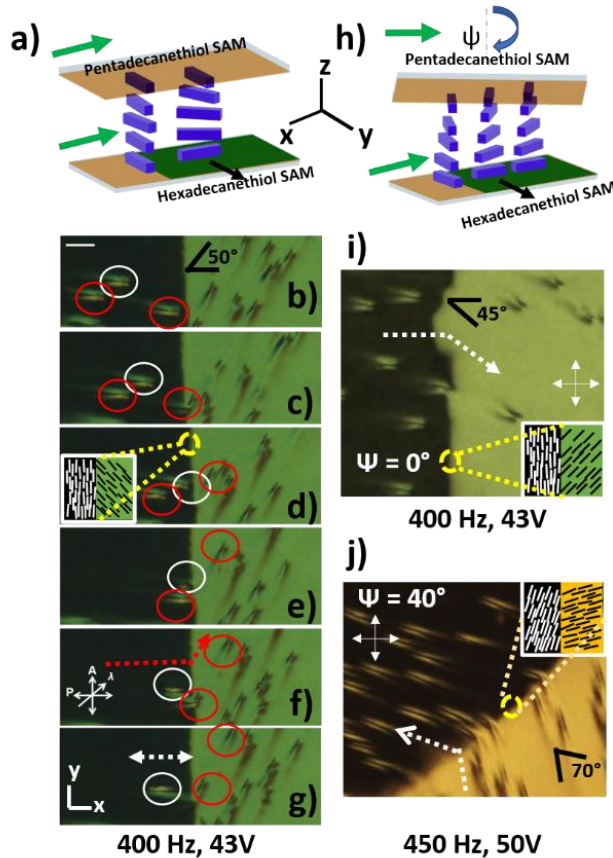


**Figure 3.** a) Schematic illustration of LC alignment in cells patterned with SAMs to create uniform and twisted LC domains. (b) Crossed polar image: the dark and bright regions correspond to uniform and twisted LC domains, respectively. (b-g) Trajectories of solitons before and after encountering the interface of uniform and twisted LC domains (400 Hz, 43 V). See text for details. The LC orientations at the mid-plane of the optical cell are indicated in the inset in (d). (h) Schematic illustration of LC samples with patterned twisted domains. The top surface is rotated by  $\psi$  to create patterned LC domains with two different twist angles. (i-j) Trajectories of a soliton across LC domains with patterned twist (h). The top surfaces are rotated by (i)  $0^\circ$  and (j)  $40^\circ$ .

LCs, including twisted domains, can be used to manipulate soliton dynamics. In the future, we will explore how solitons interact with inclusions (colloids) in LCs and how motion of the solitons couples to colloidal transport processes. In addition, we will explore soliton dynamics in chiral nematic systems, to understand further how the presence of twist in the LC influences the formation of solitons, their dynamics in the presence of AC electric fields and interactions.

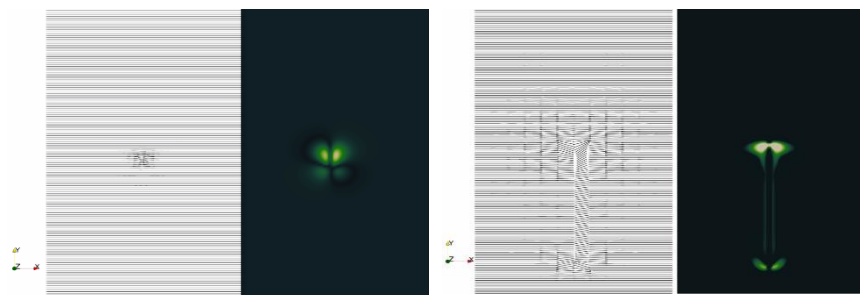


**Figure 4:** Simulations of solitons. Left: Director orientation for a “butterfly” structure and the calculated polarizing microscopy image. Right: Director profile for a “bullet” structure and the calculated polarizing microscopy image.

Overall, the future plans for this project will lead to designs of active soft matter that provide new modes of energy transduction, opening up the possibility of new approaches to active transport with applications, for example, to nanoscale separations and assembly processes.

## Publications

- (1) Fuster, H. A.; Wang, X.; Wang, X. G.; Bukusoglu, E.; Spagnolie, S. E.; Abbott, N. L. Programming van der Waals interactions with complex symmetries into microparticles using liquid crystallinity. *Science Advances* 2020, 6 (25).
- (2) Kim, Y. K.; Noh, J.; Nayani, K.; Abbott, N. L. Soft matter from liquid crystals. *Soft Matter* 2019, 15 (35), 6913.
- (3) Nayani, K.; Cordova-Figueroa, U. M.; Abbott, N. L. Steering Active Emulsions with Liquid Crystals. *Langmuir* 2020, 36 (25), 6948.
- (4) Nayani, K.; Yang, Y.; Yu, H. Z.; Jani, P.; Mavrikakis, M.; Abbott, N. Areas of opportunity related to design of chemical and biological sensors based on liquid crystals. *Liquid Crystals Today* 2020, 29 (2), 24.
- (5) Pantoja, M. A. B.; Yan, Y.; Abbott, N. L. Toluene-induced phase transitions in blue phase liquid crystals. *Liquid Crystals* 2019, 46 (13-14), 1925.
- (6) Sadati, M.; Martinez-Gonzalez, J. A.; Zhou, Y.; Qazvini, N. T.; Kurtenbach, K.; Li, X.; Bukusoglu, E.; Zhang, R.; Abbott, N. L.; Hernandez-Ortiz, J. P. et al. Prolate and oblate chiral liquid crystal spheroids. *Science Advances* 2020, 6 (28).
- (7) Senyuk, B.; Mozaffari, A.; Crust, K.; Zhang, R.; De Pablo, J. J.; Smalyukh, I. Transformation between elastic dipoles, quadrupoles, octupoles, and hexadecapoles driven by surfactant self-assembly in nematic emulsion. *Science Advances* 2021, 7 (25).
- (8) Wang, X.; Zhang, R.; Mozaffari, A.; de Pablo, J. J.; Abbott, N. L. Active motion of multiphase oil droplets: emergent dynamics of squirmers with evolving internal structure. *Soft Matter* 2021, 17 (10), 2985.
- (9) Wang, X.; Zhou, Y.; Palacio-Betancur, V.; Kim, Y. K.; Delalande, L.; Tsuei, M.; Yang, Y.; de Pablo, J. J.; Abbott, N. L. Reconfigurable Multicompartment Emulsion Drops Formed by Nematic Liquid Crystals and Immiscible Perfluorocarbon Oils. *Langmuir* 2019, 35 (49), 16312.
- (10) Zhang, R.; Mozaffari, A.; de Pablo, J. J. Autonomous materials systems from active liquid crystals. *Nature Reviews Materials* 2021, 6 (5), 437.

# Biomimetic Self-Growing Modular Materials with Encoded Morphologies and Deformabilities

J. Aizenberg, Harvard University, A. C. Balazs, University of Pittsburgh

## Program Scope

Our aim is to design a new type of growing synthetic polymer material that encompasses “living” chain ends and can continually incorporate nutrient, i.e., monomer and cross-linker. The interactions between the reactive chain ends and “nutrient” monomer and cross-linkers enable the material to grow in a controllable isotropic or anisotropic manner into programmable shapes and sizes. The experimental part is focused on incorporating modular, environment-responsive units into the network of the growing polymeric materials, in particular, novel liquid crystal elastomers (LCEs) that display extremely broad varieties of deformation and morphology changes. The modeling part of the program is focused on building theoretical and computational models that capture key features of the growth modes observed experimentally and predicting the effects of varying key elements of the parameter space involved.

## Recent Progress

### New dynamic materials platforms

*Solvent-induced topological transformations of liquid crystalline polymer (LCP)-based cellular microstructures<sup>1</sup>.* Biology’s multicellular networks have inspired microscale materials made of interconnected circles, squares, triangles, and other lattice geometries. The networked topologies lead to novel energy transport and chemical reaction capabilities. Biological materials constantly adapt by merging,

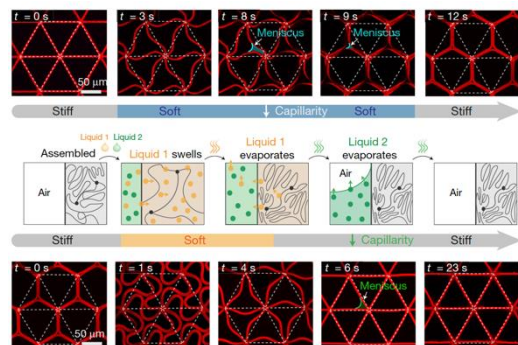


**Figure 2.** Fluorescence confocal images of the LCP microstructures at different stages of the liquid-induced assembly and disassembly and the schematic representation of the generalized mechanism of the disassembly process, showing how the mixture of two liquids decouples the two scales, with one—highly volatile—liquid acting at the molecular scale and another—chemically inert, less volatile—liquid returning the structure to its original state at the micron scale.

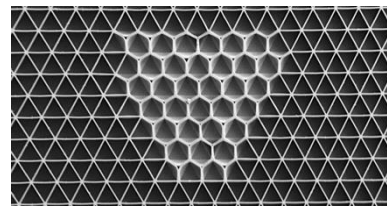


**Figure 1.** A drop of liquid applied to the center of a stiff triangular micro-lattice transiently softens and zips together the walls to transform the material into a hexagonal lattice

cellular boundaries. But in the synthetic case, nothing can change the basic topology. This study introduces a way to

manipulate material topology at the microscale using a simple liquid. Starting with a triangular lattice made of stiff polymer, the liquid first infiltrates and temporarily softens the material. Next, as the liquid evaporates, local capillary forces – usually too weak but aided by the softened structure – zip together the walls of the triangles. The result is a hexagonal lattice with half as many compartments and double the nodes. Finally, the polymer rapidly dries and re-stiffens, trapping the hexagonal topology (Fig. 1). The new topology can be switched back by applying a mix of two liquids: one temporarily swells the polymer to pry apart the zipped walls, allowing the lattice to relax back to its original topology, and a second, less volatile liquid delays

capillary forces until after the first liquid has evaporated and the material has regained its stiffness. In this way, the topologies can be switched back and forth repeatedly and trapped in any intermediate configuration (Fig. 2). These controlled transformations allowed us to modulate acoustic, resilience, frictional, and wetting properties and open new possibilities for using dynamic topology to control energy transmission and generation in materials.

*Reversibly growing crosslinked silicone-based polymers with programmable sizes and properties*<sup>2</sup>. Inspired by flatworms *Planaria*, we developed a growing-degrowing strategy of enabling thermoset materials to either absorb or release components for continuously changing their sizes, shapes, compositions, and a set of properties simultaneously. The strategy is based on the monomer-polymer equilibrium of networks in which supplying or removing small polymerizable components would drive the networks toward expansion or contraction. Using acid-catalyzed equilibration of siloxane as an example, we demonstrate that the size of the resulting silicone materials can be significantly or finely tuned in both directions of growth and decomposition. The equilibration can be turned off to yield stable products or reactivated again. Our strategy can endow the materials with many appealing capabilities including environment adaptivity, self-healing, and switchability of surface morphologies, shapes, and optical properties.

### Computational Modeling

We developed a theoretical model to devise a scheme that leads to the formation of either an interpenetrating polymer network (IPN) or a random copolymer network (RCN). In our approach, synthetic polymer networks “grow” irreversibly by “consuming” monomer and crosslinker from the surrounding solution and transforming them into a new polymer network. We focused on two different mechanisms for growing the polymer networks. Both mechanisms are initiated by immersing a primary gel (the “seed”) into a mixture of solvent and monomer (Fig. 3; Stage 0). The latter species diffuse into the gel, causing it to swell and expand in size.

At the outset of Stage 1, the absorbed monomers are polymerized to form secondary chains (magenta-colored lines in Fig. 3). These secondary chains are then used to form a new network within the body of the gel. In the first mechanism of growth, the secondary chains form crosslinks to create an interpenetrating polymer network. In the second mechanism, the secondary chains undergo exchange reactions with the primary gel to form a random copolymer network (RCN). After removal of the sol (a mixture of disconnected, small gel-like pieces and uncrosslinked chains), the IPN and RCN are each placed in a bath that is identical to the initial mixture (as in the center of Fig. 1). In the last step of Stage 1, these gels swell (“grow”) by incorporating monomeric units from the solution into their network.

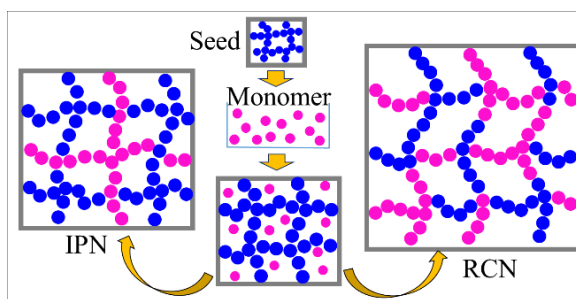


**Figure 3.** Schematics of the gel growth. Stage 0: A primary gel network (“seed”) is immersed and swollen in a solution of the secondary monomer (magenta circles) Stage 1: The absorbed secondary monomers are polymerized and either: form crosslinks among themselves to create the interpenetrating network (IPN), or undergo the simultaneous crosslinking among themselves and interchain exchange with the primary gel to form the random copolymer network (RCN). The blue- and magenta-colored lines depict the respective primary and secondary polymer chains. After removal of the sol fraction, the formed gels are swollen in the same monomer solution as depicted at the top. Stage 2: The steps in Stage 1 can now be repeated to continue the growth process.

Through our theoretical model, we determined how the structures of these IPNs and RCNs affect the uptake of the monomer and solvent and thus, control the gel growth. In particular, we found that due to the residual elastic stresses from the stretched primary network, the IPN is always stiffer (i.e., swells less) than the RCN. The swelling of both the IPN and RCN, however, can be tailored to yield the softness required for a variety of applications. Specifically, if the primary networks are immersed in a solution with a high monomer volume fraction (e.g.  $\phi_m^{(s)} = 1$ ), the swelling of both the IPN and RCN can be controlled by increasing the crosslinker fraction,  $\alpha$ .

If the primary network is placed in a solution with a low monomer volume fraction ( $\phi_m^{(s)} = 0.3$ ), the degree of swelling of both IPN and RCN is low; also, the IPN is less sensitive to changes in  $\alpha$ . In this scenario, however, the swelling of both the IPN and RCN can be controlled through the appropriate choice of the Flory-Huggins  $\chi$ -parameters, which characterize interactions between the different components.

These effects and the greater swelling of the RCN over IPN, as well as the sensitivity of the swelling to the various control parameters, are magnified in Stage 2 of growth. Moreover, if the crosslinker fraction is kept sufficiently low, the gel grows more in Stage 2 in comparison with Stage 1, whereas at high crosslinker fraction the growth in Stage 2 is less than in Stage 1. Due to accumulation of stress in the IPN because of the stretching of chains, the repeated growth of this material is hindered. In contrast, the RCN can undergo subsequent interchain exchange reactions and thereby expand in size.

This growth process can potentially be used to repair damaged gels that encompass voids. The entire damaged sample would now serve as the “seed” that is immersed into a bath of monomers and crosslinkers (equivalent to Stage 0). The voids left by the damage are more accessible and permeable than the intact portions and hence the solution would preferentially diffuse to these damaged regions. With these latter regions being preferentially swollen by the monomer solution, polymerization and crosslinking of the absorbed species (Stage 1) can lead to “regeneration” of the gel within the voids and a degree of material’s repair.

These different processes are controllable and introduce a new method for manufacturing polymeric materials with specified sizes and shapes. The systems, however, are sufficiently complex (with a large number of control parameters) that these calculations can provide valuable guidelines for tailoring the properties of the growing gels. The theoretical model provides the necessary quantitative detail to facilitate experimental realization of such stepwise growth processes. Consequently, the findings can provide valuable guidelines for fine-tuning the growth process to yield gel samples of specified size and mechanical properties.

## Future Plans

**Experimental Part.** The synthesis and fabrication work of the *Aizenberg* group will focus on: i) studying base-catalyzed growth processes in silicone-based elastomers; ii) fabricating and studying a range of compositionally uniform, but molecularly anisotropic photosensitive LCE microstructures and their arrays, with a goal of programming in their design the light-induced formation of transient, but controllable bimorphs consisting of ordered and disordered layers; iii) expanding the developed silicone materials platform towards incorporating in it the identified above stimuli-responsive LC moieties capable of eliciting programmable deformation modes; iv) studying growth and degrowth processes of the hybrid silicone/LCE materials and their effects on the resulting ability of these materials to convert thermal and light energy into mechanical

deformations; v) interacting with the *Balazs* group in order to adjust the synthetic efforts and direct them along the paths that optimize and amplify the emergent dynamic behaviors of the developed hybrid materials.

### Computational Modeling.

*Develop a DPD model for the growth of a living seed.* As the next step in our computational efforts, we will develop a dissipative particle dynamics (DPD) approach to model growth from a living seed. We must now augment our DPD models to account for the exchange reactions triggered by the stretching of the polymer chains. Since the DPD chains are simulated by a bead-spring model, which encompasses an elastic constant and equilibrium bond distance,  $r_0$ , we can track chains that are stretched significantly beyond  $r_0$  and specify an exchange reaction between neighboring beads to elevate this stretching. To test our newly developed model, we will compare the simulation results with experiments by monitoring the morphology of the growing network at different incubation times for fixed concentrations of monomer, catalyst, and cross-linker. Through interactions with the *Aizenberg* group, the *Balazs* group will attempt to match the degree of cross-linking and the average length of the polymer strands between the cross-links to the experimentally observed values. These studies will allow us to validate our new DPD model that incorporates the exchange reactions and calibrate the simulation parameters.

*Developing a gel lattice spring model (gLSM) for growth of a living seed.* Via the DPD approach, we can capture critical dynamic processes—the chemical reactions, diffusion and hydrodynamic interactions—that are occurring within the material on length scales of hundreds of nanometers. To simulate the dynamic behavior on larger length (and time) scales considered in the experiments, we will develop a new gel lattice spring model (gLSM), which combines finite element and finite difference methods to capture the elastodynamics of the gel and the chemical reaction-diffusion processes occurring within the gel. We propose to use a multi-scale approach, where our DPD simulations will yield relationships between the growth of the living seed and the reaction parameters. These relationships will then serve as phenomenological inputs to our larger scale gLSM for the growth of the polymer network. These new studies will be formulated through iterative interactions with the *Aizenberg* group, in much the same manner that we previously employed to develop a gLSM for thermo-responsive gels that accurately described the experimental system fabricated by the *Aizenberg* group.<sup>3</sup>

### References

- 1) Li, S.; Deng, B.; Grinthal, A.; Scheneider-Yamamura, A.; Kang, J.; Martens, R.; Zhang, C.; Li, J.; Yu, S.; Bertoldi, K.; Aizenberg, J.; “Liquid-induced topological transformations of cellular microstructures”, *Nature*, **2021**, 592, 386–391.
- 2) Zhou, X.; Zheng, Y.; Zhang, H.; Yang, L.; Cui, Y.; Krishnan, B. P.; Dong, S.; Aizenberg, M.; Zeng, A.; Hu, Y.; Aizenberg, J.; Cui, J. “Reversibly growing crosslinked polymers with programmable sizes and properties”, *submitted*.
- 3) He, X.; Aizenberg, M.; Kuksenok, O.; Zarzar, L. D.; Shastri, A.; Balazs, A. C.; Aizenberg, J. Synthetic homeostatic materials with chemo-mechano-chemical self-regulation. *Nature* **2012**, 487, 214-218.

## Publications

- 1) Li, S.; Deng, B.; Grinthal, A.; Scheneider-Yamamura, A.; Kang, J.; Martens, R.; Zhang, C.; Li, J.; Yu, S.; Bertoldi, K.; Aizenberg, J. “Liquid-induced topological transformations of cellular microstructures”, *Nature*, **2021**, 592, 386–391; DOI: 10.1038/s41586-021-03404-7.
- 2) Zhou, X.; Zheng, Y.; Zhang, H.; Yang, L.; Cui, Y.; Krishnan, B. P.; Dong, S.; Aizenberg, M.; Zeng, A.; Hu, Y.; Aizenberg, J.; Cui, J. “Reversibly growing crosslinked polymers with programmable sizes and properties”, *submitted*.
- 3) Chatterjee, R.; Biswas, S.; Yashin, V. V.; Aizenberg, M.; Aizenberg, J.; Balazs, A. “Controllable Growth of Interpenetrating or Random Copolymer Networks”, *Soft Matter*, *accepted for publication*.
- 4) Lerch, M. M.; Grinthal, A.; Aizenberg, J., “Viewpoint: Homeostasis as Inspiration – Toward Interactive Materials”, *Adv. Mater.* **2020**, 32(20). 1905554. DOI: 10.1002/adma.201905554.
- 5) Waters, J. T.; Li, S.; Yao, Y.; Lerch, M. M.; Aizenberg, M.; Aizenberg, J.; Balazs, A. C., “Twist Again: Dynamically and Reversibly Controllable Chirality in Liquid Crystalline Elastomer Microposts”, *Sci. Adv.* **2020**, 6 (13), eaay5349, DOI: 10.1126/sciadv.aay5349.
- 6) Korevaar, P. A.; Kaplan, C. N.; Grinthal, A.; Rust, R. M.; Aizenberg, J. “Non-equilibrium signal integration in hydrogels”, *Nat. Comm.* **2020**, 11 (1), 386. DOI: 10.1038/s41467-019-14114-0.

## **Self-assembled adaptive materials via 3D printed active programmable building blocks**

**Igor S. Aronson<sup>1</sup> and Ayusman Sen<sup>2</sup>**

**Departments of <sup>1</sup>Biomedical Engineering and <sup>2</sup>Chemistry**

**The Pennsylvania State University**

**University Park, Pennsylvania 16802**

### **Program Scope**

State-of-the-art biomolecular materials inspired by living systems are at the heart of multiple emerging technologies, such as additive manufacturing, soft robotics, and nanofabrication. The overarching goal of our work is to understand the fundamental principles controlling the hierarchical organization of out of equilibrium bio-inspired soft materials at different length scales. This program harnesses the progress in self-assembly, soft materials, and additive manufacturing to design a new class of multi-responsive microscopic building blocks. The microblocks will be based mostly on 3D printed, self-propelled particles that respond to chemical concentration gradients, light, and external magnetic or electric fields. The proposed research advances the DOE mission on controlling matter and energy far away from equilibrium and creating new technologies rivaling those of living organisms.

### **Recent Progress**

**Focusing and alignment of acoustically active nanorods.** We investigated the effects of acoustic field combined with a more conventional method for flow-induced focusing and alignment of metallic particles in nozzles [1]. We observed that in a microchannel with a nozzle, the particle dynamics depends on the balance between the acoustophoretic force and the fluid drag due to streaming flows generated by the acoustic field. Our results show that at a specific frequency, gold-platinum nanorods move to the center of the channel under the effects of the streaming flow and align perpendicular to the direction of the channel. When particles start to accumulate, the force balance changes and, as a swarm, they start moving with the acoustophoretic forces against the pressure gradient. The observed phenomena are explained by multiphysics finite-element modeling. The results shed light on the control of anisotropic particles in microfluidic geometry and may have applications for acoustic drug delivery and particle injection.

**Collective behavior of chiral self-propelled nanomotors.** We examined the interaction of chiral micropropellers. The propellers, having size of 2 to 8 microns, were manufactured by 3D printing using the photolithography system Nanoscribe with the resolution of 200-500 nm. To make them catalytically active, a 30-40 nm platinum layer is deposited. Also, a thin nickel layer (10-20 nm) is deposited under the platinum layer to enable the magnetic response. We studied how the propellers respond on magnetic field and what kind of bound states the propellers form when energized by hydrogen peroxide.

**Guidance and stacking of gold-platinum nanodiscs.** We fabricated bi-metallic gold-platinum nanodiscs. To enable magnetic response, a thin layer of magnetic material was introduced between gold and platinum halves. The discs have a size of approximately 3 microns and thickness about 100 nm and are produced by maskless photolithography. We observed that the discs move autonomously in hydrogen peroxide solution and respond on the applied magnetic field created by a tri-axial Helmholtz coil. We were able to guide the discs along an arbitrary trajectory. Also, multiple discs interact and stuck up sequentially, creating a self-assembled nanobattery.

**Computational modeling of 3D microtori.** In collaboration with the group of Prof. Raymond Kapral, at the University of Toronto, we studied the dynamics of self-propelled microtori previously described by us [2]. The main computational tool is the multi-particle collision dynamics (MPCD), versatile mesoscale hydrodynamic framework perfectly suited for this problem. The MPCD allows to introduce realistic chemical kinetics on the catalytic surface of the torus. Using the MPCD we uncovered the balance of forces, angle distributions, and the bound states formed by the interacting tori. We have found the angular distribution of the tori near the surface. Our analysis revealed necessary condition for the onset of the spontaneous symmetry breaking: chemical activity and electrostatic interaction with the surface. We explored interaction between a microtorus and a wall, and interactions between multiple tori, Fig. 1.

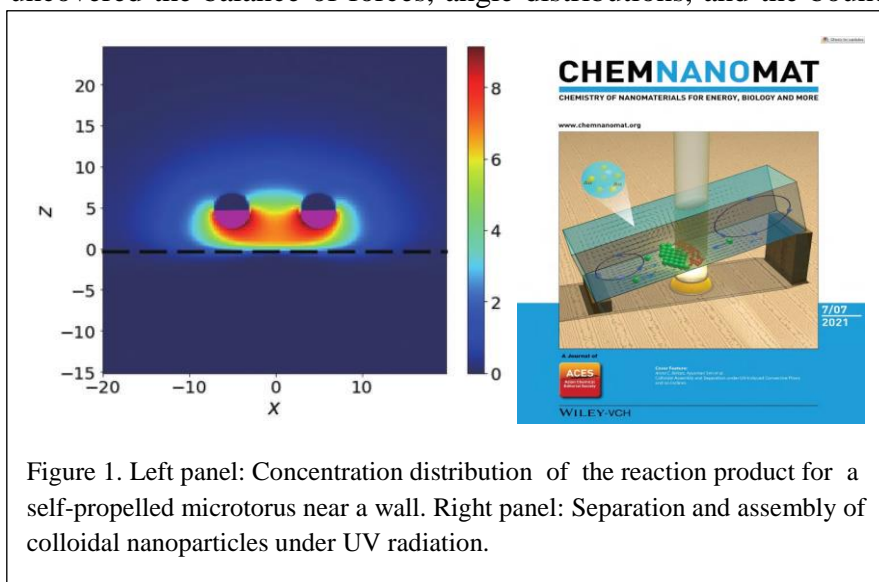


Figure 1. Left panel: Concentration distribution of the reaction product for a self-propelled microtorus near a wall. Right panel: Separation and assembly of colloidal nanoparticles under UV radiation.

**Colloidal Assembly and Separation under UV-Induced Convective Flows** [3]. We have designed a system that exploits the photothermal properties of plasmonic nanoparticles for the assembly and separation of larger microparticles, Fig. 1. Irradiating an aqueous suspension of gold or silver nanoparticles with UV light generates thermal convection which can be used to move and organize larger particles. Moving the UV light source allows the relocation of the particle cluster. In addition, thermal convection can be used to separate inert particles of different sizes on an inclined plane. Since fluid motion stems from thermal convection, collection and separation can be reversed simply by turning off the UV light enabling a rapid on-demand response system.

**Light-Powered, Continuous Pickup, Transport, and Delivery of Multiple Cargo Types by Micromotor Swarms** [4]. The three outstanding challenges in the expanding field of autonomous nano/microparticle systems are: 1) to design fuel-free systems in which directed motion of nano/microparticle swarms can be powered solely by light, 2) to demonstrate function that can only be carried out by swarms, rather than by individual particles, and 3) to repeatedly pickup, transport, and deliver multiple cargo types. We have successfully demonstrated all three

capabilities using TiO<sub>2</sub> microparticle swarms. Using the photothermal effect, the swarms can be moved directionally using light. The swarms can collect and release a variety of inert cargo particles on demand. Moreover, the cargo particles of different sizes can be sorted and released sequentially.

## Future Plans

Moving forward, we plan to continue our work on engineering collective behavior and long-range coherence among structured nano and microscopic active elements to uncover fundamental laws of self-organization and self-assembly in complex hierarchical systems out-of-equilibrium. We will study the formation of collective bound states in a system of chiral propellers energized by hydrogen peroxide and spun by a rotating magnetic field. Using the MPCD simulations, we will establish how chemical interactions and hydrodynamic forces control the formation of bound states in the system of self-propelled microtori. We will also explore self-organization of active microblocks functionalized by different enzymes forming a catalytic cascade. The ability to control out-of-equilibrium functional assemblies and bound states at the microscale will lead to new classes of bio-mimetic responsive materials with potential applications in microrobotics, fluidics, and chemical/biochemical sensing.

## References

- [1] Leonardo Dominguez Rubio, Mykhailo Potomkin, Remmi Danae Baker, Ayusman, Leonid Berlyand, Igor S Aranson, Self-Propulsion and Shear Flow Align Active Particles in Nozzles and Channels, *Advanced Intelligent Systems*, **2021**, 3, 2000178
- [2] Remmi D. Baker, Thomas Montenegro-Johnson, Anton D. Sediako, Murray J. Thomson, Ayusman Sen, Eric Lauga, Igor S. Aranson, “Shape-programmed 3D Printed Swimming Microtori for the Transport of Passive and Active Agents,” *Nature Commun.*, **2019**, 10, 4932.
- [3] Joshua E. Kauffman, Benjamin M. Tansi, Christopher LaSalle, Raj Kumar Manna, Oleg E. Shklyae, Anna C. Balazs, Ayusman Sen, “Colloidal Assembly and Separation under UV-Induced Convective Flows and on Inclines,” *ChemNanoMat*, **2021**, 7, ASAP.
- [4] Jianhua Zhang, Jiaqi Song, Fangzhi Mou, Jianguo Guan, and Ayusman Sen, “Titania-Based Micro/Nanomotors: Design Principles, Biomimetic Collective Behavior, and Applications,” *Trends Chem.*, **2021**, 3, 387.

## Publications

- [1] German V. Kolmakov, Igor S. Aranson, “Superfluid Swimmers,” *Physical Review Research*, **2021**, 3, 013188.
- [2] Cody Reeves, Igor S. Aranson, Petia Vlahovska, “Emergence of Lanes and Turbulent-like Motion in Active Spinner Fluid,” *Communications Physics (Nature)*, **2021**, 4, 92.

- [3] Benjamin M. Tansi, Raj Kumar Manna, Oleg E. Shklyaev, Matthew L. Peris, Anna C. Balazs, Ayusman Sen, "Achieving Independent Control over Surface and Bulk Fluid Flows in Microchambers," *ACS Appl. Mater. Interfac.*, **2021**, *13*, 6870.
- [4] Joshua E. Kauffman, Benjamin M. Tansi, Christopher LaSalle, Raj Kumar Manna, Oleg E. Shklyaev, Anna C. Balazs, Ayusman Sen, "Colloidal Assembly and Separation under UV-Induced Convective Flows and on Inclines," *ChemNanoMat*, **2021**, *7*, ASAP.
- [5] Jianhua Zhang, Jiaqi Song, Fangzhi Mou, Jianguo Guan, and Ayusman Sen, "Titania-Based Micro/Nanomotors: Design Principles, Biomimetic Collective Behavior, and Applications," *Trends Chem.*, **2021**, *3*, 387.
- [6] Matthew Collins, Leonardo Dominguez Rubio, Ayusman Sen, and Igor S. Aranson, "Acoustic Focusing and Swarming of Nanorods in a Microfluidic Nozzle," submitted to *Small*, 2021
- [7] Koohee Han, Gašper Kokot, Oleh Tovkach, Andreas Glatz, Igor S. Aranson, and Alexey Snezhko, "Emergence of Self-organized Multivortex States in Flocks of Active Rollers," *Proceedings of the National Academy of Sciences*, **2020**, *117*, 9706.
- [8] Jiyuan Wang, Mu-Jie Huang, Raymond Kapral, and Igor S Aranson, "The MPCD Analysis of Janus Chemically-active Microtori," in preparation

## **Principles of de novo protein nanomaterial assembly in 1, 2 and 3 dimensions**

**David Baker, Ph.D. (Principal Investigator) HHMI Investigator Professor of Biochemistry, Director of the Institute for Protein Design, University of Washington.**

**Jim De Yoreo, Ph.D. (Co-PI) Chief Scientist, Physical Sciences Division, Pacific Northwest National Laboratory, Richland, Washington 99352, United States and Affiliate Professor, Materials Science and Engineering, University of Washington.**

### **Program Scope**

We are exploring the *de novo* design of multi-component protein nanomaterials that self-assemble into 1D (fiber), 2D (array), or 3D (crystal) architectures. We have designed, with near atomic accuracy, 1D helical filaments with a wide range of diameters that assemble both *in vivo* and *in vitro* into precisely ordered micron scale fibers. We have designed, again with atomic level accuracy, 2D hexagonal arrays that assemble rapidly upon mixing the two designed protein components. The arrays span multiple microns and are robust to fusion of a wide range of functional groups enabling the precise arraying in 2D of multiple functionalities. We have extended these approaches to design of protein-inorganic hybrid materials. We have shown that lattice-matched interfaces between proteins and inorganic crystal interfaces can be designed with Rosetta, and that these interfaces promote the assembly of liquid crystal-like monolayers that amplify subtle asymmetry in muscovite mica in millimeter-scale co-alignment of proteins along one mica lattice direction. Incorporation of designed end to end interactions between the designed proteins leads to formation of unbounded 1D fibers on mica, and incorporation of designed trimeric interactions directs formation of highly ordered hexagonal arrays on the mineral surface.

### **Recent Progress**

***Aim 1: Design self-assembling unbounded 1D protein fibers, and characterize the assembly pathways and interfacial energies that lead to the designed versus off-target versions of these materials.***

We have achieved our goal of designing new self-assembling, unbounded 1D fibers by creating a class of proteins we call designed helical fibers (DHF). We experimentally tested 124 DHFs built from design helical repeat (DHR) protein subunits and found that 34 produced 1D structures visible with negative stain TEM. Six of these representing a diverse set of the designed structures were selected for structural determination with cryo-EM. In all characterized filaments, the position of the monomers closely matched the design model, demonstrating the accuracy of the design strategy. Leveraging the modularity of the DHR building blocks, we tuned the width of one fiber by changing the length of its monomer subunit. We found this yielded fibers of variable width with otherwise similar architecture, as expected, by generating 2D averages from negative stain TEM images.

Fiber assembly dynamics were studied using light scattering, fluorescence microscopy and AFM. For the protein named DHF119, we found the elongation rate was linearly related to the protein concentration and has a critical concentration of 3  $\mu\text{M}$ . We demonstrated that oligomeric fiber ‘anchors’, in which six building blocks are preorganized into the arrangement in the fiber by genetic fusion to six-fold symmetric designed oligomers, could be used to control where fibers nucleation and growth occurred. Additionally, we showed we could induce anisotropic disassembly of the fibers by adding ‘capping’ monomers, which contain only one of the two

interfaces in the fiber-forming monomer. These results and additional characterization of the DHF proteins were described in a publication titled: “De novo design of self-assembling helical protein filaments”(1).

**Aim 2: Design self-assembling unbounded two dimensional (2D) protein arrays, and characterize the assembly pathways and interfacial energies that lead to the designed versus off target versions of these materials.**

We succeeded in designing two-dimensional (2D) protein arrays that co-assemble from two different component proteins (**Figure 1**). Requiring multiple components for assembly is a feature not seen in most natural 2D structures, such as S-layers, and allows us to easily control the assembly of our arrays. The protein components can be purified separately as oligomers using standard methods for soluble proteins and then mixed together to induce the assembly of the layers. We computationally explored layers that could be generated by designing a single interface between two dihedral protein oligomers. The internal symmetry of these dihedral building blocks inherently corrects for small angular deviations from the design model, thus yielding large flat assemblies. We experimentally tested 45 such assemblies by co-expressing the two proteins in *E. coli* and characterizing fractions of the cell lysates with negative stain TEM. We selected one with hexagonal symmetry resembling the design for further characterization. We next expressed and purified the two components separately to allow the assembly of the layers to be characterized with SAXS, TEM, and AFM (**Figures 1** and **2**). After making solubilizing mutations, the individual components could be stored separately for months at millimolar concentrations without forming any observable higher-order structures. Mixing the purified components together in equimolar ratios in solutions with mid-nanomolar concentrations produced nearly crystalline arrays that were more extensive than arrays assembled from co-expressing components in bacteria. Averaged density maps from electron microscopy clearly showed the two components were present in their designed conformations. SAXS confirmed the arrays formed in solution in the absence of any solid support. AFM allowed growing assemblies to be viewed in real-time as components were added and defects were healed and provided relative free energies of terminating sites (**Figure 3**). This work was included in a publication titled “Design of biologically active binary protein 2D materials” (2).

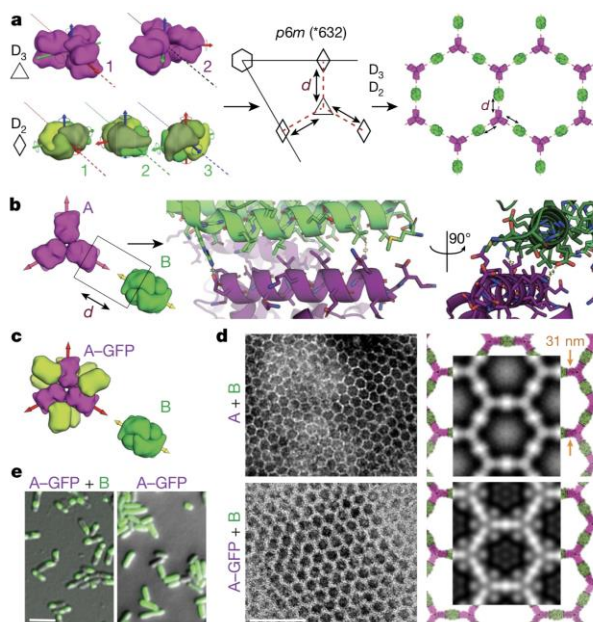
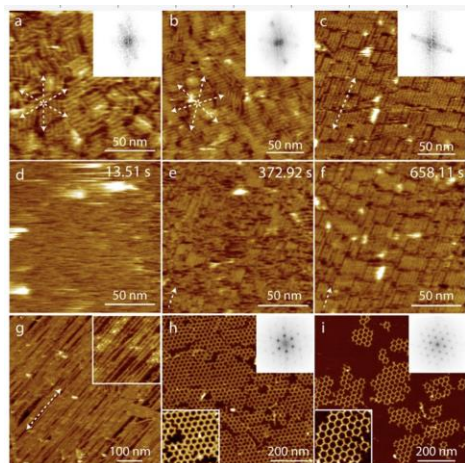


**Figure 1. In vivo assembly of 2D two-component self-assembling unbound protein arrays.**

**a.** Left, orientations of D3 and D2 building blocks for generating p6m lattice. One two-fold symmetry axis of each building block must coincide with each other and with a plane reflection axis (dashed line). Middle, top view of the p6m symmetry operators and the lattice spacing DOF (dashed line, d). Right, a possible p6m array configuration using D3 and D2 building blocks. Dashed lines indicate the direction along which building blocks slide into contact; outlined shapes indicate the symmetry group to which the building blocks belong. **b.** Left, top view of building-block configurations. In-plane close-up view of the configuration of residues at the hetero-interface (middle) and view rotated 90°, perpendicular to the plane (right). **c.** Model of A-GFP, with A in magenta and GFP in light green. **d.** Negative-stain TEM images of 2D arrays formed in *E. coli* coexpressing A and B (top left) or A-GFP and B (bottom left). Right, corresponding averaged images superimposed with the



design model (A, magenta; B, green; GFP is omitted). **e**, Confocal microscopy imaging of cells expressing A-GFP (right) or A-GFP and B (left). Scale bars, 100 nm (d), 5  $\mu$ m (e).

**Figure 2. The combination of designed protein-protein and -substrate interfaces with electrostatic and entropic forces leads to a range of 2D ordered and transient disordered DHR-mica-N liquid crystal phases.** (a-c) assemblies of 0.1  $\mu$ M DHR10-mica18 with 0.1 M, 1 M and 3 M KCl, respectively. Insets are FFTs. (d-f) consecutive AFM images showing assembly of 0.1  $\mu$ M DHR10-mica18 with 3 M KCl. (g) assembly DHR10-mica6-N with 3 M KCl into single protein diameter nanowires. Inset is a higher magnification image (50 nm by 50 nm). (h, i) assemblies of DHR10-mica6-H and DHR10-mica7-H with 3 M KCl, respectively. Insets (upper-right) FFTs and (lower-left) higher-magnification images (200 nm by 200 nm). The dashed arrows indicate orientations of assemblies.

**Aim 3: Design and characterize the dynamics, energetics, and order of self-assembly of mixed protein-inorganic systems, specifically multi-component protein nanorods on mica layers.**

To study protein inorganic crystal interfaces and protein assembly on a mineral template, we developed a model system of a designed repeat protein that presents a periodic array of negatively charged residues closely matched to the potassium ion sublattice formed on the mica (001) surface (**Figures 2 and 3**). Using AFM, we found that at ten millimolar concentration of KCl individual proteins adsorbed parallel to the mica lattice, and at higher concentrations the proteins assembled into liquid crystal-like arrays as intended. At [KCl] > 1M these arrays were extremely anisotropic on muscovite mica (m-mica), with nearly all proteins aligned along just one of the three mica lattice directions across areas tens of millimeters in width, representing  $10^9$  aligned proteins. In some ways our assemblies behaved like colloidal nanocrystals, for example they depended on the proteins having a sufficient aspect ratio, but in other ways the assemblies were unique, for example forming a phase resembling a 2D smectic liquid crystal, suggesting the assemblies were affected by a balance of specific protein-mica and protein-protein interactions, as well as by non-specific entropy-driven interactions.

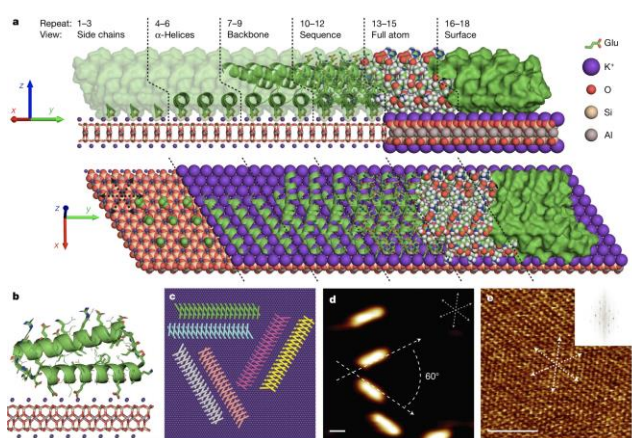


**Figure 3. We have designed repeat proteins which the carboxyl side groups are in registry with the mica lattice.** **a**, Model of DHR10-mica18 protein lattice-matched to mica (001) surface through the K<sup>+</sup> sublattice. One 18-repeat DHR10-mica18 molecule is shown from the side (top panel) and from the top (bottom panel). Repeats 1–3 illustrate the lattice-matched glutamate (Glu) side chains. Repeats 4–6 show the  $\alpha$ -helical secondary structures that contain the matched glutamates. Repeats 7–9 show the full DHR protein backbone. Repeats 10–12 show the full backbone and all amino acid side chains. Repeats 13–15 show all atoms as spheres. Repeats 16–18 show the external surface of the protein. The arrows indicate the orientations of the mica lattice. **b**, Projection view looking along the y direction.

Lattice-matched glutamates are shown as sticks and other side chains as thinner lines. **c**, DHR10-mica18 bound to K<sup>+</sup> sublattice in the six symmetry-equivalent orientations predicted by the protein-mica interface design model. **d**, AFM image of DHR10-mica18 adsorbed on mica, showing two of the three predominant orientations that are distinguishable by AFM (anti-parallel orientations look similar). The protein concentration is 0.1  $\mu$ M and the buffer contains 10 mM KCl and 20 mM Tris. The arrows in the top right corner indicate the orientations of the K<sup>+</sup> sublattice and mica lattice.

The scale bar is 5 nm. **e**, AFM of mica (001) beneath the proteins in **d**, showing the mica lattice directions (dashed arrows). The fast Fourier transform is shown in the inset. The scale bar is 5 nm.

---

Next, we demonstrated that we could modulate these assemblies by designing explicit interfaces between the proteins adsorbed on the mica surface. Adding anisotropic head-to-tail interactions caused stable liquid-crystal-like phases to form from protein building blocks that were otherwise too short to assemble. Adding a three-fold symmetric interface broke the long-range anisotropy induced by the m-mica template and caused the proteins to form an open hexagonal network with pore sizes that could be tuned by changing the length of the modular protein building block. This work was described in a publication titled “Controlling protein assembly on inorganic crystals through designed protein interfaces”(3).

### Future Plans

The long-term vision of the future of this project is to develop a fundamental understanding of the physical and chemical principles that govern robust multi-component protein self-assembly, and to use these principles to create computationally-designed, atomically-precise, hierarchical structures with novel functionalities that emerge through assembly. We seek to develop general principles for designing synthetic light-harvesting and conductive protein assemblies. We will design protein materials and characterize the kinetics of self assembly, and the incorporation of chlorophyll molecules at specific sites in these materials.

### References

1. H. Shen, J. A. Fallas, E. Lynch, W. Sheffler, B. Parry, N. Jannetty, J. Decarreau, M. Wagenbach, J. J. Vicente, J. Chen, L. Wang, Q. Dowling, G. Oberdorfer, L. Stewart, L. Wordeman, J. De Yoreo, C. Jacobs-Wagner, J. Kollman, D. Baker, De novo design of self-assembling helical protein filaments. *Science*. **362**, 705–709 (2018).
2. A. J. Ben-Sasson, J. L. Watson, W. Sheffler, M. C. Johnson, A. Bittleston, L. Somasundaram, J. Decarreau, F. Jiao, J. Chen, I. Mela, A. A. Drabek, S. M. Jarrett, S. C. Blacklow, C. F. Kaminski, G. L. Hura, J. J. De Yoreo, J. M. Kollman, H. Ruohola-Baker, E. Derivery, D. Baker, Design of biologically active binary protein 2D materials. *Nature*. **589**, 468–473 (2021).
3. H. Pyles, S. Zhang, J. J. De Yoreo, D. Baker, Controlling protein assembly on inorganic crystals through designed protein interfaces. *Nature*. **571**, 251–256 (2019).

### Publications

1. A. J. Ben-Sasson, J. L. Watson, W. Sheffler, M. C. Johnson, A. Bittleston, L. Somasundaram, J. Decarreau, F. Jiao, J. Chen, I. Mela, A. A. Drabek, S. M. Jarrett, S. C. Blacklow, C. F. Kaminski, G. L. Hura, J. J. De Yoreo, J. M. Kollman, H. Ruohola-Baker, E. Derivery, D. Baker, Design of biologically active binary protein 2D materials. *Nature*. **589**, 468–473 (2021).
2. Z. Chen, M. C. Johnson, J. Chen, M. J. Bick, S. E. Boyken, B. Lin, J. J. De Yoreo, J. M. Kollman, D. Baker, F. DiMaio, Self-Assembling 2D Arrays with de Novo Protein Building Blocks. *J. Am. Chem. Soc.* **141**, 8891–8895 (2019).
3. H. Pyles, S. Zhang, J. J. De Yoreo, D. Baker, Controlling protein assembly on inorganic crystals through designed protein interfaces. *Nature*. **571**, 251–256 (2019).

# Controlling Physical and Chemical Dynamics of Heterogeneous Networks Constructed from Soft Macromolecular Building Blocks

Anna C. Balazs<sup>1\*</sup>, Krzysztof Matyjaszewski<sup>2</sup>, Tomasz Kowalewski<sup>2</sup>

<sup>1</sup> Chemical Engineering Department, University of Pittsburgh, Pittsburgh, Pennsylvania 15261, United States

<sup>2</sup> Department of Chemistry, Center for Macromolecular Engineering, Carnegie Mellon University, 4400 Fifth Avenue, Pittsburgh, Pennsylvania 15213, United States

## Program Scope

Inspired by the modular assemblies of biomacromolecules that form complex, dynamic architectures with sophisticated functions, this current program aims to contribute to the *energy-efficient manufacturing by designing macromolecular building blocks* (macromolecular “Lego” blocks, or *mLB*) that can be reversibly linked to form a broad range of functional polymer networks with controllable composition, morphology and behavior (**Figure 1**). The concept of *mLB* was inspired by our recent work on transformable “Structurally Tailored and Engineered Macromolecular (STEM)” gels<sup>1</sup> that mimic natural stem cells. The current research involves experimental work on the “understanding, controlling, and building complex hierarchical structures” by using rationally designed *mLB*s and different types of reaction to construct materials with distinctive structures. In addition, our current simulation work also studies dynamic and reversible interactions and reactions within the networks that will guide the development of “biomimetic and/or bioinspired routes for the synthesis of energy relevant materials”, which will direct the design of macromolecular materials with transformability and degradability.

## Recent Progress

Over the past 2 years, we developed STEM gels into dynamic, transformable platforms for “macromolecular manufacturing” of soft materials. Controlled/“living” radical polymerization (CRP) methods, such as atom transfer radical polymerization (ATRP), enabled the “evolution” of the same STEM gel into multiple materials with distinctive properties. CRP provided unprecedented control over the composition and architecture of STEM gels. Simulation work over this period led to deepening of our understanding of the structure-property relationship in STEM gels, and of the origin of the unusual

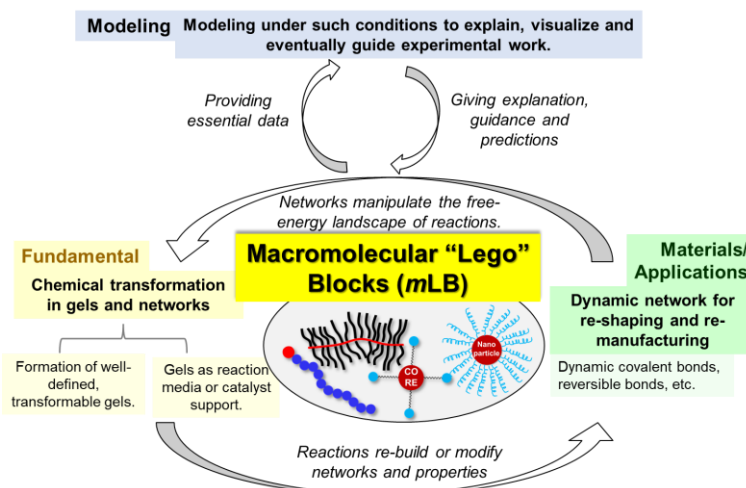


**Figure 1.** Transformable materials based on gels prepared from macromolecular “Lego” building blocks and their application as soft reaction media.



**Figure 2.** The STEM gel review was featured on the cover of *Trends in Chemistry*.<sup>2</sup>

softness. The development of STEM gels was summarized in our recent review in *Trends in Chemistry*,<sup>2</sup> which was featured on the cover of the journal (**Figure 2**).

Key results published:

**1.** Reversible addition-fragmentation chain-transfer (RAFT) polymerization using a dual-wavelength approach was developed.<sup>3</sup> The parent gel can be transformed into STEM gels that *either expand from the original gel (“E-STEM” gel), or generate additional dangling chains from latent functional groups (“D-STEM” gel)* (**Figure 3**), resulting in gels with distinctive structures such as different mesh sizes.

**2.** We developed *non-tacky, elastomeric STEM networks* based on fluorinated monomers.<sup>4</sup> Poly(octafluoropentyl acrylate) (POFPA) with a  $T_g = -35\text{ }^\circ\text{C}$  was selected to build soft (Young’s modulus = 104-178 kPa) STEM gels with low surface energy that do not adhere to glass surfaces (**Figure 4**).

**3.** We used *dissipative particle dynamics (DPD) simulations* to study the mechanical response of the modified STEM gels under compression for various values of the side chain length,  $n_{sc}$  (**Figure 5**).<sup>5</sup> We found that the mechanical properties can be tuned by varying the grafting density and  $n_{sc}$ . Increases in  $n_{sc}$ , lower the modulus of the networks up to certain saturation value; increasing  $n_{sc}$  beyond that point does not lead to any further softening of the sample. The latter findings agree with the experimental results.

**4.** A new class of water-soluble fluorescent polymers were prepared from polyacrylonitrile (PAN).<sup>6</sup> A one-step hydrothermal method was developed (**Figure 6**). This report will assist the study of photoluminescent gels based on the *interactions between dangling chains facilitated by the congested environment of the network*.

**5.** We developed a degradable star-shaped polymer scaffold as a preliminary step method towards *degradable gels and subtractive manufacturing*.<sup>7</sup> The core of the star polymers was composed of tannic acid, which is generally recognized as a safe compound by US FDA (**Figure 7**). The tannic acid was modified with ATRP initiators, and polymer arms were grown from the core using biocompatible ethylene glycol.<sup>7</sup> We demonstrated that the tannic acid polymer stars can be

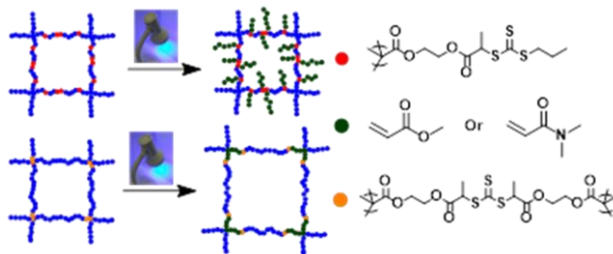


**Figure 3.** An illustration of the idealized network structure from post-synthesis modification to make: 1) “D-STEM” gels; or 2) “E-STEM” gels (bottom).<sup>3</sup>

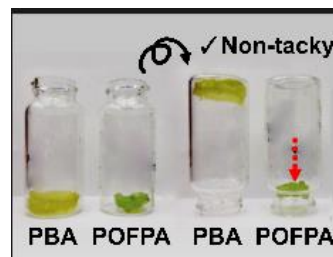


**Figure 4.** The STEM gel with dangling POFPA chains that is non-tacky is shown.<sup>4</sup>

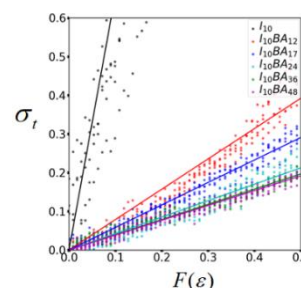


**Figure 5.** Simulated results of the mechanical properties for STEM gels with different chain lengths.<sup>5</sup>

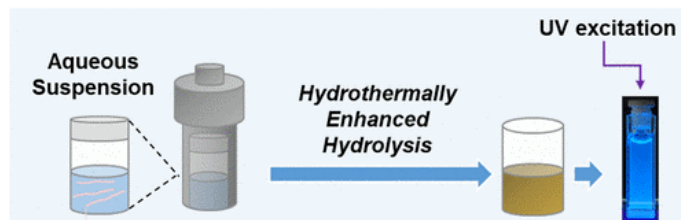


**Figure 6.** Synthesis of water-soluble photoluminescent polymers via the hydrothermal reaction of polyacrylonitrile.<sup>6</sup>

degraded under mild basic conditions. Such degradable stars can be incorporated into STEM gels to advance our efforts in subtractive manufacturing.

6. *Degradable polymer brushes* were synthesized from cellulose, a natural polymer composed of repeating glucose units.<sup>8</sup> Cellulose-based polymer brushes

were prepared by functionalizing cellulose with ATRP initiator sites and subsequently used to grow polymer side chains (**Figure 8**). The cellulose-based polymer brushes can be degraded through two different pathways, either cleavage of the main chain or detachment of the side chains. And the cellulose-based polymer brushes showed tunable degradation rates dependent on the grafting density of the brush. The cellulose-based polymer brushes will provide additional *mLBs* with *potential degradability* for the synthesis of gels in the next step.

### Future Plans

Our experimental and simulation work planned for the near future addresses the following specific questions regarding the formation and dynamic interactions within gels (

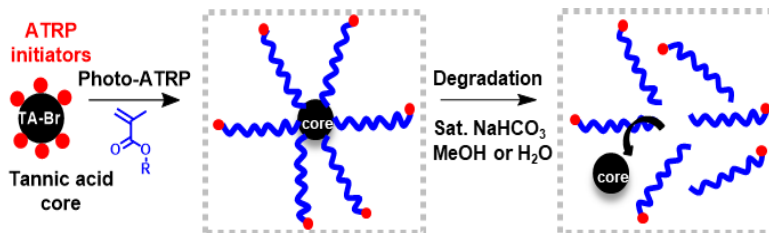


**Figure 7.** The synthesis of polymer stars, from a modified tannic acid core (TA-Br) and the subsequent degradation of the star.<sup>7</sup>

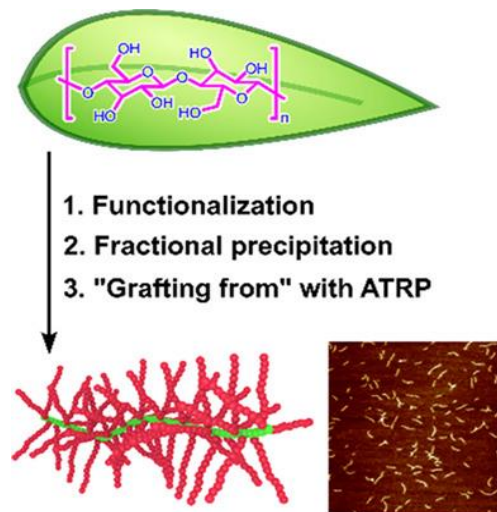


**Figure 8.** The synthesis of polymer brushes with cellulose backbones.<sup>8</sup>

### Figure 9):

- 1) Studying how different controlled radical polymerization (CRP) methods (i.e., ATRP, vs. RAFT polymerization) that are used to build macromolecular networks affect the structural defects and physical properties (i.e., swelling ratios) of the network.
- 2) Designing structurally tailored and engineered macromolecular (STEM) gels with specific dangling chains, whose interaction can induce unusual photoluminescence derived from the dipole interaction or “through-space conjugation”.
- 3) Developing “inverted” polyethylene glycol-based monomer and networks with enhanced chemical stability and resistance toward harsh chemical conditions (i.e., strong base).

4) Developing models to study STEM gels with gradient structures that encompass variations in the local polymer density, matching the structures to be fabricated by the CMU group. In the reaction-diffusion component within the gLSM, we can specify that the chemical reactions (e.g., catalytic reactions) depend on the local polymer density. The simulation results can reveal how to tailor the gradients in the gel to provide effective “reaction chambers” for catalytic processes. These studies will facilitate progress in the research described below

The long-term research in the scope of this program will also focus on:

1) Developing polymer networks with reversible transformability and degradability. In order to prepare reversibly transformable or degradable gels, we will incorporate dynamic covalent bonds or degradable macromolecular scaffold that we previously developed (i.e., tannic acid-based degradable star polymers) into STEM gels.

2) Combining experimental work and simulation work on transformable polymer networks to promote the understanding of the dynamic and reversible structure.

3) Inspired by biochemical reactions that occur within confined environments, we also plan to use rationally-designed polymer networks as reaction vessels or support materials for catalysts.

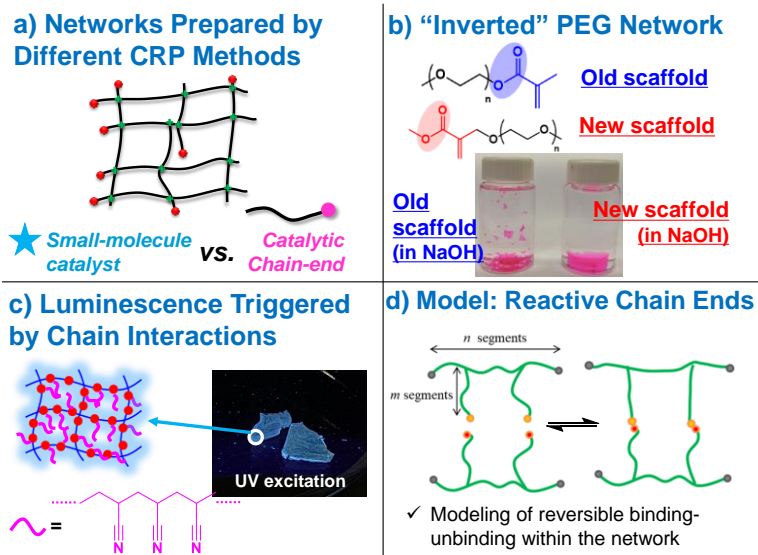


**Figure 9.** Summary of future plans. a) Study of the structure differences of networks prepared by different CRP methods. b) Development of more chemically stable network based on “inverted” PEG scaffold. c) STEM gel with luminescence triggered by chain interactions. d) Visualization of a model that studies reactive chain ends and reversible coupling in the network.

## References

- (1) Cuthbert, J.; Beziau, A.; Gottlieb, E.; Fu, L.; Yuan, R.; Balazs, A. C.; Kowalewski, T.; Matyjaszewski, K., Transformable Materials: Structurally Tailored and Engineered Macromolecular (STEM) Gels by Controlled Radical Polymerization, *Macromolecules* **2018**, *51*, 3808-3817.
- (2) Cuthbert, J.; Balazs, A. C.; Kowalewski, T.; Matyjaszewski, K., STEM Gels by Controlled Radical Polymerization, *Trends. Chem.* **2020**, *2*, 341-353.
- (3) Shanmugam, S.; Cuthbert, J.; Flum, J.; Fantin, M.; Boyer, C.; Kowalewski, T.; Matyjaszewski, K., Transformation of gels via catalyst-free selective RAFT photoactivation, *Polym. Chem.* **2019**, *10*, 2477-2483.
- (4) Cuthbert, J.; Martinez, M. R.; Sun, M.; Flum, J.; Li, L.; Olszewski, M.; Wang, Z.; Kowalewski, T.; Matyjaszewski, K., Non-Tacky Fluorinated and Elastomeric STEM Networks, *Macromol. Rapid. Comm.* **2019**, *40*, 1800876.

- (5) Zhang, T.; Biswas, S.; Cuthbert, J.; Kowalewski, T.; Matyjaszewski, K.; Balazs, A. C., Understanding the origin of softness in structurally tailored and engineered macromolecular (STEM) gels: A DPD study, *Polymer*. **2020**, *208*, 122909.
- (6) Sun, M.; Gottlieb, E.; Yuan, R.; Ghosh, S.; Wang, H.; Selhorst, R.; Huggett, A.; Du, X.; Yin, R.; Waldeck, D. H.; Matyjaszewski, K.; Kowalewski, T., Polyene-Free Photoluminescent Polymers via Hydrothermal Hydrolysis of Polyacrylonitrile in Neutral Water, *ACS Macro Lett.* **2020**, *9*, 1403-1408.
- (7) Cuthbert, J.; Yerneni, S. S.; Sun, M.; Fu, T.; Matyjaszewski, K., Degradable Polymer Stars Based on Tannic Acid Cores by ATRP, *Polymers* **2019**, *11*, 752.
- (8) Olszewski, M.; Li, L.; Xie, G.; Keith, A.; Sheiko, S. S.; Matyjaszewski, K., Degradable cellulose-based polymer brushes with controlled grafting densities, *J. Polym. Sci. A Polym. Chem.* **2019**, *57*, 2426-2435.

## Publications

- [1] Cuthbert, J.; Balazs, A. C.; Kowalewski, T.; Matyjaszewski, K., STEM Gels by Controlled Radical Polymerization. *Trends Chem.* **2020**, *2*, 341-353.
- [2] Sun, M.; Gottlieb, E.; Yuan, R.; Ghosh, S.; Wang, H.; Selhorst, R.; Huggett, A.; Du, X.; Yin, R.; Waldeck, D. H.; Matyjaszewski, K.; Kowalewski, T., Polyene-Free Photoluminescent Polymers via Hydrothermal Hydrolysis of Polyacrylonitrile in Neutral Water. *ACS Macro Lett.* **2020**, *9*, 1403-1408.
- [3] Zhang, T.; Biswas, S.; Cuthbert, J.; Kowalewski, T.; Matyjaszewski, K.; Balazs, A. C.; Understanding the origin of softness in Structurally Tailored and Engineered Macromolecular (STEM) Gels: A DPD study. *Polymer* **2020**, *206*, 122909.
- [4] Olszewski, M.; Li, L.; Xie, G.; Keith, A.; Sheiko, S. S.; Matyjaszewski, K., Degradable cellulose-based polymer brushes with controlled grafting densities. *J. Polym. Sci. A Polym. Chem.* **2019**, *57*, 2426-2435.
- [5] Cuthbert, J.; Yerneni, S. S.; Sun, M.; Fu, T.; Matyjaszewski, K., Degradable Polymer Stars Based on Tannic Acid Cores by ATRP. *Polymers* **2019**, *11*, 752.
- [6] Cuthbert, J.; Martinez, M. R.; Sun, M.; Flum, J.; Li, L.; Olszewski, M.; Wang, Z.; Kowalewski, T.; Matyjaszewski, K., Non-Tacky Fluorinated and Elastomeric STEM Networks. *Macromol. Rapid Commun.* **2019**, *40*, 1800876.
- [7] Shanmugam, S.; Cuthbert, J.; Flum, J.; Fantin, M.; Boyer, C.; Kowalewski, T.; Matyjaszewski, K., Transformation of gels via catalyst-free selective RAFT photoactivation. *Polym. Chem.* **2019**, *10*, 2477-2483.

## Bio-inspired Shape-morphing and Self-propelled Active Sheets

Anna C. Balazs, Chem. Engr. Dept. University of Pittsburgh, Pittsburgh, PA

### Program Scope

Using theory and simulation, our aim is to design chemically active, flexible sheets that convert chemical energy into mechanical motion to achieve functionality that is not possible with active stationary walls or mobile hard particles. In nature, the energy released from enzymatic reactions “fuels” a range of mechanical processes, from metabolic events to large-scale motion. Inspired by this mode of biological chemo-mechanical transduction, we design 2D catalyst-coated, flexible sheets that generate chemical energy, which drives the sheets to spontaneously morph into 3D structures and perform mechanical work within fluids. Previously, researchers have coated synthetic nano- and micro-scale particles in solution with various catalysts that react with species in the fluid and thus drive the

spontaneous motion of both the fluid and the particles. In effect, the catalysts on the mobile particles act as chemical “motors” that transduce the energy from the chemical reactions into mechanical movement. In the prior studies, however, the catalyst-coated microscopic objects were rods, filaments or spheres. The geometry of the object is important because its shape will affect the surrounding fluid flow, which in turn will affect the movement of the object. The behavior is particularly complex with flexible, active sheets; the fluid not only affects the motion of the sheet, but also drives the deformable sheets to exhibit unprecedented forms of structural reconfiguration and self-organization. In these studies, we interrelate the arrangement of catalysts on the sheet, the chemically-generated pattern of fluid flow and the final 3D shape of the sheet (see Fig.1). The potential of harnessing the fluid flow to controllably “mold” and organize the deformable sheets remains largely unexplored. Hence, the proposed studies can spearhead new research in active matter and pinpoint regions in parameter space that will lead to the most fruitful experimental investigations.

### Recent Progress

Using theoretical and computational modeling, we integrated bio-inspired structural motifs and responsive gels to design materials that undergo morphological reconfigurations, which enhance the materials’ mechanical properties and/or endow the system with new functionality.<sup>1-7</sup> Below, I summarize some of our recent results.

#### *Chemically Controlled Shape-morphing of Elastic Sheets*<sup>1</sup>

Using theory and simulation, we designed a catalyst-coated 2D sheet that controllably morphs into multiple 3D structures in fluid-filled microchambers (Fig 1). The advent of materials where a single sample morphs on-demand into various 3D shapes can dramatically simplify manufacturing processes and enable the creation of stand-alone, multi-functional soft robots. Currently, shape-morphing 2D structures encompass non-uniform internal stresses that yield a

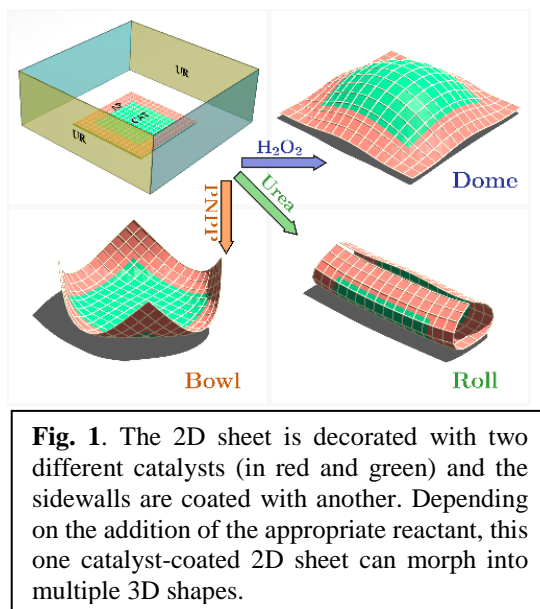


**Fig. 1.** The 2D sheet is decorated with two different catalysts (in red and green) and the sidewalls are coated with another. Depending on the addition of the appropriate reactant, this one catalyst-coated 2D sheet can morph into multiple 3D shapes.

specific 3D form with the application of external stimuli. This final 3D configuration is unique and predetermined through the materials' processing. We use theory and simulation to devise a distinctive approach for driving shape changes of 2D elastic sheets in fluid-filled microchambers. We harness the inherent chemo-mechanical transduction that occurs when the sheets are coated with catalyst. When a reactant is added to the solution, it initiates a catalytic reaction and the resultant chemical energy is transduced into the flow of the surrounding fluid. The generated flows in turn "sculpt" the flexible sheet into 3D shapes. We also exploit the fact that catalytic reactions can only be initiated by specific reactants. Hence, for a sheet encompassing multiple catalytic patches, the 3D shape can be controlled through the addition of a particular reactant or combination of reactants, enabling one sheet to form multiple architectures. Our models provide new insights into the relationships among catalytic reactions, patterns on the sheet, and generated flows, providing guidelines for driving novel 2D-to-3D shape transformations. The work was featured on the cover of *Materials Horizons* (see Fig. 2).



Fig. 2. Our work featured on cover of *Materials Horizons*<sup>1</sup>

***Self-morphing, chemically driven gears and machines*<sup>2</sup>**

Building on our observations that catalysis on the sheet generates flow, which morphs the 2D layer into 3D shapes, we designed flat, wheel-shaped sheets that morph into gears that rotate with specified directionality. We further showed that multiple gears interact to form "chemical machines" that perform mechanical work. Figure 3 shows an image of this system: deformable, catalyst-coated sheets that resemble a flat wheel, with spokes that interconnect an outer rim and inner center. The catalysis not only generates fluid flow, but the generated flow also morphs the 2D layer into 3D shapes that spontaneously rotate (see side view in Fig. 3). With the addition of cogs to the outer rim, the structure forms a chemically-driven, active gear, which can drive the motion of passive, non-coated units (in black). The studies provide design rules for creating "chemical machines" from chains of active and passive gears that act in concert to perform mechanical work. The machine's motion does not require external power, just the addition of reactants to the solution.

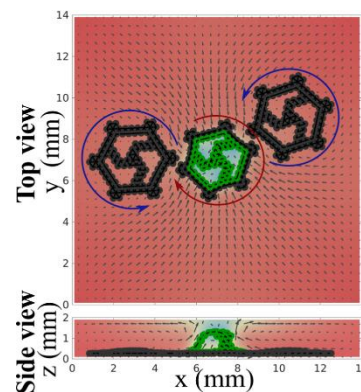
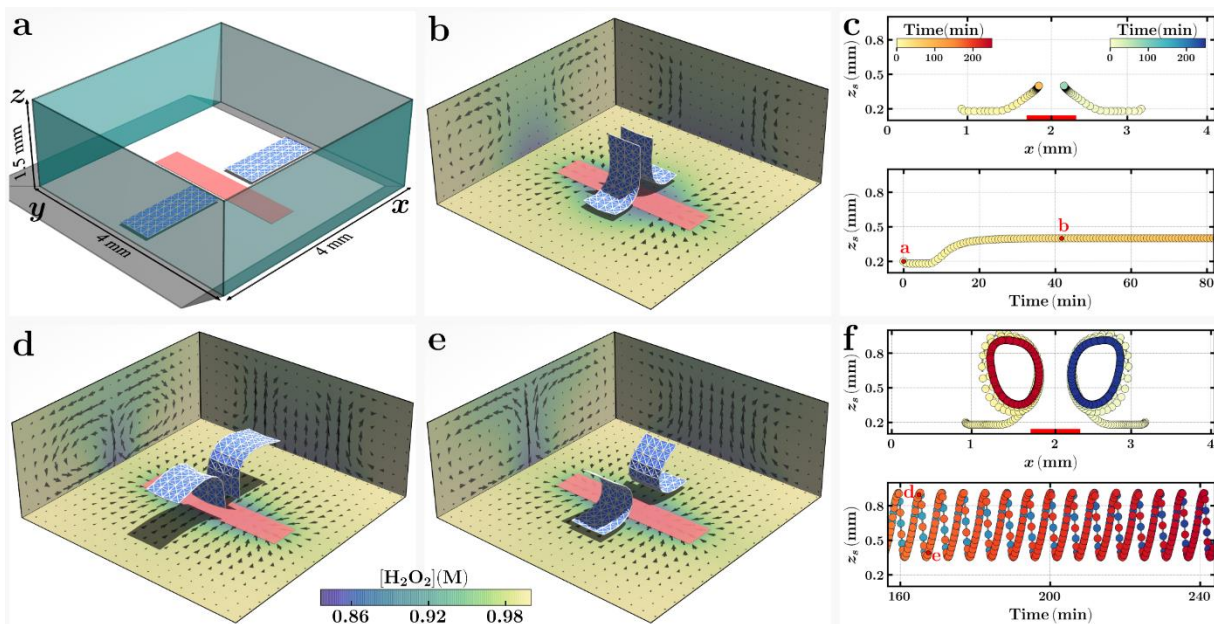


Fig. 3. Transmission of rotational motion from an active gear to two passive gears. In a fluidic chamber, an active gear can rotate multiple passive gears,<sup>2</sup>

***Chemical pumps and flexible sheets spontaneously form self-regulating oscillators in solution*<sup>3</sup>**

The synchronization of self-oscillating systems is vital to various biological functions, from the coordinated contraction of heart muscle to the self-organization of slime molds. Using computational modeling, we designed a new self-oscillating materials system that is driven by a non-periodic chemical reaction to undergo both periodic shape changes and motion. Catalytic reactions in a fluid-filled microchamber drive the movement of the fluid and immersed flexible sheets. The fluid affects the sheets' shape, and the sheets affect the fluid flow. This feedback enables remarkably complex oscillatory behavior: a single sheet fish-tails periodically across the

chamber or circulates continuously within a narrow region. Two sheets form coupled oscillators displaying not only synchronized temporal behavior, but also unique, coordinated morphological reconfigurations (Fig. 4). We developed a heuristic model that rationalizes this behavior.



**Fig. 4.** Autonomous coupled oscillations of two passive sheets. (a) Two passive sheets (marked in blue) are placed on either side of the chemical pump (marked in red) in a fluid-filled chamber. (b) At low reaction rate at the catalytic pump,  $r_m^{\text{patch}} = 52 \text{ mmol m}^{-2} \text{ s}^{-1}$ , the sheets form a stable tower like structure. (c) The height ( $Z_s$ ) of the center of the sheets remains constant for a long time. The left and right color bars indicate the time elapsed during the motion of left and right sheets, respectively. (d-e) For a higher reaction rate,  $r_m^{\text{patch}} = 96 \text{ mmol m}^{-2} \text{ s}^{-1}$ , both sheets oscillate about the center of each half domain. (f) The trajectory of the center of the sheets lie either side of the catalytic path (top). The heights of the center of the sheets as a function of time show are identical and thus indicate that the sheets are synchronized in in-phase (bottom). The stretching and bending modulus of the sheets are taken as  $k_s = 60 \text{ pN}$  and  $k_b = 2.2 \text{ pN mm}^2$  respectively.<sup>3</sup>

These coupled self-oscillators exhibit rich and tunable phase dynamics, which depends on the sheets' initial placement, coverage by catalyst and relative size. Moreover, through variations in the reactant concentration, the system can switch between the different oscillatory modes. This breadth of dynamic behavior expands the functionality of the coupled oscillators, enabling soft robots to display a variety of self-sustained, self-regulating moves. These oscillators also enable development of soft robots that operate through an inherent coupling of chemistry and motion, permitting novel autonomous and self-regulating behavior.

#### ***Colloidal Assembly and Separation under UV-Induced Convective Flows on Inclined Surfaces<sup>4</sup>***

We also considered how the application of light can be used to regulate the effects of thermal buoyancy in solutions containing a heterogeneous mixture of microparticles. Achieving directed motility and separation of colloidal particles is a crucial requirement in a range of technological areas. We described a system that exploits the photothermal properties of plasmonic nanoparticles for the assembly and separation of larger microparticles. Irradiating an aqueous suspension of gold or silver nanoparticles with UV light generates thermal convection, which can

be used to move and organize larger particles. Moving the UV light source allows the relocation of the particle cluster. In addition, thermal convection can be used to separate inert particles of different sizes on an inclined plane. Since fluid motion stems from thermal convection, collection and separation can be reversed simply by turning off the UV light enabling a rapid on-demand response system. This work was highlighted on the cover of the journal (Fig. 5)

***Harnessing biomimetic cryptic bonds to form self-reinforcing gels***<sup>5</sup> In finalizing the work from the previous grant period, we focused on two ubiquitous structural motifs in biology: loops<sup>5,6</sup> and fibers.<sup>7</sup> In the case of loops, we considered cryptic sites, which bind to form a loop and lay hidden in folded biomolecules. The sites become exposed by applied force and form new bonds that reinforce the biomaterial. We showed that these binding interactions act as “struts” that reinforce the network, as indicated by a significant decrease in the volume of the gel (from 44% to 80%) and shifts in the volume phase transition temperature. These findings provide guidelines for designing polymer networks with reversible, mechano-responsive bonds, which allow gels to undergo a self-stiffening behavior in response to a temperature-induced internal stress or external force. In a coating, these gels can prevent the underlying materials from undergoing damage and thus, extend the lifetime of the system.

### Future Plans

We will design: 1) hierarchical structures through approaches that harness chemo-mechanical transduction; 2) systems that demonstrate energy conversion and storage; 3) systems with functionality that cannot be achieved by a single entity. For example, we will:

- ***Examine the self-organization of multiple strips*** By analyzing the factors that contribute to the self-organization of these systems (as in Fig. 4), we will establish how to combine chemical pumps with multiple passive and/or active sheets to create a system that spontaneously performs work in a fluidic device.
- ***Design mechanically patterned sheets*** In the latter studies,<sup>1</sup> we considered a sheet that is mechanically uniform. We will tailor the local values of the moduli to design “mechanically patterned” sheets. By combining such mechanical patterning with the chemical patterning of catalyst on the sheet, we significantly expand the design space for controllably altering the shape of the sheet, both temporally and spatially.
- ***Devise self-regulating system*** We will design a self-regulating system where the product of the reaction affects or modifies properties of the sheet, which in turn, counteracts the force from the convective fluid. Such self-regulating systems are useful because they autonomously adjust their behavior without the need for external intervention and hence, they reduce the cost in energy of monitoring the system’s performance. In addition, self-regulating behavior is vital for creating the next generation soft robots.



Fig. 5. Journal cover featuring our work.<sup>4</sup>

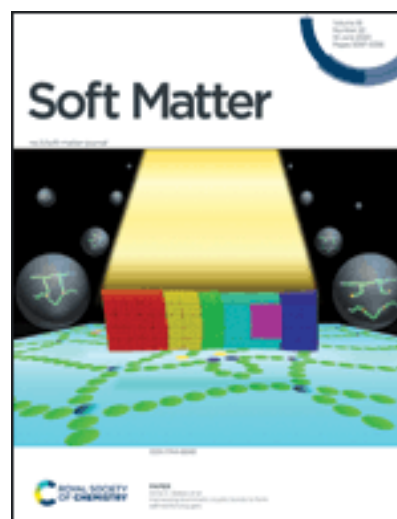


Fig. 6. Journal cover featuring our work.<sup>5</sup>

### Publications supported by this DOE grant

1. Manna, R.K., ShklyaeV, O.E., Stone, H.A., and Balazs, A.C., “Chemically controlled shape-morphing of elastic sheets” *Mater. Horiz.*, **7** (2020) 2314-2327
2. Laskar, A., ShklyaeV, O.E., and Balazs, A.C., “Self-Morphing, Chemically Driven Gears and Machines” *Matter* **4** (2021) 600-617. <https://doi.org/10.1016/j.matt.2020.11.014>
3. Manna, R.K., ShklyaeV, O.E., and Balazs, A.C., “Chemical pumps and flexible sheets spontaneously form self-regulating oscillators in solution” *PNAS* **118** (2021) e2022987118 [doi.org/10.1073/pnas.2022987118](https://doi.org/10.1073/pnas.2022987118)
4. Kauffman, J.E., Tansi, B.M., LaSalle, C., Manna, R.K., ShklyaeV, O.E., Balazs, A.C., and Sen, A. “Colloidal Assembly and Separation under UV-Induced Convective Flows and on Inclines” *CHEMNANOMAT* (2021) doi: 10.1002/cnma.202100082
5. Biswas, S., Yashin, V.V., and Balazs, A.C. “Harnessing biomimetic cryptic bonds to form self-reinforcing gels”, *Soft Matter*, **16** (2020) 5120-5131.
6. Oshri, O., Biswas, S., and Balazs, A.C., “Buckling-induced interaction between circular inclusions in an infinite thin plate” *Phys. Rev. E* **102** (2020) 033004 (17 pages).
7. Zhang, T., Yashin, V.V., Waters, J.T. and Balazs, A.C. “Formation of helices with controllable chirality in gel-fiber composites”, *Polymer* **212** (2021) 123191 Elsevier BV. doi: 10.1016/j.polymer.2020.123191

**Self-Assembly and Self-Replication of Novel Materials from Particles with Specific Recognition DE-SC0007991 . Paul M. Chaikin, David Pine, Dept. of Physics, New York University, Nadrian C. Seeman, Marcus Weck, Dept. of Chemistry, New York University.**

**Program Scope**

This program seeks to extend the use of specific DNA recognition and hybridization from the nanoscale to the micro scale. We have exhibited self-replication of DNA origami motifs in one and two dimensions and have recently extended the replication procedure to three dimensions and also shown mutation, selection and competition. We have shown that DNA functionalization allows programmed colloidal assembly and architecture of arbitrary design. A current goal is DNA assisted self-assembly and activation of colloidal micro-machines.

**Two-Dimensional Superstructures from DNA-Coated Colloidal Particles, Pine, Weck**

We have developed a method to synthesize ellipsoidal di-patch particles with DNA-coated patches and their assembly via cooperative depletion and DNA-mediated interactions. Through fine tuning of the colloidal building block architecture and the assembly conditions, namely, patch size, annealing temperature, and depletant concentration, 2D or quasi-2D colloidal superstructures can be constructed. The di-patch particles are based on azide-containing poly(styrene) (PS-N<sub>3</sub>) as the patches and 3-(trimethoxysilyl)propyl methacrylate (TPM) as the matrix. By tuning the concentration of TPM during the cluster encapsulation, the half opening angle can be varied between 55° and 97°. The di-patch particles were functionalized on the patches with palindromic DNA strands (sticky end, GCGC, melting temperature  $T_m \sim 42^\circ\text{C}$ ) through strain-promoted azide-alkyne cycloaddition (SPACC)<sup>[1]</sup> between dibenzocyclooctyne-modified DNA strands (DBCO-DNA) and the azide groups on the patches. To ease the visualization of the particles, the DNA strands were labelled with a fluorescent tag (Cy5, excitation 633 or 647 nm, emission maximum, 668 nm), (red) whereas the TPM matrix is undyed.

For assembly studies, the DNA-coated particles were then dispersed in a PBS buffer solution containing Pluronic F127. The suspension was put into a glass capillary tube, which was then sealed and affixed to a slide with UV-curable glue. The temperature of the sample slide was controlled by a thermal stage. Typically, the sample was left within a designated temperature range for about twelve hours to allow the assembly to develop. The resulting assemblies were characterized by bright-field, fluorescent, and confocal laser scanning microscopies. Figures 1 and 2 show two examples of the 2D superstructures that were obtained

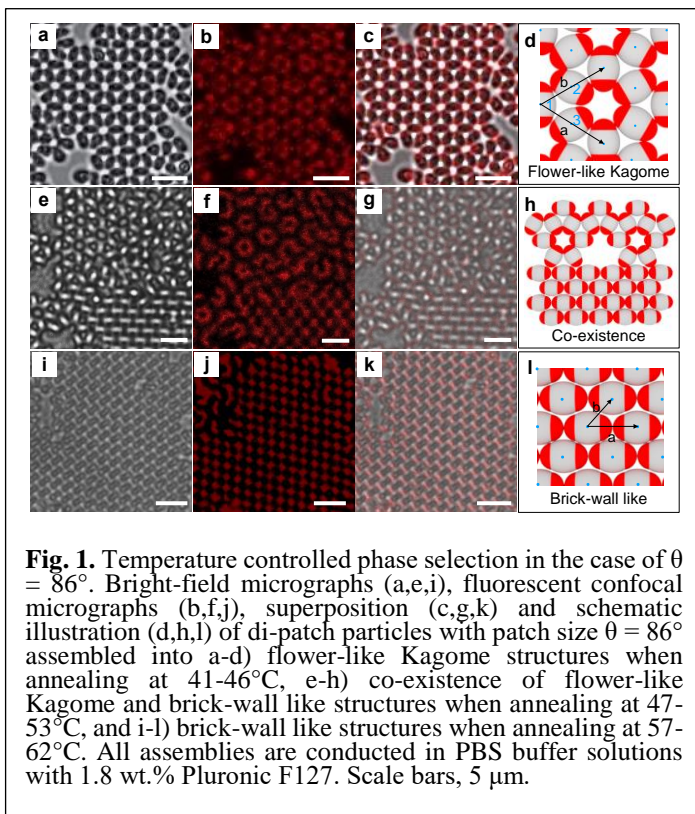


**Fig. 1.** Temperature controlled phase selection in the case of  $\theta = 86^\circ$ . Bright-field micrographs (a,e,i), fluorescent confocal micrographs (b,f,j), superposition (c,g,k) and schematic illustration (d,h,l) of di-patch particles with patch size  $\theta = 86^\circ$  assembled into a-d) flower-like Kagome structures when annealing at 41-46°C, e-h) co-existence of flower-like Kagome and brick-wall like structures when annealing at 47-53°C, and i-l) brick-wall like structures when annealing at 57-62°C. All assemblies are conducted in PBS buffer solutions with 1.8 wt.% Pluronic F127. Scale bars, 5  $\mu\text{m}$ .

through variations of assembly conditions. Figure 1 shows dipatch particles with patches of  $\theta = 86^\circ$  that assemble into flower-like Kagome structures while at higher temperatures brick-wall like superstructure were obtained. Figure 2 shows assembled particles with patches of  $\theta = 70^\circ$  that yield structures of orthogonal packing, wrinkled monolayers or co-existence of both by tuning the concentration of the depletant.

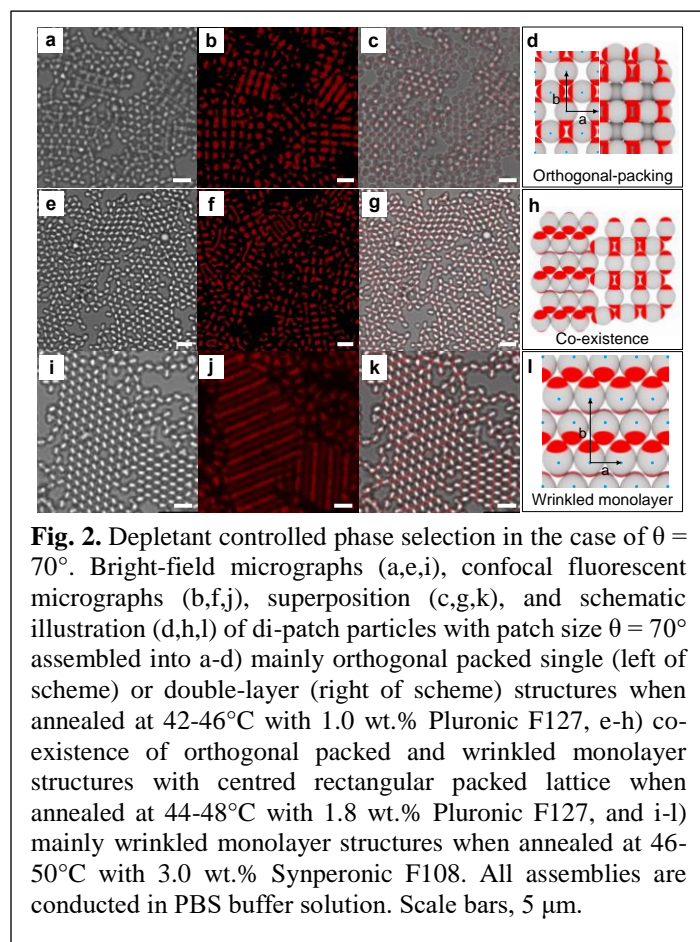


**Fig. 2.** Depletant controlled phase selection in the case of  $\theta = 70^\circ$ . Bright-field micrographs (a,e,i), confocal fluorescent micrographs (b,f,j), superposition (c,g,k), and schematic illustration (d,h,l) of di-patch particles with patch size  $\theta = 70^\circ$  assembled into a-d) mainly orthogonal packed single (left of scheme) or double-layer (right of scheme) structures when annealed at 42-46°C with 1.0 wt.% Pluronic F127, e-h) co-existence of orthogonal packed and wrinkled monolayer structures with centred rectangular packed lattice when annealed at 44-48°C with 1.8 wt.% Pluronic F127, and i-l) mainly wrinkled monolayer structures when annealed at 46-50°C with 3.0 wt.% Synperonic F108. All assemblies are conducted in PBS buffer solution. Scale bars, 5  $\mu\text{m}$ .

structures of orthogonal packing, wrinkled monolayers or co-existence of both by tuning the concentration of the depletant.

To aid our characterization of these superstructures, we have also developed algorithms capable of image analysis for classifying colloidal structures based on abstracted interparticle relationship information and quantitatively analyzing the abundance of each structure in mixed pattern assemblies. The algorithms provide a labelled image comprising classification results and particle counts of each defined class. The yielded classification data allows for more in-depth image analysis of mixed pattern particle assemblies. We envision that these algorithms will have utility in quantitative analysis of images comprised of ellipsoidal colloidal materials, nanoparticles, or biological matter. Our results provide guidance in designing and fabricating 2D colloidal superstructures from bottom-up assembly.

### Autonomous hybrid DNA- Colloid Machine using RNA as Fuel, Chaikin, Seeman

In previous work, we have demonstrated hybrid DNA - colloid machines based on hinges made with two DNA origami six helix bundle (6HB) arms joined at their vertex by semi-rigid ssDNA strands and closed with complementary DNA sticky ends attached on either arm a short distance ( $\sim 20\text{nm}$ ) from the vertex.<sup>[2]</sup> When the sticky ends open on heating or exposure to light the hinge opens. On cooling the hinge closes and with a mechanical advantage of  $\sim 50$  (arm length  $\sim 1$  micron/ $20\text{nm}$  hybridized sticky ends from vertex) we were able to move 1 micron diameter colloids at  $> 25$  microns/sec. However, the open-close cycle was slow,  $\sim$  minutes, and under the control of the experimenter. We therefore aimed at making a faster autonomous motor. We took the idea from Ref. [2] who used hybrid DNA-RNA hybridization and the remarkable enzyme RNase H to make an autonomous colloidal roller.

RNase H is an enzyme found in similar form in every living organism. When it comes upon a DNA-RNA hybrid duplex it hydrolyzes the RNA into small fragments while leaving the DNA single strand intact. It does not interact with DNA or RNA single strands or duplexes. As shown in Figure 3a) we modified our hinge design such that the DNA sticky ends on each arm are not complementary to each other but rather each is complementary to half of a RNA linker strand

which serves as fuel. When the RNA hybridizes with the DNA sticky ends the hinge closes. When the enzyme diffuses to the hybrid duplex it 'eats' the RNA linker, releases the two arms and the hinge opens completing the cycle. The cycle repeats when another RNA hybridizes with the DNA sticky ends. With optical microscopy we can track the 1 micron diameter colloid attached to a hinge arm as the hinge opens and closes. In Figure 3b) we see the stochastic opening and closing. Enzymes work better at body temperature (37°C) than at low temperature and the cycle time becomes of order a second.

The 6HB arms are not completely rigid. The bending of the arms is different for opening and closing of the hinge. The motion is not reciprocal so that we might expect some small drive even at low Reynolds number. We therefore used a DNA origami belt<sup>[31]</sup> to attach a colloid with ssDNA (with no torsional rigidity) to the substrate and a hinge/motor aligned to open and close along the colloid's equator. The aim is a rotary motor, Figure 3c). We measured the angular mean squared displacement by optically tracking the particle on the hinge/motor. With no RNA or RNase H we observed the expected rotational diffusion. But when the fuel and enzyme were added we observed both enhanced diffusion and a small but finite rotational velocity (on  $\sim 4$  samples) Figure 3d).

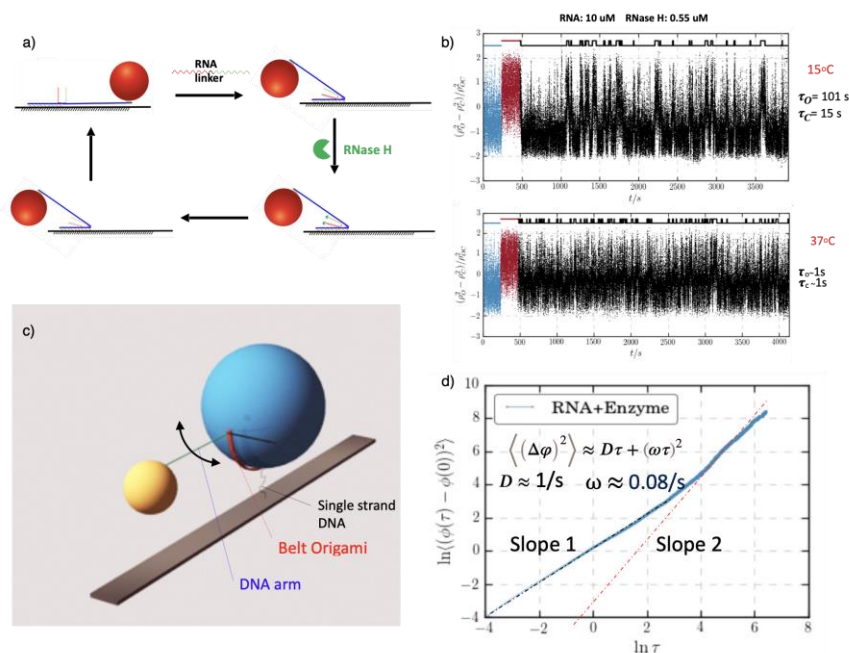


**Fig. 3:** a) Hinge/motor cycle. An RNA linker binds to opposing DNA sticky ends on hinge arms closing the hinge. RNase H enzyme 'eats' linker opening the hinge. b) Hinge time open,  $\tau_o$ , time closed,  $\tau_c$ . Blue is open position of the colloid, Red is closed, Black is the stochastic opening and closing at 15C and 37C.  $\tau_o$  and  $\tau_c$  computed from measured distribution. c) Rotary motor with hinge/motor driving yellow particle back and forth on equatorial plane. d) Angular mean squared displacement of central colloid.

### Self-assembling 3D DNA motifs with metal-mediated base pairing, Seeman

There exists a critical need for nanoelectronics technologies that utilize fabrication and degradation pathways which are both energetically sustainable and provide access to molecular electronic dimensions. The overall goal of this project is to utilize metal-mediated base pairing in DNA to self-assemble one-dimensional (1D) conductors consisting of single metal ions inside precisely defined 3D nanostructures for the development of biologically derived, recyclable nanoelectronics. This will be accomplished by utilizing the self-assembling tensegrity triangle as a powerful screening tool to assay a wide variety of DNA metalation conditions through x-ray diffraction to build a library of metal base pairs.

Metal base pairs are obtained through hydrogen bond replacement within the double helix. In our system, we modify the center base of each arm of a tensegrity triangle to have a generalized pyrimidine:pyrimidine mismatch (Fig. 4). This gap is selectively filled by a metal ion, typically  $Ag^+$  or  $Hg^{2+}$ , during the self-assembly process. By altering the identity of the pyrimidines and the

metals inside our designer DNA crystals, we are able to rapidly assay a variety of assembly conditions to determine the structures of metal-derivative pairs using x-ray diffraction. Our structural library now includes 33 metal-mediated DNA (mmDNA) base pairs using cytosine-like nucleobases (cytosine, 5-methyl-isocytosine, 5-methyl-cytosine), thymine-like bases (thymine, uracil, 5-iodo-uracil), and “hachimoji” bases in 8-letter DNA (5-methyl-isocytosine, 6-amino-5-nitropyridin-2-one [dZ]) to coordinate silver(I) and mercury(II). Previous work has shown silver ions within the double helix to possess superior molecular electronic behavior, while bulk mercury is known to exhibit low-temperature superconductivity. Leveraging these metals in a self-assembling platform will allow for future low-energy electronic device design and fabrication.

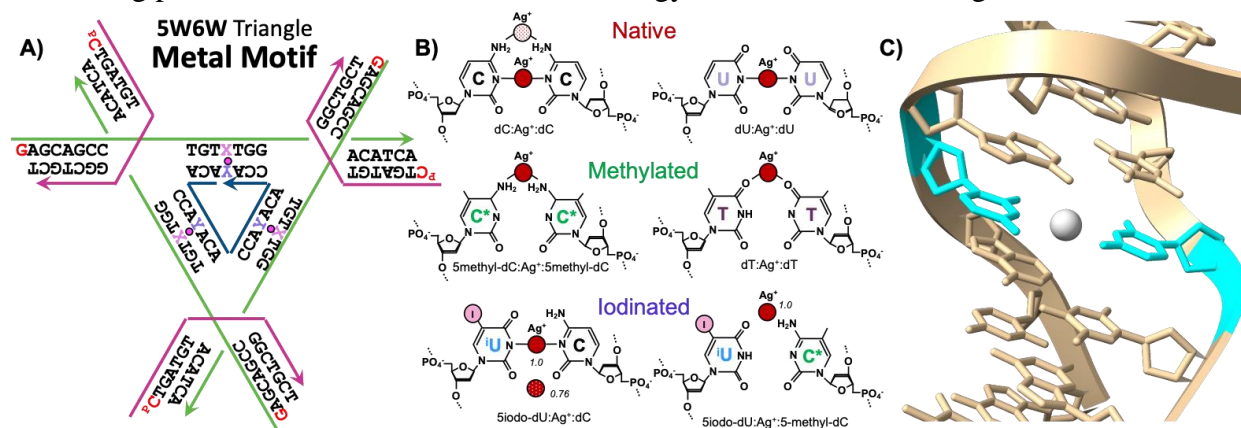


**Fig. 4:** Metal base pairs in self-assembling DNA crystals. **A)** Each triangle edge of this motif contains a pyrimidine:pyrimidine mismatch filled by a metal ion ( $\text{Ag}^+$ ,  $\text{Hg}^{2+}$ ). **B)** Ring modifications at the 5 position, opposite the metal interface, have a dramatic effect on metal coordination. Unmodified bases possess N3 (cerntrosymmetric)  $\text{Ag}^+$  coordination. Methylation at the 5 position drives major groove coordination at the 4 position, while iodination drives minor groove coordination at the 2 position. **C)** Structure of hitherto unknown  $\text{dU}:\text{Ag}^+:\text{dU}$  base pair at slightly basic pH, zoomed in from full triangle.

We report that the use of 8-letter “hachimoji” DNA allows for much stronger control of metal pairing. The expanded code letter “dS,” or 5-methyl-isocytosine, strongly disfavors mercury base pairs, while allowing for up to three silver ions in each base pair (Figure 5). By contrast, the 6-amino-5-nitropyridin-2-one dZ:dZ base pair does not bind any metal ions at neutral pH (all the standard transition metals have been assayed), while dT:dZ and dU:dZ mismpairs each bind mercury with high affinity. This fills a critical design need for our metal pairing language: we have now identified a DNA letter that can only bind silver (dS), a pair which can only bind mercury (dT:dZ), and a homopair which cannot bind any metal at all (dZ:dZ).

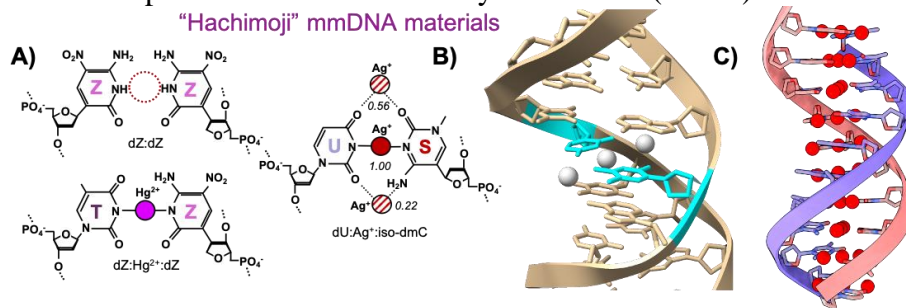


**Fig. 5:** Hachimoji, 8-letter DNA pairing. **A)** The dZ:dZ homopair does not bind any metals at neutral pH. By contrast, dU:dZ and dT:dZ mismpairs bind mercury ions with high affinity. The dS

(isocytosine) nucleobase has a high affinity for silver, and in conjunction with uracil binds up to three silver ions per base pair. **B)** Structure determination of the three-ion  $\text{dU}:\text{Ag}^+:\text{dS}$  base pair from a self-assembling DNA triangle crystal. **C)** Proposed scheme of a nanowire consisting entirely of the  $\text{dU}:\text{Ag}^+:\text{dS}$  base pair.

## References

1 Y. Wang, Y. Wang, X. Zheng, E. Ducrot, M. G. Lee, G. R. Yi, M. Weck, D. J. Pine, *J. Am. Chem. Soc.* **2015**, *137*, 10760-10766; Y. Wang, Y. Wang, X. Zheng, E. Ducrot, J. S. Yodh, M. Weck, D. J. Pine, *Nat. Commun.* **2015**, *6*, 7253; E. Ducrot, M. He, G. R. Yi, D. J. Pine, *Nat. Mater.* **2017**, *16*, 652-657; Y. Wang, I. C. Jenkins, J. T. McGinley, T. Sinno, J. C. Crocker, *Nat. Commun.* **2017**, *8*, 14173.

2. Yehl, Kevin, Andrew Mugler, Skanda Vivek, Yang Liu, Yun Zhang, Mengzhen Fan, Eric R. Weeks, and Khalid Salaita. "High-speed DNA-based rolling motors powered by RNase H." *Nature nanotechnology* 11, no. 2 (2016): 184-190.

3. Zion, Matan Yah Ben, Xiaojin He, Corinna C. Maass, Ruojie Sha, Nadrian C. Seeman, and Paul M. Chaikin. "Self-assembled three-dimensional chiral colloidal architecture." *Science* 358, no. 6363 (2017): 633-636.

#### **Publications 2020 -2021**

1."Quantifying Patterns in Optical Micrographs of One- and Two-Dimensional Anisotropic Particle Assemblies" Veronica Grebe, Mingzhu Liu and Marcus Weck\* *Soft Matter* **2020**, *16*, 10900-10909 (DOI: 10.1039/D0SM01692F).

2."Tunable Assembly of Hybrid Colloids Induced by Regioselective Depletion" Mingzhu Liu, Xiaolong Zheng, Veronica Grebe, David J. Pine and Marcus Weck\* *Nat. Mater.* **2020**, *19*, 1354-1361 (DOI: 10.1038/s41563-020-0744-2).

3. Seeman, Nadrian C. "DNA Nanotechnology at 40." (2020): 1477-1478.  
<https://doi.org/10.1021/acs.nanolett.0c00325>

4. Oh, Joon Suk, Gi-Ra Yi, and David J. Pine. "Reconfigurable Transitions between One-and Two-Dimensional Structures with Bifunctional DNA-Coated Janus Colloids." *ACS nano* 14, no. 11 (2020): 15786-15792. <https://doi.org/10.1021/acsnano.0c06846>

5. Oh, Joon Suk, Gi-Ra Yi, and David J. Pine. "Reconfigurable Self-Assembly and Kinetic Control of Multiprogrammed DNA-Coated Particles." *ACS nano* 14, no. 4 (2020): 4595-4600. <https://dx.doi.org/10.1021/acsnano.0c00164>

6. Oh, Joon Suk, Mingxin He, Gi-Ra Yi, and David J. Pine. "High-density DNA coatings on carboxylated colloids by DMTMM-and azide-mediated coupling reactions." *Langmuir* 36, no. 13 (2020): 3583-3589. <https://doi.org/10.1021/acs.langmuir.9b03386>

7. Zion, Matan Yah Ben, Yaelin Caba, Ruojie Sha, Nadrian C. Seeman, and Paul M. Chaikin. "Mix and match—a versatile equilibrium approach for hybrid colloidal synthesis." *Soft matter* 16, no. 18 (2020): 4358-4365. DOI: [10.1039/D0SM00202J](https://doi.org/10.1039/D0SM00202J) (Communication) *Soft Matter*, **2020**, *16*, 4358-4365

8. Oh, Joon Suk, Gi-Ra Yi, and David J. Pine. "Photo-printing of faceted DNA patchy particles." *Proceedings of the National Academy of Sciences* 117, no. 20 (2020): 10645-10653. [www.pnas.org/cgi/doi/10.1073/pnas.1918504117](http://www.pnas.org/cgi/doi/10.1073/pnas.1918504117)
9. Liu, Mingzhu, Fangyuan Dong, Nicolle S. Jackson, Michael D. Ward, and Marcus Weck. "Customized chiral colloids." *Journal of the American Chemical Society* 142, no. 39 (2020): 16528-16532. <https://doi.org/10.1021/jacs.0c07315>
10. "Two-Dimensional (2D) or Quasi-2D Superstructures from DNA-Coated Colloidal Particles" Mingzhu Liu, Xiaolong Zheng, Veronica Grebe, Mingxin He, David J Pine and Marcus Weck\* *Angew. Chem. Int. Ed.* **2021**, 60, 5744-5748 (DOI: [10.1002/anie.202014045](https://doi.org/10.1002/anie.202014045)).
11. Zhu, Guolong, Mark Hannel, Ruojie Sha, Feng Zhou, Matan Yah Ben Zion, Yin Zhang, Kyle Bishop, David Grier, Nadrian Seeman, and Paul Chaikin. "Microchemomechanical devices using DNA hybridization." *Proceedings of the National Academy of Sciences* 118, no. 21 (2021). <https://doi.org/10.1073/pnas.2023508118>

## Design Principles of Biomolecular Metamaterials

Jong Hyun Choi, Purdue University

### Program Scope

Architected metamaterials are engineered artificial systems with mechanical properties defined by their geometric structures, exhibiting unique auxetic behaviors that are distinct and different from those of regular materials. For example, mechanical metamaterials have negative Poisson's ratios and enhanced toughness and shear resistance.<sup>1</sup> The majority of such metamaterials are constructed by top-down approaches and macroscopic with unit cells of microns or larger.<sup>2</sup> There are also molecular auxetics including natural crystals which are not designable.<sup>1</sup> There is a wide gap in length scale of well-defined auxetic units, which may be addressed by biomolecular self-assembly. The overarching goal of this project is to (1) construct auxetic nanostructures from DNA, (2) understand their mechanics, and (3) develop design principles. We use self-assembled DNA origami to create auxetic nanomaterials with programmability and structural diversity. Our approach demonstrates several auxetic designs using DNA origami from periodic geometries to finite deployable structures. We aim to investigate their structural properties and deformation behaviors under external loading. From elasticity theory, we provide fundamental requirements for designing auxetic DNA metamaterials.

### Recent Progress

#### 1. Demonstrating auxetic nanostructures from DNA

We constructed several 2D auxetic nanostructures using wireframe DNA origami. Each DNA origami wireframe is constructed with edges and multi-arm joints at vertices. Few dsDNA helices form an edge, while ssDNA segments are used for the joint. dsDNA has two orders of magnitude greater modulus than ssDNA. Thus, dsDNA provides the rigidity in edges for overall designed geometries. ssDNA based joints have flexibility needed for structural deformation. We constructed periodic geometries, including re-entrant honeycomb, re-entrant triangle, and rotating square, and finite deployable structures. Figure 1 shows re-entrant honeycombs made of a single DNA origami. The design includes four intact unit cells (shown in black in (a) and (b)). To enable structural deformation, 'jack' edges shown in red are also included. The structures can change the conformation by modulating the length of the jack. We characterized the designed 2D DNA structures with AFM imaging. To complement the experiment, we performed coarse-grained molecular dynamics (MD) simulations with oxDNA, an open-source computational platform. Both experiment and

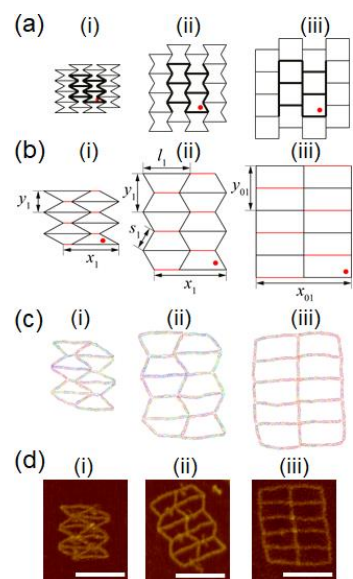


**Figure 1. Re-entrant honeycomb.** (a) Periodic geometries. (b) Designs for DNA origami. (c) MD simulation results. (d) AFM images. Scale bar = 100 nm.

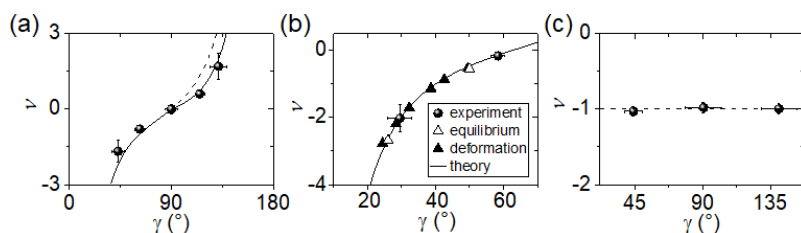


**Figure 2.** Poisson's ratio  $\nu$  of (a) re-entrant honeycomb, (b) re-entrant triangle, and (c) rotating square as a function of angle  $\gamma$  indicated as red dots in Fig. 1(b). Objects represents experimental or computational data, while the lines indicate theoretical predictions.

computation results closely follow the design. Similarly, we also demonstrated the re-entrant triangle and rotating square.

We investigated the Poisson's ratio ( $\nu$ ) of the re-entrant honeycomb, re-entrant triangle, and rotating square (Fig. 2).

Here the objects represent experimental or computational data, while solid or dashed lines indicate theoretical predictions. The auxetic DNA architectures all demonstrate negative Poisson's ratios as designed. Both re-entrant structures are asymmetric, thus their  $\nu$  varies from 0 to negative  $\infty$  (when approaching  $\gamma = 0^\circ$ ). The rotating square has a uniform  $\nu = -1$  due to its centrosymmetric design. Note that regular honeycomb structures ( $\gamma > 0^\circ$ ) in (a) shows positive  $\nu$ , as expected. Ideally, mechanical behaviors of metamaterials are determined by the designed geometry. We theoretically modelled our DNA structures assuming that edges are infinitely rigid and joints are infinitely flexible, which we termed *infinite* model. This approach provides a good estimation of Poisson's ratio vs. conformation as shown in Fig. 2.

We also explored deployable nanostructures – finite auxetic geometries that preserve their overall shapes during expansion and contraction. We constructed a deployable nanoscale flight ring, inspired by the Hoberman sphere, using wireframe DNA origami. Figure 3(a)-(f) shows the design process: conversion of 3D Hoberman sphere to 2D geometry, simplification, and wireframe designs. Three jack edges were also included which are shown in black in (f). MD simulation and AFM imaging results show open (left) and closed (right) structures in detail. Both experiment and simulation confirm  $\nu = -2.0$  and  $-1.67$ , respectively. The topology of the DNA flight ring is a trefoil knot.

**2. Elucidating mechanical behaviors under external loading**

We studied deformation behaviors of the auxetic DNA under external loads experimentally and computationally. Since the origami nanostructures are too small to apply external mechanical forces directly and accurately, we used two-step DNA reactions (toehold-mediated strand displacement and reannealing) to modulate the length of the jack edges in our experiment. This chemical loading resulted in reconfiguration of the entire structure, either expansion or shrinkage, as shown in Fig. 3(i)-(j).

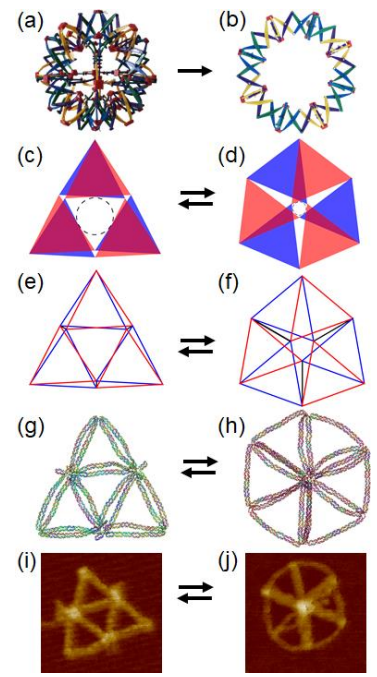


**Figure 3. Hoberman flight ring.** (a) 3D Hoberman sphere. (b) 2D version. Simplified designs of (c) open and (d) closed structures. (e)-(f) Wireframe designs. (g)-(h) MD simulations. (i)-(j) AFM data.

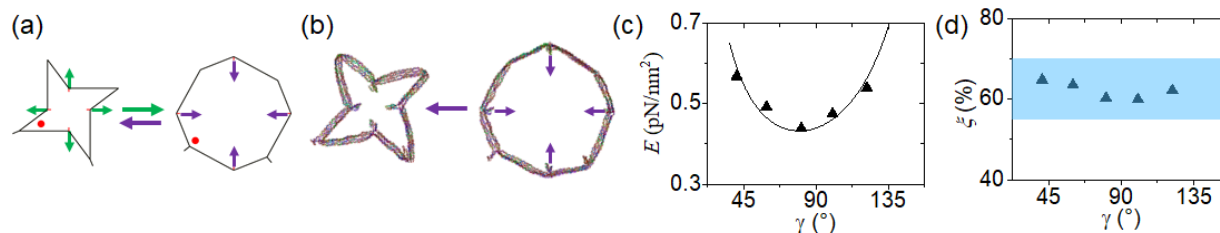


**Figure 4. Rotating square.** (a) Design and (b) MD simulations of mechanical deformation. (c) Young's modulus  $E$  as a function of the angle  $\gamma$  (denoted as red dot in (a), i.e., conformation). (d) Stretch level  $\xi$  of ssDNA joint.

In parallel, we performed mechanical deformations using MD simulations, where external forces were applied directly on the origami structures. In the equilibrium structure, the jack edges were cut off to free up space which was subsequently subject to loading (Fig. 4a). In oxDNA, we used the moving harmonic trap to pull the jack residues until the structure reaches another desired conformation (Fig. 4b). During the deformation, forces and displacements were recorded and converted into stress-strain, from which Young's modulus  $E$  was calculated (Fig. 4c, triangles). The computational results show the angle dependence, and  $E$  is on the order of few pN/nm<sup>2</sup>, comparable with that of ssDNA. This is expected in the cellular structures, due to ssDNA at the joints, serving as the determinant of  $E$ .

To understand chemical vs. mechanical deformations, we estimated the deformation forces by considering the free energy change ( $\Delta G$ ) and the displacement. The average force per jack edge for reconfiguring the re-entrant triangle in our experiment was estimated to be  $\sim 55$  pN. Since the free energy change is the maximum driving potential for structural transformation, this should be the upper limit of the force. In the computational studies, the displacements were caused directly by the applied forces. The calculated force ( $\sim 21$  pN) was the minimum needed for mechanical deformation, thus it is smaller than the force associated with chemical deformation. Similarly, the chemical and mechanical forces for the rotating square were approximately 72 and 35 pN, which are the upper and lower limits, respectively.

### 3. Developing mechanics-based design guidelines

While the infinite model is useful for designing auxetic DNA architectures, it does not provide detailed information on actual mechanical behaviors. For example, Young's modulus varies with conformation (or angle) as shown in Fig. 4c, but the model does not capture the behavior. We thus developed another model that accounts for finite rigidity in edges and finite flexibility in joints (which we term *finite* model). This model includes three deformation modes, flexing ( $K_f$ ), stretching ( $K_s$ ), and hinging ( $K_h$ ), which all resemble the Hooke's law. The model predicts the angle dependence of  $E$  (curved line in Fig. 4c). The theoretical prediction is in excellent agreement with the MD calculation data. The finite model prediction also matches well for other DNA structures. Moreover, it shows that even though the components are assumed to have linear elasticity, the overall elastic properties can be nonlinear due to the complex geometry.

The finite model allowed us to study nonideal structural effects, i.e. curved edges and loose joints. We analyzed the deformation modes upon external loads. With an applied force, for example, an internal force is generated to hold the edges in place against falling apart, and flexure is observed. To suppress the flexure, we developed a design recommendation that an edge must have a thickness larger than 10% of its length to be rigid enough to avoid any significant curvature. For a joint, the structural accuracy is better maintained with a shorter ssDNA segment. If it is too short, however, it will lead to a deformation. At the same time, the joint shall have enough flexibility such that as neighboring edges are pulled around the joint upon loading, the edge curvature can be avoided. This may be achieved by adding longer ssDNA at a joint, which could also compromise the structural integrity. Considering these aspects, we developed another design recommendation that a joint must have a stretch level between 55 and 70%, which is shown as blue shade in Fig. 4d. Overall, the edges and joints must satisfy the respective design requirements, together ensuring the integrity of the auxetic DNA architectures.

### **Future Plans**

Our work will continue in all three areas outlined above. We aim to study several other auxetic designs to examine the applicability and generality of the design guidelines. Here we are interested in both 2D and 3D architectures. Their structural properties and deformation behaviors will be studied experimentally and computationally. We also plan to investigate various mechanisms for structural transformation. In particular, we are interested to explore elastic forces in addition to chemical deformation mechanisms. Finally, we will explore additional characterization methods such as optical and other analytical measurements to visualize and study assembled structures and transformations.

### **References**

1. K. E. Evans, A. Alderson, *Advanced Materials*, 12, 617-628 (2000).
2. J.H. Lee, J.P. Singer, E.L. Thomas, *Advanced Materials*, 24, 4782-4810 (2012).

### **Publications supported by DOE grant**

- R. Li, H. Chen, and J.H. Choi, Auxetic Two-Dimensional Nanostructures from DNA, *Angewandte Chemie International Edition*, 60, 7165-7173 (2021)
- R. Li, H. Chen, and J.H. Choi, Topological Assembly of a Deployable Hoberman Flight Ring from DNA, *Small*, 17, 2007069 (2021)
- R. Li, H. Chen, H. Lee, and J.H. Choi, Elucidating the Mechanical Energy for Cyclization of a DNA Origami Tile, *Applied Sciences*, 11, 2357 (2021)
- R. Li, H. Chen, H. Lee, and J.H. Choi, Conformational Control of DNA Origami by DNA Oligomers, Intercalators and UV Light, *Methods and Protocols*, 4, 38 (2021)
- H. Qiu, F. Li, Y. Du, R. Li, J.Y. Hyun, S.Y. Lee, and J.H. Choi, Programmable Aggregation of Artificial Cells with DNA Signals, *ACS Synthetic Biology*, 10, 1268-1276 (2021)

## Energy-Efficient Self-Organization and Swarm Behavior in Active Matter

Jerome Delhommelle, Dept. of Chemistry, University of North Dakota

Paul Chaikin, Dept. of Physics, New York University

Stefano Sacanna, Mark Tuckerman, Dept. of Chemistry, New York University

### Program Scope

Living systems have the unique ability to form hierarchical assemblies, in which individual constituents can perform tasks cooperatively and emergently. Harnessing these properties is a long-standing challenge for the rational design of dynamic materials, that respond to their environment, communicate with each other, and undergo a rapid, reversible, assembly through the transduction of energy. In this project, we develop a combined experimental, computational, theoretical and Machine Learning framework to shed light on the physical underpinnings of these processes and program the assembly of smart active materials.

### Recent Progress

*Directed assembly and motion of active clusters via external stimuli*

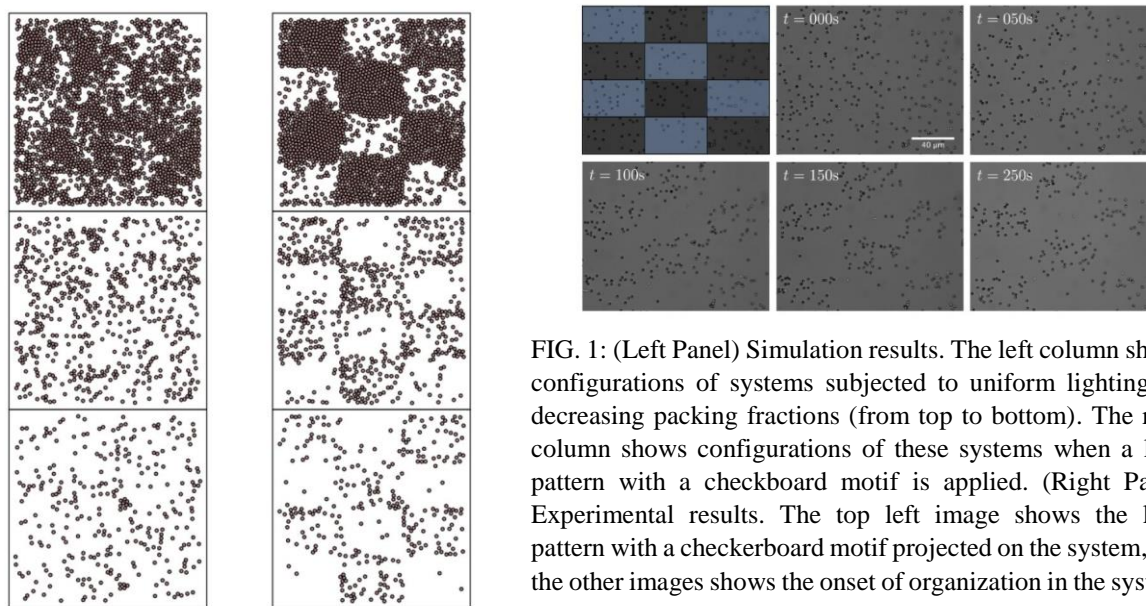


FIG. 1: (Left Panel) Simulation results. The left column shows configurations of systems subjected to uniform lighting for decreasing packing fractions (from top to bottom). The right column shows configurations of these systems when a light pattern with a checkerboard motif is applied. (Right Panel) Experimental results. The top left image shows the light pattern with a checkerboard motif projected on the system, and the other images show the onset of organization in the system.

During the past grant period, we have studied the effect of light patterns on 2D Brownian microswimmers, with a light-activated self-propulsion mechanism, through a combined experimental-computational approach. To this end, we switch off the light in regions of space in which the particles become passive and keep the light on in the rest of the system, leaving all other particles active. This allows us to form particle clusters under conditions for which phase separation is not observed with uniform lighting, and to control the shape of the cluster to match a

specific light pattern. Furthermore, we identify the threshold values for the Peclet number and run length beyond which the application of a specific light pattern promotes the formation of disk-shaped clusters. Modifying the light pattern, we show that, under the same conditions, we can achieve the formation of bubbles, through the inversion of the light pattern, or of strips, through the design of specific light patterns. Finally, through the application of light patterns with a checkerboard motif, we show that the same principles apply over a wide range of packing fractions. Fig. 1 shows a comparison between simulations and experiments. These protocols suggest new ways of inducing phase separation and controlling the morphology of the incipient new phase in these fascinating systems. We then control the motion of particles clusters in the fluid through the application of dynamic light patterns. This suggests that the formation, as well as the motion, of particle clusters can be induced and controlled through the application of specific spatiotemporal clusters of arbitrary shapes and dimensions for applications in soft matter microrobotics.

### *Assembly control through the design of novel active particles*

We developed colloidal rods with tunable aspect ratio in bulk, by sol-gel reaction of tetraethylorthosilicate (TEOS) inside water droplets containing polyvinylpyrrolidone (PVP) and ammonia in pentanol. These “reactive” water droplets are attached to preexisting colloidal seeds and used to grow well defined anisotropic particles (Fig. 2A). Specifically, we used photocatalytic seeds such as  $\text{TiO}_2$  and  $\alpha\text{-Fe}_2\text{O}_3$  particles to fabricate composite matchstick-like colloids with tunable aspect ratio and composition (Fig. 2B). By destabilizing the growing end of the rods during synthesis we promote coalescence events between reactive droplets, resulting in termination reactions where rods connect to form a single unit with catalysts at both ends. While we obtained promising results using hematite catalysts, more work is necessary for a good control of the coalescence step and obtain monodispersed samples. Moving forward, we plan to mix different rod suspensions and carefully time their coalescence to achieve full control on both particle geometry and composition (Fig. 2C). The propulsion mechanism of the rod-like swimmers, based on self-diffusiophoresis, requires light to catalyze the breakdown of a chemical fuel added to the colloidal suspension. We performed preliminary tests using the same catalyst-fuel combination as for spherical swimmers [1]. We anticipate that rods with one catalyst will behave as polar swimmers, while colloidal particles with two catalysts will be dipolar swimmers. Of particular interest will be rods with distinct catalysts, that respond to different wavelengths. Controlling light will enable us to continuously switch on and off the two catalytic ends and thus dynamically switch the system between polar and dipolar swimmers. This unique feature will enable us to seamlessly control the particles swimming behaviors of in space and time.

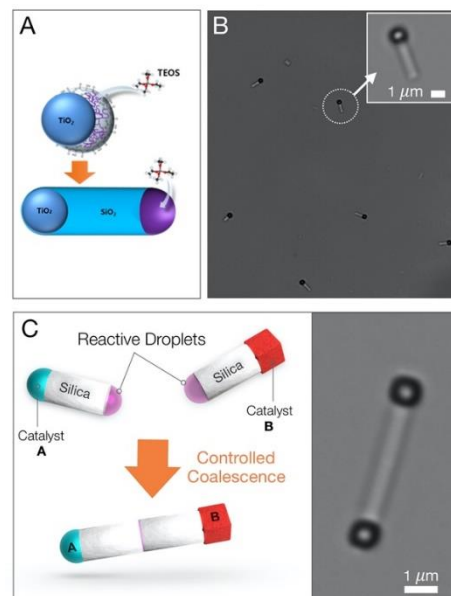


FIG. 2: Colloidal silica rods with photocatalysts attached at either one or both ends. (A) mechanism of anisotropic silica growth seeded by a  $\text{TiO}_2$  particle (B) matchstick-like colloids synthesized in bulk using hematite seeds (C) left: formation of bi-functional rods via controlled coalescence. *Right*: dipolar rod-like swimmer with hematite catalysts on both ends.

### Local Entropy Production

The signature of living systems and nonequilibrium phenomena is the production of entropy as identified by the violation of detailed balance and the presence of processes that are not time reversible. Recently Nardini et al. [3] have introduced the concept of local entropy production to see what parts of a complex dynamical are most effective in producing entropy. Presumably these are the places where work can most readily be extracted from the system. We have developed a technique based on information theory and data compression which allows us to calculate the local entropy production from both dynamical models and from experiments.

According to stochastic thermodynamics the entropy production can be obtained by calculating

$$\dot{S} = k_B \lim_{\tau \rightarrow \infty} \frac{1}{\tau} \left\langle \ln \frac{p(x)}{p^R(x)} \right\rangle$$

where  $p(x)$  is the probability of a forward trajectory and  $p^R(x)$  is the probability of the time reversed trajectory. This is easily associated with the Kullback-Leibler divergence from information theory with  $q(x) = p^R(x)$  which is the cross entropy  $H(p|q)$  minus the entropy.

$$D(p||q) = \sum_x p(x) \log \frac{p(x)}{q(x)} = H(p|q) - H(p)$$

Entropies can be computed from data compression by using, e.g. the Lempel-Ziv or Ziv–Merhav algorithms, to compress the second half of a string by the first half,  $c(x_1|x_2)$ . The K-L divergence then relates to  $c(x_1|x_2^R) - c(x_1|x_2)$ . To proceed we develop a method to obtain a string representing the local dynamics of a system. We define an overlay grid on our active Brownian particle, ABP, simulation such that no two particles occupy the same box. For each grid box, e.g. the red one in Fig. 3a, we use four squares aligned as shown from which we record an occupation number 1-16. Our string is the time sequence of numbers. Using a theoretical model with a scalar density field, Nardini et al. [3] find that the only sizable entropy production occurs at the boundary between the dense cluster and the gas phase. Using the 2x2 arrangement of squares on a particulate model we obtain a similar result in Fig. 3b. However, we can investigate more degrees of freedom, for example from particle collisions in the gas that also add to the entropy production, if we use 3x3 or 4x4 boxes.

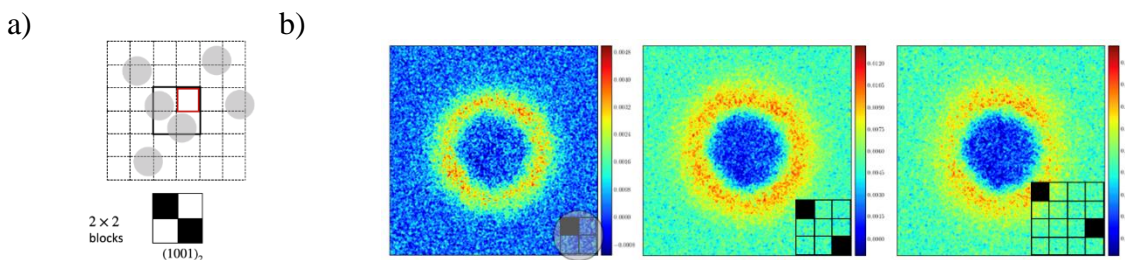


FIG. 3. a) Grid superposed on a frame from a simulation of ABP's. b) Entropy production computed from data compression/information theory for MIPS. The left most figure indicates a predominance of entropy production at the boundary of the cluster similar to [3]. As more degrees of freedom are included, we see that considerable entropy is produced by collisions in the gas phase.

## Fuel-free swimmers

During the past grant period we have been investigating a new type of microscale swimmer which is light activated but is “fuel-free” and has the potential of swimming in three dimensions instead of on a surface. The swimmer consists of a light absorbing colloidal particle attached to an oil droplet as illustrated in Fig. 4a. When heated with a broad laser beam the colloidal particle heats up and produces a temperature gradient across the droplet. The composite swimmer then propels in the direction from the colloidal bead to the droplet. The initial idea was to use the temperature gradient to induce Marangoni flows on the droplet. The hotter part of the droplet surface (near the light absorbing bead) has a higher surface tension than the colder part. This pulls the surface toward the bead and induces flow both inside and outside the droplet propelling the swimmer forward. The surfactant at the droplet water interface is only soluble in the oil. It dissociates from the hot side and recondenses on the cold side of the droplet following the internal flow and assuring that the surfactant is not lost to the exterior water phase. The swimmer is effectively powered by a heat engine and no chemical fuel is used so the swimmer can swim forever, as long as the light is on. We are still investigating whether the driving force is Marangoni or the more elusive Soret effect, thermophoresis, or a combination of the two. The colloid is either a purchased magnetic dynabead or a magnetic hematite “peanut” prepared by the Sacanna group so that the swimming direction can be controlled with magnetic fields (see Fig. 4b). Preliminary experiments indicate that this system undergoes MIPS and is also able to swim in 3D.

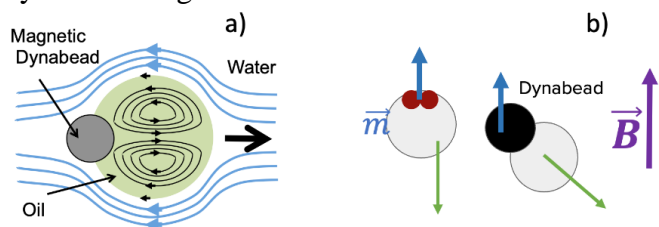


FIG. 4. a) We make a Marangoni swimmer by attaching a light absorbing particle to an oil droplet. The particle induces a temperature gradient across the droplet inducing a surface tension gradient and an internal and external flow. b) The absorbing particles are magnetic allowing directional control of the swimmers

## Future Plans

- Generalization of assembly principles through external stimuli, such as light patterns magnetic field and shear
- Development of micron sized colloidal swimmers with either polar or dipolar character for the assembly of high-density 2D samples, and exploration of more complex particles geometries (e.g., banana-like [2] swimmers) to study how shape affects motility.
- Comparison between entropy production calculated via CID and through the fluctuation theorem.
- Algorithmic development for rigid body and multi-bead swimmers and spinners

## References

- [1] Living Crystals of Light Activated Colloidal Surfers, J. Palacci, S. Sacanna, A. P. Steinberg, D.J. Pine, P.M. Chaikin, *Science* 339, 936-940 (2013)
- [2] Shaping colloidal bananas to reveal biaxial, splay-bend nematic, and smectic phases, C. Fernández-Rico, M. Chiappini, T. Yanagishima, H. de Sousa, D. G.A.L. Aarts, M. Dijkstra, R. P.A. Dullens, *Science* 369, 950-955 (2020)

[3] C. Nardini, E. Fodor, E. Tjhung, F. van Wijland, J. Tailleur, and M. E. Cates, Entropy production in field theories without time-reversal symmetry: quantifying the non-equilibrium character of active matter, *Phys. Rev. X* 7, 021007 (2017)

### **Publications 2020-2021**

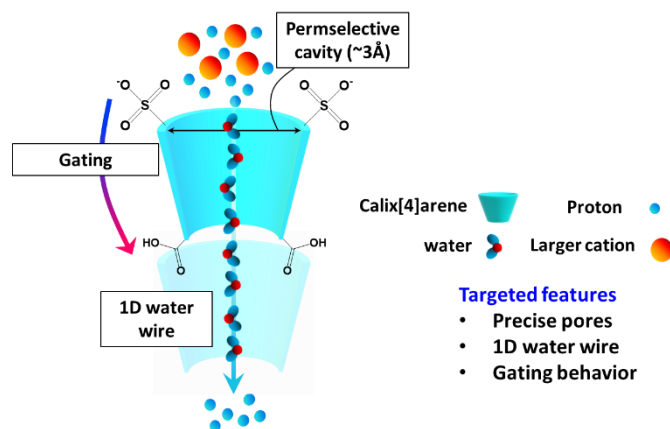
1. Entropy production in model colloidal suspensions under shear via the fluctuation theorem. C. Desgranges and J. Delhommelle. *J. Chem. Phys.* 153, 224113 (2020)
2. Play. Pause. Rewind. Measuring local entropy production and extractable work in active matter Buming Guo, Sunghan Ro, Aaron Shih, Trung V. Phan, Robert H. Austin, Stefano Martiniani, Dov Levine, and Paul M. Chaikin, <https://arxiv.org/abs/2105.12707> (2021)
3. Microswimmers under the spotlight: interplay between active and passive agents. C. Desgranges, M. Ferrari, P. M. Chaikin, S. Sacanna, M. Tuckerman, J. Delhommelle, in preparation (2021)
4. Directed assembly and motions of patterns in active matter. C. Desgranges, M. Ferrari, P. M. Chaikin, S. Sacanna, M. Tuckerman, J. Delhommelle, in preparation (2021)
5. Cooperation in a fluid swarm of fuel-free microswimmers, M. Yah Ben-Zion, A. Modin, Y. Caba and P. M. Chaikin, <https://arxiv.org/abs/2012.15087> (2021)

## Porin-Inspired Ionomers with sub-nm Gated Ion Channels for High Ion Conductivity and Selectivity

Shudipto Konika Dishari, University of Nebraska-Lincoln

### Program Scope

Bringing the capabilities of natural living systems into synthetic polymeric materials design approaches as well as controlling and understanding the molecular level self-assembly<sup>1</sup> can inform and guide the design principles of next-generation energy technologies. In living systems, porins self-assemble within biological membranes and are responsible for controlled transport of water and ions across living cells leveraging gating principles.<sup>2</sup> Inspired by nature, this DOE Early CAREER project aims to achieve molecular level control over ion conduction pathways by bringing the capabilities of biological gated ion channels into the design of a novel class of ion-conducting molecules (ionomers) containing hollow, macrocyclic repeat units (3-5 Å) (Figure 1). These sub-nm-sized cavities (unlike conventional ionomeric systems having > 1 nm-sized ionic domains) can leverage the 1D water wire effect to boost the ionic conductivity. Even when the phase segregation is hindered (happens in sub- $\mu\text{m}$  thick films of conventional ionomers at electrode interfaces),<sup>3,4,5</sup> these ionomers can still maintain molecular-level ionic conduction across single macrocyclic repeat units within ionomer chains. This way, they can bypass the absolute need for phase segregation to conduct ions, a must for conventional ionomers. By understanding and guiding the nanoscale self-assembly of calix[4]arene-containing ionomers in solution and solid-state, long-range ion conduction channels can also be created to achieve better ionic conduction even under thin-film confinement. The narrow pores of these macrocyclic units can not only act like size-exclusive ion transporters, but also act like voltage-responsive gates and selective ion transporters/blockers when asymmetric charge distribution is created at the upper and lower rims of these macrocycles. By hierarchical synthesis of an array of model, gated, calix[4]arene-based monomers and oligomers, and inducing predictive, but structure-driven ionomer alignment and self-assembly, this project aims to unravel new ways to gain unprecedented control over ionic conductivity and selective ion transport at the molecular level.



### Recent Progress

In the last 2 years, a number of calix[4]arene-based ion-conducting monomers and oligomers

having calix[4]arene and biphenyl-based repeat units were synthesized in which gating functionalities were imparted and ion exchange capacities (IECs) were varied. The dibromo derivatives of calix[4]arene-based monomers were Suzuki cross-coupled to boronic acid-functionalized biphenyl monomers to yield neutral calix monomers/oligomers which were then sulfonated using chlorosulfonic acid. Proton conductivity, nanoscale structure, and voltage gating behavior of these ionomers were studied in thin films and membranes. Out of them, the properties of two representative ionomers ( $n=1$  (calix mono),  $n=7$  (calix oligo), Figure 2a) are shown here. Both ionomers have 2  $-SO_3H$  groups at the upper rim of calix[4]arene units, while no  $-SO_3H$  groups at the lower rim which created asymmetric charge distribution across the macrocycle. The biphenyl units, alternating with calix[4]arene units, were also sulfonated. These ionomers made nice and smooth films within the thickness range ( $\sim 15$ -100 nm) comparable to the catalyst-binding ionomer layer over fuel cell electrodes.

In  $\leq 100$  nm thick films, the proton conductivity of calix oligo was up to 8 times higher than the current benchmark ionomer Nafion at 85% RH (Figure 2c), while it was 1-2 orders of magnitude higher than Nafion at 20-25% RH (Figure 2d). Even the monomeric ionomers (like calix mono) showed conductivity better than Nafion at all %RHs. Such unprecedented improvement in the thin film ionic conductivity was attributed to the 1D, ordered water wires formed through sub-nm sized macrocyclic cavities of calix mono/oligo. Poor ionic conductivity in Nafion thin films typically limits the ion

transport within the catalyst binder layer of electrodes and slows down the electrochemical reactions in fuel cells. If such macrocycle-based ionomer design approaches are adopted, interfacial ion transport limitations can be effectively addressed.

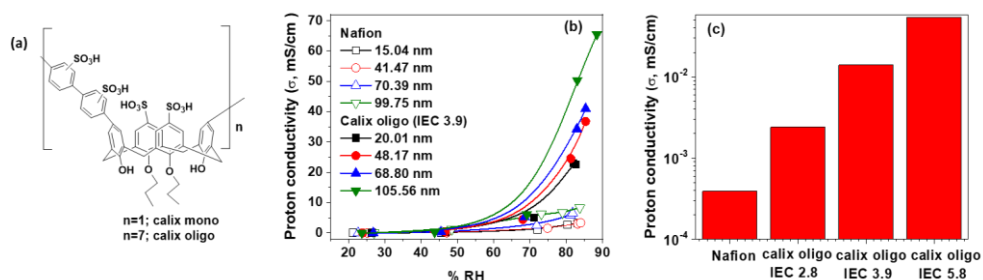


**Figure 2.** (a) Chemical structures of representative macrocyclic calix[4]arene-based oligomeric ionomers (calix mono, calix oligo). (b) Proton conductivity of calix oligo (IEC 3.9) and Nafion films at different thicknesses as a function of %RH. (c) proton conductivity of calix oligo and Nafion films ( $\sim 15$  nm) at 20-25% RH.

In addition to the molecular level ionic conduction, macrocycle-based ionomers can self-assemble and produce long-range proton conduction pathways (Figure 3) as seen from AFM (Figure 3a, b) and GISAXS (Figure 3c) measurements. While Nafion films were almost featureless (Figure 3a), calix oligo films formed ellipsoidal features which was in agreement with self-assembly studies on calix[4]arene-based monomers.<sup>6,7</sup> Molecular dynamics simulations<sup>8</sup> suggested that calix[n]arene-based molecules can form multiple bilayer-like arrangements where the calix[4]arene units of neighboring layers can sit in an up-and-down fashion to bring similar functional groups at the lower rims close to each other. Such orientation can be favorable for the

formation of ion-conduction pathways as supported by GISAXS. Calix oligo film showed two out-of-plane scattering peaks ( $q \sim 4.02, 6.46 \text{ nm}^{-1}$ ). The d-spacing of  $\sim 1.56 \text{ nm}$  for the first scattering peak could be attributed to the ionic domains through macrocyclic cavities of calix[4]arene repeat units as this spacing was similar to the distance between two macrocyclic units, spaced by a biphenyl unit, in a calix oligo chain. The other domain spacing ( $\sim 0.97 \text{ nm}$ ) may correspond to the gap between two consecutive lateral proton hopping pathways since this gap was equivalent to the width of one bilayer (calculated as  $\sim 1.10 \text{ nm}$ ). These evidence supported our hypothesis on multi-length scale pathways for ionic conduction through self-assembled features of calix oligo films.

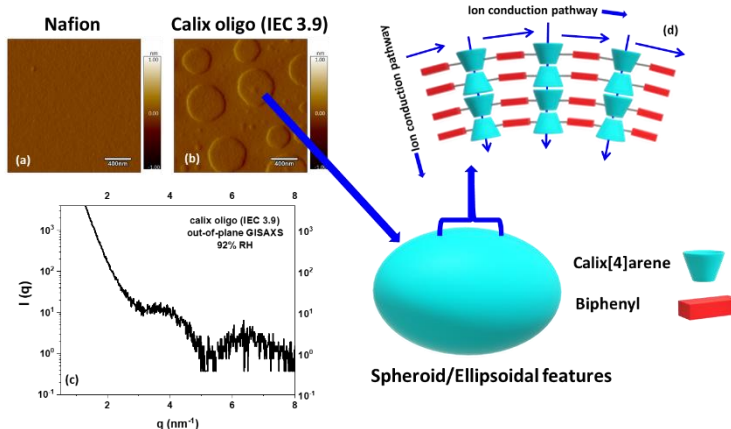


**Figure 3.** AFM amplitude images of Nafion (a) and calix oligo (IEC 3.9) (b) films. (c) Out-of-plane GISAXS of  $\sim 140 \text{ nm}$  thick calix oligo (IEC 3.9) film at 92% RH. (d) Proposed self-assembly modes and ionic conduction pathways within calix oligo films based on AFM and GISAXS data.

Having trace amounts of calix mono or calix-oligo (Nafion: calix oligo = 1:0.05 (w/w)) within Nafion membrane matrices made the proton permeation through bulk composite membranes much faster than pure Nafion membrane (Figure 4a). This again demonstrated the potential of these ionomers to create unique and efficient proton conduction pathways. Calix oligo also acted like ionic diodes (like nature-mimicking and Janus systems<sup>9,10</sup>) and showed different ionic currents at forward and reverse bias voltages. The voltage gating behavior was apparent for Nafion-calix oligo composite membranes showing ionic rectification ratio ( $|I_{+2V}/I_{-2V}|$ ) values of  $\sim 2.21$  (IEC 3.9) and  $\sim 4.55$  (IEC 5.8) (Figure 4b). At forward bias, the applied electric field drove the transport of  $\text{K}^+$  ions along the axes of calix[4]arene units from upper-to lower rim side of calix[4]arene units. The  $-\text{SO}_3^-$  groups at the upper rim of calix[4]arene units also facilitated the  $\text{K}^+$  ion transport. At the same time,  $\text{Cl}^-$  ions were transported in the reverse direction. On the other hand, at reverse bias,  $\text{K}^+$  ions got transported from lower to upper-rim side, but  $\text{Cl}^-$  ions were blocked by anionic  $-\text{SO}_3^-$  groups at the upper rims of the macrocycles. This led

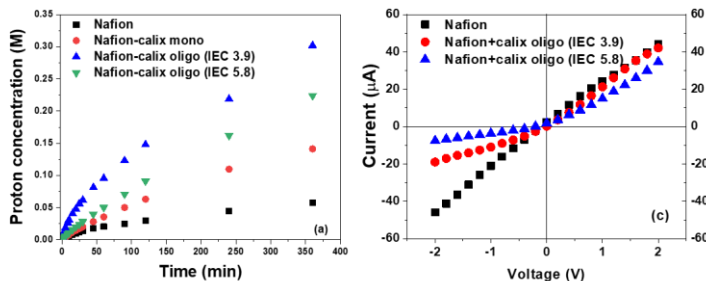


**Figure 4.** (a) Time-dependent proton permeation (measured as proton concentration in the receiving compartment) through pure Nafion and Nafion-calix mono/oligo composite membranes at 1 M HCl. (b) I-V curves of Nafion and Nafion-calix oligo (IEC 3.9, 5.8) composite membranes recorded in 0.1 M KCl in DI water.

to decrease in ionic current in reverse bias. We can, therefore, control and manipulate ion permselectivity by leveraging the gating functionalities, in addition to the size-exclusion via sub-nm molecular cavities.

## Future Plans

In coming years, the asymmetric charge distribution at the rims of macrocycles, the key to attaining voltage gating and permselectivity, will be varied continually to deeply understand the ion transport and blocking mechanisms across macrocycle-based ionomers against a range of small-to-large ions. In addition, the repeat units used in alternate to macrocyclic units will be altered to identify the conditions giving rise to distorted/well-organized self-assembly. These studies will help us to well-control the long-range connectivity of ion conduction pathways within sub- $\mu\text{m}$  thick films and guide the design principles of more practical ionomers for proton conduction at catalyst interfaces on fuel cell electrodes.

## References

- (1) Portfolio description: Biomolecular Materials, Materials Science and Engineering Division, Basic Energy Science, Department of Energy.
- (2) DeCoursey, T. E. Voltage-Gated Proton Channels: Molecular Biology, Physiology, and Pathophysiology of the HV Family. *Physiol. Rev.* **2013**, *93*, 599–652.
- (3) Kusoglu, A.; Weber, A. Z. New Insights into Perfluorinated Sulfonic-Acid Ionomers. *Chem. Rev.* **2017**, *117*, 987–1104.
- (4) Dishari, S. K.; Hickner, M. A. Confinement and Proton Transfer in Nafion Thin Films. *Macromolecules* **2013**, *46*, 413–421.
- (5) Farzin, S.; Zamani, E.; Dishari, S. K. Unraveling Depth-Specific Ionic Conduction and Stiffness Behavior across Ionomer Thin Films and Bulk Membranes. *ACS Macro Lett.* **2021**, *10*, 791–798.
- (6) Jie, K.; Zhou, Y.; Yao, Y.; Huang, F. Macrocyclic Amphiphiles. *Chem. Soc. Rev.* **2015**, *44*, 3568–3587.
- (7) Houmadi, S.; Coquie, D.; Legrand, L.; Faure, M. C.; Goldmann, M.; Reinaud, O.; Remita, S. Architecture-Controlled “SMART” Calix[6]Arene Self-Assemblies in Aqueous Solution. *Langmuir* **2007**, *23*, 4849–4855.
- (8) Martin, A. D.; Raston, C. L. Multifunctional P-Phosphonated Calixarenes. *Chem. Commun.* **2011**, *47*, 9764–9772.
- (9) Tunuguntla, R. H.; Zhang, Y.; Henley, R. Y.; Yao, Y. C.; Pham, T. A.; Wanunu, M.; Noy, A. Enhanced Water Permeability and Tunable Ion Selectivity in Subnanometer Carbon Nanotube Porins. *Science (80-. )*. **2017**, *359*, 792–796.
- (10) Yang, H. C.; Xie, Y.; Hou, J.; Cheetham, A. K.; Chen, V.; Darling, S. B. Janus Membranes: Creating Asymmetry for Energy Efficiency. *Adv. Mater.* **2018**, *30*, 1801495 (1-11).

## Publications

Dishari, S. K. Ionomers with Macrocyclic Moieties for Ion conductivity and Permselectivity. **2021** (Patent, PCT/US21/70432).

Chatterjee, S.; Zamani, E.; Farzin, S.; Obewhere O. A.; Johnson, T. J.; Dishari, S. K. Molecular-Level Control over Ionic Conduction and Ionic Current Direction by Designing Macrocyclic-based Ionomers. **2021**, submitted to *JACS Au*.

Chatterjee, S.; Zamani, E.; Farzin, S.; Dishari, S. K. Ionic Rectification Behavior of Styrene-Calix[4]arene-based Ionomers in Bulk Membranes, to be submitted.

Chatterjee, S.; Zamani, E.; Farzin, S.; Dishari, S. K. Membranes Containing Ion-conducting Calix[4]arene-based Monomers: The Role of Charge Distribution Asymmetry in Controlling Ion Permselectivity, to be submitted.

## **Microtubule-based three-dimensional active matter**

**Principle Investigator: Zvonimir Dogic, Department of Physics, University of California at Santa Barbara, Santa Barbara, CA 93106.**

**Program Scope:** Active matter is an assembly of microscopic objects, each consuming energy to generate continuous dynamics. Interactions between such animate units lead to emergent properties that are strikingly different from those found in conventional materials assembled from inanimate passive objects. The field of active matter aims to develop a theoretical framework that robustly predicts the emergence of large-scale dynamical behaviors, given elemental units of known structure dynamics and interactions. Such advances will yield new insights into non-equilibrium statistical mechanics, while also providing a powerful platform for developing synthetic materials that can more closely mimic biology and living organisms.

Several unique features of microtubule-based active matter provide a distinctive opportunity for elucidating the properties of internally-driven active matter. With these broad goals, we made several specific advances over the past two years. We have developed novel methods of driving the active dynamics with unique force-sensing motors. In turn, these have provided new insight into mechanisms by which thousands of molecular motors collectively generate mesoscopic active stresses. In a complementary effort we have created the first example of 3D active matter. Using state-of-the-art imaging techniques we have analyzed their unique topological structure and dynamics. Finally, in a major new direction, we have merged properties of active isotropic liquids with the conventional liquid-liquid phase separation to elucidate a range of intriguing non-equilibrium phenomena, ranging from self-splitting droplets to giant active interfacial fluctuations, to active wetting phenomena.

### **Recent Progress:**

*Elucidating mechanisms of active stress generation:* So far, studies of active nematics have mainly described large-scale defect-driven dynamics, while overlooking their mechanical characterization and the molecular origin of the non-equilibrium dynamics. However, active stresses are a defining feature of active matter, and understanding their properties is essential for further progress. To address this knowledge gap we developed DNA-based kinesin clusters, which can simultaneously power the non-equilibrium dynamics of active nematics while sensing and reporting the force-loads experienced by the kinesin motors. The unique features of this systems revealed two essential properties of active nematics. First, we estimated the magnitude of the average load experienced by the kinesin motors, which is comparable to their stall forces. Second, we measured the nematic order of motor clusters, which revealed the direction of the applied load. When combined, these findings suggest a new mechanism by which motors generate interfilament sliding, with crucial differences from the mechanism that has been assumed in the active matter community over the past decade.

In a complementary effort we related the large-scale dynamics of microtubule-based active nematics to the motion of the constituent filaments. We found that the extension speed of microtubule pairs is related to the molecular motor stepping speeds. We then probed the

mesoscopic flows of the dense 2D nematics, by labeling the fluid through photobleaching and by tracking the movement of individual filaments. Average nematic flows were dipolar extensile with an ATP-dependent strain rate. The microscopic motion of individual microtubules was widely distributed about this average. These measurements underline the challenge of connecting the dynamics of isolated bundles to the multi-motor and multi-filament interactions present in dense active nematics.

*Active three-dimensional liquid crystals:* In comparison to widespread ongoing work on 2D active nematics, there are essentially no studies of analogous 3D materials. However, one expects that system dimensionality critically affects the properties of equilibrium and non-equilibrium systems alike. In particular, the nature of the extended topological defects in 3D nematics is fundamentally different from the point-like singularities found in analogous 2D systems. Therefore, it is not straightforward to extend the known defect-driven dynamics of 2D active nematics to higher dimensions. Using a unique combination of state-of-the-art imaging techniques with a new system of composite active liquid crystals we measured the full spatiotemporal evolution of the nematic director field on a millimeter-scale with a single filament resolution. Using such information we extracted the structure of the defect lines and characterized the dynamics of the topological defects. When combined with theoretical modeling, such measurements led to a simple finding: the dynamics of 3D active nematics are dominated by a subfamily of topologically neutral disclination loops. These experimental findings were reinforced with numerical simulations of 3D active nematics.

*Active liquid-liquid phase separation:* By merging a polymer mixture with a model system of microtubule-based isotropic active fluids we created active liquid-liquid phase separation (LLPS). Phase separated binary polymer mixtures have an exceedingly low interfacial tensions, which allows for strong coupling of the active stresses to the interfacial deformations, a feature that is critical for the unique properties of the active-LLPS. We found that activity fundamentally alters the extensively studied dynamics of passive liquid-liquid phase separation. The active components strongly partition into one type of droplets, wherein they generate localized flows that enhance the droplet's motility. This increases the likelihood of droplets encountering each other and coalescing. Thus the average droplet size is significantly larger when compared to passive samples that lack the chemical fuel. Intriguingly, at late stages of phase separation, large droplets start to exhibit deviations from the surface tension minimizing circular shapes.

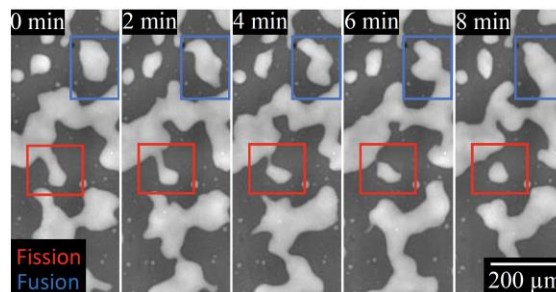


**Fig. 1. Droplet dynamics in active emulsion.**  
The finite size droplet size is maintained by droplet fusion and fission events indicated with blue and red squares.

Increasing the motor cluster concentration leads to the emergence of new processes that have no equilibrium analogs. Initially, increased activity increases the droplet motility, and the growth rate.

However, as the droplet gets larger their interfaces exhibit significant deformations due to the strong coupling of the active stresses to the soft interfaces. This generates droplets with distinct non-circular shapes (**Fig. 1**). The activity-driven shape distortions are strong enough to induce spontaneous droplet fission, where a mother droplet spontaneously divides into two daughter droplet fission (**Fig. 1**). In this regime, the active-LLPS attains a steady state, in which the average droplet size remains constant over time (**Fig. 4d**). The finite droplet size is maintained by continuous fusion and fission of droplets. The small droplets are highly mobile and are thus more likely to merge and increase in size. As they grow, the active stresses distort their shape leading to their spontaneous break-up. This non-equilibrium phase with finite-sized droplets is distinct from both the uniformly miscible phase and the bulk-demixed phase. We call it an *active emulsion*. Similar to conventional emulsions it maintains droplet of finite size. However, in contrast to conventional emulsions, active emulsions are surfactant-free and their droplet content is continuously exchanged and mixed.

*Active interfacial fluctuations:*

Understanding the stability of active emulsions requires a quantitative model of how active flows drive the non-equilibrium interfacial fluctuations. To quantify such fluctuations we used gravity to create bulk phase separated samples. In passive mixtures the interface exhibits thermally driven fluctuations. The magnitude of these fluctuations which are expected to be  $\sim 100$  nm, is determined by the surface tension and the sample temperature. Thus, for passive samples one observes an entirely flat interface with an optical microscope (**Fig. 2**). Adding ATP generates active stresses that deform the soft interface. A time sequence reveals that the interface deformations change on the time scale of minutes. The magnitude of the active stresses is determined by the concentration of the kinesin clusters. Consequently, the interfacial roughness increases with increasing concentration of kinesin motors (**Fig. 2**). For large motor concentrations the interface became very jagged. In this regime interfacial fluctuations are sufficiently large to be visible to the naked eye. To obtain equilibrium fluctuations that are comparable to those in active samples one would need  $\sim 10^8$  K temperature, which is clearly not attainable.

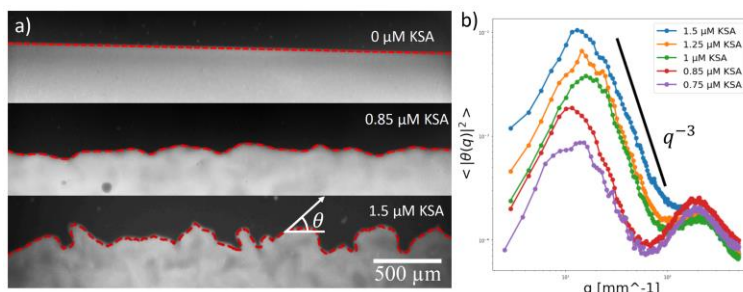


**Fig 2. Kinesin concentration controls active interfacial fluctuations.** a) Active interface configuration roughens with increasing concentration of kinesin motors. b) Fluctuation spectrum measured for different kinesin concentrations.

*Activity controlled contact angle:* In a complementary effort, we studied the contact angle that an active interface makes with a glass boundary. In the absence of chemical fuel the top phase preferentially wets the treated glass surface of the confining chamber. Correspondingly, in this regime we observed that the angle at which the interface meets the glass boundary is positive (**Fig. 3**). Unexpectedly, we found that activity influences the wetting angle. Increasing the activity decreases the magnitude of the contact angle. For high activities the contact angle switches sign

and becomes negative (**Fig. 3**). These experiments strongly suggest that activity changes the wetting angle of the active interface, but the mechanism by which activity controls the wetting angle remains unknown. Our hypothesis is that the interfacial wetting is associated with the wall-induced nematic-like alignment of the filamentous microtubules. To test this hypothesis we are developing experiments that will simultaneously visualize the microscopic structure of the active isotropic fluid and the active interface to which it is coupled.

**Future Plans:** The development of active liquid-liquid phase separation is a major advance that provides a fertile ground for numerous foundational experiments. For example, so far all experiments were carried in quasi-2D geometries. In the future, our focus will shift towards characterizing the full three-dimensional active interfaces, where internally generated flows couple more strongly to the interfacial fluctuations. Preliminary data, for instance, suggests that the active wetting transitions are significantly enhanced in such geometries. In a different direction, we are developing new methods of confining active 3D nematics and studying how point-like topological defects open up into extended disclination lines. In a bulk liquid crystal, each loop has a finite lifetime, which greatly limits the opportunity to explore how the local topology affects the dynamics of the evolving disclination line. Our goal is to create isolated loops to quantitatively characterize this poorly understood phenomenon.

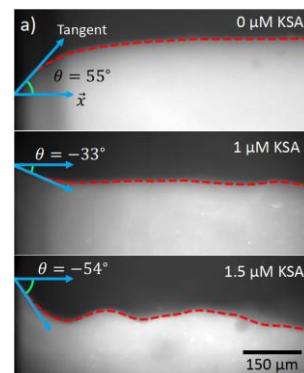


**Fig 3. Activity controlled wetting.** Top image lacks activity. Kinesin concentration increases in the bottom two images.

#### Publications which acknowledge full or partial DOE support:

1. “Active liquid crystals powered by force-sensing DNA-motor clusters,” A. M. Tayar, M. F. Hagan, Z. Dogic, *Proc. Nat. Acad. Sci.*, in press (2021)
2. “Static adhesion hysteresis in elastic structures,” E. Memet, F. Hilitski, Z. Dogic, L. Mahadevan, *Soft Matter*, **17**, 2704-2710 (2021).
3. “Machine learning active-nematic hydrodynamics,” J. Colen, M. Han, R. Zhang, S. A. Redford, L. M. Lemma, L. Morgan, P. V. Ruijgrok, R. Adkins, Z. Bryant, Z. Dogic, M. L. Gardel, J. J. de Pablo, V. Vitelli, *Proc. Nat. Acad. Sci.*, **118**, e2016708118 (2021).
4. “Topological structure and dynamics of three-dimensional active nematics,” G. Duclos, R. Adkins, D. Banerjee, M. S. E. Peterson, M. Varghese, I. Kolvin, A. Baskaran, R. A. Pelcovits, T. R. Powers, A. Baskaran, F. Toschi, M. F. Hagan, S. J. Streichan, V. Vitelli, D. A. Beller, Z. Dogic, *Science*, **367**, 1120–1124 (2020).
5. “Shear-induced gelation of self-yielding active networks,” D. A. Gagnon, C. Dessi, J. P. Berezney, R. Boros, D. T.-N. Chen, Z. Dogic, D. L. Blair, *Phys. Rev. Lett.*, **125**, 178003 (2020). [
6. "Confinement controls the bend instability of three-dimensional active liquid crystals," P. Chandrakar, M. Varghese, S. A. Aghvami, A. Baskaran, Z. Dogic, G. Duclos, *Phys. Rev. Lett.*, **125**, 257801 (2020).

## Reactive, Functional Droplets in Bio-inspired Materials and Smart Interfaces

PI: Todd Emrick

Polymer Science & Engineering Department

University of Massachusetts

Amherst, MA 01003

Email: tsemrick@mail.pse.umass.edu; phone: 413-577-1613

**Program Scope.** The scope of this project is centered on a biomolecular materials design of smart, functional droplets and their associated interfaces, drawing upon rich biological inspiration that ranges from recognition processes of living cells to macromolecular systems that work in conjunction with the body's immune response.<sup>1-3</sup> The immune system exhibits fundamentally instructive elements that are ideal for directing dynamic, responsive materials design. Consider the case of leukocytes (*i.e.*, macrophages, T cells, *etc.*) traversing the lymphatic and circulatory system to identify disease and infection, and to provide protective and healing measures *via* recognition and signaling. These and related biological processes, such as the bone-structuring action of osteoclasts (bone tissue absorbing) and osteoblasts (bone matrix secreting), inspire new materials concepts. While the biological aspects of cell signaling and response are complex, the fundamental actions—*seek, recognize, build, heal, reconfigure*—reflect materials opportunities that hinge on the translation of biological principles to simpler synthetic tools in non-biological environments. Achieving our objectives in this program requires attention to interfacial energies and principles of encapsulation that direct structures to desired locations within materials systems. *In essence, the effective translation of these fundamental biological principles to materials, such as coatings, self-healing systems, and autonomous surface-cleaning structures, is vital for advancing the energy efficiency and versatility of modern materials.*

In accord with this scope, our specific objectives include: 1) building “smart droplets” from novel polymer surfactants, inspired by conceptual designs of biology; and 2) fabricating new droplet architectures that possess unprecedented reach and functionality *via* the connection of macroscale structures to fluid interfaces. These objectives contribute to fulfilling over-arching goals of producing novel, bio-inspired synthetic polymers that engage in materials recognition, transportation, and interfacial assembly. In this way, the scope of the program is aligned with the mission of the DOE Biomolecular Materials program by emphasizing advances in 1) design and synthesis of functional, complex, multi-length scale materials; 2) incorporation of autonomous healing and regrowth processes in bio-inspired materials designs that promote energy efficiency; and 3) the preparation of materials with selective reactivity that are placed precisely at interfaces.

**Recent Progress.** Our recent progress led to the discovery of new types of polymer zwitterions that merge the design principles of biology with modern synthetic methodology. For example, as illustrated in **Figure 1**, we recently described the synthesis of sulfothetin (ST)-containing polymer zwitterions and their use as polymer surfactants that both stabilize emulsion droplets and function to capture and transport nanoparticles (NPs) through a flowing aqueous fluid.<sup>4</sup> In contrast to conventional zwitterions, which are chemically inert, the multifunctional ST-containing

copolymers we synthesized *both participate in droplet stabilization and embed reactive functionality directly into the zwitterionic framework*. Moreover, advantageously including these ST zwitterions in phosphorylcholine (PC)-containing copolymers proved particularly useful for producing surfactants that contributed characteristics of droplet stabilization and interfacial reactivity. This was demonstrated by NP pickup, or “capture”, experiments that were performed by circulating ST-coated emulsion droplets across a substrate, in a flow cell, containing amine-functionalized silica NPs. The resultant NP adherence to the fluid-fluid interface of the droplets hinged on the available reactivity of both the electrophilic (from ST) and nucleophilic (from the NPs) components as well as the solution pH and extent of amine functionality on the NPs.

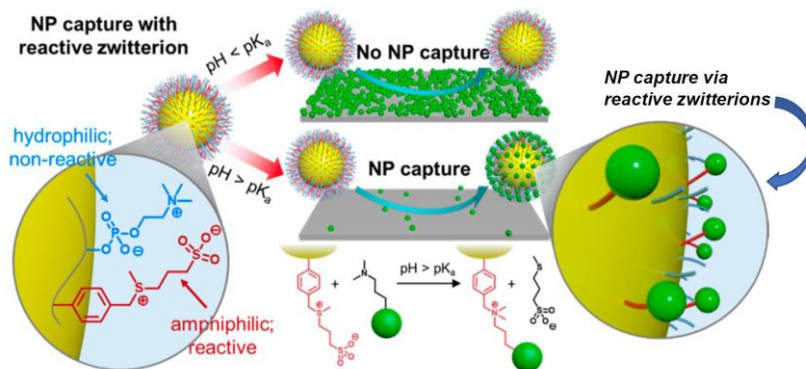


**Fig 1.** Illustration of ST-zwitterions that participate in droplet stabilization while providing reactive handles for recognizing, capturing, and transporting NPs from surfaces to droplet interfaces and through fluidic media (*ACS Applied Materials & Interfaces*, 2021).

Building on the theme of smart, bio-inspired functional droplets, we recognize that Nature is remarkably adept at using interfaces to build structures, encapsulate reagents, and regulate

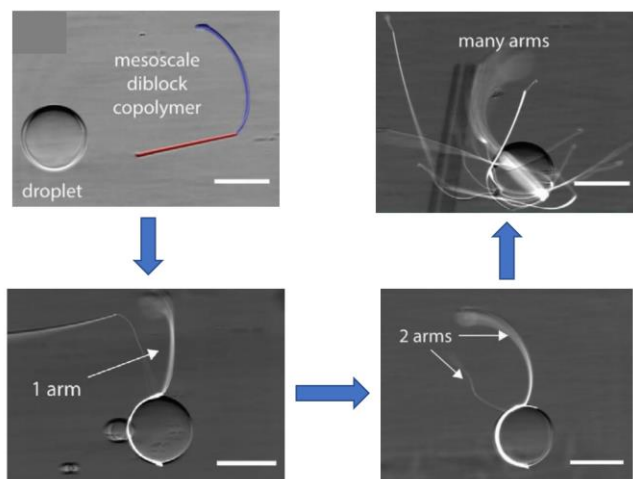


**Fig 2.** Optical micrographs showing “block polymer” ribbons wrapped around fluid droplets, giving structures with extended arms; scale bars = 200 microns (*Advanced Functional Materials*, 2020).

biological processes. Inspired by Nature, we designed meso- and macroscale surfactant-like structures for interaction with, and stabilization of, the fluid-fluid interface of droplets.<sup>5</sup> As shown in the optical micrographs of **Figure 2**, the ribbon-like geometry of these structures serves to modulate interfacial interactions with liquid droplets; such structures connected to the droplet surface may provide access to droplets with unprecedented reach and opportunities to capture reagents, clean surfaces, and engulf materials. Preparing these flagellum-like hybrid assemblies hinged on our ability to prepare polymer-based objects containing domains possessing

distinctly different affinity for fluids, substrates, and fluid-fluid interfaces. This was accomplished by subjecting light-activatable polymers to flow-coating conditions to prepare the ribbon-like structures, followed by irradiation through a photomask to produce regions of the structures with

an affinity for fluid-fluid interfaces, and other regions that prefer extension into the surrounding fluid. The products of these meso/macroscale polymer formulations and droplet attachment may have any number (from one to several) polymeric ‘arms’ adhering to the fluid-fluid interface. Using ribbons derived from photo-crosslinkable polymer structures, pH-dependent ribbon-droplet interactions were mapped to uncover conditions that afford weak adhesion (pH 1-8) and spontaneous wrapping (pH 10) that produced spools amenable to unwrapping and rewrapping multiple times over. Remarkably, “block polymer” macroscale ribbons lead to droplet wrapping of the hydrophobic block until reaching the junction point, affording wrapped (stabilized) droplets with extended hydrophilic arms. Photoacid generators built into the polymer structure afforded spatial control over the length of both the wrapped and extended components of the structures. Moreover, experiments confirmed that the bending compliance and strong interfacial activity of these ribbon-like structures affords elastoadhesive lengths of microns or smaller. Going forward, we project that these pH-, light- and spatially programmable structures represent a robust platform to transform simple soft materials building blocks into sophisticated bio-inspired assemblies.

**Future Plans.** Building upon our prior “repair-and-go”<sup>6</sup> and “clean-and-repair”<sup>7</sup> bio-inspired systems, we seek to more closely mimic osteoblast action *via* “make-and-repair” designs, in which functionalized droplets promote *in-situ* NP nucleation on droplets, then deposit the formed NPs in a controlled manner. NP nucleation will be facilitated through binding and localizing metal ions ( $\text{Ca}^{2+}$ ,  $\text{Ti}^{4+}$ , *etc.*) with functional groups such as catechols, crown ethers, carboxylates, phosphates, and choline phosphates. NP deposition will be studied by competitive NP-substrate attraction and by disruption of NP-droplet interactions *via* enzymatic or pH-induced disruption of NP binding.

In parallel, as illustrated in **Figure 3**, we will extend the capabilities of smart droplets using new designer ribbons prepared by photolithographic methods from functional polymers. Functionality embedded into the hydrophilic (extended arm) portion of the ribbons will equip the droplets with NP capture capabilities and allow droplets to reach far beyond their inherent fluid-fluid interface. Following NP capture, digestion of the hydrophobic portion of ribbons (a phagocytosis-like process) may be realized by employing suitable organic solvents in the emulsion droplet design, resulting in release of the hydrophilic part of the arm into the aqueous phase. Moreover, we plan to study fundamental rheological properties of droplets with arms, exploiting their inherent stimuli-responsive features in a triggered fashion.

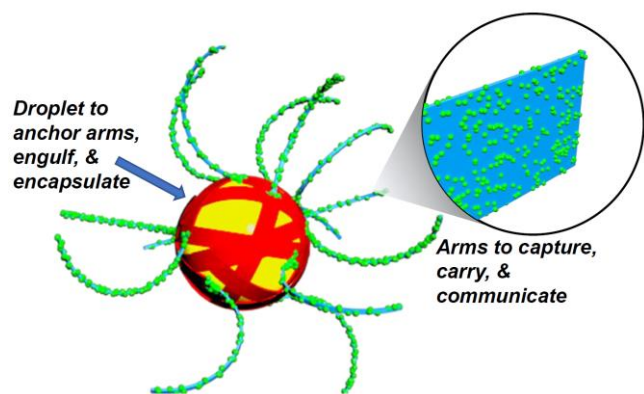


**Fig 3.** Illustration of ribbon-stabilized emulsion droplet: the hydrophobic portion of the ribbon wraps the droplet while the hydrophilic portion extends into the liquid to capture, deliver, or relocate particles, reagents, *etc.*

## References

1. Gabbiani, G. The Myofibroblast in Wound Healing and Fibrocontractive Diseases. *J. Pathol.* **2003**, *200*, 500–503. DOI: 10.1002/path.1427
2. Kirsner, R. S.; Eaglstein, W. H. The Wound Healing Process. *Dermatol. Clin.* **1993**, *11*, 629–640. DOI: 10.1016/S0733-8635(18)30216-X
3. Barrick, B.; Campbell, E. J.; Owen, C. A. Leukocyte Proteinases in Wound Healing: Roles in Physiologic and Pathologic Processes. *Wound Repair Regen.* **1999**, *7*, 410–422. DOI: 10.1046/j.1524-475X.1999.00410.x
4. Yang, Z.; Zhao, J.; Emrick, T. Functional Polymer Zwitterions as Reactive Surfactants for Nanoparticle Capture. *ACS Appl. Mater. Interfaces.* **2021**, *13*, 21898–21904. DOI: 10.1021/acsami.1c05955
5. Barber, D. M.; Yang, Z.; Prévost, L.; du Roure, O.; Lindner, A.; Emrick, T.; Crosby, A. J. Programmed Wrapping and Assembly of Droplets with Mesoscale Polymers. *Adv. Funct. Mater.* **2020**, *30*, 2002704. DOI: 10.1002/adfm.202002704
6. Bai, Y.; Chang, C. C.; Zhao, X.; Ribbe, A.; Bolukbasi, I.; Szyndler, M. J.; Crosby, A. J.; Emrick, T. Mechanical Restoration of Damaged Polymer Films by “Repair-and-Go”. *Adv. Funct. Mater.* **2016**, *26*, 857–863. DOI: 10.1002/adfm.201503947
7. Sathyan, A.; Yang, Z.; Bai, Y.; Kim, H.; Crosby, A. J.; Emrick, T. Simultaneous “Clean-and-Repair” of Surfaces Using Smart Droplets. *Adv. Funct. Mater.* **2019**, *29*, 1805219. DOI: 10.1002/adfm.201805219

## Publications

1. Yang, Z.; Zhao, J.; Emrick, T. Functional Polymer Zwitterions as Reactive Surfactants for Nanoparticle Capture. *ACS Appl. Mater. Interfaces.* **2021**, *13*, 21898–21904. DOI: 10.1021/acsami.1c05955
2. Barber, D. M.; Yang, Z.; Prévost, L.; du Roure, O.; Lindner, A.; Emrick, T.; Crosby, A. J. Programmed Wrapping and Assembly of Droplets with Mesoscale Polymers. *Adv. Funct. Mater.* **2020**, *30*, 2002704. DOI: 10.1002/adfm.202002704
3. Sathyan, A.; Yang, Z.; Bai, Y.; Kim, H.; Crosby, A. J.; Emrick, T. Simultaneous “Clean-and-Repair” of Surfaces Using Smart Droplets. *Adv. Funct. Mater.* **2019**, *29*, 1805219. DOI: 10.1002/adfm.201805219

## EARLY FORMATION STAGES AND PATHWAY COMPLEXITY IN FUNCTIONAL BIO-HYBRID NANOMATERIALS

PI: Lara A. Estroff; Co-PI: Ulrich Wiesner

Department of Materials Science and Engineering, Cornell University, Ithaca, NY 14853

### Program Scope

In order to help establish a synthesis science for hierarchically-organized, functional organic-inorganic hybrid materials, we propose to study three synthetic systems in which organic molecule self-assembly directs the formation of inorganic nanostructured materials: In System 1, surfaces of organic cationic-surfactant micelle-assemblies in aqueous solutions will direct amorphous inorganic silica clusters to form ultrasmall nanostructures with sizes around 10 nm and below with complex topologies, including rings and cages, which in turn will be used to generate functional, hierarchically porous, silica bulk materials via 3D printing. The overall goal for System 1 is to develop a synthesis science for the formation of amorphous inorganic nanoscale building blocks with complex topologies and their assemblies into hierarchically porous materials with controlled 3D shapes and functions. In System 2, we will explore solution-solid interfaces to direct the growth of porous, crystalline inorganic materials with curved, smooth surfaces. This approach will use nanostructured block copolymer (BCP)-derived gyroidal templates to study the combined effects of nanoscopic confinement and surface chemistry on nucleation and growth of inorganic crystals in 2D and 3D. The overall goal for System 2 is to develop a synthesis science for the formation of nanostructured crystals with complex topologies based on the interplay of nanoscale confinement, topology, and surface chemistry. Finally, in System 3, we will use peptide-decorated, fluorescent silica nanoparticles to study the entrapment of secondary phases by single crystals. We will probe these processes with a combination of *in situ* fluid cell atomic force microscopy (AFM) and optical super-resolution microscopy (OSRM). The overall goal for System 3 is to develop a synthesis science for the formation of nanoparticle-single crystal composites.

### Recent Progress

We have worked on projects originally proposed as well as new directions based on recent developments and discoveries. Specifically, in System 1 we have taken the first steps towards creating 3D printed complex mesoporous materials with tunable interior structures. In System 2, we have demonstrated the use of BCP-derived gyroidal templates to synthesize nanostructured superconductors in both bulk and thin-film configurations. Finally, we have laid the groundwork for both the OSRM and *in situ* AFM experiments proposed in System 3.

#### **3D Printing of Mesoporous Silica Nanoparticles.**

During the last funding period, we reported on the synthesis, characterization, and assembly of ultrasmall (~10 nm) silica nanocages.<sup>1</sup> We have now developed a methodology to generate an ink from these nanosized cages surface functionalized with photocrosslinkable ligands enabling 3D printing of structures with intrinsic porosity without the need for an additional post-printing thermal processing step (Fig. 1).<sup>2</sup> By taking advantage of our ability to orthogonally modify the interior and exterior of these cages, we

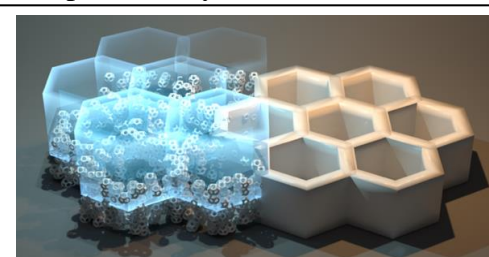


**Fig. 1.** Silica cages with photoresponsive ligands are used for the direct 3D printing of mesoporous parts with tunable internal structure. Making use of the intrinsic porosity, a new concept of internal 3D printing for complex material architectures is demonstrated, paving the way to new material and device designs with ever-increasing capabilities.<sup>2</sup>

demonstrated the positioning of functionalities throughout 3D printed objects. Furthermore, taking advantage of the internal porosity of the printed parts, an internal printing approach was realized that allows for the localized deposition of a guest material within a host matrix, enabling complex 3D material designs.

**Superconducting Quantum Metamaterials.** Mesoscale order can lead to emergent properties including phononic bandgaps or topologically protected states. Block copolymers (BCPs) offer a route to mesoscale periodic architectures, but their use as structure directing agents for metallic materials has not been fully realized. To that end, in a first study we developed a versatile approach to mesostructured metals via bulk BCP self-assembly derived ceramic templates.<sup>3</sup> Molten indium was infiltrated into mesoporous, double gyroidal silicon nitride templates under high pressure to yield bulk, 3D periodic nanocomposites as free-standing monoliths, which exhibit emergent quantum-scale phenomena. We demonstrated that the confinement in the BCP-directed nanostructure changed fundamental properties of the indium superconductor (here the correlation length of the Cooper pairs), leading to a switch from type-I to type-II superconducting behavior. Furthermore, we saw strong evidence for pinning of magnetic vortices arrayed on the order of the double gyroid lattice size. Sample behavior is stable and reproducible over months.

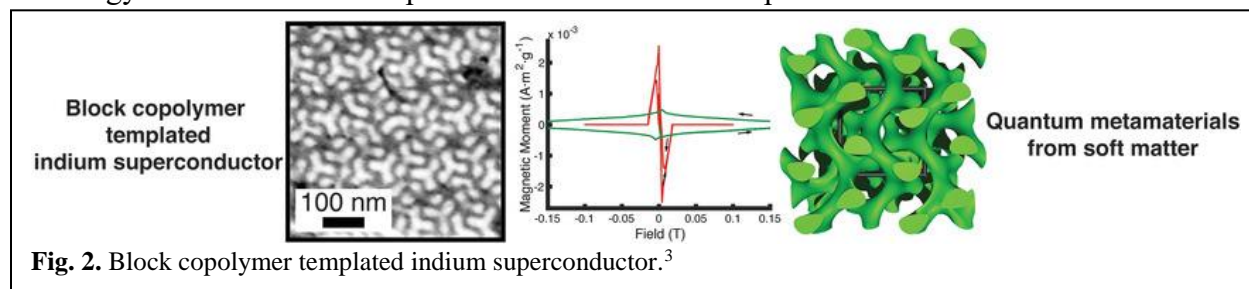
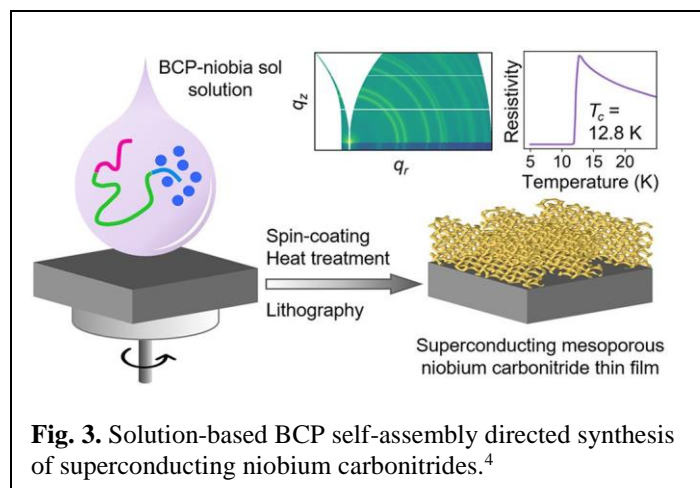


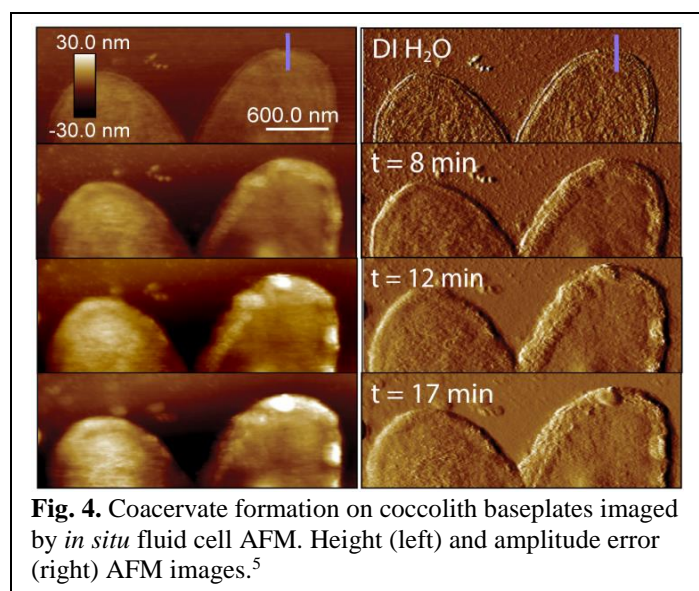
**Fig. 2.** Block copolymer templated indium superconductor.<sup>3</sup>

These results are quite exciting. High pressure infiltration of bulk block copolymer self-assembly based ceramic templates is an enabling tool for studying high-quality metals with previously inaccessible architectures, and paves the way for the emerging field of BCP-derived quantum metamaterials (Fig. 2). To the best of our knowledge, this approach has not been used before and as we showed, allows successful backfilling of quite large area and thick (i.e., bulk) monolithic templates. The resulting composites are interesting materials in their own right, e.g., with respect to their mechanical properties, which we have not yet looked at. Moreover, the switch from type-1 to type-2 superconducting behavior is significant, as type-2 superconductors have much higher critical field,  $B_{02}$ , than type-1 superconductors, above which the superconducting state disappears. In turn, this is important for applications, e.g. involving the use of strong magnetic fields (like e.g. in NMR). The properties of the superconductor are thus not only determined by the atomic structure of the metal, but by its mesostructure directed by BCP self-assembly, which makes it effectively a quantum metamaterial.

In a second study, we demonstrated access to mesostructured superconducting thin films by spin-coating a solution of BCP plus niobium oxide sol-gel precursors, optional photolithographic definition of the thin film composite structure, and subsequent thermal processing under various gases in order to generate superconducting niobium carbonitrides (Fig. 3).<sup>4</sup> This study represents a significant step forward, as it demonstrated that the solution-based BCP self-assembly directed synthesis of quantum materials is fully compatible with semiconductor



coccoliths, which form within the intracellular environment, at very low calcium concentrations. Coccolith formation provides a model system in which to examine the role of polymer-directed mineralization. We used coccolith-derived and synthetic polymers to study, *in vitro*, the chemical interactions between calcium ions and organic macromolecules that precede coccolith formation.<sup>5</sup>



processing. We therefore see this work as breaking new ground in the emerging field of soft matter self-assembly based quantum materials, with substantial academic as well as industrial interest.

***In Situ AFM studies of Surface-Induced Coacervation in Biomineralization.*** We have used *in situ* fluid cell AFM to track the kinetics of formation of a surface-induced coacervation process. Coccolithophores are a type of marine microalgae that produce crystalline calcium carbonate structures, known as

Specifically, we used liquid-cell atomic force microscopy, to visualize the process by which a functional surface, e.g., the coccolith baseplate, induces the precipitation of a polymer–Ca dense phase, or a coacervate, at chemical conditions where precipitation in solution is kinetically inhibited (Fig. 4). This strategy demonstrates how organisms can form dense Ca-rich phases from the submillimolar concentration of calcium within organelles. The *in situ* AFM techniques developed in this study will play a central role in the coming year as we begin to explore the formation of single crystal composites.

***Development of Functionalized Probes for Optical Super Resolution Microscopy.*** Building upon results from the previous funding period,<sup>6</sup> we have continued to expand our library of optical super-resolution microscopy (OSRM) probes in the form of ultrasmall (diameters <10 nm) aluminosilicate nanoparticles encapsulating different fluorescent dyes. Specifically, we have designed the nanoprobe surface chemical properties to facilitate selective compatibilization of the nanoparticles with nonpolar polymers, such as polystyrene.<sup>7</sup> Using a model block copolymer, we have used these nanoparticles, together with previously report thiol-functionalized particles to

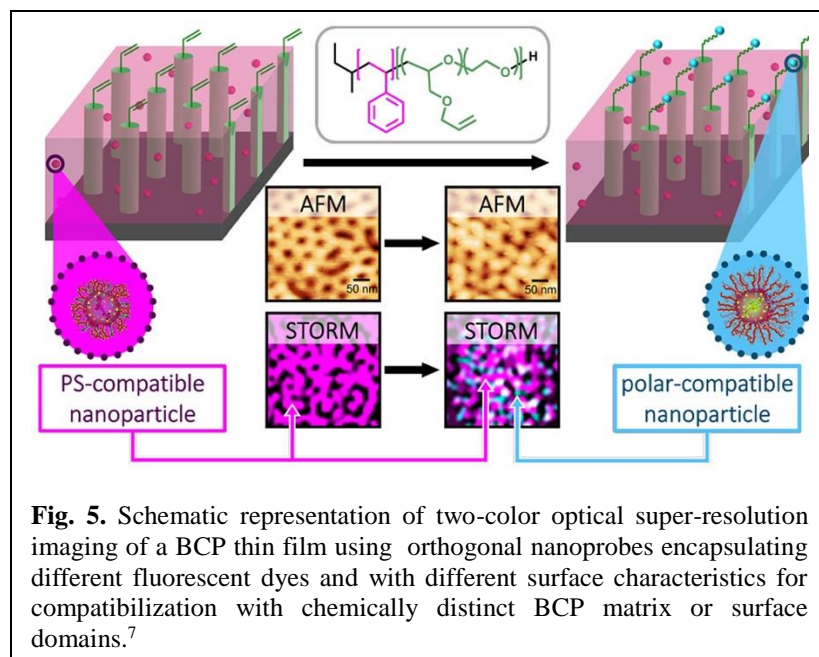


**Fig. 5.** Schematic representation of two-color optical super-resolution imaging of a BCP thin film using orthogonal nanoprobe structures encapsulating different fluorescent dyes and with different surface characteristics for compatibilization with chemically distinct BCP matrix or surface domains.<sup>7</sup>

demonstrate two-color OSRM (Fig. 5). Stochastic optical reconstruction microscopy (STORM) shows nanodomain features of two chemically dissimilar blocks consistent with atomic force microscopy results. This work paves the way for multiplexed OSRM analysis of single crystal composites in the coming year.

**Future Plans.** For System 1 we will continue to look at silica cage structures. This includes the identification of additional cages that are formed using surfactant micelles as structure

directing agents. It also comprises the further use of porous silica cage structures as novel building blocks for additive manufacturing, i.e. 3D printing of novel functional materials. The latter work will build on the results reported in our *Nat. Commun.* paper on the development of novel inks for 3D printing (Fig. 1).<sup>2</sup> These original results were quite encouraging and suggested that the use of silica cages as building blocks in inks for 3D printing may provide the basis for the development of novel materials with unusual property profiles, which we will continue to explore.

For System 2, we are exploring the versatility of using the BCP-derived templates to structure directed a range of superconducting materials. For example, we are excited about the possibility of using the single-crystal gyroid templates developed during the last funding period<sup>8</sup> to now template single atomic-scale crystals to investigate the emergent properties of a “single crystal within a single crystal”. We are finally pursuing similar techniques to fabricate 3D batteries using ultrahigh molecular weight polymers.

For System 3, we will begin the crystal growth experiments using the super resolution silica nanoparticles developed during the last project period (Fig. 5).<sup>7</sup> Using the fluid cell AFM techniques optimized over the last year (Fig. 4),<sup>5</sup> we will perform the first imaging studies of single crystal growth in the presence of these silica nanoparticles with variable surface chemistries, including peptides.

**References.** 1) Aubert, T., Ma, K., Tan, K.W., Wiesner, U., *Adv. Mater.*, **2020**, *32*, 1908362. 2) Aubert, T., Huang, J.Y., Ma, K., Hanrath, T., Wiesner, U., *Nature Commun.*, **2020**, *11*, 4695. 3) Thedford, R.P., Beaucage, P.A., Susca, E.M., Caho, C.A., Nowack, K.C., Van Dover, R.B., Gruner, S.M., Wiesner, U., *Adv. Funct. Mater.*, **2021**, *31*, 2100469. 4) Yu, F., Thedford, R.P., Hedderick, K.R., Freychet, G., Zhernenkov, M., Estroff, L.A., Nowack, K.C., Gruner, S.M., Wiesner, U.B., *ACS Appl. Mater. Interface*, **2021**, *in press*, [acsami.1c09085](https://doi.org/10.1021/acsami.1c09085). 5) Krounbi, L., Hedderick, K., Eyal, Z., Shimoni, E., Estroff, L.A., Gal, A., *Chem. Mater.* **2021**, *33*, 3534. 6) Hinckley, J.A., Chapman, D.V., Hedderick, K.R., Oleske, K.W., Estroff, L.A., Wiesner, U.B., *ACS MacroLett.* **2019**, *8*, 1378-1382. 7) Chapman, D.V., Hinckley, J.A., Erstling, J.A., Estroff, L.A., Wiesner, U.B., *Chem. Mater.* **2021**, *33*, 5156–5167. 8) Susca, E., Beaucage, P., Thedford, R.P., Singer, A., Gruner, S.M., Estroff, L.A., Wiesner, U., *Adv. Mater.*, **2019**, *31*, 1902565.

## Publications Supported by BES 2019-2021

- 1) Kohle, F.F.E., Hinckley, J.A., Li, S.Y., Dhawan, N., Katt, W.P., Erstling, J.A., Werner-Zwanziger, U., Zwanziger, J. Cerione, R.A., **Wiesner, U.B.** “Amorphous Quantum Nanomaterials”, *Adv. Mater.*, **2019**, *31*, 1806993.
- 2) Kohle, F.F.E., Hinckley, J.A., **Wiesner, U.B.** “Dye Encapsulation in Fluorescent Core-Shell Silica Nanoparticles as Probed by Fluorescence Correlation Spectroscopy”, *J. Phys. Chem. C.*, **2019**, *123*, 9813-9823.
- 3) Susca, E., Beaucage, P., Thedford, R.P., Singer, A., Gruner, S.M., **Estroff, L.A., Wiesner, U.** “Preparation of Macroscopic Block Copolymer-Based Gyroidal Mesoscale Single Crystals by Solvent Evaporation” *Adv. Mater.*, **2019**, *31*, 1902565. *adma.201902565*
- 4) Hinckley, J.A., Chapman, D.V., Hedderick, K.R., Oleske, K.W., **Estroff, L.A., Wiesner, U.B.** “Quantitative Comparison of Dye and Ultrasmall Fluorescent Silica Core-Shell Nanoparticle Probes for Optical Super-Resolution Imaging of Block Copolymer Thin Film Surfaces”, *ACS MacroLett.* **2019**, *8*, 1378-1382. *acsmacrolett.9b00675*
- 5) Aubert, T., Ma, K., Tan, K.W., **Wiesner, U.** “Two-dimensional Mesoporous Superlattices of Silica Cages”, *Adv. Mater.*, **2020**, *32*, 1908362
- 6) Aubert, T., Huang, J.Y., Ma, K., Hanrath, T., **Wiesner, U.** "Porous cage-derived nanomaterial inks for direct and internal three- dimensional printing", *Nature Commun.*, **2020**, *11*, 4695.
- 7) Chapman, D.V., Du, H., Lee, W.Y., **Wiesner, U.B.** "Optical super-resolution microscopy in polymer science", *Prog. Poly. Sci.*, **2020**, *111*, 101212.
- 8) Palin, D., Style, R.W., Zlopasa, J., Petrozzini, J.J., Pfeifer, M.A., Jonkers, H.M., Dufresne, E.R., **Estroff, L.A.** “Forming Anisotropic Crystal Composites: Assessing the Mechanical Translation of Gel Network Anisotropy to Calcite Crystal Form”, *J. Am. Chem. Soc.*, **2021**, *143*, 3439-3447. <https://doi.org/10.1021/jacs.0c12326>
- 9) Thedford, R.P., Beaucage, P.A., Susca, E.M., Caho, C.A., Nowack, K.C., Van Dover, R.B., Gruner, S.M., **Wiesner, U.**, "Superconducting Quantum Metamaterials from High Pressure Melt Infiltration of Metals into Block Copolymer Double Gyroid Derived Ceramic Templates", *Adv. Funct. Mater.*, **2021**, *31*, 2100469.
- 10) Krounbi, L., Hedderick, K., Eyal, Z., Shimoni, E., **Estroff, L.A., Gal, A.** “Surface-induced coacervation facilitates localized precipitation of mineral precursors from dilute solutions” *Chem. Mater.* **2021**, *33*, 3534. <https://doi.org/10.1021/acs.chemmater.0c04668>
- 11) Chapman, D.V., Hinckley, J.A., Erstling, J.A., **Estroff, L.A., Wiesner, U.B.** “Orthogonal Nanoprobes Enabling Two-Color Optical Super- Resolution Microscopy Imaging of the Two Domains of Diblock Copolymer Thin Film Nanocomposites”, *Chem. Mater.* **2021**, *33*, 5156–5167.

- 12) Yu, F., Thedford, R.P., Hedderick, K.R., Freychet, G., Zhernenkov, M., **Estroff, L.A.**, Nowack, K.C., Gruner, S.M., **Wiesner, U.B.** “Patternable Mesoporous Thin Film Quantum Materials via Block Copolymer Self-Assembly: An Emergent Technology?” *ACS Appl. Mater. Interface*, **2021**, *in press*. <https://doi.org/10.1021/acsami.1c09085>

## **Programmable Dynamic Self-Assembly of DNA Nanostructures**

**Elisa Franco**

Mechanical and Aerospace Engineering University of California, Los Angeles.

**Rebecca Schulman**

Chemical and Biomolecular Engineering and computer science Johns Hopkins University

### **Program Scope**

The synthesis of novel materials with self-regulation properties akin to those of biological cells is a central challenge in biomolecular materials research<sup>1,2</sup>. In biological systems, behaviors such as growth, division, and self-repair emerge because molecular self-assembly processes are coupled to and directed by signal transduction and gene expression networks. The overall goal of this project is to program synthetic materials to, analogously, respond adaptively and dynamically to their environments by coordinating synthetic self-assembly processes with synthetic molecular circuits and control systems, and controlling the flow of energy during self-assembly. This project's central question during this funding cycle is to understand how to provide fuel to artificial self-assembling materials so they can execute sustained and repeated tasks over extended periods of time. We are addressing this question by designing chemical systems that regulate the influx of high-energy precursors (fuel components) and enzymes and the removal of waste products. These systems are composed of biochemical reaction systems and hierarchically organized materials, so that the release of biochemical energy in different forms and the management of waste products is regulated by chemical reactions and controlled transport across different phases. This work on regulating fuel and waste availability will next allow us to design new classes of sophisticated, multi-component materials with complex, programmed chemomechanical behaviors, *i.e.* the ability to perform work. We use DNA nanotubes<sup>3-5</sup> as components of dynamic materials and couple far-from-equilibrium genelet and strand-displacement nucleic acid circuits to nanotube self-assembly using short nucleic acid message strands<sup>6-8</sup>. Mechanisms for the production and transport of fuel for assembly and reorganization are present in processes as diverse as active microtubule assembly and nanoparticle assembly; this suggests that the systematic framework for controlling fuel and waste availability and material responses will broadly advance DNA self-assembly and the design of dynamic biomolecular materials and materials systems as a whole.

### **Recent Progress**

**Controlled dynamic self-assembly of encapsulated nanotube systems and circuits** Cells achieve sustained behaviors by isolating their operation from the environment and regulating influx of fuel and outflux of waste. Toward the development of encapsulated systems with the capacity for regulated flux of components, we have demonstrated methods to self-assemble DNA scaffolds as well as circuits controlling their assembly inside water-in-oil droplets as model microscopic compartments. We have demonstrated encapsulated polymerization of four different classes of DNA tiles, using different protocols that include vortexing and microfluidics. To track polymerization across a large droplet population we have established a qualitative approach that uses statistical properties of droplet images (skewness and kurtosis). This method made it possible to compare how quickly nanotubes assemble under different conditions. We have further shown the encapsulated control of assembly via synthetic genes transcribing RNA molecules that activate assembly. We have also shown the emergence of autonomous pulse-like self-assembly occurs when enzymes transcribing and degrading RNA are present. Transient assembly is controllable by regulating the concentration of enzymes, and its kinetics are recapitulated by a simple

mathematical model. Current work is dedicated to controlling assembly inside compartments via different fueling mechanisms provided by the external environment, with the overall goal of eventually converting energy stored in the fuel into mechanical changes of the compartment shape and size. As a first fueling mechanism, we have designed DNA tiles that can be activated by UV light via photocleavable domains, and we are characterizing temporal protocols for achieving linear nanotube growth. We have also combined photoactivation and transcription-based activation, demonstrating that both are necessary for nanotube assembly. In collaboration with the Simmel lab at TU Munich we are also engineering synthetic genes that are activatable via small molecules like IPTG, which can permeate adjacent compartments in the presence of alpha hemolysin pores. These methods will expand our toolkit to precisely control and sustain nucleation, growth rates, and length of DNA nanotubes.

**Controlled hydrogel release of DNA assembly regulators** Another route to control the release of biochemical fuel is through the adoption of hydrogel compartments loaded with fuel molecules whose release can be controlled by a specific triggering signal. We have demonstrated the control of nanotube assembly and disassembly via DNA inputs localized in a polyacrylamide hydrogel via acrydite conjugation and a UV-photocleavable spacer. We have completed a quantitative characterization of DNA “load” release as a function of gel matrix density, UV irradiation duration and intensity, and concentration of DNA incorporated in the gel, developing protocols that suppress un-triggered leak of DNA fuel. By releasing DNA load that is a regulator for nanotube assembly, we showed that nanotubes present in the aqueous phase external to the gel can be disassembled and assembled through various reaction pathways. We are exploring methods to release multiple regulators with distinct timescales and delays, so that autonomous dynamic steps of nanotube formation could be achieved via gel-stored strands. Preliminary experiments and coarse-grained models indicate that both the timescale of DNA release from the gel and the

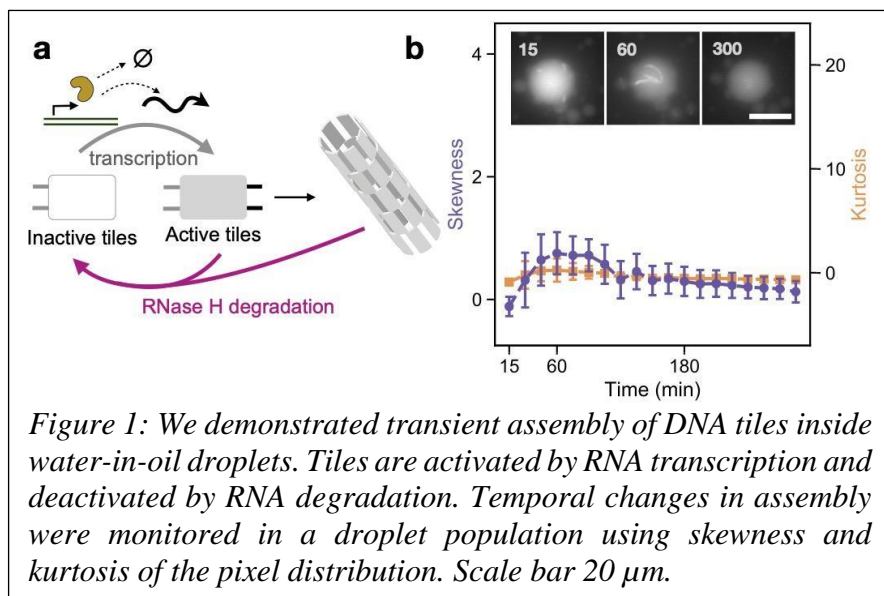


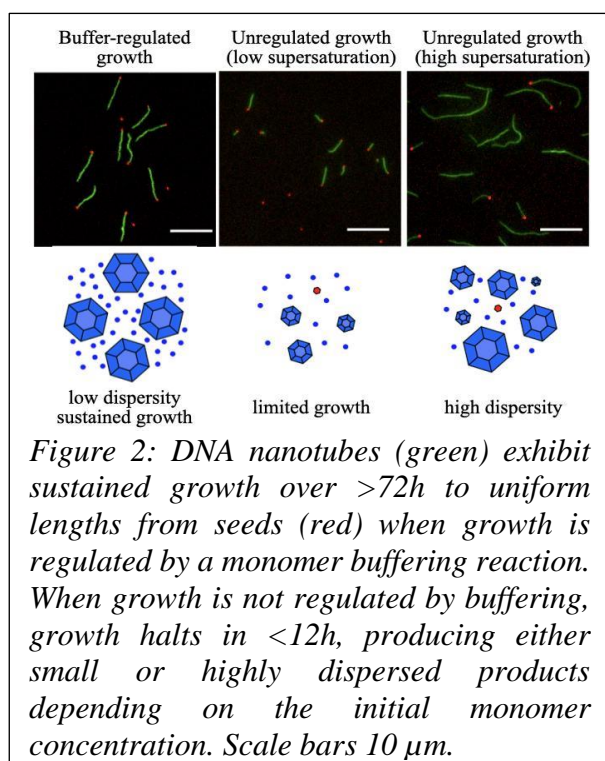
*Figure 1: We demonstrated transient assembly of DNA tiles inside water-in-oil droplets. Tiles are activated by RNA transcription and deactivated by RNA degradation. Temporal changes in assembly were monitored in a droplet population using skewness and kurtosis of the pixel distribution. Scale bar 20  $\mu$ m.*

timescale of tile assembly need to be taken into account to obtain sequential steps of nanotube assembly and disassembly. These results point to the need for releasing regulator strands with specific temporal delays. We are characterizing strand displacement reactions loaded in the gel to obtain tunable delays of release.

**Fueling and regulating nanostructure growth**

**processes.** Crystallization is a ubiquitous means of self-assembly that can organize matter over length scales orders of magnitude larger than those of the monomer units. Yet crystallization is notoriously difficult to control because it is exquisitely sensitive to monomer concentration, which changes as monomers are depleted during growth. Living cells control crystallization using chemical reaction networks that offset depletion by synthesizing or activating monomers to regulate monomer concentration, stabilizing growth conditions even as depletion rates change, and

thus reliably yielding desired products. Using DNA nanotubes as a model system, we have shown that coupling a generic reversible bimolecular monomer buffering reaction to a crystallization process leads to reliable growth of large, uniformly sized crystals even when crystal growth rates change over time. Buffered growth of nanotubes increases the yield, uniformity and quality of assembled structures by maintaining the physical conditions for growth in the weakly supersaturated regime. Buffering allows such maintenance without reliance on typical protocols such as annealing that modulate physical conditions over time and performs better than such protocols because conditions for growth are altered in a closed loop fashion dependent on the current level of supersaturation. The regulation mechanism is also easily tunable and performs in a manner quantitatively consistent with molecular simulations. Buffering could be applied broadly as a simple means to regulate and sustain batch crystallization and could facilitate the self-



assembly of complex, hierarchical synthetic structures.

**Turnkey dissipative networks for driving repeated material reconfiguration.** Engineered far-from-equilibrium synthetic chemical networks that pulse or switch states in response to environmental signals could precisely regulate the kinetics of chemical synthesis or self-assembly pathways. Extensive tuning of such networks has generally been required to compensate for the different activities of and unintended reactions between a network's chemical elements, making integration with material processes challenging. Elements with standardized performance could be rapidly integrated to build far-from-equilibrium networks with designed function. During this cycle we have developed standardized excitable chemical elements, termed genelets, for constructing complex *in vitro* transcriptional networks. We developed a protocol for

identifying >15 interchangeable genelet regulatory elements with uniform performance and minimal crosstalk. These elements can be combined to engineer feedforward and feedback modules whose dynamics are predicted by a simple kinetic model. We have also shown that modules can be rationally integrated and reorganized into networks that produce tunable temporal pulses and act as multi-state switchable memories. Standardized genelet elements should make engineering complex far-from-equilibrium chemical dynamics routine and allow the direction of complex, repeated tasks by self-assembling biomolecular materials.

**Growing complex structures from fiber primitives.** A longstanding goal of nanotechnology is to develop methods for synthesizing custom matter from the ground up in a hierarchical fashion. To help understand how directed dynamic process could regulate and fuel such complex growth processes, and therefore make them practical, we have developed a system for assembling extended networks of semiflexible DNA nanotubes and developed a predictive model of the assembly process that will allow it to be tuned and therefore to be predictive coupled with chemical

and physical mechanisms for regulating energy flow and controlling dynamics. In this system, nanotubes assemble from nanometer scale tiles into materials via nucleated growth from sites on rigid, Y-shaped nanotube seeds. These architectures then, in turn, assemble into networks that include as many as 80 seeds and can extend over areas as large as  $900 \mu\text{m}^2$ . We have measured the kinetics of network growth and found that the pathways of assembly of these networks are well predicted by a stochastic model of hierarchical assembly that assumes a single joining rate between DNA nanotube ends. Because the number of nucleation sites on the seeds and their spatial arrangement can be systematically varied by design, this system allows the assembly of a wide variety of networks and characterization of the assembly mechanisms that lead to different types of material architectures at length scales of tens to hundreds of microns. We have identified the ratio of inter-network vs intra-network joining events as a key parameter that controls whether networks develop into “open-branching” topologies or “closed-loop” topologies. Further, by activating or deactivating the incorporated Y-shaped DNA origami junctions via strand displacement, we are also able to direct networks to change form. This system will serve as model for understanding the formation and reconfiguration of filament networks at this length-scale.

### Future Plans

Our research advances make it possible to control the self-assembly of nanotubes through diverse fuel storage and delivery mechanisms including chemical reactions (dissipative genelet systems, buffering reactions), compartmentalization (hydrogels, droplets), and light. These mechanisms make it possible to program the release of chemical or electromagnetic energy toward the spontaneous assembly of biomolecular structures. We plan on integrating these chemical and physical means to control and coordinate the formation of hierarchical structures that include multiple types of nanotubes and their organizing components. Our overall goal is to demonstrate multi-scale architectures whose kinetics can be sustained for long periods of time. In addition, we will develop programs that direct the hierarchical structure formation, dissolution, and reconfiguration through pathways that include multiple steps. The formation of distinct architectures will be achieved by modulating the relative abundance of molecules that fuel assembly or disassembly of specific components at different points in time.

### References

1. Balazs, A. C. et al. Designing Biomimetic, Dissipative Material Systems. (2016) doi:10.2172/1235400.
2. McEvoy, M. A. & Correll, N. Materials science. Materials that couple sensing, actuation, computation, and communication. *Science* 347, 1261689 (2015).
3. Rothemund, P. W. K., Papadakis, N. & Winfree, E. Algorithmic self-assembly of DNA Sierpinski triangles. *PLoS Biol.* 2, e424 (2004).
4. Mohammed, A. M., Šulc, P., Zenk, J. & Schulman, R. Self-assembling DNA nanotubes to connect molecular landmarks. *Nat. Nanotechnol.* 12, 312–316 (2017).
5. Green, L. N. et al. Autonomous dynamic control of DNA nanostructure self-assembly. *Nat. Chem.* 11, 510–520 (2019).
6. Franco, E. et al. Timing molecular motion and production with a synthetic transcriptional clock. *Proc. Natl. Acad. Sci. U. S. A.* 108, E784–93 (2011).
7. Schaffter, S. W. & Schulman, R. Building in vitro transcriptional regulatory networks by successively integrating multiple functional circuit modules. *Nat. Chem.* 11, 829–838 (2019).
8. Kim, J. & Winfree, E. Synthetic in vitro transcriptional oscillators. *Molecular Systems Biology* vol. 7 465 (2011).

### **Publications (2019-2021)**

Siddharth Agarwal, Elisa Franco. Enzyme-driven assembly and disassembly of hybrid DNA–RNA nanotubes. *Journal of the American Chemical Society* 141 (19), 7831-7841, 2019.

Siddharth Agarwal, Melissa A Klocke, Passa E Pungchai, Elisa Franco. Dynamic self-assembly of compartmentalized DNA nanotubes. *Nature Communications* 12 (1), 1-13, 2021.

Deepak Agrawal and Rebecca Schulman Modular protein-oligonucleotide signal exchange *Nucleic Acids Research*, 48, 12, pp 6431-6444, 2020.

Kurt J Cox, Hari KK Subramanian, Christian Cuba Samaniego, Elisa Franco, Amit Choudhary. A universal method for sensitive and cell-free detection of CRISPR-associated nucleases *Chemical science* 10 (9), 2653-2662, 2019

Christian Cuba Samaniego, Elisa Franco Ultrasensitive molecular controllers for quasi-integral feedback. *Cell Systems* 12 (3), 272-288, e3, 2021.

Leopold N Green, Hari KK Subramanian, Vahid Mardanlou, Jongmin Kim, Rizal F Hariadi, Elisa Franco Autonomous dynamic control of DNA nanostructure self-assembly. *Nature chemistry* 11 (6), pp 510-520, 2019

Michael Pacella, Vahid Mardanlou, Siddharth Agarwal, Anusha Patel, Elizabeth Jelezniakov, Abdul Mohammed, Elisa Franco and Rebecca Schulman Characterizing the Length-Dependence of DNA Nanotube End-to-End Joining Rates. *Molecular Systems Design & Engineering*, 5, pp 544-558, 2020.

Samuel Schaffter, Kuan-Lin Chen, Jackson O'Brien, Madeline Noble, Arvind Murugan and Rebecca Schulman Standardized excitable elements for scalable engineering of far-from-equilibrium chemical networks. <https://www.researchsquare.com/article/rs-247740/v1>, 2021.

Samuel Schaffter, Dominic Scalise, Terence Murphy, Anusha Patel and Rebecca Schulman Feedback regulation of crystal growth by buffering monomer concentration. *Nature Communications*, 10.1038/241467-020-19882-8, 2020.

Samuel Schaffter, Joanna Schneider, Deepak Agrawal, Michael Pacella, Eric Rothchild, Terence Murphy and Rebecca Schulman Reconfiguring DNA Nanotube Architectures via Selective Regulation of Terminating Structures. *ACS Nano*, 10.1021/acsnano.0c05340, 2020.

Samuel Schaffter and Rebecca Schulman Building *in vitro* transcriptional regulatory networks that integrate multiple functional circuit motifs. *Nature Chemistry*, 11, pp 829-838, 2019.

## Program Title: Bioinspired Design of Multifunctional Dynamic Materials

**Principle Investigator: Zhibin Guan, Ph.D.**

**Mailing Address: 1102 Natural Sciences II, Irvine, CA 92697**

**Email: zguan@uci.edu**

### Program Scope

The overall objective of this project is to mimic nature's out-of-equilibrium self-assembly processes to develop dissipative self-assembly of active materials using redox chemistry. Fuel driven dissipative, out-of-equilibrium assemblies, such as microtubule and actin filaments, are at the heart for many cellular processes, including cellular transport, cell motility, proliferation, and morphogenesis. Such dissipative processes in nature have inspired the design of synthetic self-assembled systems driven by chemical fuels. Nevertheless, relatively few systems of chemical-fueled dissipative assembly have been developed and the toxicity of the chemical fuels and harsh conditions used in many designs further limit their applications. With the DOE support, we recently developed a transient, out-of-equilibrium self-assembly system based on a new chemical redox reaction network. By using a mild redox reaction network, we could simultaneously create and destroy a disulfide-based hydrogelator, leading to transient, active behavior.

### Recent Progress

#### 1. Active Supramolecular Materials Fueled by Electricity

We recently demonstrated a dissipative self-assembly materials system by using chemical redox reaction network to fuel the dissipative self-assembly. In the current study, we explored a new type of out-of-equilibrium design by using an electrochemical redox reaction network to fuel active material. This allows us to directly use electricity to fuel dissipative self-assembly of active materials. We sought to achieve our initial goal by modifying our previous redox-based approach with an oxidant that is activated electrochemically. Ferricyanide ( $\text{Fcn}^{3-}$ ) has been previously shown to oxidize cysteine in aqueous solution after being generated electrochemically from the reduced form, ferrocyanide ( $\text{Fcn}^{4-}$ ). In our design, we used the electrochemically generated  $\text{Fcn}^{3-}$  to oxidize our thiol precursor (CSH) to the self-assembling disulfide species (CSSC). Furthermore,  $\text{Fcn}^{3-}$  is nontoxic and has been previously used to control biological systems. We decided to continue using dithiothreitol (DTT) as reductant because oxidized DTT can be reduced electrochemically to regenerate the reductant. Therefore, this system can be designed to produce no chemical waste. The design and principle of our initial electrochemically fueled (**e-fueled**) dissipative self-assembly is shown in Figure 1A-B.

To directly visualize the e-fueled dissipative self-assembly process, we conducted *in situ* electrochemical confocal laser scanning microscopy (CLSM) experiments with CSH,  $\text{Fcn}^{4-}$ , and DTT present. The working electrode where oxidation occurs is a glassy carbon rod, imaged at the interface between the electrode and solution where gelation is expected. Cyclic voltammetry (CV) was conducted before the experiment to ensure proper electrical connection. The CLSM image clearly showed that the fibers began to grow from the surface of the working electrode which continued to grow outwards when the potential was maintained (Figure 1C). When the current was

turned off at 5 minutes, the fibers began to disassemble and eventually disappear, demonstrating the transient, dissipative assembly of the system.

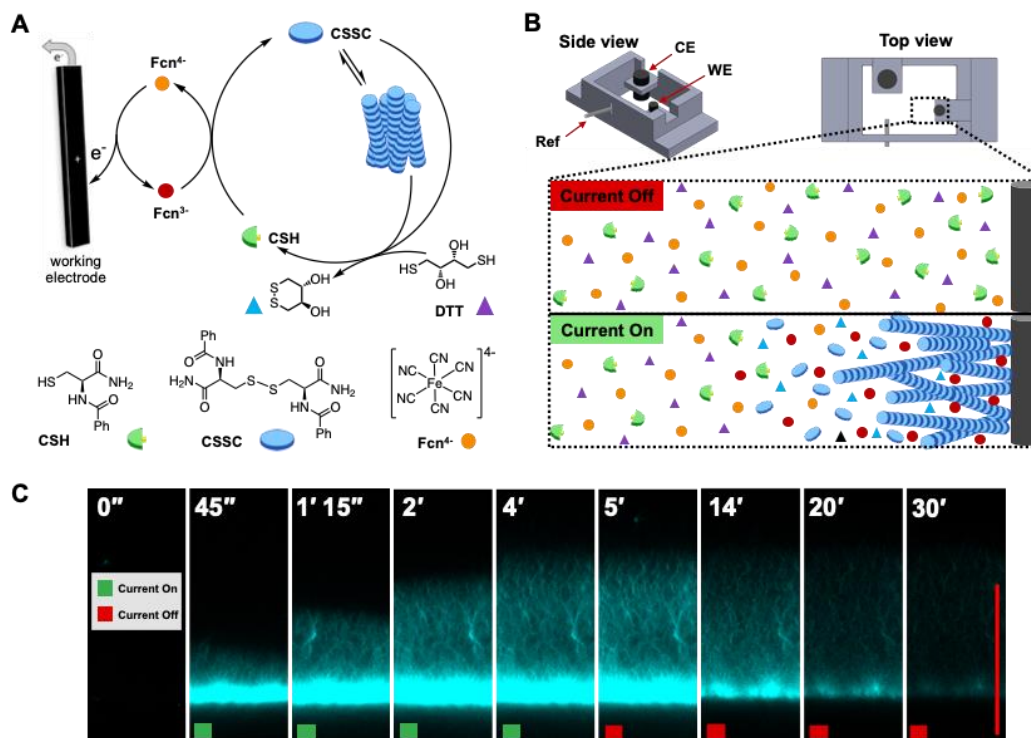


**Figure 1.** Electrically fueled dissipative self-assembly of active materials. (A) and (B) Schematic for electrically-fueled dissipative assembly. Upon application of an electric potential, ferricyanide ( $\text{Fcn}^{3-}$ ) is generated near the anode, causing subsequent thiol oxidation to disulfide and subsequent gel growth. When the potential is no longer applied, DTT present in solution reduces the disulfide to the thiol precursor, and the gel dissolves. (C) CLSM snapshots showing fiber growth while potential was applied (green square), and dissipation when potential was absent (red square) ( $\text{pH } 8$ ,  $[\text{CSH}]_0 = 2.5 \text{ mM}$ ,  $[\text{DTT}]_0 = 20 \text{ mM}$ ,  $[\text{Fcn}^{4+}]_0 = 150 \text{ mM}$ , Scale bar =  $50 \text{ }\mu\text{m}$ ).

Furthermore, we observed highly dynamic, active assembly process in this e-fueled dissipative assembly system. CLSM videos captured various modes of activities for the self-assembly fibers, including simultaneously growing and shrinking, waving, and looping. Lastly, we demonstrated precise spatiotemporal control for the e-fueled dissipative self-assembly system. Using a microfabricated interdigitated microelectrode with individually addressable working electrodes, we could turn on and off fiber assembly at each specific working electrode at desired duration.

Electrochemical process is unique and powerful because it provides a very convenient way to sustainably fuel the active material system and offers both spatial and temporal control to the process. Successful development of electrochemical reaction networks will open the door to the design of highly functional active materials with precise spatiotemporal control. Given electricity is the most common power source and the default information carrier for manmade devices, the described approach offers a unique opportunity for integrating active materials into electronic devices for active soft electronic applications.

## 2. Chemothermally Driven Out-of-Equilibrium Materials

In this study, we demonstrated a chemically fueled out-of-equilibrium system that can perform macroscopic actuation and do work by lifting objects. Specifically, we achieved this by driving a lower critical solution temperature (LCST) phase transition of poly(*N*-isopropylacrylamide) (pNIPAAm) hydrogels with heat generated by a copper-catalyzed azide-alkyne cycloaddition (CuAAC) reaction (Figure 2A). To realize macroscopic motion using out-of-equilibrium processes, the fuels are the azide and alkyne, and the system is the pNIPAAm gel with the copper catalyst in presence. Upon addition of the fuels (azide and alkyne), the system moves out of equilibrium due to the energetically downhill CuAAC reaction, raising the temperature of the system and inducing an LCST transition to the pNIPAAm gel. As the fuels run out, the heat generated by the CuAAC reaction dissipates to the environment, driving the re-swelling of the gel, completing an out-of-equilibrium cycle (Figure 2A). The same process can be repeated multiple cycles by repetitively adding new chemical fuel.

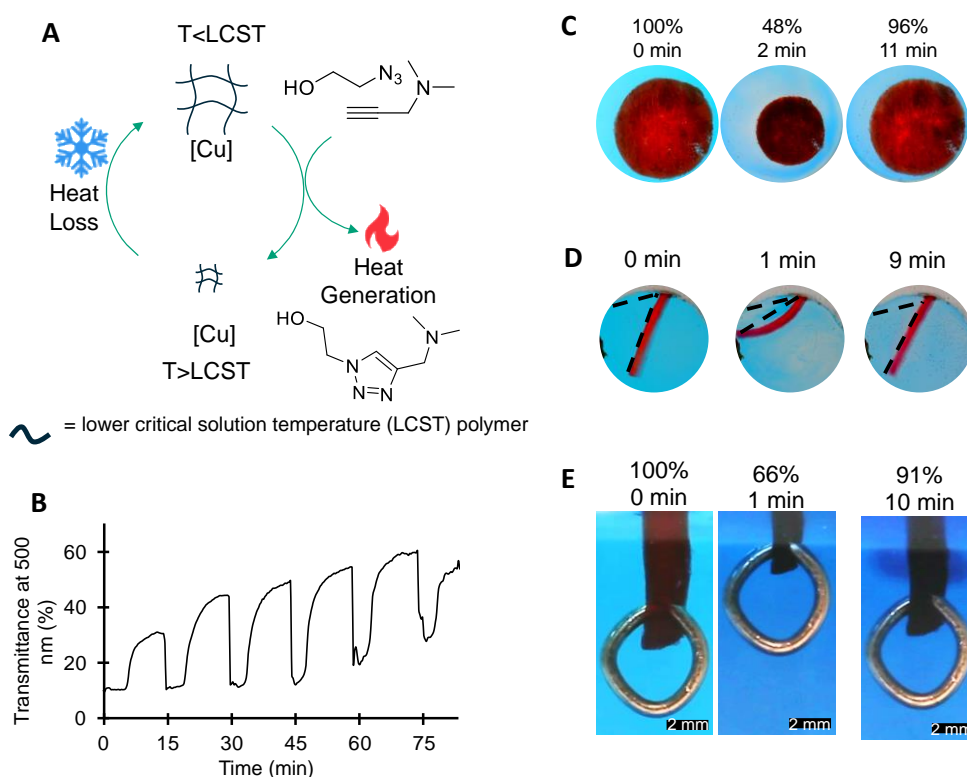


**Figure 2.** (A) Design concept of chemothermally driven out-of-equilibrium bulk materials and small molecule heat generation studies. Scheme showing the out-of-equilibrium system composed of a temperature responsive pNIPAAm hydrogel with a lower critical solution temperature (LCST) phase transition along with a Cu catalyst to catalyze the azide-alkyne cycloaddition (CuAAC) of 2-azidoethanol and 3-dimethylaminopropyne, which are the fuels. The heat from the exothermic CuAAC drives the LCST phase transition. Heat dissipation then completes the cycle by lowering the temperature of the system. (B) Chemothermally driven out-of-equilibrium system demonstrated for a colloidal solution of pNIPAAm NPs. Transmittance at 500 nm of a water solution containing a Cu catalyst and pNIPAAm NP with 1 mmol of fuels (2-azidoethanol and 3-dimethylaminopropyne) added ever 15 min. (C) The transient volume/size change of a pNIPAAm hydrogel sphere (1.56 cm diameter, stained with Congo Red) after the addition of 1 mmol fuels. (D) Transient actuation of an asymmetrical hydrogel film upon the addition of chemical fuels. (E) Demonstration of chemothermal approach for performing macroscopic work by lifting an object following the addition of 1 mmol fuel at 0 min.

In our study, the transient out-of-equilibrium behavior was demonstrated in cyclic changes of turbidity (Figure 2B), volume change (Figure 2C), and actuation of asymmetric hydrogels (Figure 2D). Furthermore, the bulk hydrogel was shown to be able to perform work by consuming chemical fuels, as demonstrated by the reversible lifting of an object two orders of magnitude heavier than itself (Figure 2E). This demonstrated bioinspired out-of-equilibrium materials capable of generating macroscopic motion by dissipating chemical energy at the molecular scale.

### III. Future Plans

#### (1) Further Investigation of Electrically Fueled Dissipative Self-assembly Materials

We will investigate the kinetic details of electrochemical redox reactions that fueled the active assembly system. To broaden the scope, we will identify other electrochemical reaction networks as well as new building blocks for the development of e-fueled dissipative materials.

#### (2) Investigation of Enzyme Network Fueled Active Materials

Another direction we will pursue is to develop a steady-state, long-lived active assembly system using redox enzyme networks. In initial study, we will use glucose oxidase (GOx)-catalyzed oxidation of glucose to continuously generate H<sub>2</sub>O<sub>2</sub> “fuel” and simultaneously use glutathione reductase (GR) to catalyze the reduction of glutathione disulfide (GSSG) to free glutathione (GSH) as the reductant.

#### **Publications in year 2019-2021 (which acknowledge DOE support):**

1. Selmani, S.; Schwartz, E.; Mulvey, J.; Wei, H.; Grosvirt-Dramen, A.; Gibson, W.; Hochbaum, A. I.; Patterson, J. P.; Ragan, R.; Guan, Z. “Electrically fueled active supramolecular materials”, manuscript submitted.
2. Ogden, W.; Guan, Z. “Redox Chemical-Fueled Dissipative Self-Assembly of Active Materials”, *ChemSystemsChem* **2020**, *2*, e1900030. <https://chemistry-europe.onlinelibrary.wiley.com/doi/epdf/10.1002/syst.201900030>
3. Muradyan, H.; Guan, Z. “Chemothermally Driven Out-of-equilibrium Materials for Macroscopic Motion” *ChemSystemsChem*, **2020**, *2*, e2000024. <https://chemistry-europe.onlinelibrary.wiley.com/doi/epdf/10.1002/syst.202000024>
4. Muradyan, H.; Mozhdehi, D.; Guan, Z. “Self-healing magnetic nanocomposites with robust mechanical properties and high magnetic actuation potential prepared from commodity monomers via graft-from approach”, *Polymer Chemistry*, **2020**, *11*, 1292–1297. <https://pubs.rsc.org/en/content/articlepdf/2020/py/c9py01700c>
5. Tretbar, C. A.; Neal, J. A.; Guan, Z. “Direct Silyl Ether Metathesis for Robust and Thermally Stable Vitrimers”, *J. Am. Chem. Soc.* **2019**, *141*, 16595 – 16599. <https://pubs.acs.org/doi/abs/10.1021/jacs.9b08876>
6. Li, C.; Tan, J.; Guan, Z.; Zhang, Q. “A Three-Armed Polymer with Tunable Self-Assembly and Self-Healing Properties Based on Benzene-1,3,5-tricarboxamide and Metal-Ligand Interactions” *Macromol. Rapid Comm.* **2019**, 1800909. <https://onlinelibrary.wiley.com/doi/epdf/10.1002/marc.201800909>

## Propulsion of synthetic protocells and coacervates driven by biochemical catalysis

**Principal Investigators: Daniel A. Hammer<sup>1,2</sup>, Daeyeon Lee<sup>2</sup> & Matthew Good<sup>1,3</sup>**

**Departments of <sup>1</sup>Bioengineering, <sup>2</sup>Chemical and Biomolecular Engineering, and <sup>3</sup>Cell and Developmental Biology, University of Pennsylvania, Philadelphia, PA 19104**

### Program Scope

An important area in the design of biomolecular materials is the recapitulation of cellular activities through the assembly of molecular components into functional synthetic cells, or protocells. By building cell-like structures that mimic the organization and size of natural cells but which incorporate novel, responsive components, we can augment their capabilities beyond biological limitations, including the ability to convert chemical and radiant energies to mechanical energy. We previously demonstrated that enzymatic reactions encapsulated within polymersomes induce large-scale motility, akin to the random motion displayed by living cells. In this project we are developing motile protocells containing a wide range of enzymatic systems and will use both surface and intra-protocell cascades to drive directed motion of protocells using gradients of substrates, heterogeneously applied stimuli, or asymmetric distributions of enzymes on the capsule surface. We will also leverage our novel protein coacervation system to make motile coacervates, and to use these materials as membrane-less organelles which will serve as hubs for enzymatic activity that drive protocells motion. The work we propose is a fundamental exploration of the design of protocells and coacervates as *adaptive, motile matter*, whose *morphology, content, behavior and performance* can be controlled through directed biochemical catalysis the reconstitution and activation of enzymes, thus leading to the conversion of chemical to mechanical energy. The aims of this project are: **Aim 1. Motility of Single Uniform Protocells**. We are developing new methods for synthesis of uniform microcapsules in high number over short time-scales which will enable us to quantify the effects of enzymatic activity on capsule motion. We will induce motility by functionalizing protocells with a spectrum of enzymes, to ascertain the fundamental relationship between enzyme force-generation and capsule motion. To guide directional motility of these capsules, we will generate microfluidic gradients of substrates. **Aim 2. Motion and fluctuation of patchy interfaces**. We will use the toolbox of molecular biology to spatially and temporally decorate the interface of capsules using light. We will measure the dynamic fluctuations of polymersome membranes caused by surface enzymatic activity. Additionally, we will measure the propulsive motion of capsules coated with patches of enzymes. **Aim 3. Enzymatic control of coacervates and membraneless organelles**. Using coacervating proteins as microcompartments in protocells we will create regulatory hubs that guide protocell motion. Our long-term goal is to expand our system to multiple discrete hubs and sequester multi-component cascades within protocells, and to embed active enzymes within or on coacervate surfaces to control their propulsion.

### Recent Progress

**Capsule motility.** We had previously shown that catalase, embedded in polymersomes, could cause spontaneous active surface protocell motility (3). Polymersomes were made from 10.4kD poly(ethylene)-b-poly(butadiene), 5% of which were functionalized with biotin, and catalase was encapsulated inside. Catalase-loaded polymersomes showed active motility on avidin substrates when the substrate H<sub>2</sub>O<sub>2</sub> was added; when H<sub>2</sub>O<sub>2</sub> was depleted, the capsules stopped moving, and the motion could be reinitiated by readding H<sub>2</sub>O<sub>2</sub>. The capsules displayed diffusive motion in a uniform field of substrate, and the diffusivity increased with decreasing particle size (3). The capsules also displayed directed motion in a gradient of substrate.

In this published study, particles were heterogeneous. We have exerted considerable effort making particles that are uniform in size by microfluidic assembly. First, we made polymersomes from di-block copolymers by a double emulsion method, followed by rapid dewetting, in which stable membranes were formed with one hour of capsule assembly, a vast improvement over the two-week annealing time we reported previously (4). Second, we have also developed a novel way to make capsules from poly-lactic glycolic acid (PLGA), with well-defined shells. PLGA is sequestered to the middle organic phase of the double emulsion, as illustrated by the concentration of Nile Red in the shells. **Figure 1** illustrates the uniform PLGA capsules that were made by a double emulsion templating method. Because of their stability, we are focusing on the use of PLGA capsules for protocell motility experiments.

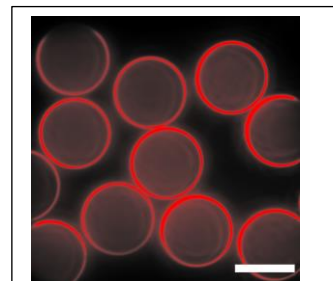


**Figure 1.** Uniform capsules made by microfluidic templating from 85:15 Poly(D,L-lactic-co-glycolic acid).  $M_w$  50-75kD. Shell is labeled with Nile Red. Scale bar, 50  $\mu\text{m}$ .

We employed the chemistry developed by Eniola et al. (5) to functionalize the PLGA capsules with biotinylated catalase, via a biotin-avidin linkage. Briefly, the carboxylic acid is activated with EDC and an amine-reactive NHS-ester to label the capsules with avidin; biotinylated catalase is then bound to the capsule surface. After passivating the surface to eliminate non-specific binding, we observe diffusive like motion of PLGA capsules against a background convective motion. We are conducting image processing of particle motion to characterize the motion of capsules. Since our observations suggest that smaller capsules exhibit greater motion, we have endeavored to process our particles using by osmotic annealing in a slightly hypertonic solution leading to a controllable reduction in size.

**Active coacervates.** We have made significant progress on the development of functional enzyme coacervates. Our engineering revolves around a subdomain of the P-granule protein Laf-

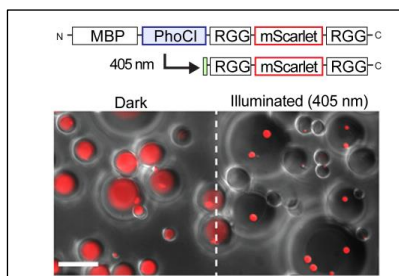


**Figure 2.** Schematic of photocleavable PhoCl tagged RGG containing mScarlet. Emulsions containing 2 mg/ml MBP-PhoCl-RGG-mScarlet-RGG, before and after exposure to 405 nm light (5 s light pulse, 7.87 mW/cm<sup>2</sup>) scale bars: 20  $\mu\text{m}$ .

1, which is known to phase separate into micron-size granules and regulates the sequestration of RNA to control germline specificity. The intrinsically disordered, arginine/glycine-rich RGG domain of Laf-1 is necessary and sufficient for protein condensation separation. We multimerized the RGG domain and demonstrated that increased valency leads to changes in the critical temperature for protein condensation (6). Regulated valency thus provides a strategy for enzymatic control of phase separation via introduction of protease cleavable sites between domains; proteases can then lead to rapid dissolution of condensates. In addition, in collaboration with J. Mittal, Texas A&M, we have also predicted and verified how changes in the sequence of amino acids in with RGG can lead to predictable changes in phase behavior (2).

We have developed a number of strategies for controlling the assembly and dissolution of condensates in response to light. Attaching maltose binding protein (MBP) a large solubilization tag, can prevent coacervation of RGG tandem. However, insertion of a cleavable domain between RGG tandem and MBP can lead to activatable coacervation. By inserting PhoCl, an engineered photocleavable protein, between MBP and RGG tandem, we induced the assembly of coacervates with light (see **Fig 2**; (7)). We have also demonstrated light-

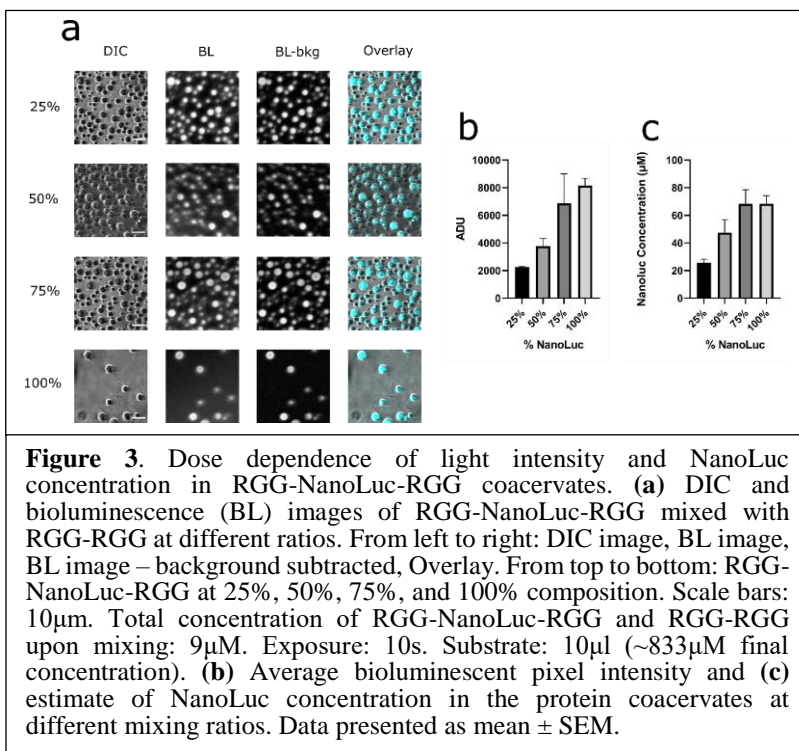
induced assembly of FRB and FKBP by the small molecule rapamycin (Rap), which can be released from a photocaged form (data not shown).

**Enzyme active coacervation.** We have followed a number of strategies for embedding enzymatic activity in coacervates. One strategy was to insert a recombinant enzyme between RGG domains, thus sequestering the enzyme to the coacervate interior. We sequestered an ultrabright version of the enzyme luciferase, NanoLuc, within two RGG domains (RGG-NLuc-RGG). This protein assembles into coacervates on its own and also can be blended with RGG-RGG in different ratios to adjust the level of light (see **Fig. 3**). Based on bioluminescent conversion of the substrate, we could determine that NanoLuc is concentrated 10-fold in the coacervates (1).

We then locally reconstituted enzymatic activity from split enzymes inside coacervates. The ability to control enzyme activity until assembly represent another way to control enzyme activity. We incorporated the split components of the NanoLuc enzyme inside the RGG protein coacervates. We used NanoBiT, an engineered split NanoLuc

system for detecting protein-protein interactions, consisting of a small 1.3 kDa peptide (SmBiT) and a larger 17.6kDa peptide (LgBiT) (1). We flanked SmBiT and LgBiT with RGG domains and fused an MBP domain at the N-termini of the recombinant proteins along with Human Rhinovirus 3C (HRV3C) protease cleavage site (MBP-x-RGG-LgBiT-RGG and MBP-x-RGG-SmBiT-RGG, where x denotes for HRV3C cut site). We confirmed that HRV3C effectively cleaved MBP domains from both of these constructs and resulted in micron-scale protein coacervates within 60 minutes. Bioluminescence images showed that LgBiT and SmBiT were reconstituted inside the RGG protein coacervates and generated a detectable light signal after addition of Nano-Glo substrate. In comparison, at 6 $\mu$ M, neither MBP-RGG-LgBiT-RGG nor MBP-RGG-SmBiT-RGG alone generated a signal after addition of HRV3C and Nano-Glo substrate, confirming that bioluminescence is a result of reconstitution and assembly of LgBiT and SmBiT. These results were confirmed using bioluminescent measurements using a plate reader (1). Thus, we reconstituted of LgBiT and SmBiT into a functional enzyme within protein condensates.

**Enzyme localization on the surface of coacervates.** Spatially distributed assembly of enzymatic activity is a hallmark of biological function and a possible gateway for enzymatic propulsion of coacervates. First, we isolated NanoLuc at the surface of an RGG droplet by attaching it to a surfactant protein with a terminal RGG domain that facilitated localization to the interface of the RGG protein coacervates. The surfactant consists of an N-terminal hydrophilic protein domain Glutathione S-transferase (GST) which is often used as a water solubility enhancer,



a C-terminal RGG domain which tends to partition into the RGG coacervates, and a fluorescent reporter mCherry (GST-mCherry-RGG). We hypothesized we could use this surfactant to recruit a NanoLuc to the surface of RGG coacervates using SynZips (SZ) – SZ1 and SZ2 bind to each other can link proteins together. We fused the surfactant GST-mCherry-RGG with SZ1 (SZ1-GST-mCherry-RGG) and then fused NanoLuc with a SZ2 (NanoLuc-SZ2). Confocal microscopy confirmed that this strategy led to the concentration of NanoLuc to the coacervate-water interface (Fig. 4A). Upon addition of the substrate Nano-Glo and imaging, we observed a ring pattern of bioluminescence indicating peripheral localization of the NanoLuc enzyme (Fig 4A).

We also achieved localization of a functional catalase at the surface of RGG droplets. An RGG dimer was terminated with a SZ1 (SZ1-RGG-RGG). Then, we used the monomeric functional

catalase from *E. coli* (HPII) and linked it to SZ2 with a terminal GFP reporter (GFP-HPII-SZ2). As seen in Fig. 4B, fluorescence was sequestered at the edge of the coacervates. These droplets undergo diffusive motion in response to the addition of H<sub>2</sub>O<sub>2</sub> and we are currently assessing whether motion results from enzymatic activity using dynamic light scattering.

### Future Plans

Our future plans are to a) measure the motion of PLGA capsules in response to catalase activity, both in uniform fields of H<sub>2</sub>O<sub>2</sub> and in gradients; b) measure the motion of coacervate droplets as a result of surface-active catalase; c) make very large coacervates and sequester catalase at the droplet surface and make measurements of shape fluctuation in response to enzyme activity. We also envision using micropipette aspiration to measure the forces to smooth out bending transitions that result from surface forces due to local enzyme activity.

### References

- (1) M. Guan, ... M. C. Good & D. A. Hammer (2021), "Incorporation and Assembly of a Light-Emitting Enzymatic Reaction into Model Protein Condensates," submitted, *Biochemistry*.
- (2) Schuster, B. S., ..., D. A. Hammer, M. C. Good and J. Mittal, (2020), "Identifying Sequence Perturbations to an Intrinsically Disordered Protein that Determine Its Phase Separation Behavior," *Proceedings of the National Academy of Sciences USA* 117 (21):11421-11431.
- (3) W.-S. Jang, ... D. Lee & D.A. Hammer, (2018), "Enzymatically powered surface-associated self-motile protocells," *Small* 14; 1801715.
- (4) N. P. Kamat, M.-H. Lee, D. Lee & D. A. Hammer, (2011), "Micropipette aspiration of double emulsion generated, unilamellar polymersomes", *Soft Matter* 7:9863-9866.
- (5) A.O. Eniola, S. D. Rodgers & D.A. Hammer. (2002), "Characterization of biodegradable drug delivery vehicles with the adhesive properties of leukocytes," *Biomaterials* 23:2167.
- (6) B. S. Schuster, ... M. C. Good & D.A. Hammer, (2018), "Controllable protein phase separation and modular recruitment to form responsive, membraneless organelles," (2018) *Nat. Comm.* 9, 2985.
- (7) Reed, E. H., B. Schuster, M. C. Good & D. A. Hammer, (2020), "SPLIT Stable Protein Coacervation Using a Light Induced Transition," *ACS Synthetic Biology* 9(3):500.

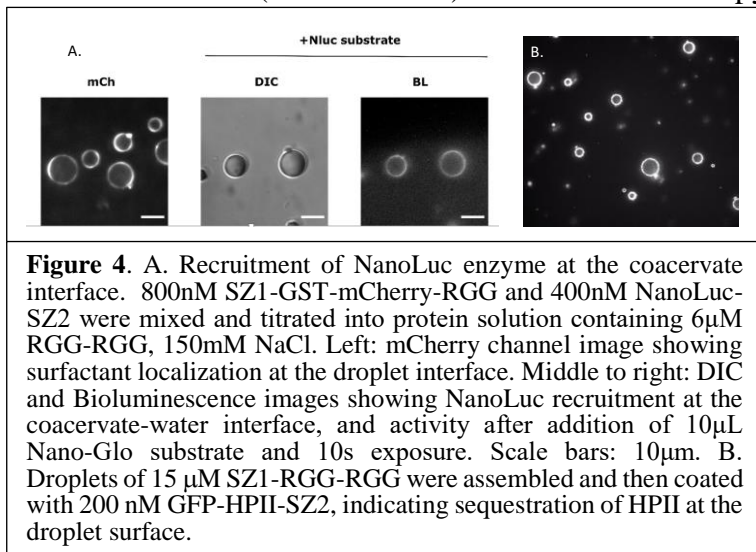


**Figure 4.** A. Recruitment of NanoLuc enzyme at the coacervate interface. 800nM SZ1-GST-mCherry-RGG and 400nM NanoLuc-SZ2 were mixed and titrated into protein solution containing 6µM RGG-RGG, 150mM NaCl. Left: mCherry channel image showing surfactant localization at the droplet interface. Middle to right: DIC and Bioluminescence images showing NanoLuc recruitment at the coacervate-water interface, and activity after addition of 10µL Nano-Glo substrate and 10s exposure. Scale bars: 10µm. B. Droplets of 15 µM SZ1-RGG-RGG were assembled and then coated with 200 nM GFP-HPII-SZ2, indicating sequestration of HPII at the droplet surface.

### **Publications (over last two years)**

Reed, Ellen H., Benjamin Schuster, Matthew C. Good, and Daniel A. Hammer, (2020), "SPLIT Stable Protein Coacervation Using a Light Induced Transition," ACS Synthetic Biology 9(3):500-507; doi:10.1021/acssynbio.9b00503.

Guan, Muyang, Mikael V. Garabedian, Marcel Leutenegger, Benjamin S. Schuster, Matthew C. Good and Daniel A. Hammer (2021), "Incorporation and Assembly of a Light-Emitting Enzymatic Reaction into Model Protein Condensates," submitted, Biochemistry.

Schuster, Benjamin S., Gregory Dignon, Wai Shing Tang, Fleurie Kelley, Aishwarya Kanchi Ranganath, Alison G. Simpkins, Roshan M. Regy, Daniel A. Hammer, Matthew C. Good and Jeetain Mittal, (2020), "Identifying Sequence Perturbations to an Intrinsically Disordered Protein that Determine Its Phase Separation Behavior," Proceedings of the National Academy, USA 117 (21):11421-11431; doi: 10.1073/pnas.2000223117.

Garabedian M.V., Wang W., Dabdoub J.B., Tong, M., Caldwell R.M., Benman W., Schuster B.S., Deiters A., Good, M.C. "Designer Membraneless Organelles Sequester Native Factors for Modular Control of Cell Behavior," in press, Nature Chemical Biology (2021).

Li, S., Xia, B., Javed, B., Hasley, W.D., Melendez-Davila, A., Liu, M., Kerzner, M., Agarwal, S., Xiao, Q., Torre, P., Bermudez, J.G., Rahimi, K., Kostina, N.Y., Möller, M., Rodriguez-Emmenegger, C., Klein, M.L., Percec, V. and Good, M.C. "Direct Visualization of Vesicle Disassembly and Reassembly Using Photocleavable Dendrimers Elucidates Cargo Release Mechanisms." ACS Nano 14: 7398-7411 (2020).

## Chemically fueled dissipative assembly of complex molecular architectures

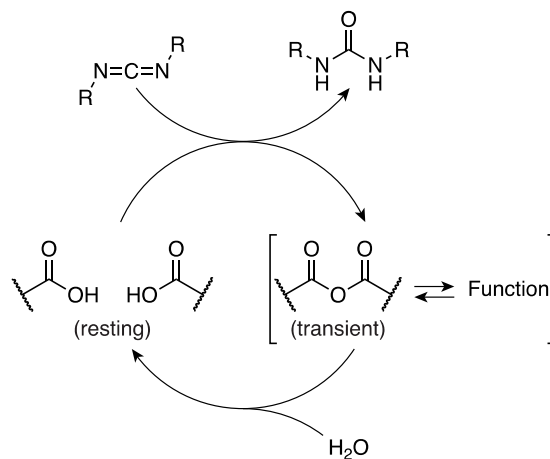
C. Scott Hartley, Department of Chemistry & Biochemistry, Miami University

Dominik Konkolewicz, Department of Chemistry & Biochemistry, Miami University

### Program Scope

The systems of biochemistry are chemical reaction networks that operate with a level of sophistication that is far beyond what chemists can currently design. Many of their most interesting functional properties result from the dissipation of energy; that is, they operate out-of-equilibrium. Often, the energy input is a chemical fuel, such as ATP, which provides selectivity and ultimately complexity over the direct use of light.<sup>1</sup>

Applying these concepts to non-biological systems—that is, developing chemical fuel chemistry that can be used in non-biological contexts—is currently of significant interest.<sup>2</sup> The goal is to achieve systems with adaptive behavior that would be impossible using thermodynamic control. In this context, many different fuel chemistries have been developed.<sup>2</sup> The hydration of carbodiimides is now among the more popular choices. As shown in Scheme 1, carbodiimide hydration is catalyzed by carboxylic acids. Carboxylic anhydrides, which spontaneously decompose if the reaction is carried out in water, are formed as intermediates. The net result is the formation of a *transient (covalent) bond*. While simple, anhydride formation can be coupled to other processes to create functional systems with time-dependent properties.



**Scheme 1.** Treatment of aqueous carboxylic acids with carbodiimides gives transient anhydrides.

The overall goal of this project is to use transient covalent bond formation in functional systems. We are currently focused on three key areas: (1) the transient generation of supramolecular hosts and related assemblies; (2) polymer materials with transient changes in mechanical properties and responsive behavior; (3) fundamental studies of carbodiimide chemistry to optimize their use as chemical fuels.

### Recent Progress

**Transient geometry changes.** ATP-induced geometry changes are found in many

functional systems in biology. We have synthesized the series of diphenic acids in Figure 1a as simple examples of this concept applied to abiotic systems.<sup>3,4</sup> On treatment with the common carbodiimide EDC (*N*-(3-(dimethylamino)-propyl)-*N'*-ethylcarbodiimide hydrochloride), bridging leads to a significant reduction in the twist about the biaryl bond. In essence, this system operates as a chemically fueled molecular clamp (Figure 1b).

Initial work on compounds **DP-Ac1**–**DP-Ac3** established the basic concept.<sup>3</sup> We have subsequently synthesized many more derivatives.<sup>4</sup> Optimization yielded conditions that are kinetically well-behaved, allowing analysis of structure–property effects, leading to several key conclusions. First, the system is surprisingly insensitive to steric effects, tolerating even fairly large substituents. Second, the kinetics are quite sensitive to electronic effects, with electron-withdrawing substituents (e.g., CN) giving reduced efficiencies (anhydride produced per EDC consumed), lifetimes, and peak anhydride concentrations.

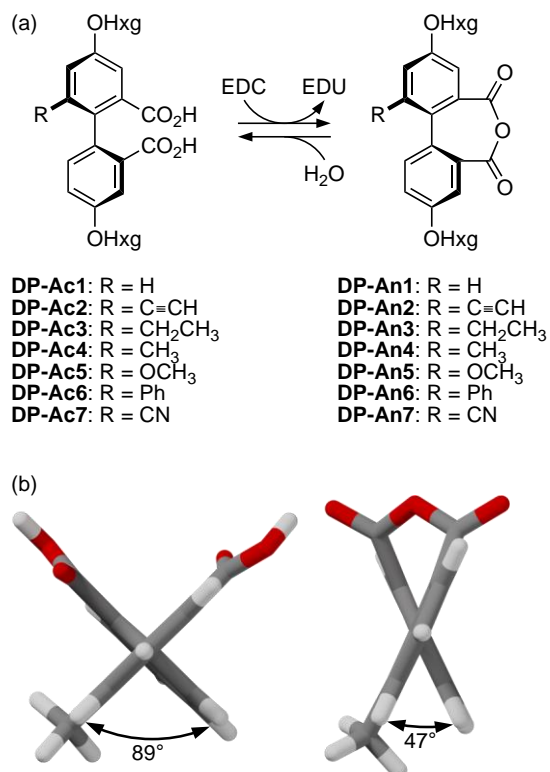
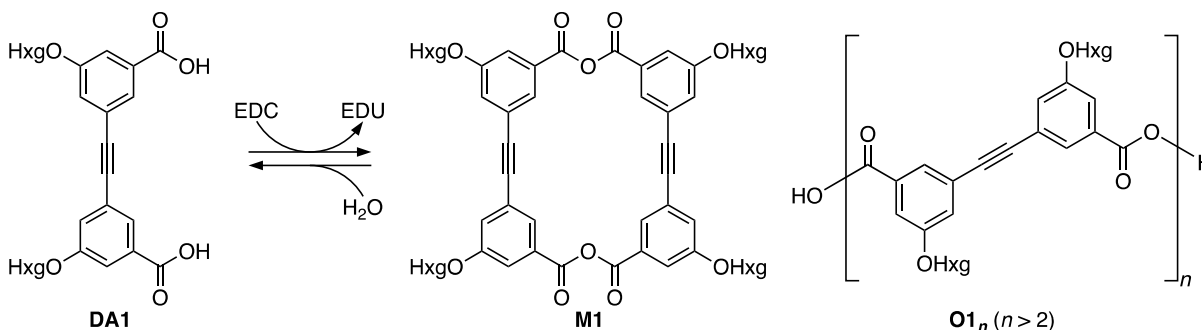


**Figure 1.** Diphenic acids undergo transient geometry changes on treatment with EDC. (a) Compounds synthesized. (b) Geometry changes on bridging.

**Structural complexity in transient assembly.** Compounds assembled through fueled covalent assembly have tended to be quite simple, comprising a single unstable covalent bond linking two components. In contrast, thermodynamically controlled assembly has long been used to prepare macrocycles and cages from multiple polyfunctional reactants, leading to new function. To extend these concepts to chemically fueled systems, diacid **DA1** was assembled using pulses of EDC as shown in Scheme 2.<sup>5</sup> This reaction yields a mixture of the target macrocycle **M1** and oligomers **O1<sub>n</sub>**. Both are observed at short reaction times, but the mixture quickly shifts to favor **M1** which is the major product as the system returns to equilibrium.



**Scheme 2.** Assembly of monomer **DA1** into macrocycle **M1** in competition with oligomerization to **O1<sub>n</sub>**.

Mechanistic studies showed that this arises from two effects. First, the anhydrides are dynamic and exchange more quickly than they decompose back to the starting acids, providing a route for the system to find **M1** as a local minimum on its free energy surface. This process is fuel-independent and continues even once the fuel is exhausted. Second, the anhydrides in **O1<sub>n</sub>** undergo faster hydrolysis and are thus preferentially removed from the reaction mixture. If fuel remains, the regenerated **DA1** is partitioned between the possible products, building up the more-persistent **M1**.

**High-affinity host systems.** In previous work,<sup>6</sup> we had showed that crown-ether-like anhydrides could be assembled with EDC, but exhibited an unusual negative templation effect (i.e., they were suppressed by the cations that best-fit their cavities). These species were only expected to bind cations weakly in water, however, and were therefore not expected to be of use in applications requiring transient hosts (e.g., active transport). We have since been exploring the synthesis and properties of cage-like crown ethers such as **C2** from macrocyclic diacids, which should have much higher cation affinities, as shown in Figure 2. The quantities of **C2** produced from EDC are dependent on the presence of small amounts of alkali metal cations, showing a mixture of positive ( $\text{Li}^+$ ) and negative ( $\text{Na}^+$ ,  $\text{K}^+$ ) templation effects, indicating interactions with the guest. The behavior of a similar cage compound with a larger cavity is distinctly different.

**Transient polymer crosslinking.** In previous work,<sup>7</sup> we had shown that acid-functionalized polymer solutions undergo crosslinking on treatment with EDC, yielding transient gels. A recent example is shown in Figure 3. We have since carried out detailed structure–property relationships on this system. As expected, the peak storage modulus ( $G'$ ) and gel lifetime are sensitive to the amount of EDC added, the proportion of acid groups in the

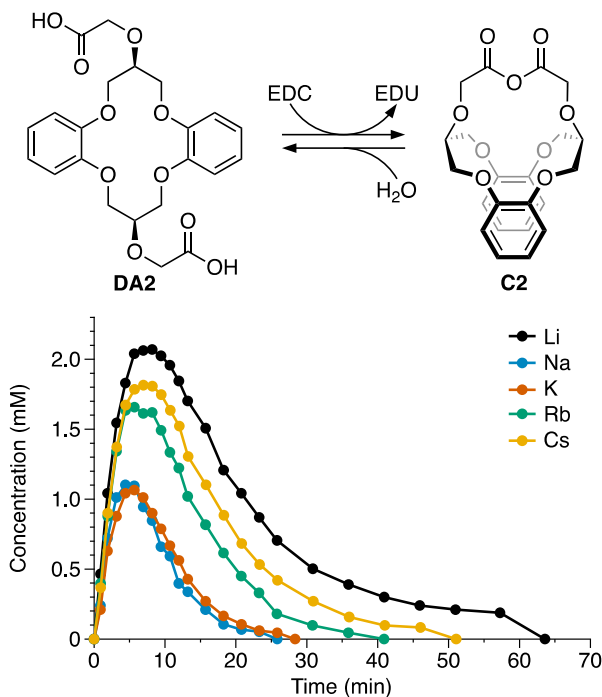


**Figure 2.** Assembly of host **C2** in the presence of various cations (20 mM **DA2**, 40 mM salts).

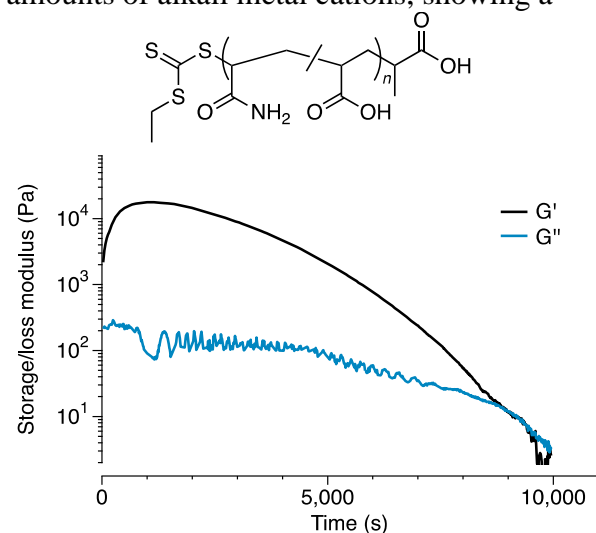


**Figure 3.** Acid-functionalized polymers (top) undergo gelation on treatment with EDC (bottom, data shown for a random copolymer with 170 acrylamide and 30 acrylic acid units).

polymer, and the temperature. The peak storage modulus is predominantly determined by the number of anhydrides that can be formed (i.e., EDC concentration and, to a lesser extent, proportion of available acid groups), whereas the lifetime further depends on hydrolysis rate and is much more sensitive to temperature. Polymer chain length has a relatively small effect.

## Future Plans

**Tuning carbodiimide structure.** EDC, which is water-soluble and readily available, is by far the most common compound used in carbodiimide-fueled assembly, although alternatives have never really been considered. We are currently studying how carbodiimide structure affects the activation rate in these systems, with the goal of identifying compounds that can be conveniently used when the anhydride formation rate needs to be tuned.

**Transient polymer systems.** Integrating transient bond formation with polymer systems is important for the creation of functional materials with responsive behavior. We are currently exploring how carbodiimides can be used to effect transient changes in materials' properties for existing gels (i.e., gel–gel as opposed to sol–gel transitions). We will then explore how polymer network architecture affects materials properties (single vs interpenetrating networks) and develop dual network systems with both permanent dynamic and transient dynamic networks. In a separate study, we will generate monomer systems that undergo transient polymerization, including an investigation of how decomposition rates can be used to organize monomer sequence in the final polymers.

**Structural complexity in transient assembly.** We are continuing our efforts to create transient structurally complex molecules using carbodiimides. We are digging deeper into the mechanism of assembly of the macrocycles in Scheme 2, and will extend these results to 3D cages. We are also incorporating the diphenic acid units in Figure 1 into foldamer backbones as a strategy for amplifying fueled geometry changes.

## References

1. Weißenfels, M.; Gemen, J.; Klajn, R. *Chem* **2021**, *7*, 23–37.
2. Kariyawasam, L. S.; Hossain, M. M.; Hartley, C. S. *Angew. Chem., Int. Ed.* **2021**, *60*, 12648–12658.
3. Jayalath, I. M.; Wang, H.; Mantel, G.; Kariyawasam, L. S.; Hartley, C. S. *Org. Lett.* **2020**, *22*, 7567–7571.
4. Jayalath, I.; Gerken, M.; Mantel, G.; Hartley, S. *ChemRxiv* **2021**, DOI: 10.26434/chemrxiv.14749170.v1.
5. Hossain, M. M.; Atkinson, J. L.; Hartley, C. S. *Angew. Chem., Int. Ed.* **2020**, *59*, 13807–13813.
6. Kariyawasam, L. S.; Hartley, C. S. *J. Am. Chem. Soc.* **2017**, *139*, 11949–11955.
7. Zhang, B.; Jayalath, I. M.; Ke, J.; Sparks, J. L.; Hartley, C. S.; Konkolewicz, D. *Chem. Commun.* **2019**, *55*, 2086–2089.

## Publications

1. Kariyawasam, L. S.; Kron, J. C.; Jiang, R.; Sommer, A. J.; Hartley, C. S. Structure–property effects in the generation of transient aqueous benzoic acid anhydrides by carbodiimide fuels. *J. Org. Chem.* **2020**, *85*, 682–690.
2. Hossain, M. M.; Atkinson, J. L.; Hartley, C. S. Dissipative assembly of macrocycles comprising multiple transient bonds. *Angew. Chem., Int. Ed.* **2020**, *59*, 13807–13813.
3. Jayalath, I. M.; Wang, H.; Mantel, G.; Kariyawasam, L. S.; Hartley, C. S. Chemically fueled transient geometry changes in diphenic acids. *Org. Lett.* **2020**, *22*, 7567–7571.
4. Kariyawasam, L. S.; Hossain, M. M.; Hartley, C. S. The transient covalent bond in abiotic nonequilibrium systems. *Angew. Chem., Int. Ed.* **2021**, *60*, 12648–12658.

## **Controlling Lattice Organization, Assembly Pathways and Defects in Self-Assembled DNA-Based Nanomaterials**

**Sanat K. Kumar and Oleg Gang**

Columbia University, New York, NY

### **Program Scope**

The major objective of this research effort is to devise platform approaches for the assembly by-design of nanoscale objects into prescribed well-organized nanomaterials using DNA programmable strategy. On a fundamental side, this effort seeks to uncover the main parameters controlling assembly processes and to establish the effective ways for creating prescribed nano-architectures through information-encoded interactions. Our integrated experimental and theoretical efforts are focused on exploring how nanoscale lattice and cluster architectures can be rationally formed through engineered nanoscale valence, specifically encoded bonds, a thermodynamic tuning of interactions and an optimization of assembly pathways. We also explore the relationship between molecular factors influencing nanoscale assembly and formed larger scale morphologies. In respect to establishing broadly applicable assembly methods, we have established a strategy of encapsulating nanoparticles (NP) and proteins into DNA frames, forming so called “material voxels”, which are basic building blocks for forming larger-scale organized nanomaterials. The frame’s shape and DNA-programmed anisotropic interactions controls the effective valence and that consequently leads to formation the crystals whose symmetry is directly correlated with the engineered valence. NP lattices are templated by the formed DNA frameworks and they, to a large degree, are independent of the NP details. Through a combination of experiment and theory, we have developed approaches for creating, probing, and understanding the valence-guided self-assembled systems.

In the next stage we plan to generalize these methods, to integrate experiment and mean-field liquid-state theory and molecular simulations to develop inverse design strategies for nanomaterial assembly. These should permit for the robust and tailorable assembly of desired NP lattice types and incorporation of multiple types of NP in the desired manner. While this concept is potentially facile for ordering NPs into arbitrarily designed crystal structures, the presence of defects limits the size and the perfection of the crystals that result. Revealing and analyzing these defects in 3D nano-arrays is a significant challenge that will be addressed by our studies. In addition, using a suite of advanced characterization and computational methods, we aim to delineate the pathways for lattice formation and to establish optimal pathways for minimizing defects and arrested states. In parallel, we are developing novel 3D electron and x-ray-based imaging techniques, and related AI-guided analysis methods to quantify defects and the local arrangements in the 3D NP lattices.

### **Recent Progress**

**Designed Lattices of Functional Inorganic Nanoparticles and Biomolecules.** In order to translate advances in nanoscale-synthesis into targeted material fabrication, it is important to establish methods for organizing nanoscale objects into well-defined three-dimensional (3D) arrays. Despite successes in nanoparticle assembly, most extant methods are system-specific and not fully compatible with biomolecules. We developed a platform approach for assembly distinct 3D ordered arrays from different nanomaterials using DNA prescribed and valence-controlled material voxels. DNA is a precisely programmable material<sup>1,2</sup> appropriate for directing 3D particle organization<sup>3-6</sup>. Typically, nanoparticles are grafted with single-stranded DNA chains, and

assembled using base-pairing of complementary sequences. This robust approach, however, cannot decouple particle properties, e.g., its shell, size, and shape, from the assembly structure. Due to the complex and often transient shapes, the problem of organizing biomolecules is even greater. Thus, an outstanding challenge is to establish a versatile methodology for assembly of nanoscale objects of different nature in 3D ordered arrays.

We addressed this challenge by using 3D DNA frameworks formed from polyhedral DNA origami frames for organizing nano-objects in space<sup>7</sup>. The approach can be extended to catalytic, biological and inorganic matrices. One of the key difficulties in realization of this strategy is to reveal relationship between the design of frame, inter-frame connectivity, and thermodynamic and kinetic effects favorable for the formation of 3D ordered framework. We used DNA frames of different shapes to host desired nano-objects. This integrated object, so called a “material voxel”, is an elemental building block with designed anisotropic interactions and encapsulated functional nano-object. The access to different lattice symmetries is provided through the design of inter-vertex hybridization of frames. Hybridization permits a great control over interactions encoding, energetics and flexibility of interframe linkages.

We demonstrated that 3D ordered lattice can be assembled purely from DNA frames with shapes of Platonic solids (octahedral, cubic and tetrahedral frames) in predetermined manner. Our detailed studies using electron microscopy (EM) methods permitted optimize the formation of voxels and incorporation of nanoparticle within them. The in-situ structural studies were conducted using in-situ small angle x-ray scattering (SAXS) and ex-situ TEM, which revealed the designed principles and assembly pathways required for the formation of 3D crystalline arrays. These experimental efforts were supported by our computational work that successfully predicted equilibrium phases for these three different shapes of voxels. The computational findings are in great agreement with our experimental observations. We applied the developed assembly method for building materials from light emitting nanoparticles, simple protein (streptavidin) and enzymatic cascades (glucose oxidase and horseradish peroxidase). The confirmation and characterization of different 3D lattices from inorganic and bio-organic materials, demonstrates the versatility of our DNA material voxel assembly approach. We used this platform to synthesize two different material organizations with properties relevant to dramatically different applications – optical, using a combination of quantum dots, and catalytic, using a cascaded enzyme network organized within a 3D lattice.

**Designed and Bioactive Protein 2D and 3D Lattices.** Broadly applicable methods to organize proteins in 2D and 3D ordered arrays are required to enable complexly designed biomaterials, engineered biomolecular scaffolds, cell-free bio-systems, and well-defined hybrid biomolecular-nanoparticle materials. The significant requirement for these novel material systems is an ability to preserve a biological activity of proteins in these formed arrays. We developed an approach (**Figure 1**) for the tailored integration of proteins into DNA-based voxels and the programmable assembly of these voxels into biologically functional protein arrays<sup>8</sup>. Our approach allows to form fully designed 2D and 3D ordered protein organizations. We applied the presented concept to ferritin, an iron storage protein, and its iron-free analog, apoferritin, in order to form single-layers, double-layers, as well as several types of prescribed 3D protein lattices. Our work demonstrates that internal voxel design and programmable inter-voxel encoding can be effectively employed to create protein lattices, as confirmed by in-situ x-ray scattering and cryo-electron microscopy 3D imaging. Furthermore, we showed that the assembled protein lattices maintain structural stability

and biological activity in environments relevant for protein functionality. The open framework of the 3D arrays allows small molecules to access the ferritins and their iron cores, and convert them into apoferritin arrays through the release of iron ions. The presented study introduces a platform approach for creating ordered bioactive protein nanomaterials with desired organizations.

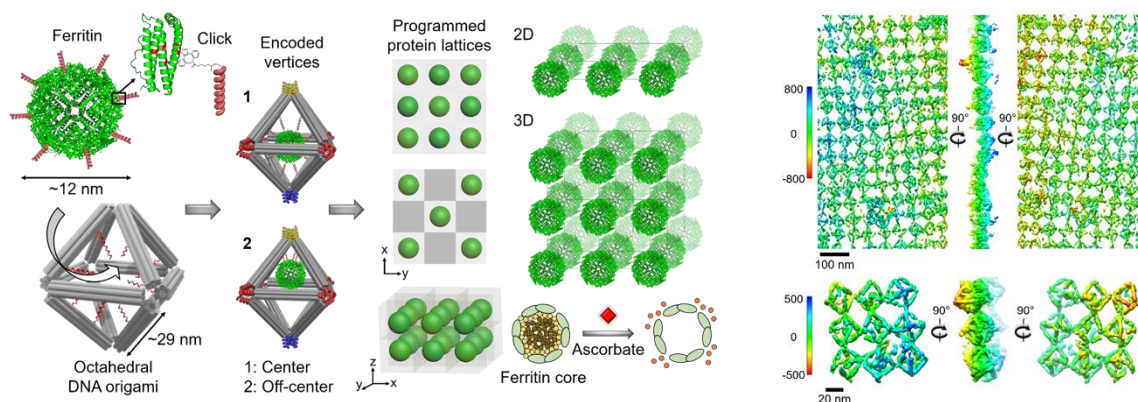


**Figure 1.** (Left) Illustration showing the approach for assembling bioactive proteins into ordered 2D and 3D arrays through programmable octahedral-shaped DNA frameworks. These frameworks can host and control the placement of the proteins internally—for example, at the center (1) or off-center (2)—and be encoded with specific sequences externally (color coding scheme) to create desired lattices. The 3D ferritin array could release iron ions and preserve lattice structure. (Right) Nanoscale tomography based on the images obtained by cryo-electron microscopy visualizes DNA-protein lattices in 3D. The color bars indicate different heights of the lattice (in angstroms).

**Complexly encoded anisotropic bonds for 1D, 2D and 3D Assembly.** We developed DNA hollow square bucket (HSB) as a basic building block which interactions can be fully encoded and regulated for achieving desired assembly state<sup>9</sup>. We demonstrated the programmable 1D, 2D and 3D hierarchical ordered arrays, assembled via DNA hybridization encoding on HSB (**Figure 2**). The HSB is fenced by double layer DNA duplexes with a height of 28 nm and a square open window in the center. Binding strands (“sticky ends”) can be prescribed independently along three dimensions of HSB, which dictate the construction of final assembled structures. To construct 1D, 2D and 3D ordered arrays, complementary sticky ends for bucket-bucket recognition are anchored along Z, XY and XYZ direction of HSB, respectively. HSB can be encoded binding strands not only for bucket-bucket recognition,

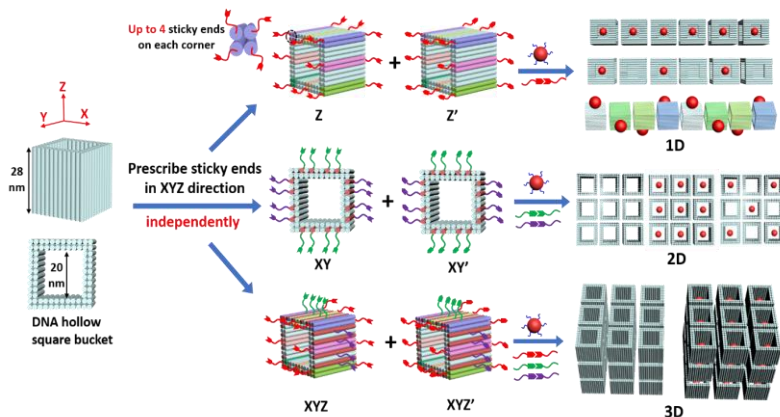


**Figure 2. Programmable assembly with differentiated and complexly encoded bonds.** Designed hollow square bucket is constructed by double layer DNA shown as cylinders. Design of DNA bonds for bucket-bucket recognition along three dimensions (XYZ) can be prescribed independently and each bond is encoded by DNA of multiple types, thus allowing for full differentiation and complex encoding of anisotropic bonds. Designed 1D, 2D and 3D organizations were realized experimentally using SAXS and electron microscopy and studied computationally.

but also for association of NP within the cavity or on the bundle of sidewalls. The resultant 1D, 2D and 3D empty ordered arrays were designated to form organizations of NPs. We showed the construction of several types of linear architectures, such as homo-chain-like and alternating-chain-like arrays, and chiral NP organizations. We applied the developed method for further generating 2D arrays and 3D lattices with prescribed NPs organizations. Different types of mesoscale 3D morphologies were observed in our computational modelling efforts of assembly process, and were found through the detailed small angle x-ray scattering (SAXS) data analysis. This study is also important for revealing the role of defects. That is, by varying the interaction energies (and the number/type of bonds on each site) and then evaluating the size of self-assembled structures formed allow us to assess factors that affect assembly and that restrict the formation of more perfect structures. Thus, for example, if the contact energy for a pair is infinitely strong, then it will pair with a favorable neighbor as quickly as possible. However, this strong binding prevents bond rearrangement that could potentially create more favorable (multi-NPs) assembly states. That is, for us to access true equilibrium requires entropy to be competitive with energetics.

**Combinatorial-Entropy-Driven Aggregation in DNA-Grafted Nanoparticles.** We used computer simulations and experiment to show that there are attractive interactions between pairs of NPs grafted with palindromic single-stranded DNA sequences<sup>10</sup> (**Figure 3**). This contribution arises purely from combinatorial entropy, i.e., from the chains deciding if they want to pair with chains grafted to the same vs different NPs. We evaluated theoretically and numerically this entropic contribution originating from the number of distinct bonding patterns associated with intra- and inter-particle binding. This entropic attraction, which becomes more favorable with decreasing inter-NP distance, allows for the NP to form condensed phases. The theoretical predictions were fully confirmed in our experiment, which probed formation of lattices for predicted NP-DNA designs.

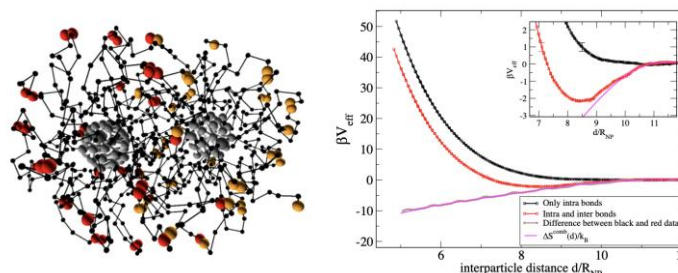


**Figure 3:** Base pairing between two NPs with palindromic DNA sequences. The yellow and red are single strand fragments on the two NPs. The proximity of yellow and red suggests that inter-NP binding happens. (right) The consequences of such binding on inter-NP potential PMF (red). The purple is the (attractive) contribution to the PMF, while the black curve is the entropic penalty for brush overlap from NPs.

### Future Plans

Our future work will develop the hierarchical assembly strategy based on the prescribed valence concept. We will combine this assembly methodology with structure-predictive inverse design strategy. In addition, to investigating questions about establishing principle and practical approaches for assembly of equilibrium structures, we aim to explore what assembly pathways can lead to the faster structure formation with minimal defects. In-situ structure probing and assembly monitoring using x-ray scattering and nanoscale tomography will be utilized. We will establish x-ray- electron microscopy-based and methods for 3D imaging of NP lattices with single NP sensitivity to obtain information about defects, interfaces and lattice imperfections. Finally, we will investigate principles and develop quantitative methods for creating complex designed lattices using systems with distinctive sequence-encoded interactions.

## References

- 1 Seeman, N. C. DNA in a material world. *Nature* **421**, 427-431 (2003).
- 2 Rothemund, P. W. K. Folding DNA to create nanoscale shapes and patterns. *Nature* **440**, 297-302 (2006).
- 3 Halverson, J. D. & Tkachenko, A. V. DNA-programmed mesoscopic architecture. *Phys. Rev. E* **87**, 062310 (2013).
- 4 Zheng, J., Constantinou, P. E., Micheel, C., Alivisatos, A. P., Kiehl, R. A. & Seeman, N. C. Two-Dimensional Nanoparticle Arrays Show the Organizational Power of Robust DNA Motifs. *Nano Letters* **6**, 1502-1504 (2006).
- 5 Nykypanchuk, D., Maye, M. M., van der Lelie, D. & Gang, O. DNA-guided crystallization of colloidal nanoparticles. *Nature* **451**, 549-552 (2008).
- 6 Vo, T., Venkatasubramanian, V., Kumar, S., Srinivasan, B., Pal, S., Zhang, Y. G. & Gang, O. Stoichiometric control of DNA-grafted colloid self-assembly. *Proc. Natl. Acad. Sci. USA* **112**, 4982-4987 (2015).
- 7 Tian, Y., Lhermitte, J. R., Bai, L., Vo, T., Xin, H. L. L., Li, H. L., Li, R. P., Fukuto, M., Yager, K. G., Kahn, J. S., Xiong, Y., Minevich, B., Kumar, S. K. & Gang, O. Ordered three-dimensional nanomaterials using DNA-prescribed and valence-controlled material voxels. *Nature Materials* **19**, 789+, doi:10.1038/s41563-019-0550-x (2020).
- 8 Wang, S.-T., Minevich, B., Liu, J., Zhang, H., Nykypanchuk, D., Byrnes, J., Liu, W., Bershadsky, L., Liu, Q., Wang, T., Ren, G. & Gang, O. Designed and biologically active protein lattices. *Nature Communications* **12**, 3702, doi:10.1038/s41467-021-23966-4 (2021).
- 9 Lin, Z., Emamy, H., Minevich, B., Xiong, Y., Xiang, S., Kumar, S., Ke, Y. & Gang, O. Engineering Organization of DNA Nano-Chambers through Dimensionally Controlled and Multi-Sequence Encoded Differentiated Bonds. *Journal of the American Chemical Society* **142**, 17531-17542, doi:10.1021/jacs.0c07263 (2020).
- 10 Sciortino, F., Zhang, Y. G., Gang, O. & Kumar, S. K. Combinatorial-Entropy-Driven Aggregation in DNA-Grafted Nanoparticles. *Acs Nano* **14**, 5628-5635, doi:10.1021/acsnano.9b10123 (2020).

## Publications

1. F. De Fazio, A. H. El-Sagheer, J. S. Kahn, I. Nandhakumar, M. R. Burton, T. Brown, O. L. Muskens, O. Gang & A. G. Kanaras. "Light-Induced Reversible DNA Ligation of Gold Nanoparticle Superlattices", *ACS Nano* (2019).
2. Chen, K. J. Gibson, D. Liu, H. C. Rees, J.-H. Lee, W. Xia, R. Lin, H. L. Xin, O. Gang & Y. Weizmann. Regioselective surface encoding of nanoparticles for programmable self-assembly. *Nature Materials* **18**, 169 (2019).
3. Lu, T. Vo, Y. Zhang, A. Frenkel, K. G. Yager, S. Kumar, and O. Gang. "Unusual Packing of Soft-Shelled Nanocubes", *Science Advances*, DOI: 10.1126/sciadv.aaw2399 (2019)
4. Z. Li, Y. Xiong, S. Xiang, O. Gang. "Controllable Covalent-bound Nano-Architectures from DNA Frame, *Journal of the American Chemical Society*", DOI: 10.1021/jacs.9b01510, (2019)
5. Hamed Emamy, Oleg Gang, Francis W Starr, "The Stability of a Nanoparticle Diamond Lattice Linked by DNA", *Nanomaterials*, (2019), **9**(5): 661; doi: 10.3390/nano9050661

6. Honghu Zhang, Mingxing Li, Kaiwei Wang, Ye Tian, Jia-Shiang Chen, Katherine T Fountaine, Donald DiMarzio, Mingzhao Liu, Mircea Cotlet, Oleg Gang. "Polarized Single-Particle Quantum Dot Emitters through Programmable Cluster Assembly". *ACS Nano* 14, 2, 1369–1378; (2019); <https://doi.org/10.1021/acsnano.9b06919>
7. C.H. Liu, E Janke, R Li, P Juhas, O Gang, D.V. Talapin, S.J.L. Billinge, "sasPDF: pair distribution function analysis of nanoparticle assemblies from small-angle-scattering data, *J. Appl. Cryst.*", (2020). 53, 699-709; <https://doi.org/10.1107/S1600576720004628>
8. JS Kahn, B Minevich, O Gang. "Three-dimensional DNA-programmable nanoparticle superlattices". DOI: 10.1016/j.copbio.2019.12.025. *Current opinion in biotechnology* (2020)
9. Ye Tian, Julien R Lhermitte, Lin Bai, Thi Vo, Huolin L Xin, Huilin Li, Ruipeng Li, Masafumi Fukuto, Kevin G Yager, Jason S Kahn, Yan Xiong, Brian Minevich, Sanat K Kumar, Oleg Gang. "Ordered three-dimensional nanomaterials using DNA-prescribed and valence-controlled material voxels". <https://doi.org/10.1038/s41563-019-0550-x>. *Nature Materials*, (2020)
10. Shih-Ting Wang, Melissa A. Gray, Sunting Xu, Yiyang Lind, James Byrnes, Andy I. Nguyen, Nevena Todorova, Molly M. Stevens, Carolyn R. Bertozzi, Ronald N. Zuckermann, and Oleg Gang. "DNA Origami Protection and Molecular Interfacing through Engineered Sequence-Defined Peptides". <https://doi.org/10.1073/pnas.1919749117>, *PNAS*, (2020).
11. Sha Sun, Shize Yang, Huolin Xin, Dmytro Nykypanchuk, Mingzhao Liu, Honghu Zhang and Oleg Gang. "Valence-Programmable Nanoparticle Architectures". *Nature Communications*, 11, 2279 (2020)
12. F. Sciortino, Y. Zhang, O. Gang, S. Kumar, Sanat, "Combinatorial-Entropy Driven Aggregation in DNA-Grafted Nanoparticles", *ACS Nano*, 14, 5628-5635, doi:10.1021/acsnano.9b10123 (2020).
13. Xiong, Y., Huang, J., Wang, S. T., Zafar, S. F. & Gang, O. Local Environment Affects the Activity of Enzymes on a 3D Molecular Scaffold. *ACS Nano* 14, 14646-14654, doi:10.1021/acsnano.0c03962 (2020).
14. Shani, L., Michelson, A. N., Minevich, B., Fleger, Y., Stern, M., Shaulov, A., Yeshurun, Y. & Gang, O. DNA-assembled superconducting 3D nanoscale architectures. *Nature Communications* 11, 5697; doi:10.1038/s41467-020-19439-9 (2020).
15. Lin, Z., Emamy, H., Minevich, B., Xiong, Y., Xiang, S., Kumar, S., Ke, Y. & Gang, O. Engineering Organization of DNA Nano-Chambers through Dimensionally Controlled and Multi-Sequence Encoded Differentiated Bonds. *Journal of the American Chemical Society* 142, 17531-17542, doi:10.1021/jacs.0c07263 (2020).
16. Sciortino, F., Zhang, Y. G., Gang, O. & Kumar, S. K. Combinatorial-Entropy-Driven Aggregation in DNA-Grafted Nanoparticles. *ACS Nano* 14, 5628-5635, doi:10.1021/acsnano.9b10123 (2020).
17. Gang, O. Reactive polymers guide nanoparticle clustering Tailored polymer shells drive the assembly of a desired class of nanoparticle architectures. *Science* 369, 1305-1306, doi:10.1126/science.abd8183 (2020).
18. Ma, N. N., B. Minevich, J. L. Liu, M. Ji, Y. Tian, and O. Gang. Directional Assembly of Nanoparticles by DNA Shapes: Towards Designed Architectures and Functionality. *Topics in Current Chemistry* 378 (2020). <https://dx.doi.org/10.1007/s41061-020-0301-0>.

19. Xiong, Y., Yang, S., Tian, Y., Michelson, A., Xiang, S., Xin, H. & Gang, O. Three-Dimensional Patterning of Nanoparticles by Molecular Stamping. *ACS Nano* 14, 6823-6833. (2020). <https://dx.doi.org/10.1021/acsnano.0c00607>
20. Michelson, A., Zhang, H. H., Xiang, S. T. & Gang, O. Engineered Silicon Carbide Three-Dimensional Frameworks through DNA-Prescribed Assembly. *Nano Letters* 21, 1863-1870, doi:10.1021/acs.nanolett.0c05023 (2021).
21. Majewski, P. W., Michelson, A., Cordeiro, M. A. L., Tian, C., Ma, C. L., Kisslinger, K., Tian, Y., Liu, W. Y., Stach, E. A., Yager, K. G. & Gang, O. L. Resilient three-dimensional ordered architectures assembled from nanoparticles by DNA. *Science Advances* Vol. 7, no. 12, eabf0617; DOI: 10.1126/sciadv.abf0617 (2021).
22. Gang, O. DNA assembles nano-objects. *Physics Today* 74, 58-59 (2021).
23. He, L., Mu, J., Gang, O., & Chen, X. Rationally Programming Nanomaterials with DNA for Biomedical Applications, *Advanced Science*, (2021); <https://doi.org/10.1002/advs.202003775>
24. S.T. Wang, B. Minevich, J. Liu, H. Zhang, D. Nykypanchuk, J. Byrnes, W. Liu, L. Bershadsky, Q. Liu, T. Wang, G. Ren, and O. Gang. Designed and biologically active protein lattices, *Nature Communications*, 12, Article number: 3702 (2021); <https://doi.org/10.1038/s41467-021-23966-4>
25. Jason Kahn and Oleg Gang, Designer Nanomaterials through Programmable Assembly, *Angewandte Chemie*, (2021) <https://doi.org/10.1002/ange.202105678>

## **Command of Active and Responsive Elastomers by Topological Defects and Patterns**

**Oleg D. Lavrentovich**

**Advanced Materials and Liquid Crystal Institute, Materials Science Graduate Program,  
Department of Physics, Kent State University, Kent, Ohio 44242**

### **Program Scope**

The goal is to establish a relationship between the spatial director gradients inscribed into the liquid crystal monomer by patterned plasmonic photoalignment and the response of the resulting liquid crystal elastomer (LCE). The focus is on photopatterned LCE coatings that offer a possibility to create and explore dynamic surface topographies and to analyze fundamental mechanisms of thermo-mechanical and photo-mechanical response. The patterns under investigation represent one-, two- and three-dimensionally varying molecular orientations.

### **Recent Progress**

Liquid crystal elastomers (LCEs) hold a major promise as a versatile material platform for smart soft coatings, since their orientational order can be pre-designed to program a desired dynamic profile. Understanding the relationship between the LCEs ordering and their response to external cues is of prime importance in the fundamental physics of out-of-equilibrium systems. Many facets of the activity-orientational order coupling can be studied in a controlled manner by using pre-designed patterns of the orientational order with topological defects as an integral part of the system. In this project, we introduce temperature-responsive and light-responsive dynamic coatings based on LCEs with various patterns of molecular orientation. At the early stages of our research we explored one-dimensionally and two-dimensionally varied patterns of molecular orientation inscribed into the LCE by plasmonic metamask photoalignment [1,2]. Within the last two years, our main focus was on a much more complex director pattern that incorporates three-dimensional director variations and singular regions in the form of topologically stable disclinations [3].

We demonstrated a deterministic relationship between the complex three-dimensional geometry of the pre-inscribed molecular orientation and the dynamic surface topography of the disclinations-containing thermally-activated LCE coatings. The disclinations are pre-designed by confining the nematic monomer between two plates with different in-plane director patterns, one unidirectional and another one periodically distorted with alternating splay and bend in the shape of letters “C”, resembling Néel walls. The disclinations form in response to the antagonistic boundary conditions as singular lines that run in the bulk of the sample parallel to the bounding plates, resolving frustrations in the regions in which the top and bottom directors are perpendicular to each other, Fig.1.

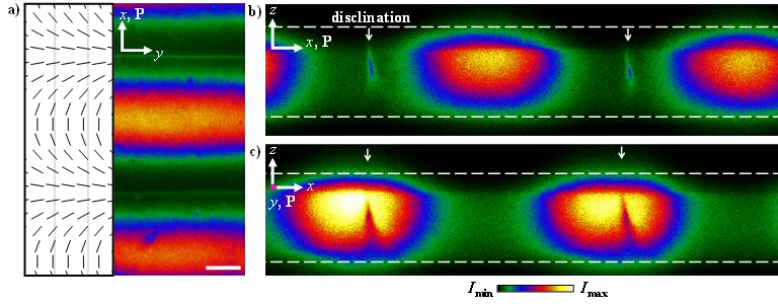


**Figure 1.** LCE coating. Fluorescence confocal polarizing microscopy of **a)**  $xy$ -scan with light polarized along the  $x$ -direction. Scale bar  $20\ \mu\text{m}$ ; **b)**  $xz$ -scan with light polarized along the  $x$ -direction; **c)**  $xz$ -scan with light polarized along the  $y$ -direction. The dotted lines in **(b)** and **(c)** represent the coating of thickness  $18\ \mu\text{m}$ . The white arrows in **(b)** and **(c)** point towards the disclination cores.

the director pattern predesigned on one of the surfaces, the microchannels-valleys form along the splay regions and elevations run along the bend regions. Besides the displacements along the normal direction, the LCE coatings also show in-plane displacements. The correspondence between the directions of profile shifts, both out-of-plane deflections, and in-plane material displacements, is easy to trace qualitatively by considering the spatial variation of the activation force  $\mathbf{f} = \alpha|\Delta S|(\hat{\mathbf{n}}\text{div}\hat{\mathbf{n}} - \hat{\mathbf{n}} \times \text{curl}\hat{\mathbf{n}})$  and Fig. 3; here  $\alpha$  is the activation coefficient,  $|\Delta S|$  is the change in the absolute value of the scalar order parameter of the LCE, and  $\hat{\mathbf{n}}$  is the spatially-varying director. The profile of the LCE coating with periodic valleys above the disclinations can be of two types: single-minimum valleys and double-minimum valleys. The latter form when the disclinations are close to the patterned surface of a heated coating. The experimentally observed modifications of the LCE profiles in response to the temperature are reproduced in detail by the linear elasticity theory and nonlinear finite-element numerical simulations, which predict a variety of outcomes, including the single and double valleys.

Qualitatively, the development of valleys at elevated temperatures can be understood as thickening of the film along the nearby locations where the director does not change along the  $z$ -axis. In these locations, the ellipsoid of nematic order parameter becomes less elongated and approaches a sphere

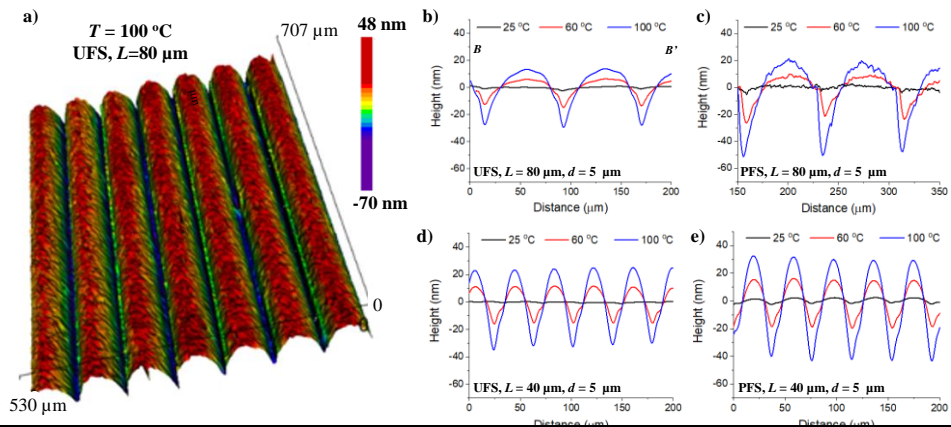


**Figure 2.** **a)** 3D image of LCE coating at  $100\ \text{°C}$ , period  $L=80\ \mu\text{m}$ . Temperature dependence of LCE surface profiles of **b)** a coating with a uniformly aligned free surface (UFS),  $L=80\ \mu\text{m}$ ; bottom substrate is patterned; **c)** Patterned free surface (PFS),  $L=80\ \mu\text{m}$ ; bottom surface is uniform; **d)** USF,  $L=40\ \mu\text{m}$ ; **e)** PFS,  $L=40\ \mu\text{m}$ . In all cases, the coating thickness is  $d = 5\ \mu\text{m}$ .

The LCE coatings prepared at room temperature with a system of disclinations are initially flat. Once the coatings are heated, a decrease in the scalar order parameter coupled to the director distortions produces a profound change in the topography of the coating, Fig.2. Namely, the thickness of the coatings decreases along the vertical planes that contain disclinations (thus forming microgrooves) and increases in the intermediate locations where the director is uniform along the normal to the coating. In terms of

upon heating, which implies thickening of the film. Conservation of mass means that the regions with disclinations develop valleys. Both the experiments and the theory demonstrate that the director distortions produce not only out-of-plane deflections but also in-plane mass transport, guided by the director pattern. The theoretical and numerical models predict not only the correct direction of material shifts but also quantify these shifts in terms of the elastic parameters of the LCE and changes of the scalar order parameter.

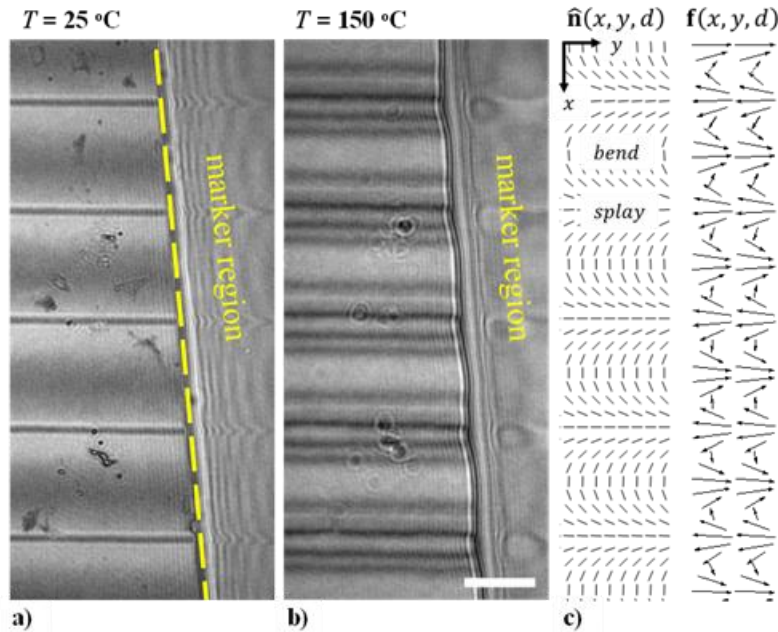


**Figure 3.** a) PFS LCE coating at  $25\text{ }^{\circ}\text{C}$ ;  $d = 7\text{ }\mu\text{m}$ ; b) Wavy appearance of initially straight line in panel (a) when LCE coating is heated to  $150\text{ }^{\circ}\text{C}$ . Note that the marker line shifts to the left in the splay regions with disclinations. Scale bar,  $25\text{ }\mu\text{m}$ ; c) Spatial variation of the director field  $\hat{n}$  and the activation force  $f$  at the patterned surface of a LCE coating;  $f$  points to the right in bend regions, to the left in the splay regions and from splay to bend regions, which explains qualitatively the experimental data on in-plane and out-of-plane profile shifts of the LCE coatings, see Fig.2.

coatings activated by an external cue such as temperature can be controlled by the gradients of director distortions at singular disclinations. The established close correspondence between the experiment and theory suggests that the proposed linear elasticity theory and nonlinear finite-element numerical simulations grasp the most salient details of responsive patterned LCEs and can be used to model other complicated geometries, in which the thermal, electromagnetic, or chemical energy can be transformed into elastic response and potentially useful mechanical work. The disclinations-containing LCEs show potential as soft dynamic coatings with a predesigned responsive surface profile.

Another notable research accomplishment was the preparation of smectic LCE coatings in which the surface topography was caused by the shrinkage of the smectic layer upon the temperature activation and preparation of nanoscale topographies that serve as substrates to various active matter systems. Lavrentovich wrote a number of invited review papers in which the discussion of LCEs was part of the analysis. Shiyanovskii developed a theory of nematics based on the nemator description that would facilitate simulations of LCE properties.

The described dynamic profile of the patterned LCE coatings should be distinguished from the wrinkles that LCE coatings and films develop under external mechanical loading, even when the director is initially uniform in space and the load is unidirectional; this wrinkling effect has been studied extensively, see the most recent papers [4-6] and references therein. In the present work, the reason for surface modulations is not an external load: it is the prepatterned director gradients that yield a non-flat surface topography once the change in the scalar order parameter is activated by the temperature, which is an external action of a scalar isotropic nature with no preferred direction in space.

The work demonstrates that the geometry and amplitude of surface deformations in LCE

## Future Plans

The plan is to explore two new mechanisms of fast dynamic control of coatings topography: one is based on visible light irradiation and another on a low-frequency electric field actuation. Surfaces in natural materials are usually static, but even a static topography brings an important functionality, examples being plant leaves and animal skins. LCEs with a controllable fast dynamic surface topography could create the next generation of advanced materials with properties superior to those found in Nature. One of the seemingly fruitful approaches is to use an electric field and light. However, explorations of the electric field effect started only very recently [7-9], and the fundamental mechanisms remain unexplored, while light effects are mostly limited by UV irradiation, see, for example, Ref. [2]. We plan to explore

1. LCE coatings which incorporate photosensitive molecules that change their conformation under blue and red light in the visible part of the spectrum.
2. LCE coating which incorporate molecules with strong permanent electric dipoles to impart a sensitivity to the electric field, to study the LCE response to the electric field and develop electrically-controlled surface topographies.

## References

- [1] G. Babakhanova, T. Turiv, Y. B. Guo, M. Hendrikx, Q. H. Wei, A. Schenning, D. J. Broer, and O. D. Lavrentovich, *Liquid crystal elastomer coatings with programmed response of surface profile*, Nature Communications **9**, 456 (2018).
- [2] G. Babakhanova, H. Yu, I. Chaganava, Q. H. Wei, P. Shiller, and O. D. Lavrentovich, *Controlled Placement of Microparticles at the Water-Liquid Crystal Elastomer Interface*, Acs Applied Materials & Interfaces **11**, 15007-15013 (2019).
- [3] G. Babakhanova, Y. M. Golestani, H. Baza, S. Afghah, H. Yu, M. Varga, Q.-H. Wei, P. Shiller, J. V. Selinger, R. L. B. Selinger, and O. D. Lavrentovich, *Dynamically morphing microchannels in liquid crystal elastomer coatings containing disclinations*, Journal of Applied Physics **128**, 184702 (2020).
- [4] H. Soni, R. A. Pelcovits, and T. R. Powers, *Wrinkling of a thin film on a nematic liquid-crystal elastomer*, Physical Review E **94**, 012701 (2016).
- [5] P. Plucinsky and K. Bhattacharya, *Microstructure-enabled control of wrinkling in nematic elastomer sheets*, Journal of the Mechanics and Physics of Solids **102**, 125-150 (2017).
- [6] M. S. Krieger and M. A. Dias, *Tunable wrinkling of thin nematic liquid crystal elastomer sheets*, Physical Review E **100**, 022701 (2019).
- [7] D. Q. Liu, N. B. Tito, and D. J. Broer, *Protruding organic surfaces triggered by in-plane electric fields*, Nature Communications **8**, 1526 (2017).
- [8] A. Agrawal, H. Y. Chen, H. Kim, B. H. Zhu, O. Adetiba, A. Miranda, A. C. Chipara, P. M. Ajayan, J. G. Jacot, and R. Verduzco, *Electromechanically Responsive Liquid Crystal Elastomer Nanocomposites for Active Cell Culture*, Acs Macro Letters **5**, 1386-1390 (2016).
- [9] H. M. van der Kooij, S. A. Semerdzhiev, J. Buijs, D. J. Broer, D. Q. Liu, and J. Sprakel, *Morphing of liquid crystal surfaces by emergent collectivity*, Nature Communications **10**, 3501 (2019).

## Publications

1. G. Babakhanova and O.D. Lavrentovich, The techniques of surface alignment of liquid crystals, Chapter 7 in *Modern Problems of the Physics of Liquid Systems*, Springer Proceedings in Physics 223, Editors L.A. Bulavin and L. Xu, Springer Nature Switzerland AG, 2019, pages 165-197.
2. C. Peng, O.D. Lavrentovich, Liquid Crystals-Enabled AC Electrokinetics, *Micromachines* **10**, 45 (2019).
3. J.-K. Guo, S.-H. Hong, H.-J. Yoon, G. Babakhanova, O.D. Lavrentovich, J.-K. Song, Laser-induced nanodroplet injection and reconfigurable double emulsions with designed inner structures, *Advanced Science* **2019** 1900785 (2019)
4. G. Babakhanova, Y. M. Golestani, S. Afghah, H. Baza, M. Varga, H. Yu, Q.-H. Wei, P. Shiller, J.V. Selinger, R. L. B. Selinger, and O.D. Lavrentovich, Dynamically morphing microchannels in liquid crystal elastomer coatings containing disclinations, *Journal of Applied Physics* **128**, 184702 (2020) Chosen as an Editor's Pick.
5. O.D. Lavrentovich, Design of nematic liquid crystals to control microscale dynamics, *Liquid Crystals Reviews* **8**, 59-129 (2020)
6. G. Babakhanova, J. Krieger, B.-X. Li, T. Turiv, M.-H. Kim, O. D. Lavrentovich, Cell alignment by smectic liquid crystal elastomer coatings with nanogrooves, *J. Biomed. Mater. Res.* **108A**, 1223–1230 (2020)
7. Taras Turiv, Jess Krieger, Greta Babakhanova, Hao Yu, Sergij V. Shiyonovskii, Qi-Huo Wei, Min-Ho Kim, Oleg D. Lavrentovich, Topology control of human fibroblast cells monolayer by liquid crystal elastomer, *Science Advances* **6**, eaaz6485 (2020)
8. O.D. Lavrentovich, Ferroelectric nematic liquid crystal, a century in waiting, *PNAS* **117**, 14629-14631 (2020)
9. R. Koizumi, T. Turiv, M. M. Genkin, Robert J. Lastowski, Hao Yu, Irakli Chaganava, Qihuo Wei, Igor S. Aranson, and Oleg D. Lavrentovich, Control of microswimmers by spiral nematic vortices: Transition from individual to collective motion and contraction, expansion, and stable circulation of bacterial swirls, *Physical Review Research* **2**, 033060 (2020).
10. O.D. Lavrentovich, Design of Chiral Domains by Surface Confinement of Liquid Crystals, *ACS Central Science* **6**, 1858-1861 (2020).
11. N. Aryasova, S.V. Shiyonovskii, Elasticity and dynamics of uniaxial nematic liquid crystal with defects: Nematic model, *Phys. Rev. Res.* **2**, 043373 (2020)
12. Mojtaba Rajabi, Hend Baza, Taras Turiv, and Oleg D. Lavrentovich, Directional self-locomotion of active droplets enabled by nematic environment, *Nature Physics* **17**, 260-266 (2021).

## **Understanding functional dynamics on the nanoscale through an integrated experimental–computational framework**

**Erik Luijten, Northwestern University**

**Qian Chen, University of Illinois at Urbana-Champaign**

### **Program Scope**

We aim to establish a closely integrated experimental–computational program of work focused on understanding and emulating the nanoscopic functional dynamics of living systems in synthetic materials. Our central hypothesis is that nanoparticles (NPs) with properly designed directional interactions will afford fine control over their equilibrium assembly, motility driven by chemical fuels or external fields, and ultimately non-equilibrium aggregation into functional materials. Our primary goals are to understand the working mechanisms of patchy machines on the nanoscale and to generate collective, spatiotemporal patterns from them as a new form of active materials, which exhibit form and function that change as needed. Specifically, cyclic spatiotemporal patterns underly most systems that perform useful work or transduce energy, yet their realization in man-made materials that are reconfigurable on the nanoscale is extremely limited. The ability of such patchy nanomachines to undergo dynamic cooperative transitions in morphology will provide radically new opportunities for controlling processes such as mass and energy transport. These materials differ from the vast majority of synthetic static materials which exist in only a single form and have limited function throughout their performance lifespan.

### **Recent Progress**

During this reporting cycle (Year 1), we have made major progress in multiple areas in joint experimental–computational work on capturing, analyzing (including machine learning, ML), and understanding of NP dynamics, the synthesis of patchy NPs as machines, and computational studies of the forces and pattern formation mechanisms associated with the driven dynamics of NPs. These efforts are described in detailed below.

#### 1. Experimental–computational collaboration on understanding the equilibrium self-assembly of anisotropic NPs captured by liquid-phase transmission electron microscopy (TEM)

We used liquid-phase TEM to achieve the first imaging of crystal growth modes for a diversity of NPs of about 50 nm in size (e.g., gold nanocubes, concave nanocubes, nanospheres) from their disordered suspended state. Unexpectedly, for all these NP shapes we discovered a universal layer-by-layer growth mode (Fig. 1a, c–d), resembling atomic crystallization but differing from the corrugated growth prevalent for colloidal crystals. We complemented our experiments with kinetic Monte Carlo simulations to understand this dependence of crystal growth mode on the size of the building blocks. The simulations cover a wide range of intrinsic diffusion rates  $D_0$  and interaction range  $\Delta$ . As shown in Fig. 1b, there exists a sharp boundary in the phase map as a function of the diffusion rate and the particle flux  $F$ , only weakly dependent on  $\Delta$ . We thus established a unified framework for understanding crystal growth modes across four orders of magnitude in length scale, from atomic to micron-sized colloids. In contrast to existing disparate concepts in crystallization, such as thin-film epitaxy in metallurgy and the semiconductor industry, ion clustering in mineralogy, and geometric packing in colloidal physics, we identified building block

size as the common factor governing crystal growth across scales, thereby connecting the historically separate communities. Several key parameters governing crystallization kinetics were measured that were until now inaccessible, which allows us to provide input and validation for predictive simulations that will enable a paradigm shift towards efficient and quantitative crystal design.

## 2. Collaborative efforts on developing unsupervised ML for shape classification of patchy NPs

We developed an unsupervised ML to quantify, in an automated manner, the morphology of patchy NPs (metallic cores and polymer patches, more details in Section 3) based on TEM images (Fig. 1e). We adapted U-Net based convolutional neural networks to identify the core and patch in the TEM images. Subsequently, the segmented contours of the patches were converted into a general

representation of shape feature as a  $d(\theta) - \theta$  function (Fig. 1f), which was then further dimension-reduced through principal-component analysis (to retain the major geometric features as inputs for shape classification). The classification identifies four classes of patchy NPs based upon their degree of symmetry using a Gaussian Mixture Model without prior knowledge or subjective interpretation of the patch geometry (Fig. 1g). The fraction of patches belonging to each class depends on the ligand concentrations. We view this method as a foundation for smart synthesis, where machine learning analyzes the products and predicts the optimal synthesis conditions to achieve high-throughput and high-precision synthesis of patchy NPs—the central materials system in this project.

## 3. Synthesis of symmetry-breaking patchy nanoprisms from cooperative polymer grafting

We advanced the synthesis of patchy NPs to introduce controlled symmetry breaking of patches through cooperative polymer grafting using gold triangular prisms as a demonstration. As illustrated in Fig. 2, we synthesized single-patched nanoprisms with preferential adsorption of polystyrene-*b*-polyacrylic acid (PS-*b*-PAA) on one of three otherwise geometrically and

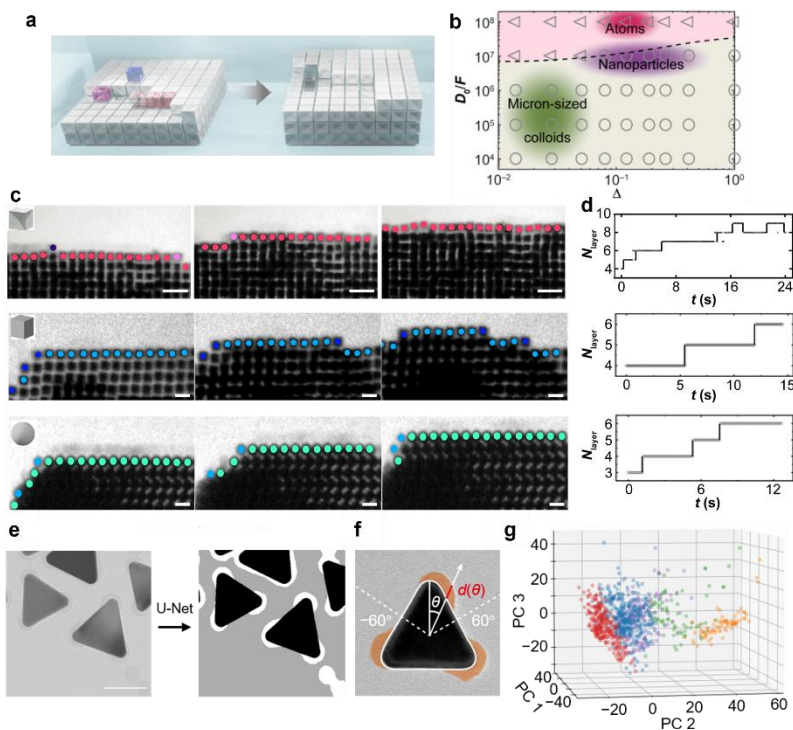


Figure 1. (a) Schematic of layer-by-layer growth of nanoparticle crystals. (b) Kinetic Monte Carlo simulations distinguish crystal growth modes for atoms, NPs, and colloids (triangles: layer-by-layer growth; circles: roughened growth). The regions where atoms, NPs, and micron-sized colloids reside are shaded in red, purple, and green, respectively. (c) Liquid-phase TEM snapshots of layer-by-layer growth modes for various NP shapes. (d) Staged growth of the number of (partial) layers  $N_{\text{layer}}$  over time  $t$ . (e) TEM images of patchy NPs and U-Net based segmentation. (f) Conversion of patch contours into shape signature. (g) Unsupervised ML-based classification of different patch geometries. Scale bars: 200 nm.

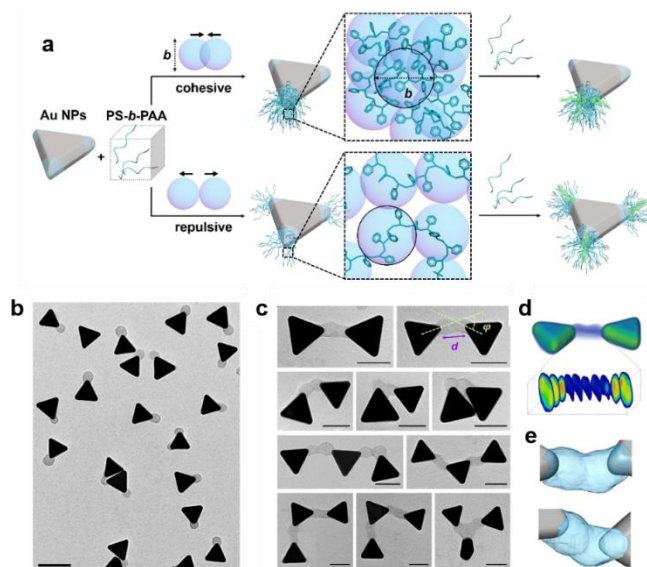


Figure 2. (a) Schematics of cooperative polymer grafting based synthesis of patchy nanoprisms. (b) TEM images of the single-patched nanoprisms. (c-d) TEM images and 3D reconstructions of the assemblies of single patched prisms. Scale bars: 100 nm in (b) and 50 nm in (c).

chemically identical prism tips. Strong polymer–polymer attraction was found crucial to induce this symmetry breaking by enabling a macromolecular “bandwagon” effect. Freely suspending polymers tend to keep joining the adsorption domains occupied by other polymers in the presence of polymer–polymer attraction, effective even on top of polymer–solvent attraction and the entropic steric hinderance. This effect, if utilized at the onset of polymer adsorption and at dilute polymer concentration, can lead to symmetry breaking if multiple identical adsorption sites are available but stochastically the initial adsorption of first few polymer molecules occurs only on one of them. The single-patched prisms can assemble into “nano-bowties” via patch interpenetration (Fig. 2c–d). We demonstrated for the first time the approach of cooperative polymer grafting to create

symmetry-broken patchy NPs, which we view as applicable to other NP shapes. Instead of generating patches coated evenly on all vertices, our method can enable selective coating on one, two, or multiple vertices, allowing us to build a library of patchy NPs as “nanomachines.”

#### 4. Inducing pattern formation through collective motion of active components

To achieve controlled large-scale organization of active components, we designed a class of systems based upon self-propelled NPs (“swimmers”) that can be controlled via an external magnetic field (Fig. 3a). Earlier work indicated that the steady state of such highly nonequilibrium systems may be predictable through concepts derived from equilibrium thermodynamics, but this hypothesis continues to be unproven beyond the prototypical symmetric two-component case. We have been able to generalize this concept in two ways, by increasing the number of components and by breaking the symmetry of the interactions that drive phase separation and pattern formation. We are studying these newly designed systems through large-scale molecular dynamics simulations. These simulations have confirmed that the concepts discovered

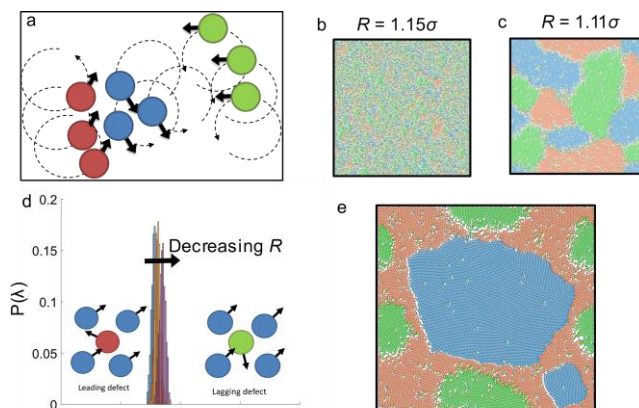


Figure 3. (a) Schematic showing three groups of colloidal particles that move  $120^\circ$  out of phase from each other. The state of a random system after being driven with a radius of (b)  $R=1.15\sigma$  and (c)  $R=1.11\sigma$  after 105 orbital cycles. (d) Histogram of out-of-phase particles present in the bulk phase of a species for  $R=1.11\sigma$  (blue),  $1.10\sigma$  (orange),  $1.09\sigma$  (yellow), and  $1.08\sigma$  (purple). (e) Steady-state structure when the blue species leads the red species by  $72^\circ$ , the red species leads the green species by  $144^\circ$ , and the green species leads the blue species by  $144^\circ$ .

in the binary case extend to ternary (Fig. 3b) and quaternary systems. Pattern formation is controlled by the orbital radius of the particles (Fig. 3c), which we surmise to represent the non-equilibrium counterpart of temperature in equilibrium thermodynamics. In addition, we realized that the interactions can be tuned through the phase difference between the orbiting components (Fig. 3d), affording control over the spatial arrangements of segregated domains (Fig. 3e). Beyond fundamental discovery, these computations will guide our subsequent experimental efforts.

## 5. Understanding entropic interactions in multicomponent fluids

On a fundamental level, the role of entropy in aggregation in multicomponent systems is known since the 1950s through the seminal work of Asakura and Oosawa on depletion interactions. However, far less is known on solutions in which the depletants comprise multiple components. Building on earlier algorithmic developments, we have developed a Monte Carlo algorithm for computing the depletion interactions induced in ternary systems with multiple size asymmetries. We have attained high-precision predictive capabilities allowing the design of systems with complex effective interactions that can be further modulated through the presence of electrostatic charges on the particles, permitting targeted design of experimental systems.

### **Future Plans**

In the next reporting period, we will continue to synthesize high-quality patchy NPs and use the patchy NP library that we have already established to perform systematic liquid-phase TEM imaging and analysis of kinetic pathways using a combination of machine learning based image analysis, simulation, and theory. We will also extend our equilibrium assembly studies to active NPs that are self-propelled by chemical fuels and by electrophoretic mechanisms. Moreover, we are in the process of extending our computational methodology to include fully resolved hydrodynamic effects.

### **Publications**

Binbin Luo<sup>†</sup>, Ziwei Wang<sup>†</sup>, Zihao Ou, Erik Luijten<sup>\*</sup>, Qian Chen<sup>\*</sup>, “Unravelling crystal growth modes at the nanoscale,” submitted to *Nature*, under review, solely acknowledging this DOE grant.

Ahyoung Kim, Thi Vo, Hyosung An, Lehan Yao, Shan Zhou, Sharon C. Glotzer, Qian Chen, “Programmable symmetry-broken patch nanoprisms from cooperative polymer grafting,” awaiting publication.

Lehan Yao, Hyosung An, Shan Zhou, Ahyoung Kim, Erik Luijten, Qian Chen, “An unsupervised machine learning for nanomorphology classification,” manuscript in preparation, solely acknowledging this DOE grant.

Garrett Watson and Erik Luijten, “Complex interactions induced by multi-component depletants,” manuscript in preparation, solely acknowledging this DOE grant.

## **Bio-mimetic material design based on principles of disorder**

Sidney R. Nagel (University of Chicago)  
Andrea J. Liu (University of Pennsylvania)

### **Program Scope**

Our overarching goal is to investigate various aspects and new principles of disordered matter that allow for innovative material design and to apply these principles to create novel and flexible biologically-inspired functions. Starting with networks created from simulated particle packings, our aim is to invent new algorithms to manipulate material in order to create novel functionality. Our program emphasizes the important role that disorder plays in creating malleable matter. By uncovering the flexibility of these materials, we can create new forms of matter with novel functions that are inspired by biological functions. There is a real potential for creating a new means of manufacturing functionality into a material that could have a broad applicability.

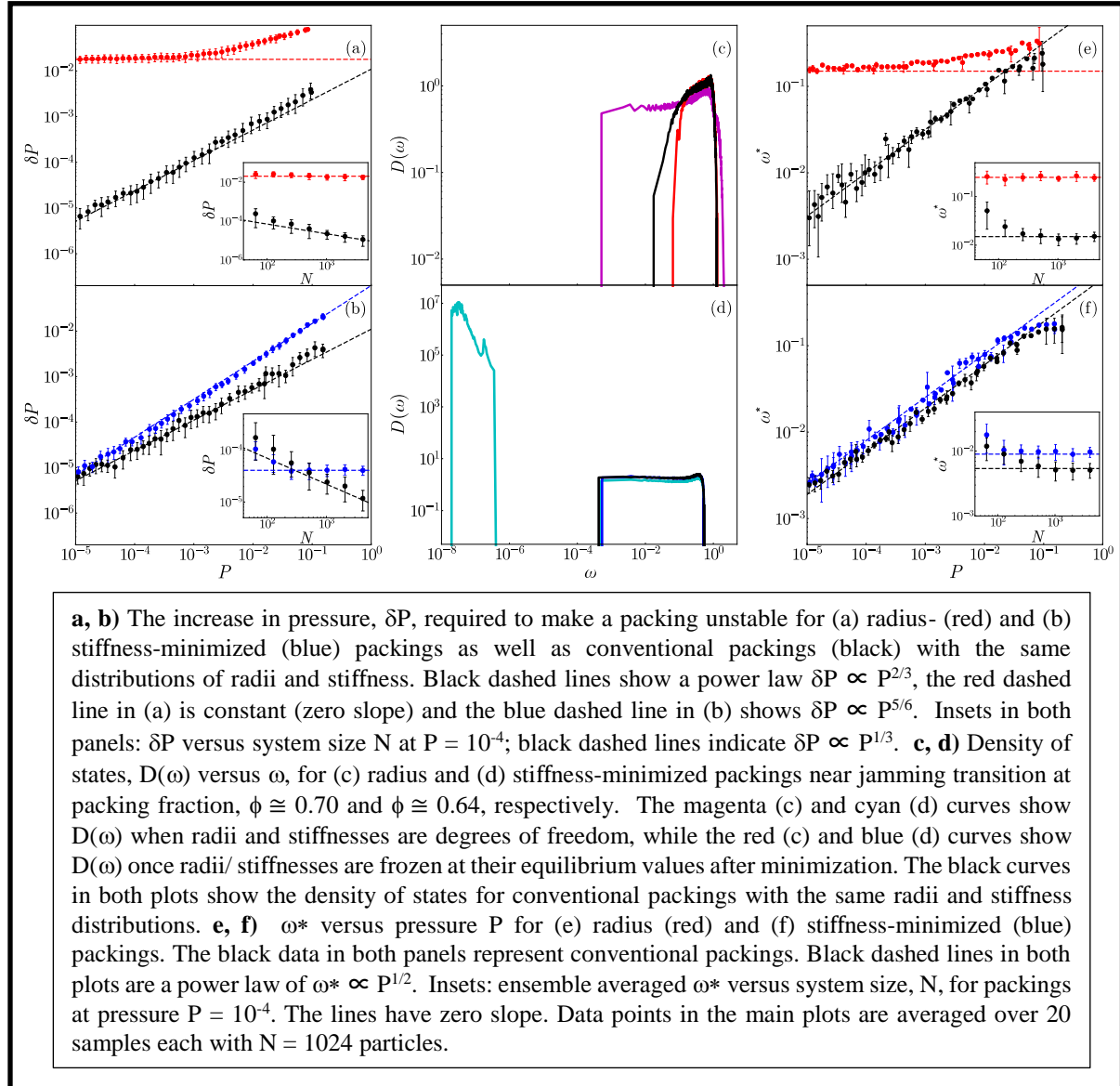
Minimization of a function to find low-lying states in a complex landscape is a daunting challenge that lies at the heart of many constraint-satisfaction statistical-physics problems, ranging from machine learning to population ecology [1-4]. One example is finding low-energy configurations of a jammed disordered packing of spherical particles. In this case, the landscape is the potential-energy surface and the  $Nd$  degrees of freedom that are varied to minimize the energy are the positions of each of the  $N$  particles in  $d$ -dimensional space. For the resulting states, rigidity or stability against applied strain requires that the number of constraints, which are the inter-particle forces or contacts shared between pairs of particles, must exceed the number of degrees of freedom:  $NZ/2 \geq Nd$  where  $Z$  is the average number of contacts per particle in the system [5]. Typically, in the thermodynamic limit a jammed system is only marginally stable to perturbations [6-13]; that is, an infinitesimal perturbation suffices to rearrange the packing, pushing the system into a new local energy minimum.

It was recently proposed that stress-induced aging can be exploited to manipulate an out-of-equilibrium solid to achieve various desired elastic responses [14]. Thus, imposing strain directs the manner in which a solid ages. This directed aging relies on the fact that straining a disordered system gives rise to a spatially varying stress pattern that depends sensitively on the applied deformation. If we consider a disordered network of nodes connected by bonds, an external force applied on such a network would result in a different stress at each bond. Each bond evolves (*i.e.*, ages) at a different rate; in many cases, the bonds under the highest stress evolve the fastest. In a particulate solid, regions under higher stress presumably deform plastically at a higher rate as well, but the effects can be highly nonlinear and how they affect material properties is not well understood. In our recent progress, we have started to extend the ideas we have developed for mechanical networks to disordered particulate solids.

### **Recent Progress**

The particle positions (and orientations for non-spherical particles) are only a subset of possible degrees of freedom that one might want to allow. The swap Monte Carlo [15-19] and breathing algorithms [20-24] have found success in producing more stable jammed states by permitting some latitude for particle radii to vary. We can view these algorithms in a broader

context in which the introduction of additional “learning” degrees of freedom [14, 25-27] such as particle radii can lead to desirable properties such as greater stability.



In general, the addition of new degrees of freedom allows more ways for the system to reach a lower energy minimum but does not necessarily guarantee that the system is more stable in the sense that there are enhanced barriers against rearrangement due to external perturbations. Indeed, one might expect that when particle radii as well as positions are allowed to vary, the resulting jammed packings may remain marginally stable even while their energies are reduced.

We have investigated [28] how the transient addition of new degrees of freedom affects the properties of jammed states. By “transient” we mean that the new degrees of freedom are accessible during minimization but are frozen once the system reaches a local minimum. The mechanical stability of a physical system plays a crucial role in determining its excitations and response to strain. Recent advances have led to protocols that can create particularly stable amorphous solids. Such systems, whether they be physical systems created using vapor-deposition

or numerical model systems created using swap or breathing algorithms, exist in exceptionally deep energy minima marked by the absence of low-frequency quasilocalized modes. As shown in the figure, we have introduced new numerical protocols for creating stable jammed packings that first introduce and subsequently remove degrees of freedom such as particle sizes or particle stiffnesses. We find that different choices for the degrees of freedom can lead to very different results. For jammed packings, degrees of freedom that couple to the jamming transition, *e.g.*, particle sizes, push the system to much more stable and deeper energy minima than those that only couple to interaction stiffnesses.

If the new learning degrees of freedom couple to the energy, minimization allows the system to find lower-energy minima than were accessible without them. Paths leading out of the minima that involve those degrees of freedom become blocked by energy barriers once those degrees of freedom are frozen. By manipulating the allowed degrees of freedom in this way, we create configurations that not only have low energy but also have high energy barriers preventing escape. However, we find that not all transient degrees of freedom are equally effective at increasing stability. Degrees of freedom that change the Maxwell count create particularly stable packings, while those that leave the isostatic point unaffected at  $Z=2d$  do not appreciably increase stability.

### **Future Plans**

Introducing learning degrees of freedom is effective in producing mechanical networks with desirable properties beyond stability, such as negative Poisson ratio [24–26, 29], allostery [26, 27, 30, 31] and classification ability [27]. We plan in our future work to generalize this idea, at least conceptually. For example, vapor-deposited glasses are observed to be much more stable than those formed from normally supercooled liquids [32]. Perhaps particles at a free surface have more degrees of freedom than those in the bulk and that those particles can then freeze as more particles are deposited on upper layers. This would be an example of a learning degree of freedom that then gets quenched or frozen out as the sample preparation continues. Relaxation pathways in a supercooled liquid that are accessible at higher temperature (or lower pressure) may effectively freeze out on certain time scales with further supercooling. Similarly, when a glassy system ages or is subjected to cyclical loading, some relaxation pathways become inaccessible that had previously been available to the system. Perhaps these pathways can be viewed as degrees of freedom that freeze out over time. We will be studying in what ways new degrees of freedom, such as these, can be introduced and then frozen in both simulations and then into experimentally accessible materials.

In addition, we plan on studying how these ideas relate to creating metamaterials with novel function. Metamaterials offer the possibility of creating a broad array of behaviors not found in ordinary, non-architected materials. By manipulating the connectivity and strength of the structural units, rather than the composition or structure of the native material itself, metamaterials with unusual elastic response—mechanical metamaterials—can be designed. While such metamaterials can be designed and built on a relatively small scale, it is not always clear how to scale up the number of components or to control the microstructure at the microscopic level in order to achieve the desired behavior – especially when the applied deformations are well outside the linear-response regime. A mechanical metamaterial with inhomogeneous response is difficult to design, since it requires detailed knowledge of structure and mechanics at the constituent scale and computer resources that grow with system size. It is also challenging to fabricate, since it requires control and manipulation at the constituent scale. The idea of “directed aging” [14] circumvents

these obstacles by starting with a disordered solid and training it while it ages by applying appropriate stresses in such a way that it ultimately evolves to have the desired functionality. Directed aging takes advantage of the natural tendency of a material to minimize its energy under stress by deforming plastically. A demonstrated process that can be understood in terms of directed aging is the heating of solid foams under pressure to create auxetic (i.e., negative Poisson's ratio) foams [13]. The concept of directed aging allows this process to be generalized to create materials with a variety of responses determined by the stresses applied [12]. Aging a system under a fixed shear stress, for example, leads to systems with high Poisson's ratios. The challenge for this general approach is to find appropriate flexible protocols for the training that will produce a broad class of response.

## References

- [1] F.Krzakala, J. Kurchan. *Phys. Rev. E*, 76(2):021122, 2007.
- [2] M. Mézard, T. Mora. *Journal of Physiology-Paris*, 103: 107–113, 2009.
- [3] A. Altieri, S. Franz. *Phys. Rev. E*, 99: 010401, 2019.
- [4] P. Mehta, W. Cui, C-H Wang, R. Marsland. *PRE*, 99: 052111, 2019.
- [5] J. Clerk Maxwell. *Philosophical Magazine and Journal of Science*, 27: 294–299, 1864.
- [6] R. Connelly, W. Whiteley. *SIAM Journal on Discrete Mathematics*, 9, 1996.
- [7] P. Charbonneau, E.I. Corwin, G. Parisi, F. Zamponi. *Phys. Rev. Lett.* 109: 205501, 2012.
- [8] C.P. Goodrich, W.G. Ellenbroek, A.J. Liu. *Soft Matter*, 9:10993–10999, 2013.
- [9] C.P. Goodrich, S. Dagois-Bohy, et al.. *Phys. Rev. E*, 90: 022138, 2014.
- [10] E.DeGiuli, A. Laversanne-Finot, G.Düring, E.Lerner, M.Wyart. *Soft Matt.* 10:5628, 2014.
- [11] R Connelly, SD Guest. Cornell Univ., College Arts Sci., 2015.
- [12] M. Müller, M. Wyart. *Ann. Rev. of Cond. Matter Phys.*, 6(1):177–200, 2015.
- [13] N. Xu, A.J. Liu, S.R. Nagel. *Phys. Rev. Letts.* 119: 215502, 2017.
- [14] N. Pashine, D. Hexner, A.J. Liu, S.R. Nagel. 5(12): eaax4215, 2019.
- [15] A. Ninarello, L. Berthier, D. Coslovich. *Phys. Rev. X*, 7: 021039, 2017.
- [16] H. Ikeda, F. Zamponi, A. Ikeda. *J. Chem Phys.* 147: 234506, 2017.
- [17] C. Brito, E. Lerner, M. Wyart. *Phys. Revi. X*, 8: 031050, 2018.
- [18] L. Berthier, E. Flenner, C.J. Fullerton, C. Scalliet, M. Singh. *J. Stat. Mech.: Theory and Experiment*, 2019: 064004, 2019.
- [19] A.D.S. Parmar, B. Guiselin, L. Berthier. *J. Chem. Phys.* 153:134505, 2020.
- [20] C. Brito, H. Ikeda, P. Urbani, M. Wyart, F. Zamponi. *PNAS* 115: 11736–11741, 2018.
- [21] G. Kapteijns, W. Ji, C. Brito, M. Wyart, E. Lerner. *Phys. Rev. E*, 99: 012106, 2019.
- [22] H. Ikeda, P. Urbani, F. Zamponi. *J. Physics A: Math and Theor*, 52: 344001, 2019.
- [23] T. Yanagishima, J. Russo, R. Dullens, H. Tanaka. *arXiv:2011.09259*, 2020.
- [24] H. Ikeda, C. Brito, M. Wyart. *J. Stat. Mech.: Th. & Exp*, 2020: 033302, 2020.
- [25] C.P. Goodrich, A.J. Liu, S.R. Nagel. *Phys. Rev. Letts.* 114: 225501, 2015.
- [26] D. Hexner, A.J. Liu, S.R. Nagel. *PNAS*, 117:31690–31695, 2020.
- [27] M. Stern, D. Hexner, J.W. Rocks, A.J. Liu. *arXiv preprint arXiv:2011.03861*, 2020.
- [28] V.F. Hagh, S.R. Nagel, A.J. Liu, M.L.Manning, E.I. Corwin. *arXiv:2105.10846*, 2021.
- [29] D. Hexner, A.J. Liu, S.R. Nagel. *Phys. Rev. E*, 97: 063001, 2018.
- [30] J.W. Rocks, N. Pashine, I. Bischofberger, C.P. Goodrich, A.J. Liu, S.R. Nagel. *PNAS*, 114: 2520–2525, 2017.
- [31] J.W. Rocks, H. Ronellenfisch, A.J. Liu, S.R. Nagel, E. Katifori. *PNAS*, 116 :2506, 2019.
- [32] M.D. Ediger. *J. Chem. Phys.* 147: 210901, 2017.

## **Publications in past 2 years supported by DOE-BES**

“The limits of multifunctionality in tunable networks,” Jason W. Rocks, Henrik Ronellenfitsch, Andrea J. Liu, Sidney R. Nagel, Eleni Katifori *PNAS* **116**, 2506–2511 (2019).

“Memory formation in matter,” Nathan C. Keim, Joseph Paulsen, Zorana Zeravcic, Srikanth Sastry, Sidney R. Nagel *Rev. Mod. Phys.* **91**, 035002 (2019).

“Directed aging, memory and Nature's greed,” Nidhi Pashine, Daniel Hexner, Andrea J. Liu, Sidney R. Nagel *Science Advances* **5**, eaax4215 (2019). arXiv:1903.05776

“Ideal Isotropic Auxetic Networks from Random Networks,” Daniel R. Reid, Nidhi Pashine, Alec S Bowen, Sidney R. Nagel, Juan J. de Pablo *Soft Matter* **15**, 8084-8091 (2019)

“Effect of directed aging on the nonlinear elasticity and memory formation in a material,” Daniel Hexner, Nidhi Pashine, Andrea J. Liu, Sidney R. Nagel *Phys. Rev. Research* **2**, 043231 (2020).

“Periodic training of creeping solids,” Daniel Hexner, Andrea J. Liu, Sidney R. Nagel *PNAS* **117**, 31690 - 31695 (2020).

“Multiple memory formation in glassy landscapes,” Chloe W. Lindeman, Sidney R. Nagel  
Accepted *Science Advances* (2021).

“Transient degrees of freedom and stability,” Varda F. Hagh, Sidney R. Nagel, Andrea J. Liu, M. Lisa Manning, Eric I. Corwin ArXiv:2105.10846

## Electrostatic Driven Self-Assembly Design of Functional Nanostructures

Monica Olvera de la Cruz (PI) and Michael J. Bedzyk (co-PI)

Department of Materials Science and Engineering, Northwestern University, Evanston, IL 60208

### Program Scope

The goal of this project is to understand the role of electrostatics in determining the equilibrium assembly structures composed of charged amphiphilic molecules in heterogenous environment. Inside cells of living organisms, aggregates of biomolecules facilitate and regulate functions. These aggregates organize the local environment to promote specific cellular functions including synthesizing molecules. The aim of this project is to design aggregates that mimic cellular aggregates by using synthetic molecules. The complexity of the interactions between components of the aggregates requires a cooperative theoretical and experimental approach.

### Recent Progress

**Functionalizing Microcompartments.** In collaboration with Northwestern's Tullman-Ercek group, we studied the physical principles of Bacterial microcompartments (MCPs) self-assembly to guide the engineering of microreactors [1]. MCPs are reactors that enclose and protect enzymes that aid in chemical and energy production. MCPs are found in various bacterial phyla and are postulated to help many of these organisms survive in hostile environments such as the gut of their hosts. By means of multiscale simulations, we identified the amino acids and interactions responsible for assembling a well-characterized MCP protein into different morphologies, including long tubular structures to enhance sequential reactions. Physical models were developed to predict the dependence of MCP morphology on the number ratio of different protein components (Fig. 1, left).

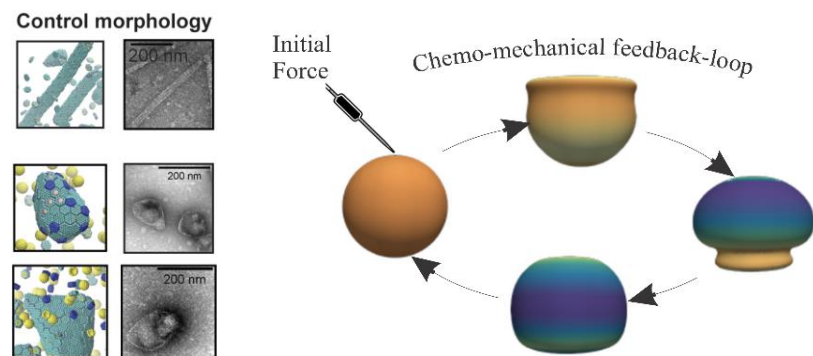


**Figure 1.** (Left) Coarse-grained model morphologies from microcompartment proteins compared to morphologies observed by transmission electron microscopy. (Right) Autonomous responsive polymer shells that undergo morphological changes triggered by an initial deformation.

We then considered functionalized hydrogels forming closed elastic vesicles as models of shape-forming processes that are controlled by chemical and mechanical signaling events [2]. In this project, we determined the chemo-response of the soft materials (hydrogels) by coupling the local mechanical response of a hydrogel model with the chemical processes that can occur on it. It was found that the chemicals can modify the local gel microenvironment, allowing swelling and deswelling of the material via chemo-mechanical stresses in an autonomous manner (Fig 1, right). This work will inspire further developments

of responsive materials, which could enhance microcompartments' and nanoreactors' functionality, such as controlled permeability and at-will release of chemicals.

**Shape Selection in Charged, Chiral membranes.** Charged chiral molecules including lipids constitute important biomaterials such as cell membranes. Molecular chirality effects are manifested at meso- and macro-scales in self-assembled structures such as twisted or helical ribbons, helical tubules and helicoidal scrolls. These chiral shapes originate from a relative tilt in the orientation of neighboring molecules that is induced by molecular chirality. However, the role of electrostatic interactions in regulating/controlling the shape selection in assemblies of charged chiral molecules is not well understood. To tackle this problem, we designed the simplest possible chiral amphiphile  $C_{16}$ -K (Fig. 2, top), where an ionizable, chiral amino acid lysine (K) is covalently linked to 16 carbon long alkyl tails. We analyzed the self-assembly in varied ionic environments, over  $\mu\text{m}$ - $\text{\AA}$  length scales using in situ atomic force microscopy (AFM), cryo-transmission electron microscopy (cryo-TEM) and solution small- and wide-angle X-ray scattering (SAXS/WAXS). We developed mean field models that combined the effects of membrane elasticity, chirality and electrostatics. The key finding of our studies is that *helicoidal scrolls (cochleates)* is the equilibrium membrane morphology when the range of electrostatic interactions ( $\lambda_s$ ) is low ( $\lambda_s < 3 \text{ nm}$ ) (Fig. 2, bottom). By contrast helical membranes are formed when the electrostatic interactions are weak, but long ranged ( $\lambda_s > 7 \text{ nm}$ ) [3]. Specifically, high aspect ratio ( $L/W > 10$ ) bilayer ribbons converted to sheets ( $L/W \sim 1$ ) and then rolled into cochleates as the electrostatic screening length was reduced by adding salt. Furthermore, the interbilayer spacing in cochleates varied linearly with the screening length and could be tuned between 13 to 35 nm.

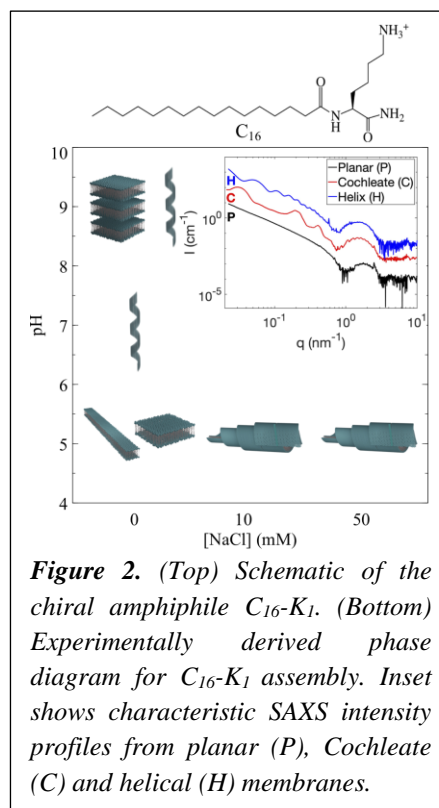


**Figure 2.** (Top) Schematic of the chiral amphiphile  $C_{16}$ -K<sub>1</sub>. (Bottom) Experimentally derived phase diagram for  $C_{16}$ -K<sub>1</sub> assembly. Inset shows characteristic SAXS intensity profiles from planar (P), Cochleate (C) and helical (H) membranes.

By contrast helical membranes are formed when the electrostatic interactions are weak, but long ranged ( $\lambda_s > 7 \text{ nm}$ ) [3]. Specifically, high aspect ratio ( $L/W > 10$ ) bilayer ribbons converted to sheets ( $L/W \sim 1$ ) and then rolled into cochleates as the electrostatic screening length was reduced by adding salt. Furthermore, the interbilayer spacing in cochleates varied linearly with the screening length and could be tuned between 13 to 35 nm.

**Hybrid Biomimetic Materials.** We aim to design polymers that would co-assemble with biomolecules to generate biomimetic membranes. In collaboration with the experimental group of Prof. Ting Xu at the University of California, Berkeley, we developed transmembrane polymers composed of four different types of monomers and are amphiphilic [4]. They exhibited selective transport of proton ions over monovalent metal ions of  $\text{Na}^+$ ,  $\text{Li}^+$ , and  $\text{K}^+$ . The efficiency in proton transport was comparable to those of natural proton channels. Via atomistic simulations we found that the inserted random polymers promote the formation of dynamic hydrogen-bonded chains, which could aid proton ion transport.

Protein surfaces are composed of all kinds of amino acids, including positively and negatively charged, polar charge neutral, and nonpolar. Protein surface domains are known to play a central role in determining protein-protein interactions and protein-ligand binding. Nevertheless, quantifying protein surface domains remain highly challenging. To characterize protein surfaces, we developed a new program [5] that can analyze the probability of all types of amino acids, their

three-dimensional distributions, and the clustering of amino acids at protein surfaces. We examined the long-range impacts of electrostatic interactions in the degree of infectability of SARS-CoV-2 [6]. In specific, we were targeting the polybasic furin cleavage site, which are positively charged and located around 10 nm away from the (highly negatively charged) human cell receptor hACE2 once hACE2 binds to the spike protein's receptor-binding domain (RBD). We found that the polybasic cleavage site enhances the RBD-hACE2 binding affinity, supporting that long-range electrostatic interactions play a crucial role in protein-protein interactions.

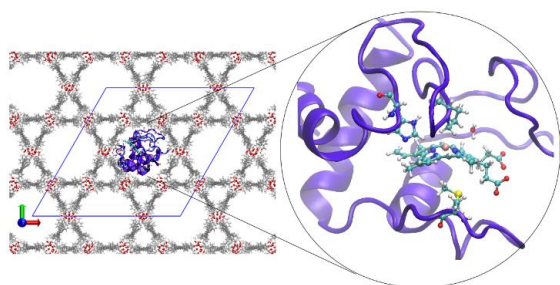


**Figure 3.** (A) Snapshot of Cyt c inside the nanopores of the nanomaterial. (B) Closeup showing the partial unfolding of Cyt c due to the hydrophobic/hydrophilic interaction with the framework, which increases the access of water to the heme active site resulting in enhanced catalytic activity due to the improved access of reaction substrates to the active center.

Encapsulation of proteins within nanomaterials may protect proteins from denaturation outside their native environment. We investigated the conformational changes of the enzyme Cyt c encapsulated within a metal-organic framework [7]. Our simulations show that the encapsulated protein partially unfolds which enhances the access of water and water-soluble reaction substrates (such as ABTS and  $H_2O_2$ ) to the enzyme active site (fig. 3). The conformational changes aid to enhance the catalytic performance of Cyt c.

Water mediates electrostatic interactions between particles and surfaces via polarization. In confinement, water displays unique features different from those in bulk solution which impact electrostatic interactions in a unique manner. We investigated a system consisting of water and ions confined between two graphene surfaces [8] relevant in different applications including water desalination, electrochemical energy storage, and energy harvesting. By considering the interaction between two ions near the graphene surface, we found that the water polarization and confinement enhance the attraction between physisorbed ions in the surface normal direction. Furthermore, the interaction energy changes by about  $5 k_B T$  by exchanging the ions' positions along the surface normal direction and, the intercalation of one ion between the graphene layers turns the ion-ion interaction repulsive. Conversely, the in-plane interaction between the ions is almost unaffected by the graphene surface. The simulation results are supported by x-ray reflectivity experiments of the water structure near a graphene surface.

## Future Plans

In the future, we will extend our work on closed membranes to develop a theory to include time dependent chemical reactions on hydrogels. We will also study how the presence of charged species, such as ions, polyelectrolytes, and proteins, affect the structure of water and polarization in confinement. We are interested in understanding the mechanisms that can increase the energy storage of nanocapacitors and studying the changes in the water polarization that can be used to detect and characterize large macromolecules, such as, polyelectrolytes, proteins, and nucleic acids. In addition, we will develop a continuum theoretical approach as well as a computational

model to study nanopatterns in multicomponent nanoshells. By combining the shape transformation and the surface pattern, the model will allow a systematic search for the ground state of crystalline nanoshells composed of multiple components.

Finally, our more recent experimental work on chiral lipids shows that in solutions containing very low salt (< 1mM), the high aspect ratio bilayers convert to helical ribbons when the average molecular charge is reduced by increasing the solution pH. Our future work will focus on developing a theoretical model for the evolution of the helical ribbon structure as a function of molecular charge, and experimentally testing the generality of the above observations. Overall, we aim to deduce simple rules for electrostatic control of chiral membrane shapes. We will include proteins in the solution, and by combining X-ray scattering experiments and molecular dynamics (MD) simulations we will determine the adsorption and assembly of proteins.

## Reference

1. Li, Y.; Kennedy, N.W.; Li, S.; Mills, C.E.; Tullman-Ercek, D.; Olvera de la Cruz, M. "Computational and experimental approaches to controlling bacterial microcompartment assembly" *ACS Central Science* **2021**, 7, 658-670; DOI: 10.1021/acscentsci.0c01699
2. Li, S.; Matoz-Fernandez, D.A.; Aggarwal, A.; Olvera de la Cruz, M. "Chemically controlled pattern formation in self-oscillating elastic shells" *PNAS* **2021**, 118 (10) e2025717118; DOI: 10.1073/pnas.2025717118
3. Gao, C.; Kewalramani, S. ; Valencia, D. M.; Li, H.; McCourt, J. M.; Olvera de la Cruz, M.; Bedzyk, M.J. "Electrostatic Shape Control of a Charged Molecular Membrane from Ribbon to Scroll" *Proc. Natl. Acad. Sci.*, **2019**, 116, 22030-22036.
4. Jiang, T.; Hall, A.; Eres, M.; Hemmatian, Z.; Qiao, B.; Zhou, Y.; Ruan, Z.; Couse, A.D.; Heller, W.T.; Huang, H.; Olvera de la Cruz, M.; Rolandi, M.; Xu, T. "Single-chain heteropolymers transport protons selectively and rapidly" *Nature* **2020**, 577, 216–220; DOI: 10.1038/s41586-019-1881-0
5. Li, Y.; Qiao, B.; Olvera de la Cruz, M. "Protein surface printer for exploring protein domains" *J. Chem. Inf. Model.*, **2020**, 60, 10, 5255–5264; DOI: 10.1021/acs.jcim.0c00582
6. Qiao, B.; Olvera de la Cruz, M. "Enhanced Binding of SARS-CoV-2 Spike Protein to Receptor by Distal Polybasic Cleavage Sites" *ACS Nano*, **2020**, 14, 10616–10623; DOI: 10.1021/acsnano.0c04798
7. Chen, Y.; Jiménez-Ángeles, F.; Qiao, B.; Krzyaniak, M.D.; Sha, F.; Kato, S.; Gong, X.; Buru, C.T.; Chen, Z.; Zhang, X.; Gianneschi, N.C.; Wasielewski, M.R.; Olvera de la Cruz, M.; Farha, O.K. "Insights into the Enhanced Activity of a Metal–Organic Framework-Encapsulated Enzyme" *JACS*, **2020**, 142, 18576–18582; DOI:10.1021/jacs.0c07870
8. Jimenez-Angeles, F.; Harmon, K. J.; Nguyen, T. D.; Fenter, P.; Olvera de la Cruz, M. "Nonreciprocal interactions induced by water in confinement" *Phys. Rev. Res.*, **2020**, 2, 043244; DOI: 10.1103/PhysRevResearch.2.043244
9. Dahal, Y.; Olvera de la Cruz, M. "Controlling protein adsorption modes electrostatically" *Soft Matter*, **2020**, 16, 5224-5232; DOI: 10.1039/D0SM00632G

**Publications** (grant number DE-FG02-08ER46539 from 06, 2019 to 06, 2021)

1. Liang, Y.; Ma, B.; Olvera de la Cruz, M. "Reverse order-disorder transition of Janus particles confined in two dimensions" *Phys. Rev. E* **2021**, 103, 062607; DOI: 10.1103/PhysRevE.103.062607
2. Li, Y.; Kennedy, N.W.; Li, S.; Mills, C.E.; Tullman-Ercek, D.; Olvera de la Cruz, M. "Computational and experimental approaches to controlling bacterial microcompartment assembly" *ACS Central Science* **2021**, 7, 658-670; DOI: 10.1021/acscentsci.0c01699
3. Wang, J.; Waltmann, C.; Kossio-Umana, H.; Olvera de la Cruz, M.; Torkelson, J. M. "Heterogeneously Charged Complexes of Random Copolymers for the Segregation of Organic Molecules" *ACS Central Science* **2021**, 7, 882-891 (2021); DOI: 10.1021/acscentsci.1c00119
4. Li, S.; Matoz-Fernandez, D.A.; Aggarwal, A.; Olvera de la Cruz, M. "Chemically controlled pattern formation in self-oscillating elastic shells" *Proc. Natl. Acad. Sci.*, **2021**, 118 (10) e2025717118; DOI: 10.1073/pnas.2025717118
5. Jimenez-Angeles, F.; Harmon, K. J.; Nguyen, T. D.; Fenter, P.; Olvera de la Cruz, M. "Nonreciprocal interactions induced by water in confinement" *Phys. Rev. Res.*, **2020**, 2, 043244; DOI: 10.1103/PhysRevResearch.2.043244
6. Chen, Y.; Jiménez-Ángeles, F.; Qiao, B.; Krzyaniak, M.D.; Sha, F.; Kato, S.; Gong, X.; Buru, C.T.; Chen, Z.; Zhang, X.; Gianneschi, N.C.; Wasielewski, M.R.; Olvera de la Cruz, M.; Farha, O.K. "Insights into the Enhanced Activity of a Metal–Organic Framework-Encapsulated Enzyme" *JACS*, **2020**, 142, 18576–18582; DOI:10.1021/jacs.0c07870
7. Li, Y.; Qiao, B.; Olvera de la Cruz, M. "Protein surface printer for exploring protein domains" *J. Chem. Inf. Model.*, **2020**, 60, 10, 5255–5264; DOI: 10.1021/acs.jcim.0c00582
8. Du, F.; Qiao, B.; Nguyen, T.; Vincent, M.; Bobbala, S.; Yi, S.; Lescott, C.; Dravid, V.P.; Olvera de la Cruz, M.; Scott, E. A. "Homopolymer self-assembly of poly(propylene sulfone) hydrogels via dynamic noncovalent sulfone-sulfone bonding" *Nature Commun.*, **2020**, 11, 4896; DOI: 10.1038/s41467-020-18657-5
9. Qiao, B.; Olvera de la Cruz, M. "Enhanced Binding of SARS-CoV-2 Spike Protein to Receptor by Distal Polybasic Cleavage Sites" *ACS Nano*, **2020**, 14, 10616–10623; DOI: 10.1021/acsnano.0c04798
10. Dahal, Y.; Olvera de la Cruz, M. "Controlling protein adsorption modes electrostatically" *Soft Matter*, **2020**, 16, 5224-5232; DOI: 10.1039/D0SM00632G
11. Jiang, T.; Hall, A.; Eres, M.; Hemmatian, Z.; Qiao, B.; Zhou, Y.; Ruan, Z.; Couse, A.D.; Heller, W.T.; Huang, H.; Olvera de la Cruz, M.; Rolandi, M.; Xu, T. "Single-chain heteropolymers transport protons selectively and rapidly" *Nature* **2020**, 577, 216–220; DOI: 10.1038/s41586-019-1881-0
12. Gao, C.; Kewalramani, S. ; Valencia, D. M.; Li, H.; McCourt, J. M.; Olvera de la Cruz, M.; Bedzyk, M.J. "Electrostatic Shape Control of a Charged Molecular Membrane from Ribbon to Scroll" *Proc. Natl. Acad. Sci.*, **2019**, 116, 22030-22036.
13. Waltmann, C; Asor, R.; Raviv, U; Olvera de la Cruz, M. "Assembly and Stability of Simian Virus 40 Polymorphs" *ACS Nano* 14, 4430-4443 (2020); DOI: 10.1021/acsnano.9b10004
14. Girard, M.; Ehlen, A.; Shakya, A.; Bereau, T.; Olvera de la Cruz, M. "Hoobas: A highly object-oriented builder for molecular dynamics" *Computational Materials Science* **2019**, 167, 25-33; DOI: 10.1016/j.commatsci.2019.05.003

15. Dannenhoffer, A.; Sai, H.; Dongxu Huang, D.; Nagasing, B.; Harutyunyan, B.; Fairfield, D.J.; Aytun, T.; Chin, S.M.; Bedzyk, M. J.; Olvera de la Cruz, M.; Stupp, S.I. "Impact of charge switching stimuli on supramolecular perylene monoimide assemblies" *Chemical Science* **2019**, 10, 5779-5786; DOI: 10.1039/C8SC05595E
16. Dahal, Y.; Olvera de la Cruz, M. "Crystallizing protein assemblies via free and grafted linkers" *Soft Matter* **2019**, 15, 4311; DOI: 10.1039/c9sm00693a

## **Active Noise to Control and Direct Self-Assembly**

Colloidal Aggregation controlled by Active Fluctuations

**Jérémie Palacci, UC San Diego (and IST Austria)**

### **Program Scope**

The aim of this program is to explore the impact of active particles on a collection of passive ones. It addresses basic science questions to understand and unlock the potential of active noise to control and direct the assembly of passive constituents. Such questions are: Can we use non-equilibrium fluctuations control the behavior of collections of passive particles? Can we use active baths to overcome metastable states and guarantee the relaxation of a system towards equilibrium? Can we control and direct the assembly of passive particles in targeted architectures or shapes, which could not be achieved in a thermal system? What is the effect of an active bath on the phase transition of passive particles? Does the transition rescale with the effective temperature or is the effect of activity altering the nature and order of the transition?

### **Recent Progress**

We investigated the behavior of passive beads with attractive (depletion) interactions in a thermal bath or in a bath of motile bacteria generating additional active noise. We observe a significant effect of the bacterial bath vs thermal bath on the morphology and dynamics of colloidal aggregates [see Figure below]. We notably show that:

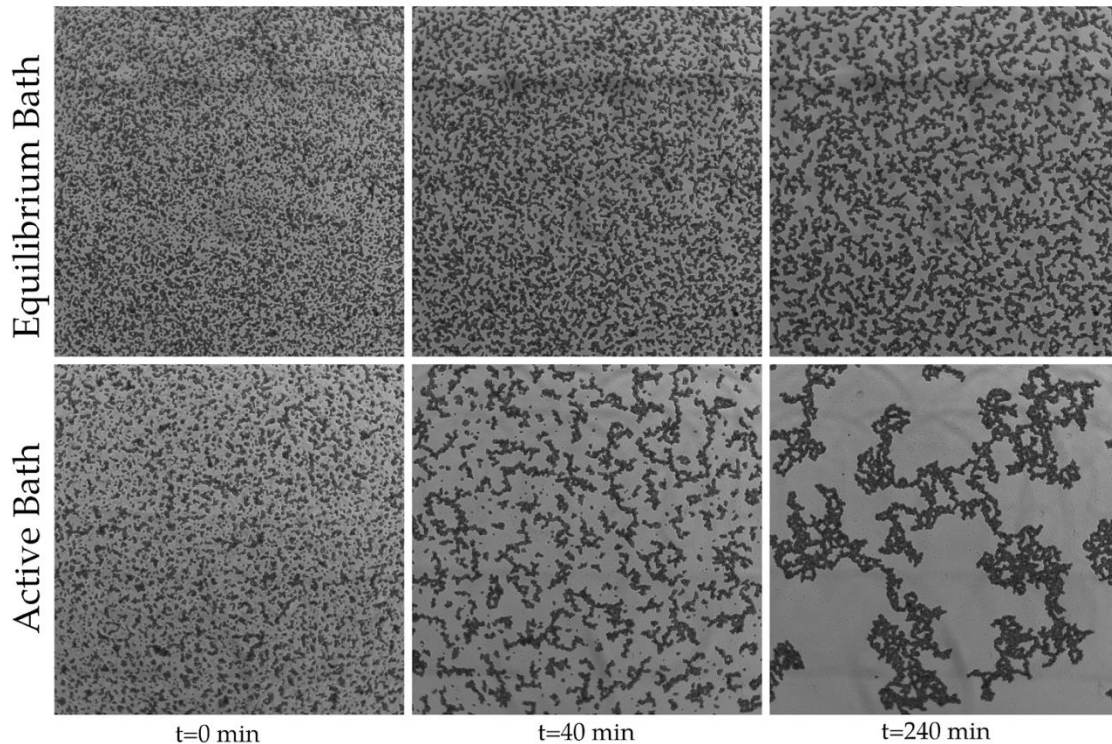
1. The translational and rotational diffusion in the active bacterial bath scale like Stokes-Einstein predictions for a system of size  $R$ .
2. The effective temperature measured through the translational or rotational diffusion is the same.
3. The amplitude of the fluctuations is a linear function of the bacteria concentration -- a result in line with [1].
4. The morphology of the aggregates, quantified by their fractal dimension, is set by the attraction strength and level of fluctuations, e.g. "temperature" of the bath.
5. The experimental measurements of fractal dimensions for aggregates in thermal and active bath collapse onto each other using the dimensionless parameter attraction strength over energy of the bath.

As a result, the active bath seems to behave like a thermal one, provided all relevant energy scales are similarly "enhanced".

## Future Plans

We will engineer a microfluidic device allowing us to control the activity of the bacteria temporally (and possibly spatially) so that we can impose time-dependent annealing or quenching to the system of colloids. This is done jointly with the development of protocols to control the speed and duration of swimming of motile bacteria, hence added fluctuations of the bath.

We are studying the nucleation crystallization of the passive beads in a thermal and active bath and notably investigate the susceptibility of the system to observe whether the addition of active fluctuations can change the order of the transition.



Time series of the formation and growth of colloidal aggregates using colloidal beads with attractive interactions, in a thermal (top) or active bacterial bath (bottom). Passive bead concentration and attractive interactions between the passive beads are the same in the two experiments. The dynamics and morphology of the aggregates differ.

## References

[1] *Enhanced Diffusion due to Active Swimmers at a Solid Surface*, Mino et al, Physical Review Letters, **106**, 2011

## Publications

*Colloidal Aggregation controlled by active fluctuations*, D. Grober & J. Palacci, in prep.

*Decision-making at a T-junction by gradient-sensing microscopic agents*, T. Gandhi, J.M. Huang, A. Aubret, Y. Li, S. Ramananarivo, M. Vergassola, J. Palacci, Physical Review Fluids, **5**, 2020

## Nanomaterial Construction through Peptide Computational Design and Hierarchical Solution Assembly

**Darrin Pochan**      **Materials Science and Engineering, University of Delaware**

**Jeffery Saven**      **Chemistry, University of Pennsylvania**

**Chris Kloxin**      **Materials Science and Engineering, Chemical and Biological Engineering, University of Delaware**

### Program Scope

Our collaborative project is based fundamentally on the computational design of non-natural, short peptides (peptides of less than 50 residues) that form well-defined, coiled coil bundle building block structures. These molecules are amenable to solution processing associated with soft materials, such as surfactants and polymers. Short amino acid sequences are robust with respect to the cycling of temperature and the use of a wide variation of solution conditions including organic solvents. Such solution processing provides control over the hierarchical assembly and desired morphology of peptide materials. The structures of oligomeric systems based on peptides, particularly coiled coil bundles of alpha helices, can be

computationally modeled, where variation of length and oligomerization state is computationally generated de novo. Computational modeling, which accounts for the atomistic details of the peptide side groups, provides enhanced versatility in specifying the shape and size of the coiled coil building blocks and incorporation of non-natural amino acids. Using solid phase peptide synthesis, there is no restriction on the number and placement of nonbiological amino acids within a peptide. Covalent and noncovalent interactions between residues are readily incorporated, greatly extending the molecular canvas beyond only the 20 natural amino acids.

Peptide sequences are computationally designed in the context of a supramolecular hierarchy. The hierarchy begins with solution assembly of computationally designed, non-natural peptides to form desired coiled coil material building blocks that display desired functionality to promote targeted, physical and/or covalent interactions between building blocks. Subsequently, different building blocks are assembled within

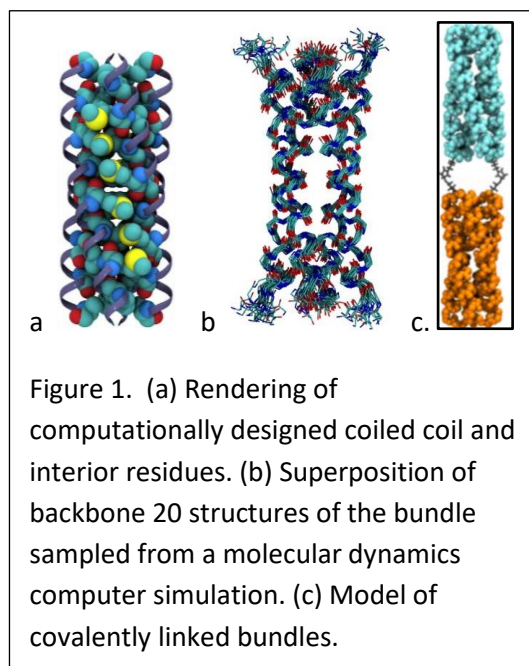


Figure 1. (a) Rendering of computationally designed coiled coil and interior residues. (b) Superposition of backbone 20 structures of the bundle sampled from a molecular dynamics computer simulation. (c) Model of covalently linked bundles.

designed, multistep, hierarchical pathways that involve variation of peptide concentrations and solution conditions to build target materials. Within this new approach, we include a variety of non-natural chemical functionalities to build a wide range of material structures with a focus on 1-D nanostructures, liquid crystal phases, and polymer fibers.

### **Recent Progress**

We have designed peptides de novo that fold into tetrahelical bundle structures which then can be used as supermonomers for hierarchical physical and/or covalent assembly into individual polymers with desired intra- and interchain characteristics. The solution behavior of the chains can be controlled in order to form liquid crystal phases and be processed into fiber materials.

Individual tetrahelical bundles when linked using nonnatural covalent “click” chemistries (e.g., thiol-maleimide conjugation reaction) can form a variety of interesting polymeric structures, comprising monomers with nanometer dimensions. One such construct forms polymeric rods having large persistence lengths (tens of microns). Importantly, the observed stiffness for the bundle chains is exceptional relative to their mass/length ratio.[Wu, et al.] The rigid bundle chains display a persistence length that is approximately two orders of magnitude more stiff than other assemblies with similar mass/length. The molecular features that underlie such rigidity are unclear, and we are employing molecular simulations to investigate the roles that interbundle interactions and covalent linkages have on the relative orientations of covalently linked bundles (see Future Plans).

Other important results from this period include our work showing the ability to form chains of bundle building blocks that contain desired patterns of both bundle building blocks as well as building blocks with desired functionalities attached in patterns. Wu et al. contains examples of our ability to include fluorescent dyes, inorganic nanoparticles, and synthetic polymer chains at desired locations within a bundlemer polymer chain. This facet of research is being explored in current research to control inter-rod interactions as well as to make rods functional.

With respect to the understanding of rod solution behavior and inter-rod interactions, extensive work has been performed on dilute solutions of rigid rod particles, particularly with small-angle neutron scattering [Sinha et al. 2019] and rheological measurements. By controlling solution conditions (pH, salt concentration), the interactions of the ultra-stiff rod particles can be controlled. With our ability to control the bundle pattern within rods/chains and our ability to computationally design new bundles with desired functional character (e.g. net charge, charge patterns), the rigid rods have the potential to be exciting, new model colloidal particles with which we can design new hierarchical assemblies and liquid crystalline materials. This work is ongoing with a focus on more concentrated rigid rod regimes to observe and control liquid crystalline behavior.

Work has continued on the solution behavior of the rigid rod chains in more concentrated solution in order to observe and control liquid crystal formation. Currently we only have a preliminary understanding of the LC behavior as shown in the attached Figure 1.

Importantly, the control of rod length and dispersity is key in formation of liquid crystal phases. Current synthetic methods to form rods has produced chains with too high of a dispersity in chain length to form regular LC phases due to very short rods and unreacted bundles effectively serving as a solvent to disrupt interchain interactions/packing needed for regular LC formation. Exceptions exist such as the apparent smectic behavior observed in Wu et al. as well as the clear LC behavior in Figure 1. Current efforts are

focusing on chain formation control so that LC behavior becomes a common occurrence that can be manipulated with inter-rod interactions, concentration, temperature, and solution conditions. Concentrated solutions of rigid rods have been successfully spun into fiber materials (Figure 1) that exhibit alignment of the constituent rods within the fibers [Kim, et al.].

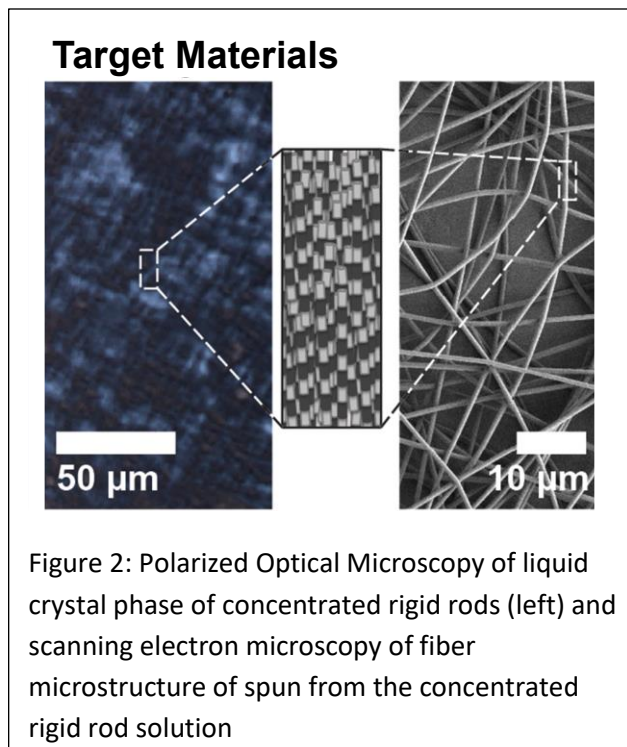


Figure 2: Polarized Optical Microscopy of liquid crystal phase of concentrated rigid rods (left) and scanning electron microscopy of fiber microstructure of spun from the concentrated rigid rod solution

## Future Plans

The molecular features that underlie rigidity of the polymeric assemblies are unclear, and we are employing molecular simulations and experimental studies to investigate the roles that interbundle interactions and covalent linkages have on the relative orientations of covalently linked bundles. The simulations are being used to suggest hypotheses regarding interactions between amino acid residues that will be assessed experimentally in collaboration with the Kloxin and Pochan groups. The Saven lab has designed sequences to probe underlying reasons for the extreme stiffness in the rigid rod chains, including the hypothesis that a certain degree of unfolding occurs at the bundle ends so that hydrogen bonding and hydrophobic interactions can persist between neighboring bundles along a chain. The new designs have modifications of the bundle building blocks an effort to probe the roles of hydrogen bonding and other intermolecular interactions between neighboring bundle in specifying the rigidity of the chains.

Helical bundles of varying charge have been computationally designed in an effort to control association and repulsion between individual bundles in solution via the design and control of electrostatic interactions. These designed sequences are presently being studied by the Pochan

and Kloxin groups and are an important part of the ability to design rods and other polymeric assemblies with desired interactions for formation of hierarchical materials assembly. New conjugation reactions including the copper-catalyzed azide-alkyne click reaction are also being employed.

### **Publications**

Wu, D.D.; Sinha, N.; Lee, J.Y., Tian, Y.; Zhang, H.; Sutherland, B.; Kloxin, C.J.; Saven, J.G.; Pochan, D.J. Polymers with Controlled Assembly and Rigidity Made with Click-functional Peptide Bundles. *Nature*, **2019**, 574, 658-662

Sinha, N.; Wu, D.; Kloxin, C.J.; Saven, J.G.; Jensen, G.V.; Pochan, D.J. Polyelectrolyte character of rigid rod peptide bundlemer chains constructed via hierarchical self-assembly, *Soft Matter*, **2019**, 15, 9858-9870.

Sinha, N.; Kloxin, C.J.; Saven, J.G.; Jensen, G.V.; Kelman, Z.; Pochan, D.J. Recombinant expression of computationally designed peptide-bundlemers in *Escherichia coli*. *Journal of Biotechnology*, **2021**, 330, 57-60.

Kim, K.; Kloxin, C.J.; Saven, J.G.; Pochan, D.J. Nanofibers Produced by Electrospinning of Ultrarigid Polymer Rods Made from Designed Peptide Bundlemers. *ACS Applied Materials and Interfaces*, **2021**, 13, 26339-26351.

## **New principles of self-organization created through the interplay of DNA condensates, microtubules, and motors**

**Paul W.K. Rothmund, California Institute of Technology**

### **Program Scope**

In self-organizing living systems, one important principle is the modular reuse of a few simple molecular components in myriad combinations to achieve more complex phenomena. For example, the mechanical tasks of a cell are driven by the nonequilibrium dynamics of cytoskeletal filaments and molecular motors—the same filaments and motors, reprogrammed by a variety of modulators, perform tasks ranging from cell movement to division. Similarly, many compartmentalization tasks are performed by liquid-like condensates of simple components, which act as membraneless organelles to localize particular molecules in space and time (e.g. for gene regulation or RNA processing). In a few cases, condensates combine and interact with the cytoskeleton to create still more complex phenomena, e.g. the nucleation of microtubule asters from the centrosome (a protein condensate) to form the mitotic spindle during cell division [1]. Despite having a few examples, the landscape of behaviors that can be achieved through the combination of condensates, filaments, and motors appears vast.

Our goal is to combine programmable DNA condensates, filamentous microtubules, and light-controlled motors into self-organizing systems whose principles go beyond those that have been observed in nature. In one limit, our systems will use microtubules and motors to create the molecular analog of a network of roads, which will organize droplets of DNA condensates capable of carrying molecular cargo. DNA condensates coupled to motors will flow from one microtubule aster hub to another, with their direction and timing controlled by DNA circuits. In another limit, microtubules will swim through bulk DNA condensates and exhibit strong interactions with boundaries between different types of condensates. Microtubule swimmers will reflect, get trapped, or refract at boundaries, under a mechanical analog of the classical optical index of refraction. DNA condensates having different mechanical indexes of refraction will be used to construct the analog of optical lenses, so that microtubule swimmers can be manipulated like light—collimated, diffracted, focused, and sorted based on properties analogous to wavelength. These two limits define two new architectures, within which multiple new mechanistic principles for self-organization will be discovered and explored. To explore these architectures, the motor-based coupling between DNA condensates and filaments will be controlled in time and space through the use of opto-proteins that create reversible links between DNA condensates and motors upon illumination. For each principle of interest, patterns of light will create virtual experiments by defining patterns of activity where DNA condensates walk along filaments, or filaments swim through condensates, and patterns of inactivity which will serve either as controls, or as boundary conditions vital to create the desired phenomena.

## Recent Progress

Under COVID restrictions we have focused on theoretical and computational explorations of the interaction of microscopic neutral swimmers with viscosity discontinuities (Fig. 1). We have ignored idiosyncratic features of microtubules, motors proteins, and condensates to yield results that should be applicable to microscopic swimmers in general.

Snell's law, which encompasses both refraction and total internal reflection (TIR), provides a foundation for ray optics and all lens-based instruments, from microscopes to telescopes. Refraction can result when light passes between media of different index of refraction, the dimensionless number

that captures how much a medium retards the propagation of light. The question arises whether Snell's law applies to other domains, e.g. when a self-propelled particle passes between two media for which it experiences different drag forces. We have derived a variant of Snell's law for neutral swimmers moving between media of different viscosity. Just as the ratio of the indices of refraction dictates the behavior of light, the ratio of viscosities is shown to determine the behavior of swimmers, but with notable differences in detail (Fig. 2). Strikingly, refraction depends strongly on swimmer shape and, in particular, aspect ratio. This enables the dispersion of a “white” beam of swimmers having many aspect ratios into monomorphic beams by a viscosity prism. In turn, monomorphic beams can be effectively focused by spherical and viscosity gradient lenses. Completing the analogy, shape-dependence of the TIR critical angle enables differential retention of multi-morphic swimmers within a viscosity trap. Such recapitulations of ray optics (Fig. 3) anticipate a universe of new devices for sorting, concentrating, and analyzing microscopic swimmers.

The amount of refraction at a viscosity discontinuity depends on the duration that the swimmer straddles the interface—there will only be torque on the body when it is moving between regions of different viscosities. Thus, using the angular velocity force coupling via the friction tensors, we calculate translational velocity and the crossing time, which allows us to integrate the forces and torques over the duration of a crossing event to calculate the angle of refraction  $\theta_f$ . For spherical swimmers of radius  $a$ , with friction coefficient  $\zeta_c$  and rotational drag coefficient  $\zeta_R$  we find that:

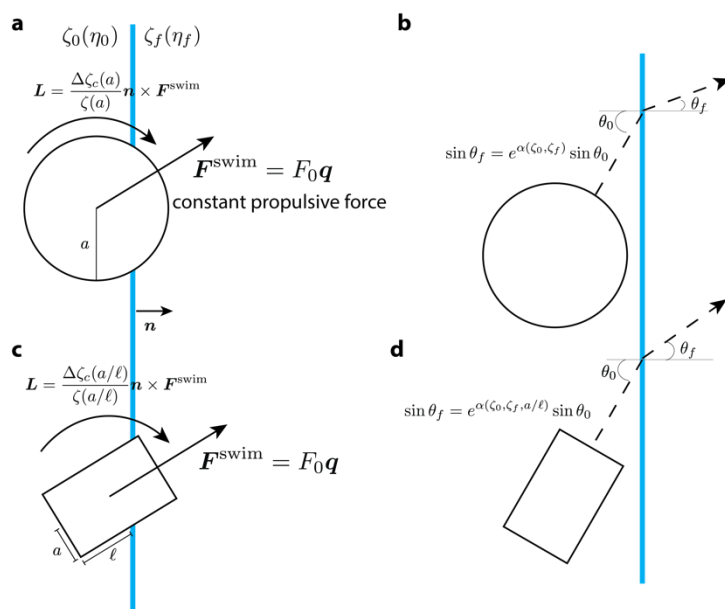


**Fig. 1.** Spherical and rectangular swimmers moving across drag (viscosity) discontinuity. Forces and torques on a swimmer (a) causes a reorientation of the swimmer's trajectory (b).

$$\sin \theta_f = e^\alpha \sin \theta_0, \quad \alpha = -\frac{2a\Delta\zeta_c}{\zeta_R}. \quad (1)$$

For a sphere,  $\Delta\zeta_c = 6\pi\Delta\eta a^2$  and  $\zeta_R = 8\pi\langle\eta\rangle a^3$  where  $\Delta\eta$  is the change in viscosity and  $\langle\eta\rangle$  is a weighted average of the viscosities. It is worth noting that the radius of the swimmer cancels out, resulting in:

$$\alpha = -1.5\frac{\Delta\eta}{\langle\eta\rangle}. \quad (2)$$

For rectangular a swimmer, where the half minor length is  $a$ , the half major length is  $l$ , and the angle of incidence is  $\theta_0$ , the appropriate analog of eqn. (1) is:

$$\sin \theta_f = e^\alpha \sin \theta_0, \quad \alpha \sim -\frac{\Delta\zeta_c}{\zeta_R} (2\ell \cos \theta_0 + 2a(1 - \cos \theta_0)). \quad (3)$$

For a rectangular swimmer,  $\Delta\zeta_c \sim \pi\Delta\eta al / \ln(l/a)$  and  $\zeta_R \sim \pi\langle\eta\rangle l^3 / \ln(l/a)$ . Therefore:

$$\alpha \sim -\frac{a}{\ell^2} (a + (\ell - a) \cos \theta_0) \frac{\Delta\eta}{\langle\eta\rangle}. \quad (4)$$

Thus the Snell's law analog for a rectangular swimmer depends on the swimmer's shape via the aspect ratio. We also note that when  $a = l$ , Eq. (3) reduces to Eq. (1). To further the analogy with optics, the aspect ratio of the rectangular swimmer corresponds to the wavelength of light.

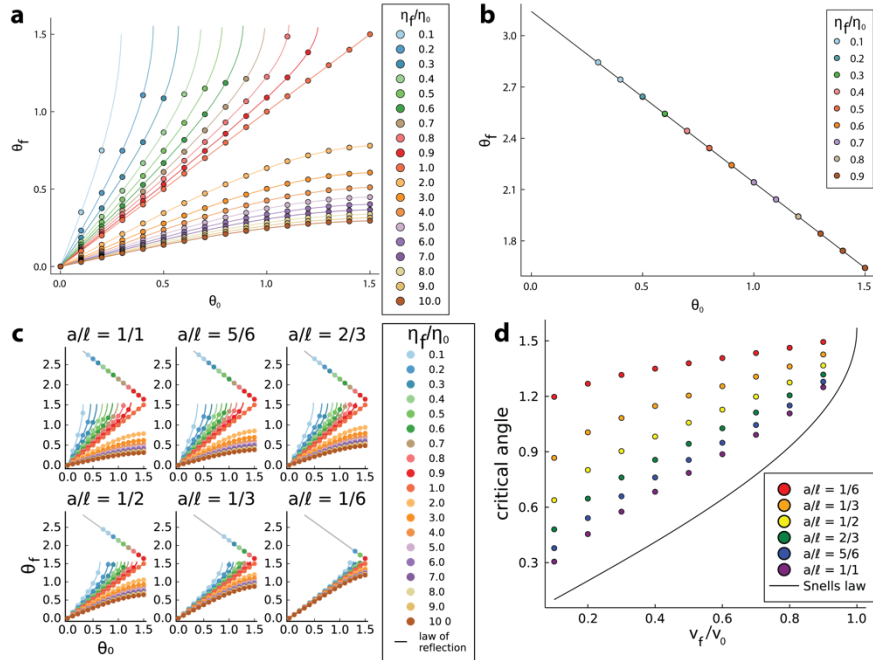


**Fig. 2.** Swimmers refract and reflect in a manner analogous to Snell's law. **a**, Spherical swimmer refraction as a function of incident angle and viscosity ratios. Curves are theoretical, and points simulations. **b**, For incident angles above the critical angle, swimmers follow the law of reflection (black line). **c**, Refraction and reflection for rectangular swimmers of varying aspect ratio  $a/l$ . **d**, Comparison between critical angle dependence on speed ratios for different swimmers and the optical Snell's law.

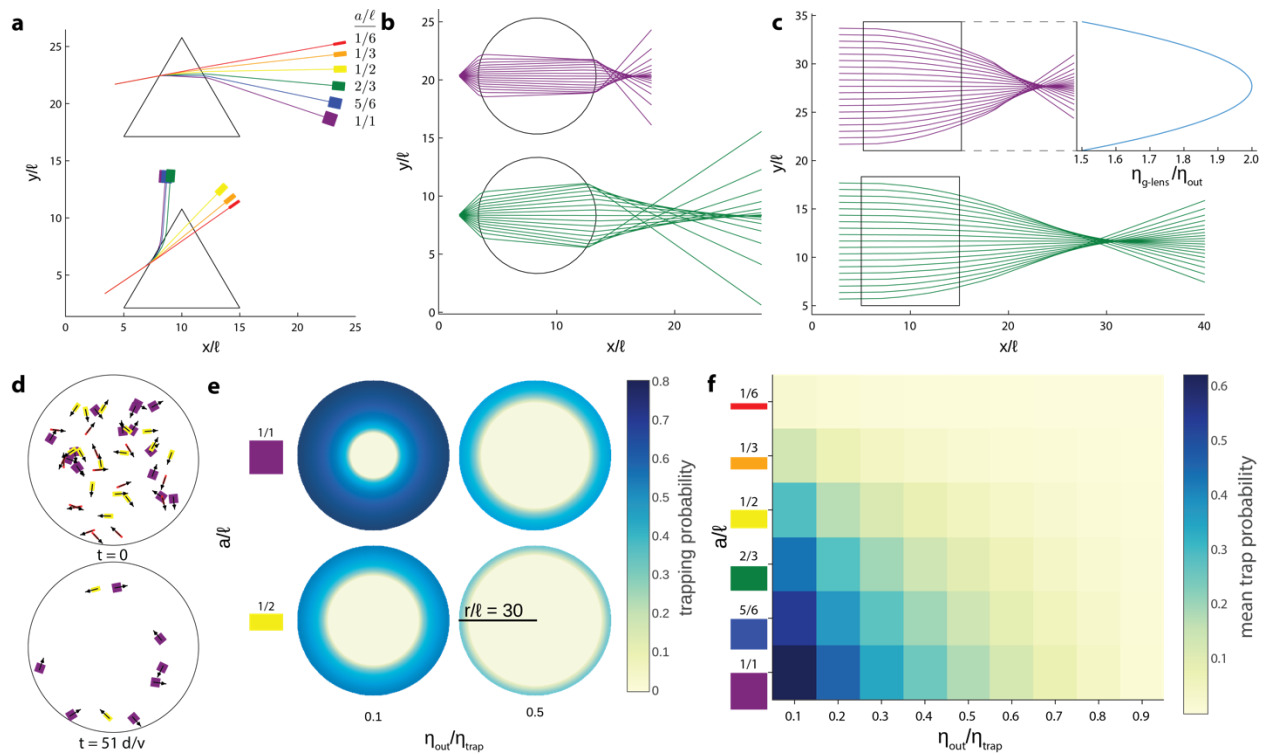


**Fig. 3.** Principles of ray optics can be similarly applied to organize swimmers. **a**, Prism analogs disperses rectangular swimmers by their shape. Top: Swimmers disperse to different angles after passing through a region of high viscosity ( $\eta_{\text{tri}}/\eta_{\text{out}} = 2$ ). Bottom: A subset of swimmers reflect at a discontinuity of lower viscosity ( $\eta_{\text{tri}}/\eta_{\text{out}} = 2/3$ ). **b**, Ball lens analog has different focal lengths and (spherical aberrations) depending on swimmer shape.  $\eta_{\text{b-lens}}/\eta_{\text{out}} = 8$ . Top:  $a/l = 1$ . Bottom:  $a/l = 2/3$ . **c**, Gradient lens analog similarly focus swimmers while minimizing aberrations  $\eta_{\text{out}} = 1$ . Top:  $a/l = 1$ , inset shows viscosity gradient of the lens. Bottom:  $a/l = 2/3$ . **d**, Frames of timelapse simulation for a swimmer trap  $\eta_{\text{out}}/\eta_{\text{trap}} = 0.1$ . Time is measured in  $d/v$  where  $d$  is the trap diameter and  $v$  is the swimmer speed. **e**, Probability of a swimmer to be trapped given a random orientation. **f**, Trapping efficiency increases for smaller viscosity ratios and decreases for thinner swimmers.

## Future Plans

After the above theoretical work is submitted, we will focus our efforts on experiments integrating DNA condensates, microtubules and motors. This will involve cloning motor proteins, coupling them to condensates via cyanobenzothiazole click chemistry, and investigating (1) the motion of small motor-coupled condensate droplets on large microtubule asters and (2) the motion of individual microtubules and microtubule bundles within bulk motor-coupled condensates.

## References

[1] David Zwicker, Markus Decker, Steffen Jaensch, Anthony A. Hyman, and Frank Jülicher, Centrosomes are autocatalytic droplets of pericentriolar material organized by centrioles. *Proceedings of the National Academy of Sciences*, **111**: E2636-E2645, (2014).

## **Publications**

Tyler D. Ross, Dino Osmanović, John F. Brady, and Paul W.K. Rothmund, Snell's Law for Swimmers, in preparation.

**Project Title: Miniaturized Hybrid Materials Inspired by Nature**

Abstract Title: Polyelectrolyte-Mediated Shape Transitions and Assembly in Microtubules and Tubulin Oligomers

**Principle Investigator (PI): C. R. Safinya**

**Co-PIs: Y. Li and K. Ewert**

**Materials Department, University of California at Santa Barbara**

**Santa Barbara, CA 93106**

**E-mail: safinya@mrl.ucsb.edu**

**Program Scope**

The objective of our research program is to develop a fundamental scientific understanding of assembly in biomolecular materials mediated by mechanisms that mimic complex events in the cellular environment. The building blocks that we study include globular, disordered, and filamentous proteins [1-8], lipids, and nucleic acids [9,11]. Notably, the nanoscale assemblies may either be similar to, *or highly distinct* from, those occurring *in vivo*, owing to the complex nature of the systems. Novel assemblies may further result due to controlled shape changes in building blocks [1,6,12].

In current work with microtubule (MT) filamentous protein building blocks, we have found a novel driving mechanism for shape transitions mediated by poly-lysine, a positively charged polymer [13]. Polycation-directed conformational changes in the longitudinal and lateral directions of tubulin protofilaments (PFs, making the wall of MTs), have led to the creation of PF double helices and various tubular architectures. The shape transitions from MTs into the new assemblies, as revealed by synchrotron small-angle X-ray scattering (SAXS) and transmission electron microscopy, are dependent on the size and concentration of the polycations. Our finding has exposed a novel new role for tubulin oligomer building blocks wherein one is able to control filament shape in two orthogonal directions (i.e. a two-dimensionally shape-controllable protein building block), which may form the template for production of novel supramolecular architectures. In parallel work we have discovered a new phase in mixtures of short DNA (sDNA) and cationic liposomes [11]. Stacking of short DNA into columns, by attractive sDNA end-end interactions, has led to the spontaneous formation of a 3D columnar geometric arrangement in multilayer membranes. Softening of the membrane bending rigidity enhances the 3D columnar phase. The findings are consistent with a model where membrane deviations and subsequent wrapping around sDNA columns are coherent across layers. The findings are significant in the area of biomaterials assembly. One may expect that nanoparticles of different shape for example, charged peptide rods with built-in end-to-end hydrophobic interactions, when coupled to membranes, may also be induced to exhibit 3D ordering for structure studies and in applications requiring a local high concentration of a biomolecule such as in sensing.

The projects utilize the broad spectrum of expertise of the PI and the two co-PIs in biomolecular self-assembling methods, custom organic/polymer synthesis and purification of biological molecules, synchrotron x-ray scattering, electron and optical microscopy, and SAXS-osmotic pressure techniques for *in-situ* force measurements.

## Recent Progress

### (I) Poly(Lysine)-Mediated Shape Plasticity in Microtubules leads to Tubulin Double Helix

**Findings and Significance.** By virtue of their native structure, tubulin dimers are protein building blocks that are naturally preprogrammed to assemble into cytoskeletal polymers known as microtubules (MTs). Here we demonstrate polycation-directed (i.e., electrostatically tunable) assembly of tubulins through conformational changes in the longitudinal and lateral directions of tubulin protofilaments (PFs), creating novel tubulin double helices and various tubular architectures (see Figure 1) [13]. Synchrotron small-angle X-ray scattering and transmission electron microscopy reveal a remarkable range of nanoscale assembly structures of the tubulin double helix building blocks, resulting in single- and double-layered tubulin tubules. The phase transitions from MTs into the new assemblies are dependent on the size and concentration of the polycations. Two characteristic scales that determine the number of observed phases are the size of the polycation compared to the size of the tubulin ( $\approx 4$  nm) and the MT diameter ( $\approx 25$  nm).

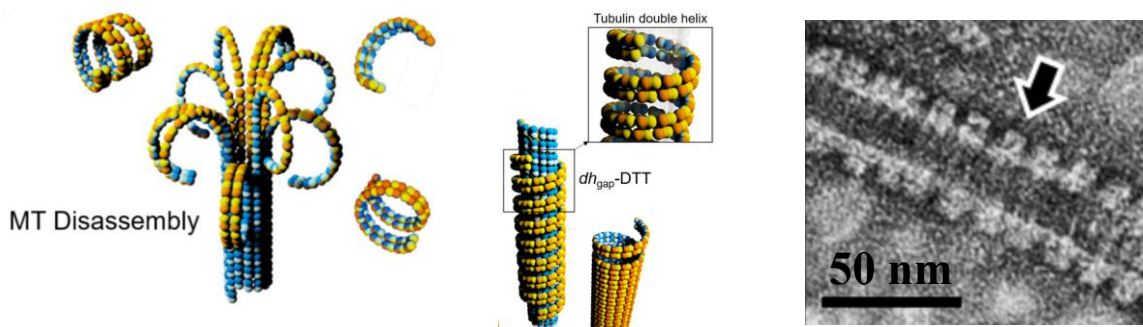


**Figure 1.** Polycation-driven transformation of microtubules into ‘tubulin double helix’-based architectures, driven by curvature changes in tubulin protofilaments along the longitudinal and lateral directions. In the presence of cationic poly(L-lysine) (PL), microtubules (MTs) undergo a depolymerization event where tubulin protofilaments curl away from the MT cylindrical axis (**Left** image) and are transformed into tubulin double helices (tubulin-*dh*) (shown floating around the depolymerizing MT on the left). These novel tubulin double helices form the building blocks of three distinct types of observed structures. Two of these structures result from the tubulin double helix wrapping around individual MTs (i.e., MTs which have not yet depolymerized). In cross-section these phases consist of double tubulin layers (DTT), with the inner/outer protofilaments crossed with respect to each other. The outer tubulin layer comprising the tubulin-*dh* may either have a large pitch with a gap (labeled  $dh_{\text{gap}}\text{-DTT}$ ; **Middle** image with the magnified insert showing the outer-layer tubulin-*dh*) or a smaller pitch with a tight gap (labeled  $dh_{\text{tight}}\text{-DTT}$ ; not shown). Alternatively, the tubulin-*dh* building blocks may directly assemble to form single-wall tubulin tubules (labeled  $dh\text{-STTs}$ ; shown on the lower right of the  $dh_{\text{gap}}\text{-DTT}$  structure in the **Middle** image). The novel structures require polycation-triggered curvature changes of tubulin protofilaments in two orthogonal directions: longitudinal and lateral. **Right:** TEM images of  $dh_{\text{gap}}\text{-DTTs}$ , showing the double helical nature of the outer layer.

The work suggests the feasibility of “programmable breakdown” of protein nanotubes, tearing MTs into double-stranded tubulin PFs and building up previously undiscovered nanostructures, by using polycations with both scissor- and glue-like properties. Importantly, we define a new role of tubulins building blocks for the fabrication of novel supramolecular architectures. These findings provide insight into the design of protein-based functional materials, for example, as metallization templates for future nanoscale electronic devices and molecular screws driven by kinesin motors.

### (II) A 3D Columnar Phase of Stacked Short DNA Organized by Coherent Membrane Undulations

**Findings and Significance.** We have discovered a method of preparing a novel new organization of short DNA structures upon intercalation of blunt duplexes of short DNA (sDNA) within cationic

multilayer fluid membranes (see Figure 2) [11]. A novel geometric arrangement of sDNA is observed in the form of a 3D columnar phase of stacked sDNA, even though direct DNA–DNA electrostatic interactions across membrane layers are screened by cationic lipids diffusing near the phosphate groups of sDNA. Softening of the membrane bending rigidity, which promotes membrane undulations, significantly enhances the 3D columnar phase. The discovery of the new phase is consistent with a model where local membrane undulations, caused by electrostatically induced wrapping of the membrane around sDNA columns, phase-lock from layer to layer. This phase-locking precipitates coherent “crystal-like” undulations coupled to sDNA columns with long-range positional and orientational order. The new phase may be thought of as a 3D crystal of membrane undulations with the repeating unit cell consisting of a curved membrane ribbon coupled to a column of sDNA, with width equal to the DNA–DNA interaxial distance and length set by the membrane size. It is analogous to bicontinuous phases with long-range positional and orientational order of curved membranes and the  $P_\beta$  “rippled” phase of multilayer membranes.

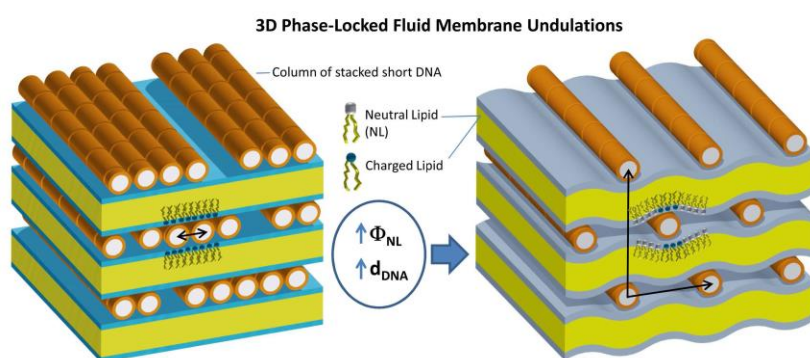


**Figure 2.** 2D ( $L_\alpha^{sDNA,2D}$ , **left**) and 3D columnar phases ( $R_\alpha^{sDNA,3D}$ , **right**) of stacked blunt short DNA (sDNA) intercalated between fluid cationic lipid membranes (CL), revealed by synchrotron-based small-angle X-ray scattering (SAXS). **Left:** Graphic illustration of CL–sDNA complexes in the  $L_\alpha^{sDNA,2D}$  phases. Formed at low mole fraction neutral lipid ( $\Phi_{NL}$ ), the stacked sDNA (depicted as short cylinders) sandwiched between

cationic membranes form columns with a well defined DNA interaxial spacing in each layer, but without correlations from layer to layer. **Right:** Illustration of CL–sDNA complexes in the  $R_\alpha^{sDNA,3D}$  phase, which forms after  $\Phi_{NL}$  is increased above a certain threshold ( $0.5 < \Phi_{NL} \leq 0.75$  for 11 and 24 bp sDNA, and  $0.52 < \Phi_{NL} \leq 0.75$  for 48 bp sDNA). In this phase, the sDNA rods across bilayers exhibit correlations, forming a centered rectangular lattice with long-range order. The stacked sDNA rods retain a sliding degree of freedom along the helical axis.

The findings of this paper have broad implications in the area of assembly in biological materials. Many of the prevailing approaches in hierarchical assembly of nanoscale building blocks involve either specific interactions, such as H-bonding of complementary nucleic acid base pairs attached to colloidal nanoparticles, or nonspecific electrostatic interactions, for example between intrinsically disordered protein biopolymers bound to the surface of other structured proteins. Here, we used the mutual electrostatic coupling of short sDNA rods and flexible membranes as the mechanism for 3D ordering of sDNA. The method may be extended to other nanoparticles of different shape with a designed-in coupling to membranes; for example, charged peptide rods with built-in end-to-end hydrophobic interactions, both for structure studies and as advanced materials in applications requiring a local high concentration such as biosensing.

## Future Plans

Microtubules (MTs) are hollow cylinders with outer and inner diameter of  $\approx 25$  and 15 nm, respectively. In earlier BES-supported study we found, by time-dependent SAXS and TEM, that the polyamine spermine( $4^+$ ) disassembles MT bundles into tubulin oligomers and rings above a critical spermine concentration [1]. Thus, multivalent ions tend to depolymerize MTs, with the MT life-time dependent on ion concentration. In the next period we will look for shape transitions in

dynamical MTs coated with intrinsically disordered protein (IDP) Tau (a very weak stabilizer of MTs). Our future plans involve experiments that will uncover structural and shape transitions in microtubule–Tau assemblies in dissipative conditions in the presence of GTP and tubulin. The methods we will employ include state-of-the-art electron microscopy and time-dependent synchrotron SAXS studies, in the presence of metal cations such as  $Mg^{2+}$ ,  $Ca^{2+}$ ,  $Mn^{2+}$ , and  $Zn^{2+}$ .

## References

1. Ojeda-Lopez, M. A.; Needleman, D. J.; Song, C.; Ginsburg, A.; Kohl, P.; Li, Y.; Miller, H. P.; Wilson, L.; Raviv, U.; Choi, M. C.; Safinya, C. R.: Transformation of taxol-stabilized microtubules into inverted tubulin tubules triggered by a tubulin conformation switch. *Nature Materials* **2014**, *13*, 195-203.
2. Deek, J.; Chung, P. J.; Kayser, J.; Bausch, A. R.; Safinya, C. R.: Neurofilament sidearms modulate parallel and crossed-filament orientations inducing nematic to isotropic and re-entrant birefringent hydrogels. *Nature Communications* **2013**, *4*, 2224.
3. Chung, P. J.; Choi, M. C.; Miller, H. P.; Feinstein, H. E.; Raviv, U.; Li, Y.; Wilson, L.; Feinstein, S. L.; Safinya, C. R.: Direct force measurements reveal that protein Tau confers short-range attractions and isoform-dependent steric stabilization to microtubules. *Proc. Natl. Acad. Sci. U. S. A. (PNAS Plus)* **2015**, *112*, E6416-E6425.
4. Safinya, C. R.; Deek, J.; Beck, R.; Jones, J. B.; Li, Y.: Assembly of Biological Nanostructures: Isotropic and Liquid Crystalline Phases of Neurofilament Hydrogels. *Ann. Rev. Cond. Matter Phys.* **2015**, *6*, 113-136.
5. Chung, P. J.; Song, C.; Miller, H. P.; Li, Y.; Choi, M. C.; Wilson, L.; Feinstein, S. C.; Safinya, C. R.: Tau mediates microtubule bundle architectures mimicking fascicles of microtubules found in the axon initial segment. *Nature Communications* **2016**, *7*, 12278.
6. Safinya, C. R.; Chung, P. J.; Song, C.; Li, Y.; Ewert, K. K.; Choi, M. C.: The effect of multivalent cations and Tau on paclitaxel-stabilized microtubule assembly, disassembly, and structure. *Adv. Colloid Interf. Sci.* **2016**, *232*, 9-16.
7. Choi, M. C.; Chung, P. J.; Song, C.; Miller, H. P.; Kiris, E.; Li, Y.; Wilson, L.; Feinstein, S. C.; Safinya, C. R.: Paclitaxel suppresses Tau-mediated microtubule bundling in a concentration-dependent manner. *Biochim. Biophys. Acta - General Subjects* **2017**, *1861*, 3456-3463.
8. Chung, P. J.; Song, C.; Deek, J.; Miller, H. P.; Li, Y.; Choi, M. C.; Wilson, L.; Feinstein, S. C.; Safinya, C. R.: Comparison between 102k and 20k Poly(ethylene oxide) Depletants in Osmotic Pressure Measurements of Interfilament Forces in Cytoskeletal Systems. *ACS Macro Lett.* **2018**, *7*, 228-232.
9. Majzoub, R. N.; Ewert, K. K.; Jacovetty, E. L.; Carragher, B.; Potter, C. S.; Li, Y.; Safinya, C. R.: Patterned Threadlike Micelles and DNA-Tethered Nanoparticles: A Structural Study of PEGylated Cationic Liposome–DNA Assemblies. *Langmuir* **2015**, *31*, 7073-7083.
10. Liu, C.; Ewert, K. K.; Wonder, E.; Kohl, P.; Li, Y.; Qiao, W.; Safinya, C. R.: Reversible Control of Spacing in Charged Lamellar Membrane Hydrogels by Hydrophobically Mediated Tethering with Symmetric and Asymmetric Double-End-Anchored Poly(ethylene glycol)s. *ACS Appl. Mater. Interfaces* **2018**, *10*, 44152–44162.

## Publications (BES-supported, last 24 months)

11. Boussein, N. F.; Leal, C.; McAllister, C. S.; Li, Y.; Ewert, K. K.; Samuel, C. E.; Safinya, C. R.: A 3D columnar phase of stacked short DNA organized by coherent membrane undulations. *Langmuir* **2019**, *35*, 11891-11901. DOI: [10.1021/acs.langmuir.9b01726](https://doi.org/10.1021/acs.langmuir.9b01726).
12. Safinya, C. R.; Chung, P. J.; Song, C.; Li, Y.; Miller, H. P.; Choi, M. C.; Raviv, U.; Ewert, K. K.; Wilson, L.; Feinstein, S. C.: Minireview - Microtubules and Tubulin Oligomers: Shape Transitions and Assembly by Intrinsically Disordered Protein Tau and Cationic Biomolecules. *Langmuir* **2019**, *48*, 15970-15978. DOI: [10.1021/acs.langmuir.9b02208](https://doi.org/10.1021/acs.langmuir.9b02208)
13. Lee, J.; Song, C.; Lee, J.; Miller, H. P.; Cho, H.; Gim, B.; Li, Y.; Feinstein, S. C.; Wilson, L.; Safinya, C. R.; Choi, M. C.: Tubulin Double Helix: Lateral and Longitudinal Curvature Changes of Tubulin Protofilament. *Small* **2020**, 2001240. DOI: [10.1002/sml.202001240](https://doi.org/10.1002/sml.202001240).
14. Wonder, E.; Ewert, K. K.; Liu, C.; Steffes, V. M.; Kwak, J.; Qahar, V.; Majzoub, R. N.; Zhang, Z.; Carragher, B.; Potter, C. S.; Li, Y.; Qiao, W.; Safinya, C. R.: Assembly of Building Blocks by Double-End-Anchored Polymers in the Dilute Regime Mediated by Hydrophobic Interactions at Controlled Distances. *ACS Appl. Mat. Interf.* **2020**, *12*, 45728-45743. DOI: [10.1021/acsami.0c10972](https://doi.org/10.1021/acsami.0c10972)
15. Brandon S. Light, Youli Li, Miguel Zepeda-Rosales, Cyrus R. Safinya: Forced Crowding of colloids by thermophoresis and convection in a custom liquid Clusius-Dickel micro-device. *Langmuir* **2021**, *37*, 2, 675–682. DOI: [10.1021/acs.langmuir.0c02721](https://doi.org/10.1021/acs.langmuir.0c02721)
16. Safinya, C. R.; Ewert, K. K.; Li, Y.; Rädler, J. O.: Cationic Liposomes as Spatial Organizers of Nucleic Acids in One, Two, and Three Dimensions: Liquid Crystal Phases with Applications in Delivery and Bionanotechnology, Handbook of Lipid Membranes: Molecular, Functional, and Materials Aspects (Cyrus R. Safinya and Joachim O. Rädler, eds.) ISBN 13: 978-1466555723 & ISBN 10: 1466555726 Publisher: CRC Press Taylor & Francis Group (scheduled publication date: **September 2021**, ebook and hardcover).
17. Smith, G. S.; Safinya, C. R.: Structures and Interactions in Freely Suspended Multilayer Membranes and Dilute Lamellar Fluid Membranes from Synchrotron X-ray Scattering, Handbook of Lipid Membranes: Molecular, Functional, and Materials Aspects (Cyrus R. Safinya and Joachim O. Rädler, eds.) ISBN 13: 978-1466555723 & ISBN 10: 1466555726 Publisher: CRC Press Taylor & Francis Group (scheduled publication date: **September 2021**, ebook and hardcover).
18. Kohl, P.; Song, C.; Fletcher, B.; Chung, P. J.; Miller, H. P.; Li, Y.; Choi, M. C.; Wilson, L.; Feinstein, S. C.; Safinya, C. R.: Metal Ions Impart Shape Plasticity on Microtubule (MT)/Tau Bundles Driving a Transition from a Loosely Organized Sliding MT Phase to an Extended Phase of MT Bundles Locked in a Hexagonal Lattice (*manuscript in preparation*).
19. Steffes, V. M.; Zhang, Z.; MacDonald, S.; Crowe, J.; Ewert, K. K.; Carragher, B.; Potter, C. S.; Safinya, C. R.: Novel Shape Transitions Revealed by Cryogenic-TEM in Lipid Nanoparticles Mediated by Multivalent Lipids. (*manuscript in preparation*).

## Tension- and Curvature- Controlled Fluid-Solid Domain Patterning in Single Lamellae

**Maria M. Santore and Gregory M. Grason**

**Department of Polymer Science and Engineering**

**University of Massachusetts, Amherst, MA 01003**

### Program Scope

This program integrates experiment and theory to facilitate the discovery of new patterning mechanisms for flexible ultrathin materials that can assume complex contours of non-zero Gaussian curvature. Patterns of interest span length scales up to that of the overall system, built from intricate shapes (flowers, circles, hexagons, diamonds) assembled in regular arrays (eg. a hexagonal lattice) or in arrangements of interconnected or parallel stripes. The program exploits phospholipid lamellae as a model for flexible, ultra-thin (4 nm) fluid-solid composite sheets. These composite lamellae integrate rigid phase-separated solid phospholipid domains in fluid bilayers (Figure 1) and can flow, stretch, and shear,<sup>1</sup> enabling them to assume complex contours. Current efforts focus on the impacts of tension, curvature, rigidity, and bending on pattern formation by assembly or crystallization. Distinguishing features include switchable pattern designs, responsive to gentle mechanical or osmotic stimuli, and process controlled pattern variations for compositionally identical systems.

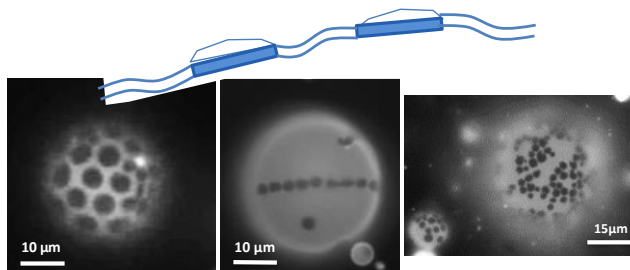


**Fig. 1.** Examples of patterns in composite lamellae.

### Recent Progress

**Overview.** Contrary to expectations that tense vesicles and sharp curvature are critical to interesting pattern formation in composite membranes, we discovered elaborate arrangements of discrete domains assembled in the near-zero tension limit over a broad range of vesicle sizes where fluid membranes were “floppy” and solid domains remained visibly flat. Progress in the last two years has therefore focused on assembly-based pattern formation near zero tension. Key advances here include the discovery and quantification of pairwise domain interactions driven by the rigidity of solid domains and the energetic cost of bending fluid lamellae; the observation of Brownian motion and its suppression by long range interactions; the ability for precise domain positioning, the response of patterns to gentle touch or osmotic forces, and counterintuitive features of multibody versus pairwise interactions. Separately, new observations regarding domain shapes motivate focus on the influence of tension on domain formation.

Pairwise interactions in the zero tension limit. Motivated by our discovery of repulsive domain ordering in slightly deflated vesicles containing moderate numbers solid domains, we more recently sought to measure the inter-domain pair potentials.<sup>2</sup> In vesicles containing exactly two similar domains and having overall solid area fractions of 10-18% (domain / vesicle diameter ratios of 0.45-0.58) Brownian motion was suppressed. This prevented quantifying the shape of the pair potential but it revealed a well-established potential minimum. We found the position of the minimum, i.e. the preferred domain separation was strongly dependent on

the “excess area”, the ratio of membrane area to that of a sphere of equal volume. For over 100 vesicles varying from 15-35  $\mu\text{m}$  in size, we generated a master curve relating domain separation (from sub micron to many tens of microns) to excess area. The master curve superposes measurements from different sized vesicles and, above excess areas of  $\sim 1.03$ , those with different relative domain sizes. At smaller excess areas, the influence of domain size grows, with smaller domains exhibiting greater separations compared with larger domains at the same excess area. Modeling predicted these essential features, requiring only bending energy, pressure, and membrane stretching and with the former dominating the energy. The qualitative agreement between modeling and experiment establishes that these interactions arise from the cost of bending the fluid membrane, without requiring complexities such as line tension. Moreover, the rigidity of the solid domain was found to be critical to these interactions, which combine repulsions and attractions and are therefore distinct from exclusively repulsive interactions between fluid domains in a fluid membrane. Future work on pairwise interactions will probe the impact of smaller domain sizes and domain size mis-match.

**Multibody Interactions.** A clear next step for domain assembly in the zero-tension limit is the study of how pairwise interactions lead to multibody interactions and patterning. Distinct from the striped phases observed at high tensions, we have observed linear arrays of small domains and have little understanding of how and when these form. Recent work, however, has established that an abrupt reduction in excess area can trigger a transition from a dynamic and loosely repulsive “gas” of small solid domains to a chain, such as that in Figure 1. The conditions and dynamics surrounding this behavior are a focus of ongoing study.

**Modeling intra-vesicle shape and inter-domain energetics.** The effect of 2-D shear rigidity qualitatively alters the shape and mechanics of solid domains relative to the well-studied case of

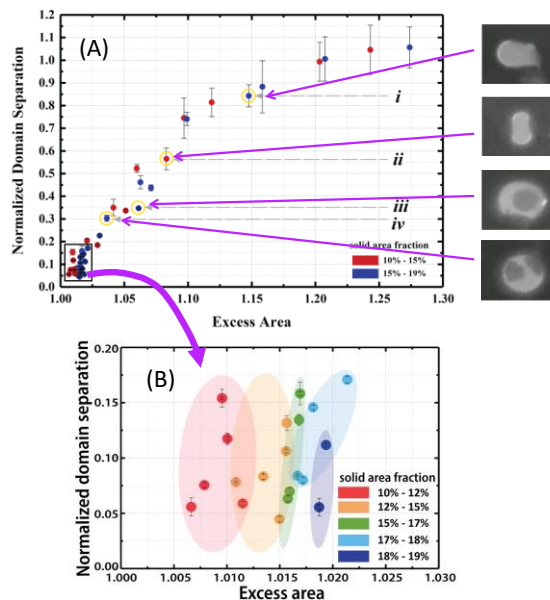


**Fig 2.** A) Master curve for pairwise domain separation as a function of excess area B) close up showing influence of domain size

fluid domain elasticity. This derives from the geometric incompatibility of planar crystals and Gaussian curvature. Unlike the case of bending mechanics, forcing a 2-D solid to conform to a spherical curvature leads to strains that grow with area. This effect amounts to a *geometric rigidification* of solid domains leading those domains to expel Gaussian curvature, effectively leading solid domains to behave as “2-D, plate-like colloids” embedded within the fluid vesicle. Recent modeling efforts have advanced the quantitative understanding of the impact of plate-like domains on fluid-solid composites in two directions.

First, we have extended the analysis of exact shape equilibria of composite vesicles based on a generalized 2D Helfrich model with rigid inclusions. Through that analysis we have shown that high-bending “hinges”, which flank solid domains, emerge at the transition between negative and positive internal pressure (see Fig 3A). In the limit of high inflation, hinges concentrate elastic energy of the fluid phase, and we have shown that relative length and curvature of hinges to be directly correlated to the internal pressure (and tension) of the vesicle. This result then provides key understanding of what then controls strength and interaction ranges of domains on the vesicle.

The second direction centers on advancing the modeling of inter-domain energetics. We have advanced our analytical multi-arc ansatz for two-domain vesicle configurations. While our previous approach facilitated prediction of the qualitative distinction between states that favor close vs. antipodal domain

arrangements, it was not able to capture nature of the transition, nor the quantitative features of associated with configurations intermediate to attractive and repulsive equilibria. The current approach captures these more complex intermediates and therefore facilitates modeling of energetics over the full range of states, as shown for example in the repulsive (low inflation) and attractive (high inflation) regimes in Fig. 3B, and proves that equilibrium domain separation vanishes in the isoperimetric limit. Additionally, we have constructed the phase diagram of attractive vs. repulsive domain interactions as a function of domain size and inflation (Fig. 3C), confirming the observations that larger domains experience attractions at lower excess area. Further study has developed the scaling behavior for the equilibrium domain spacing as function of excess length.

Influence of tension and curvature on domain shape. While we have long observed a variety of complex domain shapes including symmetric hexagons, notched hexagons, ninja stars, diamonds, and different types of flowers, we have come to believe that domains with more

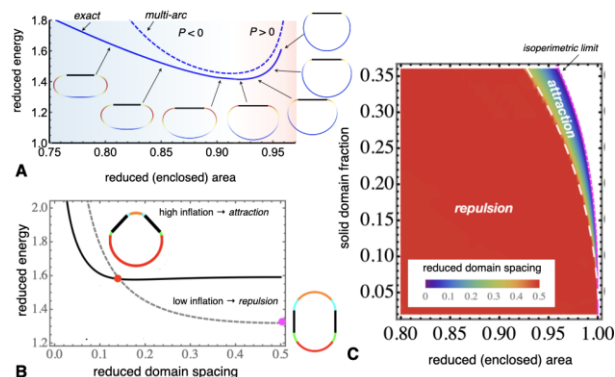


**Fig 3.** (A) Evolution of single domain morphology and energy of 2D vesicle model with increasing inflation (i.e. reduced area); (B) Inter-domain potential of from 2D vesicle model showing respective attraction and repulsion at high- and low-inflation; (C) phase diagram of domain interactions.

elaborate shapes generally form at higher tensions. Because domains nucleate and grow upon cooling, the membrane tension at any point in domain development can influence current and future growth patterns. Yet, because membrane tension is controlled by the relative rates of cooling, thermal membrane contraction, solid area fraction, and water loss, it is difficult to anticipate. It had been a long-standing puzzle, for instance, why flower shapes tended to be observed in one compositional side of the phase diagram. Also a puzzle was the counterintuitive but highly reproducible observation of regular compact domains on smaller vesicles and instabilities on large vesicles.

New studies tracking the evolving domain shapes have led to hypotheses now being tested: We posit that the tension during nucleation is higher when the phase transition temperature is lower, on the low DPPC side of the phase diagram, producing small irregular domains from the start. Conversely with lower tensions during nucleation, where the binodal curve traverses higher temperatures, regular domains can develop instabilities only once they grow to substantially larger sizes, producing domains of fundamentally different character. Ongoing work employs micropipettes to test and quantify these behaviors.

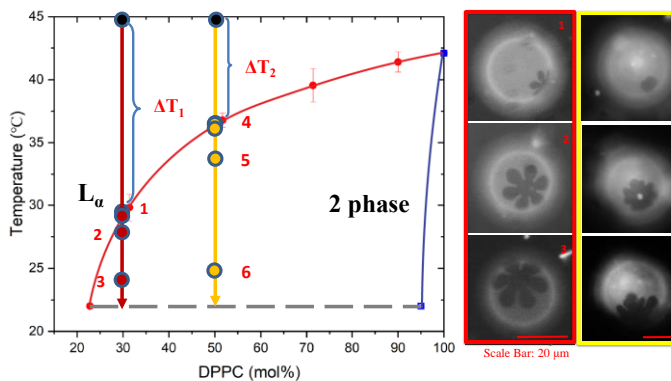


**Fig 4.** Cooling histories and morphologies for two lipid compositions parts in the phase diagram.

## Future Plans

Future work extends from pairwise multibody effects, including 3- and 4- domain interactions and prioritizing behaviors such as domain chaining, that are difficult to anticipate from the pairwise interactions. Ex-situ tension measurements on vesicles having different domains shapes and subject to different processing histories will test hypotheses correlating processing tensions to domain features and enabling detailed modeling explanations of domain morphologies.

## References

1. Evans, E.; Needham, D. Physical Properties of Surfactant Bilayer Membranes - Thermal Transitions, Elasticity, Rigidity, Cohesion, and Colloidal Interactions. *Journal of Physical Chemistry* **1987**, *91*, 4219-4228.
2. Xin, W. Y.; Wu, H.; Grason, G. M.; Santore, M. M. Switchable positioning of plate-like inclusions in lipid membranes: Elastically mediated interactions of planar colloids in 2D fluids. *Science Advances* **2021**, *7*, eabf1943.

## **Publications**

Li, S.; Zandi, R.; Travasset, A.; Grason, G.M. “Ground States of Crystalline Caps: Generalized Jellium on Curved Space”, *Physical Review Letters*, **2019**, *123*, 145501, DOI: 10.1103/PhysRevLett.123.145501

Xin, W. Y.; Wu, H.; Grason, G. M.; Santore, M. M. “Switchable positioning of plate-like inclusions in lipid membranes: Elastically mediated interactions of planar colloids in 2D fluids”, *Science Advances* **2021**, *7*, eabf1943, DOI: 10.1126/sciadv.abf1943

## Controlling exciton dynamics with DNA origami for quantum information science

Gabriela S. Schlau-Cohen (PI), Department of Chemistry

Mark Bathe (co-PI), Department of Bioengineering

Adam Willard (co-PI), Department of Chemistry

Massachusetts Institute of Technology

### Program Scope

The overall goal of our program is to design, synthesize, and characterize DNA-chromophore constructs that encode programmable spatiotemporal exciton dynamics upon photoexcitation for applications such as quantum information processing and energy transport. Control over excited-state properties in the condensed phase requires control over chromophore position and orientation, which is challenging in synthetic systems<sup>1</sup>. By scaffolding molecular chromophores into DNA origami we achieve the requisite nanometer precision for arbitrary 2 and 3D structures.<sup>2-3</sup> Combining this synthetic strategy with high-resolution spectroscopy<sup>4</sup> and advanced theoretical modeling, we have developed a design framework for these photoactive materials.

### Recent Progress

#### Engineering couplings for energy transfer

Exciton dynamics in the condensed phase depend on the electronic coupling between chromophores and between chromophores and their surrounding environment, termed the system-bath coupling. Without tractable model systems, the relative contributions of these two couplings and their interplay have been challenging to explore. In particular, the system-bath coupling has been extensively investigated theoretically but underutilized experimentally. Through phosphoramidite modified chromophore-DNA assemblies we generate cyanine (Cy3) monomers, dimers, and trimers scaffolded within DNA duplexes<sup>5</sup>.

By changing the number of nucleotides separating the chromophores of the Cy3 dimers, we systematically decreased the magnitude of electronic coupling (Figure 1a). Using multidimensional spectroscopy and molecular dynamics (MD) simulations, we experimentally measured the relative magnitude and then computationally quantified the electronic coupling, observing tunability from hundreds down to tens of wavenumbers (Figure 1b,c).

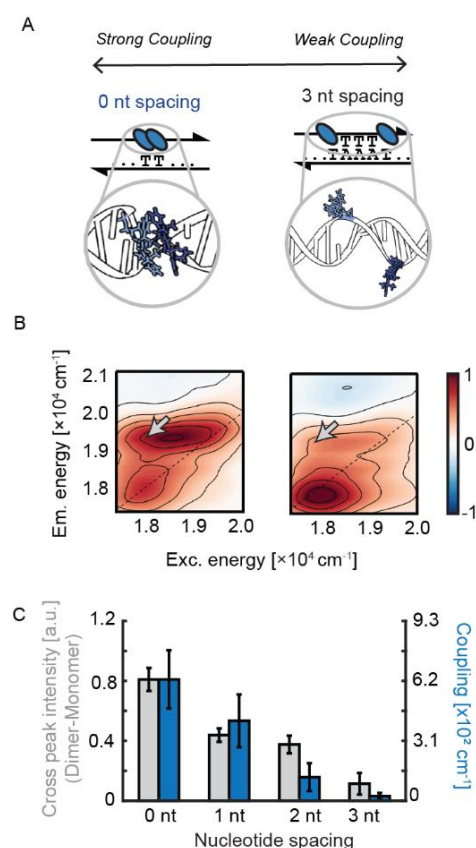


**Figure 1:** Control over electronic coupling. (A) Schematic and MD snapshots of Cy3 dimers with varying coupling. (B) 2D electronic spectra ( $T=250$  fs) for 0 and 3 nucleotide separated dimers. (C) Calculated electronic coupling and 2D spectrum cross peak intensity for varying nucleotide spacing.

In order to investigate the impact of system-bath coupling, we scaffolded chromophores in both DNA duplexes and DNA double-crossover (DX) tiles, which have a persistence length twice that of duplexes (Figure 2a). The more rigid scaffold led to a narrower distribution of lifetimes (not shown), slowed the structural fluctuations of the chromophore-DNA assembly (as measured by fluorescence anisotropy, Fig. 2b), and gave rise to a more structured distribution of transition dipole angles (Figure 2c).

We evaluated the role of the different system-bath couplings in energy transfer by incorporating a Cy5 acceptor dye to the end of the DNA constructs and measuring the energy transfer efficiency from Cy3 to Cy5 (Figure 2d). The more rigid DX tile transferred energy less efficiently than the more flexible duplex. Simulations suggest the efficiency decrease in the DX tile is from inefficient subpopulations, whereas in the duplex the fast fluctuations access a favorable configuration during the excited-state lifetime, increasing the overall efficiency of energy transfer.

### *Geometric control over exciton properties*

To build on our advances in phosphoramidite excitonic circuitry, we developed a facile approach to vary the geometry and photophysics of the Cy3 dimer. The excited-state lifetime of the Cy3 dimer is sensitive to the relative position and orientation of the two chromophores and the local environment. By designing DNA structures with a strongly coupled molecular dimer and variable complementary strands (adding up to five additional bases), we introduced geometric distortion (schematic in Figure 3a) that yielded variation in the excited state lifetime (Figure 3b)<sup>6</sup>. In an orthogonal method of tuning, we showed that the dimer excited state lifetimes are also sensitive to solvent polarity. Single-molecule measurements (Figure 3d-e) show that variation in excited-state lifetime from differences in complementary strands is visible with limited heterogeneity on the single-molecule level, suggesting potential utility as probes for fluorescence imaging of the local chemical environment.

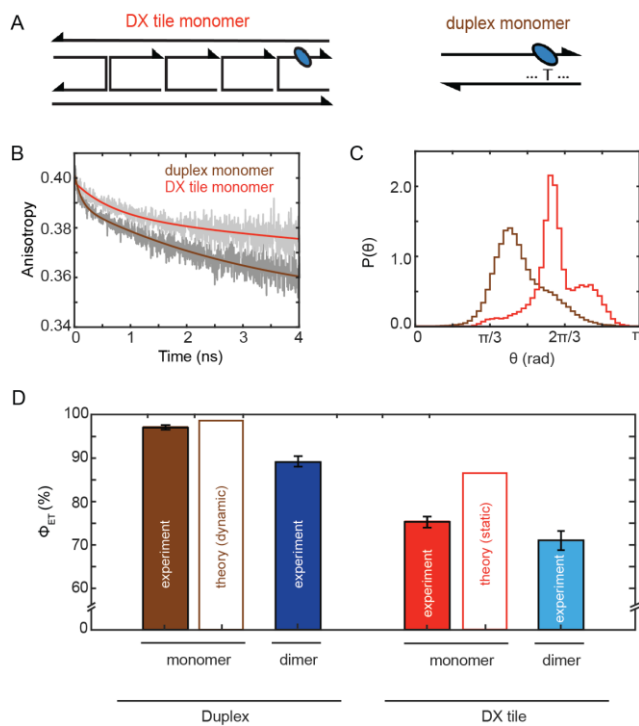


**Figure 2:** Control over system-bath coupling and energy transfer. (A) Schematic of duplex and DX tiles (B) fluorescence anisotropy decay for Cy3 scaffolded within duplexes (0.19 ns) and DX tiles (0.62 ns). (C) MD derived dipole angles between the Cy3 chromophore and the DNA backbone for duplexes and DX tiles. (D) Energy transfer efficiency between Cy3 monomers and dimers and an attached Cy5 acceptor.

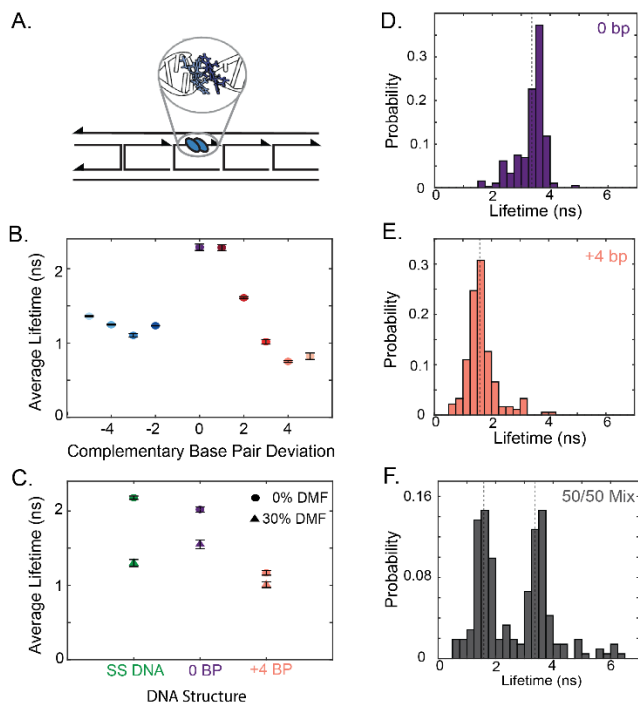


**Figure 3:** Tuning excitonic properties with geometric distortion. (A) Schematic of DNA-chromophore dimer. (B) Emission lifetime of dimers with a distortion of -5 to +5 bases. (C) Emission lifetime variation of dimer configurations and single-stranded (ss) DNA in environments of varying polarity. (D) Single molecule lifetime distributions of dimers with 0 and (E) 4 base distortions and a (F) 50/50 mixture of dimers, highlighting that the two species are distinguishable.

### Towards application in quantum computing

We demonstrated that molecular chromophore based excitonic circuits can be programmed to perform specific unitary operations through the reconfiguration of the constituent dye molecules<sup>8</sup>. The output of the computation is encoded in the state of the system at a given time after initializing the circuit by optical excitation. For a system undergoing a set of unitary transformations,  $\hat{U}_{target}$ , such as gates in a quantum circuit, the system Hamiltonian,  $\hat{H}_\tau$ , can be represented in terms of the transformation time,  $\tau$ , at which  $\hat{U}_{target}$  is realized (Figure 5a). Chromophores organized with a defined geometry can be identified to satisfy  $\hat{H}_\tau$  under a Frenkel exciton model of single excitations. We were able to determine the chromophore geometry for a set of universal quantum gates: the 1-qubit NOT, Hadamard, and  $\pi/8$  gates, and the 2-qubit CNOT gate (Figure 5b-d).

### Understanding & optimizing chromophore photophysics

We used femtosecond spectroscopy to map out the non-radiative pathways in Cy3, the presence of which shortens the excited-state lifetime and hinders fluorescence emission. By identifying nodes in the time-domain oscillatory signal (Figure 4), we were able to identify a previously unknown non-emissive state<sup>7</sup>. Computational modeling, spectroscopic analysis of vibrational modes, and synthetic structure tuning allowed us to identify potential nuclear design principles for suppression of this pathway, which would enhance the fluorescence from this widely used chromophore. This work also highlights the role of nuclear motion in tuning excited state molecular properties, a feature that could be incorporated into synthetic multichromophoric systems.

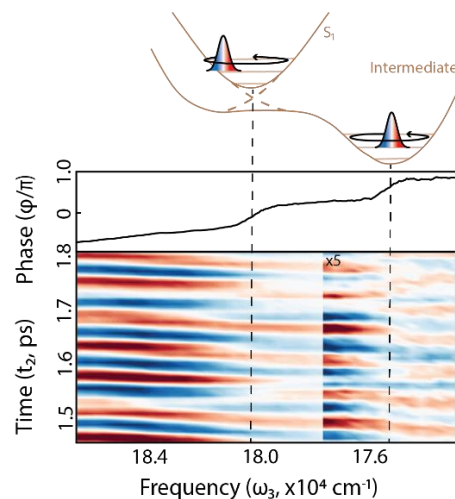


**Figure 4:** Identification of a dark intermediate state in a commonly used cyanine chromophore through coherent femtosecond vibrational dynamics

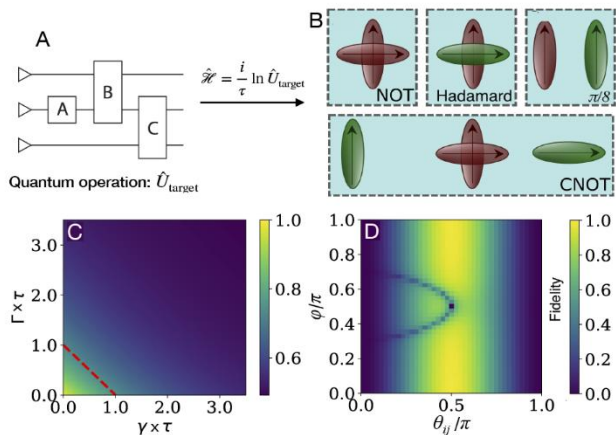


**Figure 5:** A universal set of quantum gates as excitonic circuits. (A) Unitary operations mapped into a Hamiltonian matrix corresponding to a physical system of interacting chromophore molecules. (B) The chromophore geometries realizing a set of universal quantum gates. (C) Fidelity of the NOT gate as a function of dissipation,  $\Gamma$ , and dephasing,  $\gamma$ , and (D) as a function of excitonic circuit geometry:  $\theta_{ij}$  is the twist angle and  $\phi$  is the angle between the chromophores.

higher fidelity. This suggests that hard-coded synthetic excitonic circuitry has the potential for more robust operation.

### Future Plans

Our ongoing and planned work is focused on both fundamental photophysics and demonstration of computational principles. In the first approach, we are exploring the use of DNA origami excitonic circuitry in tuning fundamental photophysical processes including delocalized states, charge separation, and triplet formation. The development of such abilities will allow for the incorporation of new functionality into these nanoscale materials. In a second approach, we are working towards experimental demonstration of an excitonic qubit, as well as optical methods of exploring 2-qubit operation including polarized excitations schemes.

### References

[1] Scholes, G. D. & Rumbles, G. *Nat. Mater.* 683 (2006). [2] Boulais, E. et al. *Nat. Mater.* 17, 159 (2018). [3] Banal, J. et al. *J. Phys. Chem. Lett.* 8, 5827 (2017). [4] Son, M. et al. *Trends Chem.* (2021). [5] Hart, S.M. et al. *Chem*, 7, 752 (2021). [6] Hart, S.M. et al. *in preparation*. [7] Hart, S.M. et al. *J. Phys. Chem. Lett.* 11, (2021). [8] Castellanos, M. et al. *Phys. Chem. Chem. Phys.*, 22 (2020). [9] Castellanos, M. et al. *Phys. Chem. Chem. Phys.* (2020).

We then expanded this approach towards larger computation algorithms, including the well-studied 2-qubit Deutsch-Jozsa (D-J) algorithm, one of the simplest algorithms for which a quantum computer can outperform a classical one. We employed two different strategies to realize this algorithm, namely, a serial approach where the three steps of the algorithm are mapped into individual circuits, and a combined approach, where the entire quantum operation is mapped into one excitonic circuit representation (Figure 6)<sup>9</sup>. In both cases, the two versions of the D-J algorithm (*i.e.*, constant and balanced) are mapped into separate constructs. We evaluated circuit fidelity in an idealized system consisting of Cy3-Cy5 dyes and found that the combined approach leads to a

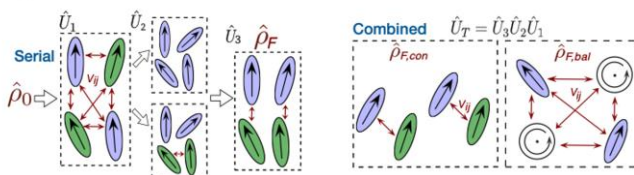


**Figure 6:** Encoding the Deutsch-Jozsa algorithm. (A) Schematic representation of the 2-qubit excitonic circuit geometry for the serial (left) and combined strategies (right).

## Publications

M. Castellanos, A. Dodin, A.P. Willard. "On the design of molecular excitonic circuits for quantum computing: the universal quantum gates" *Physical Chemistry Chemical Physics*, 2020, 22.

S.M. Hart, J.L. Banal, M. Bathe, G.S. Schlau-Cohen. "Identification of Non-Radiative Decay Pathways in Cy3". *Journal of Physical Chemistry Letters*, 2020, 11, 5000.

S.M. Hart\*, W.J. Chen\*, J.L. Banal\*, W.P. Bricker, A. Dodin, L. Markova, Y. Vyborna, A.P. Willard, R. Haner, M. Bathe, G.S. Schlau-Cohen. "Engineering couplings for exciton transport using synthetic DNA scaffolds" *Chem*, 2021, 7, 752.

M. Castellanos, A.P. Willard. "Implementation of the Deutsch-Jozsa algorithm in excitonic circuits with quantum dynamics and classical molecular dynamics simulations" *Physical Chemistry Chemical Physics*, 2021.

M. Son, S.M. Hart, G.S. Schlau-Cohen. "Investigating carotenoid photophysics in photosynthesis with 2D electronic spectroscopy" *Trends in Chemistry*, 2021

S.M. Hart, X. Wang, J. Guo, M. Bathe, G.S. Schlau-Cohen. "Geometric control over chromophore photophysics via DNA scaffolds" *In preparation*.

## Title: What are the principles controlling biomimetic heteropolymer secondary structure?

PI: Michael R. Shirts, Department of Chemical & Biological Engineering, University of Colorado Boulder

### Program Scope

Nature carries out an astonishing variety of biological functions with a very limited set of chemical building blocks. Biological heteropolymers can achieve highly specific functions because of their well-defined three-dimensional arrangements, controlled by the chemistry of the monomer backbone and specified sequences of side chains. The expansive range of function achieved with a small set of chemical building blocks implies that there is a much larger range of materials that could be built with human-engineered heteropolymers that draw from a wider palette of chemical functionality. If we better understand how to design the structures of nonbiological heteropolymers and modulate their relative stability, we can make materials that are more chemically resilient, more responsive, and mechanically tougher, and that act as more adaptable smart materials, more efficient catalysts, and better electron conductors.

The ultimate aim of this research program is to understand the guidelines, based on the underlying physical principles, by which nonbiological heteropolymers with sequence specificity can fold into well-defined three-dimensional structures with desired relative thermodynamic stabilities. The scope of the project during the current funding increment is a first step along that process: to develop the computational infrastructure and underlying general theory for the important intermediate goal of understanding the creation and control of secondary structure elements by which larger assemblies are formed. These initial studies will pave the way for more extensive and realistic modeling of the proposed heteropolymers, as well as design schemes to enable their synthesis, characterization and application.

### Recent Progress

*Infrastructure for discovering and characterizing model foldamers: thermodynamic modeling.* We have developed computational infrastructure to build and simulate coarse-grained oligomers using advanced sampling techniques and analyze them for thermodynamic and structural characteristics of cooperative folding transitions. This is done via a Python package, *cg\_openmm*, which allows us to easily construct and simulate these foldamers and perform thermodynamic characterization (Fig. 1).

*cg\_openmm* uses the highly optimized OpenMM molecular dynamics simulation package, which makes it easy to customize and add arbitrary additional functional forms. This software

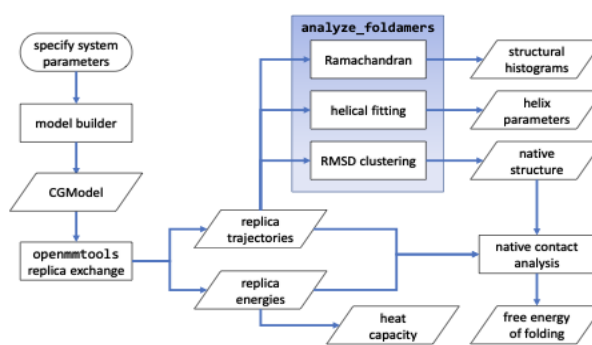


Figure 1: Data flow within *cg\_openmm* and *analyze\_foldamers* infrastructure. Input parameters are rounded rectangles, processes are rectangles, and data are parallelograms.

infrastructure enables large-scale screening of potential foldamer models, allowing specific tests of hypotheses and design models to for foldamers.

We demonstrated the capabilities of our workflow on a simple helix-forming homo-oligomer, systematically varying sets of force field parameters and studying the effects on folding cooperativity and helix stability [1]. Among other findings, we showed that small changes to force field parameters in the homo-oligomer model can dramatically affect cooperativity, stability, and even lead to helix-to-helix transitions (Fig. 2). We also showed that weakening of internal dihedral barriers leads to both lower stability and higher cooperativity. These studies prepare the way for further efforts to understand general properties of non-peptidic foldamers.

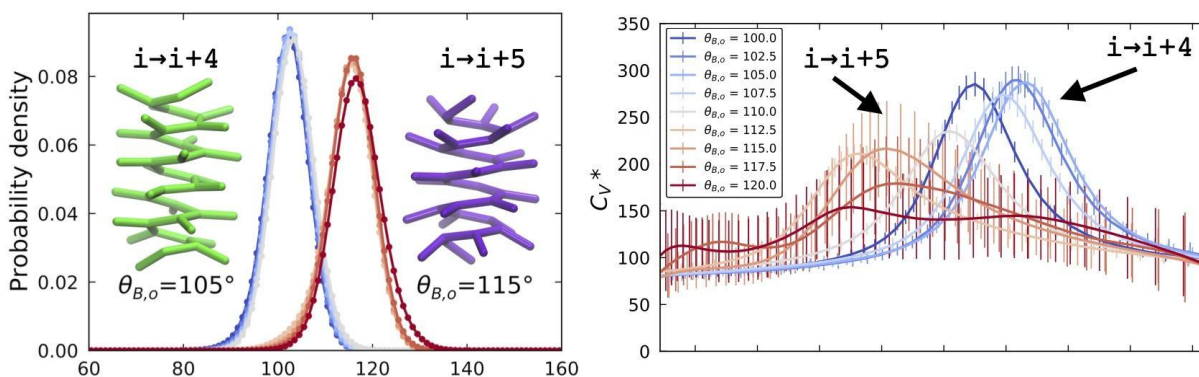


Figure 2: Two different helices form stably with small changes in angle-bending parameters (left), characterized by different melting points (heat capacity peaks) and cooperativity (heat capacity widths) (right). Such small changes could be induced by external effects such as pH or light, enabling switchable molecular scaffolds.

*Infrastructure for discovering and characterizing model foldamers: minimum energy structure searching:* As a complementary foldamer design tool, we have incorporated the capability to sample coarse-grained nonbiological oligomers in the Rosetta protein folding package, using existing protein folding algorithms, in a Python package that uses the pyrosetta Python interface to Rosetta. Fast searches of structurally well-defined minimum energy structures form a useful screening tool for further thermodynamic screening with our other analysis tools. Building into Rosetta infrastructure rather than building our own infrastructure has a long-term purpose of taking advantage of highly successful protein-design algorithms for future testing of atomistic structures.

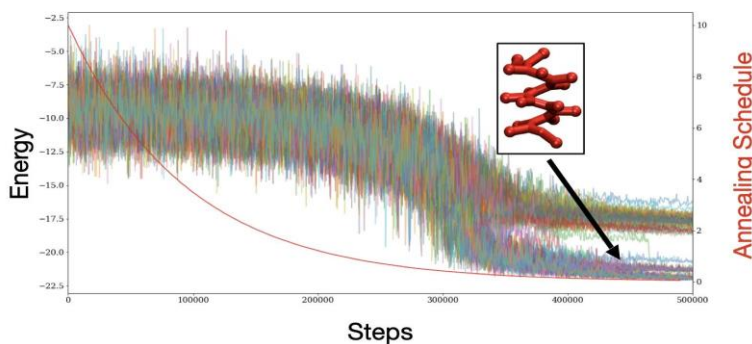


Figure 3: Coarse-grained integration into Rosetta minimum energy searches can be used to consistently find the folded structures for models capable of folding.

### *Atomistic modeling with experimental collaborators:*

We have been working with Sam Gellman (UW-Madison) to understand the structures of a terphenyl oligomer that shows signs of helix formation [2]. Experimental evidence showed clear evidence of chiral secondary structure formation, but no crystal structures could be obtained, and NMR diffusion experiments suggest dimer formation. Our simulations explain how the hypothesized secondary structure cannot form in the monomer, as formation of single helical turns destabilize subsequent turns. The utility of these simulations to one of the major experimentalists in the field demonstrates that modeling can offer real guidance.

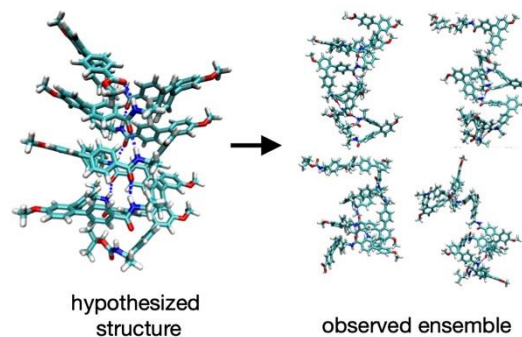


Figure 4: Experimental data are better described by the observed simulated ensemble than the hypothesized structure

*Creation of cooperatively folding knotted homopolymers:* Homopolymer theory suggests that simple random homopolymers cannot form structurally well-defined cooperative collapsed structures, and sequence specificity is needed to produce them. Additionally, there are no examples of knotted model homopolymer structures. Our initial foldamer exploration has found at least one new type of trefoil-like knot that cooperatively and stably forms from a homopolymer. Remarkably, knotting is achieved using a model with a symmetric torsion potential containing a single minimum, and equivalent backbone and sidechain particle types. This simplicity allows for investigation into knotting thermodynamics at a fundamental level. Small knots could serve as a new cooperative secondary structure building element if appropriate chemical bonds with sufficiently stiff backbone could be identified.

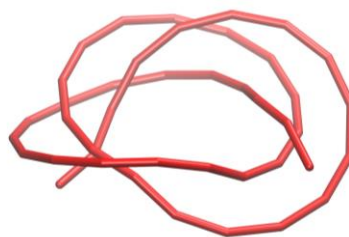
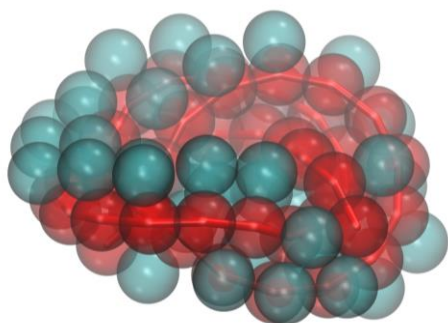


Figure 5: Thermodynamically stable knotted homo-oligomer (left, backbones in red, side chains in teal), with the backbone trace (right). The structure shown is the medoid from RMSD-based clustering of replica exchange MD trajectories

### **Future Plans**

*In the next project year:* We plan to complete key infrastructure tools to improve our ability to understand the determinants of folding behavior. These include 1) wrapping our thermodynamic functionality in an optimization framework in order to optimize models for cooperativity or stability, 2) developing statistical reweighting tools for rapid sequence design given a single simulated ensemble, and 3) synchronizing *cg\_openmm* and *cg\_pyrosetta* in single workflow,

screening for potential foldamers motifs with *cg\_pyrosetta* and optimizing and characterizing these putative foldamers with *cg\_openmm*.

We will use our infrastructure to look at fundamental hypotheses about the determinants of folding, including how the strength of directional interactions such as hydrogen bonds modulates cooperativity as well as the effect of monomer entropy on cooperativity and stability. We will test these simple hypotheses over ensembles of optimized folded helical structures, to ensure that the results are not specific to single structures but are more generalizable principles.

We are continuing our collaboration with the Gellman group by using atomistic simulations to resolve questions of experimentally suggested dimerization of terphenyl-oligomers, by simulating of dimers and examining the effect of proposed modulations of their terphenyl folding framework.

*Plans for future funding periods:* With the addition of the capability to rapidly investigate sequence-dependent behavior, we will be able to test more complex hypotheses and design principles, such as examining the minimum levels of sequence and structural complexity required to stabilize multiple folded states, characterize monomer geometries that form more inherently stable secondary structures, and examine and the effects of solvent on stabilizing folded states. We have started to work more closely with Ken Dill (SUNY Stony Brook), one of the pioneers of coarse-grained protein modeling, and will test and adapt some of the hypotheses he originally examined for lattice proteins with the additional freedom of our continuous models and the ability to design for any chemical structure, not only peptides. We will eventually work towards design rules for assembly of larger structures, both covalently linked and non-covalently assembled.

We will also continue our collaboration with the Gellman group to investigate hypotheses discovered in our coarse-grained research. For example, our hypotheses that modulating the torsional barriers can affect the cooperativity can be experimentally tested by changing the location and number of withdrawing groups on phenyl-based monomers. We aim to eventually work towards “back-map” coarse-grained models into atomistic structures that are amenable to experimental synthesis and characterization.

### **Publications during the last 2 year period (all also referenced in Abstract)**

1. Christopher C. Walker, Garrett L. Meek, Theodore L. Fobe, Michael R. Shirts, “Using a Coarse-Grained Modeling Framework to Identify Oligomeric Motifs with Tunable Secondary Structure”, in revision *J. Chem. Theory Comput.*, preprint available at ChemRxiv: 10.26434/chemrxiv.14687463.v1).
2. Adam F. Kleman, Deseree L. Dufek, Theodore L. Fobe, Darrell R. McCaslin, Brian P. Cary, Michael R. Shirts, and Samuel H. Gellman, ”Potential Foldamers Based on an *ortho*-Terphenyl Amino Acid”, *Org. Lett.* 2021, 23, 12, 4855–4859

## **Bio-inspired Polymer Membranes for Resilience of Electrochemical Energy Devices**

**Meredith N. Silberstein, Sibley School of Mechanical and Aerospace Engineering, Cornell University**

### **Program Scope**

Like biological cell membranes, polymer membranes for electrochemical energy storage and conversion devices must control ion transport and be mechanically robust. Biological membranes are constantly assessing evolving “operating” conditions such as electric field and optimizing their function by dynamically adjusting their material state; the current generation of synthetic polymer membranes are static. *Synthetic membrane performance and durability can be dramatically improved by imbuing the membrane with the ability to sense and adapt to the local electrochemical environment.* One key enabler of biological self-regulation is ionic interactions. We are applying this biological concept to modulating ionic crosslinking within synthetic polymers, considering two classes of approaches – (1) polymers with dual charged sidechains that ionically bond directly with each other; (2) polymers with like-charged sidechains that ionically bond through either multivalent ions or nanoparticles of the opposite charge.

The scope of this program is to discover the fundamental physical mechanisms for self-regulation of polymers and gels under electric fields by focusing on the following three aspects: (I) The influence of an external electric field on the strength of ionic bonds between polymer chains and how this interaction depends on concentration of ionic bonds, any solvent, free ions, polymer backbone rigidity, chemical details of the polymer; (II) How ionic bond strength and concentration among linear polymer chains influences polymer mechanical properties and self-healing for different polymer backbone rigidities and chain lengths; (III) Complete mechanical property dependence on electric fields by adding to I and II, key coupled aspects such as polymer reconfiguration guided by locally high electric field gradient. We are approaching this unexplored concept computationally, utilizing molecular dynamics (MD) simulations and constitutive modeling and validating our findings using synthesis, solution-based experiments, spectroscopy, and mechanical testing.

### **Recent Progress**

Over the last year, we have continued to progress our work on polymer networks formed from combining two sets of polymer chains with matched charge of opposite sign (Figure 1a). This work has consisted of synthesis aimed at controlling the composition, mechanical properties,

and hydrophilicity of the polymer, experimental characterization of mechanical and electrical properties, constitutive modeling, and molecular dynamics (MD) simulations. We have also performed some computational analysis on electric field dependence of anionic polymer networks bonded by divalent cations (Figure 1b).

MD simulations were used to investigate how the mechanical properties of polyelectrolytes with entirely attached charges can be tailored through application of DC electric fields with blocking electrodes. These simulations used a Kremer-Grest approach to explore the role of chain architecture. We examined four different architectures that all had very similar mechanical properties in the absence of an electric field. The key finding from this work was that the electric field influences the mechanical properties of the polyelectrolyte by reorganizing the charged molecules, which can lead to both changes in electrostatic interactions between chains and chain orientation. The effects on mechanical properties were strongest for polyelectrolytes with charges directly on the backbone. Another interesting finding was that the overall influence of the electric field depended heavily on when in the simulation it was first applied and for how long it was applied prior to the start of mechanical testing. Part of this dependence is certainly an artifact of MD simulations, but it also suggests there will be a strong dependence on polymer chain mobility for the success of our overall concept.

In parallel, we have been focused on synthetically tailoring the polyelectrolytes to achieve an understanding of and control over the mechanical properties and hydrophilicity as a function of ionic concentration and backbone composition. We are utilizing pairs of oppositely charged copolymers synthesized independently via free radical polymerization and then mixed and dialyzed to form a solid polyelectrolyte complex (PEC) with minimal free counter ion content. The non-ionic monomers are given in Table 1: in all cases a negatively and positively charged version was made. The PECs formed from these polymers range from highly stretchable (> 40x the initial length) to brittle (cannot even be gripped) in the dried state, and also in terms of how well they self-heal. These PECs also vary widely in terms of how much they will swell when submerged in water. The ability to move away from water swollen PECs without sacrificing ductility will facilitate testing within the electric field. An example stress-strain response is given in Figure 2 for one of these PECs at different strain rates and at two different ratios of the ionic component. The ionic, rather than covalent, crosslinking between the polymer chains, leads to substantial strain rate dependence. The PEC with the larger portion of ionic monomers is stiffer, has a sharper yield, and is less stretchable than that with the smaller portion of ionic monomers at the same strain rate.

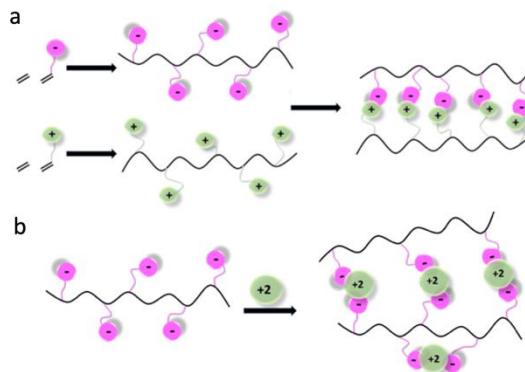


Figure 1. Schematic of polyelectrolytes. (a) Oppositely charged chains. (b) Anionic chains bonded with divalent cations.

Table 1. Monomers explored for tailoring polyelectrolyte copolymer mechanical behavior.

Monomer	Hydrophilicity	T <sub>g</sub> (°C)	Ionic ratios
2-hydroxyethyl acrylate	Highest	-14	5,10,20:1
Acrylamide	Highest	165	5:1
2-hydroxyethyl methacrylate	High	57	5,20:1
Ethyl acrylate	Low	-24	10,20:1
Butyl acrylate	Lowest	-54	20:1
2-ethylhexyl acrylate	Lowest	-50	20:1
2-methoxyethyl acrylate	Medium	-50	10,20:1

The constitutive model for these PEC is hyperelastic-viscoplastic and currently assumes that all ionic bonds that break are instantly reformed (therefore acting as viscous elements rather than contributing to damage). This model captures the substantial rate dependence and is consistent with the overall shape of the cyclic response – large plastic deformation upon unloading, gradual recovery, and decreased yield stress upon reloading. However, the model is not yet capable of quantitatively matching the observed behavior.

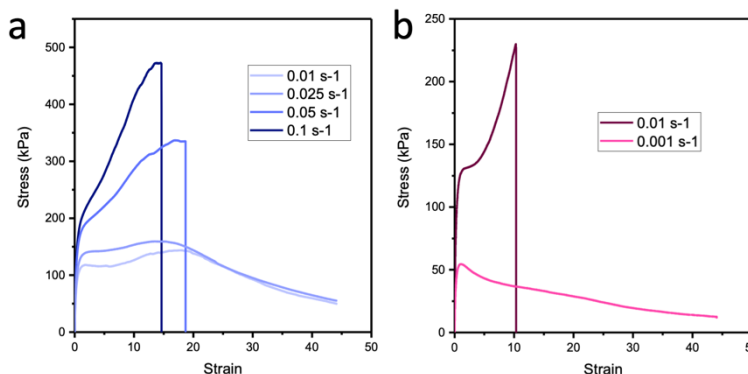


Figure 2. Monotonic stress-strain response of moderately hydrophobic polyelectrolyte. (a) 5% ionic monomers. (b) 10% ionic monomers.

The work on electric field dependence of anionic networks bonded by divalent cations has focused on establishing length scales over which cation concentration can be depleted by application of a DC electric field. Specifically, we looked at depletion on the positively charged side on which the relations should deviate from the Debye length due to the lack

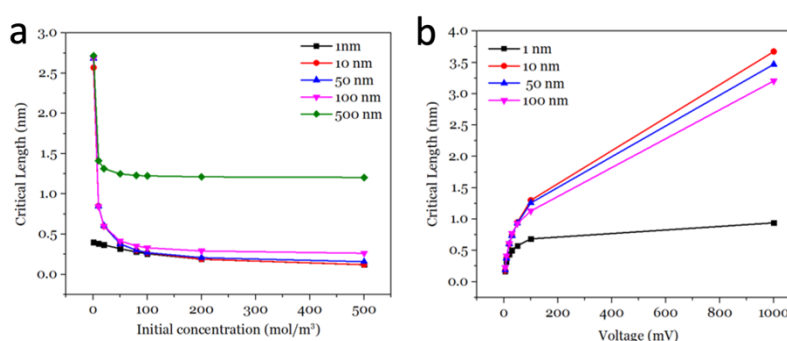


Figure 3. Length scale results from charge redistribution analysis of divalent cations in a fixed anionic matrix. (a) Initial concentration at different total lengths. (b) Voltage at different total lengths.

of mobile charges to accumulate at the interface. A subset of results is presented in Figure 3. We found that this mode of stiffness modulation is plausible for sub-100nm thick specimens, especially under bending modes. However, the methods used in this analysis assume no interactions among the ions, which is only appropriate for the low concentration limit. Moving

forward, we will use molecular dynamics simulations to investigate how these relations are affected at higher concentrations.

## **Future Plans**

Following on work from this past year, we will be completing the experimental study on tailoring PEC mechanical behavior, hydrophilicity, and propensity for self-healing. This will entail completing the thorough chemical and mechanical characterization of the hydroxyethyl acrylate, ethyl acrylate, and methoxyethyl acrylate PECs that is currently underway. The associated constitutive model will be revised and fit to the behavior of each of these materials. The model parameter dependence on material composition will help yield insight into how molecular design choices govern aspects of the bulk behavior.

Building from the PEC library, we will continue to work towards clear experimental demonstrations of electric field driven self-healing in both these bulk polymers and in versions for which each polyelectrolyte component is interpenetrated into a neutral gel matrix. This effort will be partially about experimental setup, partially about chemistry/labeling, and partially about solvent. In terms of solvent, our move this past year to a hydrophobic ionic copolymer will enable us to use organic solvents moving forward for the tests under electric fields. This will enable us to control polymer chain mobility while avoiding electrically driven water splitting and the environmental sensitivity characteristic of most hydrogels. In terms of chemistry/labeling, we will include acrylate dyes in the copolymer to better visualize where the anionic and cationic polymers are. Again, the move away from hydrogels will make these dyes more effective than in our previous attempt at using them because we will not have the same dramatic pH changes near the electrodes. In terms of experimental setup, we will be pursuing the non-blocking electrode / current driven approaches. Relatively short distances between the electrodes and a clear damaged interface are ideal for measurable healing, and the results be easily comparable with and without an applied field. Therefore, we will utilize a double cantilevered setup in the horizontal configuration of the testing setup, with compliant (carbon grease) electrodes on the upper and lower planes. A crack of set length will be introduced once the specimen is in place through a razor blade. Healing time and applied field will be controlled and then load-displacement to propagate the crack will be measured. In parallel with this experimental effort, we will be augmenting the constitutive model for PECs in the absence of electric field (described above), to include electric field effects. We expect this model to help in material and experimental design in subsequent years.

## **Publications**

1. Raiter P, Vidavsky Y, Silberstein MN. Can Polyelectrolyte Mechanical Properties Be Directly Modulated By an Electric Field? A Molecular Dynamics Study, *Adv Funct Matl*, 2020, 31, p.2006969

## **Biomimetic Strategies for Defect Annealing in Colloidal Crystallization**

**Michael J. Solomon and Sharon C. Glotzer, University of Michigan Ann Arbor**

### **Program Scope**

The purpose of this project is to discover fundamental principles that govern the control of defect kinetics and dynamics in colloidal crystals. Annealing is the chief method used to manipulate the defects and trapped states in a wide range of crystalline materials, yet current annealing methods are blunt tools that do not offer the level of control required to orchestrate defect correction with orientational, rotational, or spatial specificity. Inspired by the ways in which life identifies, controls, and corrects for defects during self-assembly, we will address: (1) how can fields be applied to anneal colloidal crystal structures with orientational specificity; (2) how can angularly oscillating and rotating applied fields couple to rotational degrees of freedom of anisotropic colloids to impact crystal quality; and (3) how can active particles function as local agents that interact directly with defects to anneal them. The ability to study these questions is supported by our recent research findings. We quantified the abundance and type of local defect structures in self-assembled colloidal crystals, thereby understanding how these two measures of crystal quality combined to determine the brilliance of structural color. We changed the shape and interactions of colloidal building blocks to understand how anisotropic colloidal properties affected the quality of crystals and their structural color. Finally, we incorporated reconfigurability into the self-assembly process to probe how kinetic pathways such as time-dependent cycling affected crystal quality.

### **Recent Progress**

We here report: (1) How adding particles of irregular size affects the crystallization and structural color of colloidal crystals; (2) How tuning the aspect ratio of colloidal discoids affects their structural color spectral response; (3) How characteristics of the annealing waveform influence the quality of colloidal crystals produced.

*Effect of particles of irregular size on the crystallization and structural color of colloidal crystals, as adapted from results reported in [1].* Structural color is most intense for highly uniform crystals; however, in practice colloidal crystals may include particles of irregular size, which can reduce the quality of the crystal. However, a quantitative relationship between particles of irregular size, crystal quality, and the resultant structural color response remains unclear. We quantitatively investigated the sensitivity of microstructural quality and structural color reflectivity of colloidal crystals to the size and volume of irregularly sized particles by experiment and simulation. When incorporated with 10 vol% of irregular particles, the structural color reflectivity of crystal films with large (small) irregular particles decreased by  $18.4\% \pm 5.6\%$  ( $27.5 \pm 5.8\%$ ), and surface crystal quality reduced by  $40.0 \pm 4.5\%$  ( $48.8 \pm 6.0\%$ ). By modeling colloidal films incorporated with irregular particles via molecular dynamics simulation and computing the reflection spectra of the modeled crystals via the finite-difference time-

domain method, we found that the peak reflectivity of the assembled structures increases monotonically with overall crystallinity, and that overall crystallinity is correlated with the volume fraction of incorporated irregular particles.

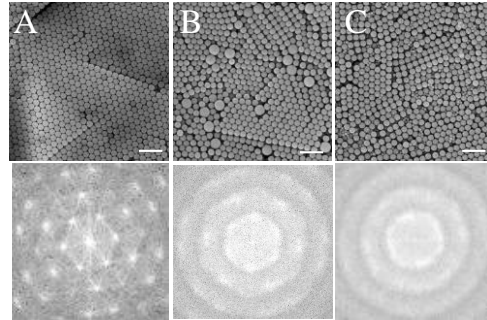


**Figure 1.** SEM (top) and FFT (bottom) images of assembled structures from (A) monosized 198 nm polystyrene (PS) spheres, (B) 198 nm PS spheres with 10 vol % of 88 nm PS spheres added, (C) 198 nm PS spheres with 10 vol % of 372 nm PS spheres added. The scale bars in SEM images are 1  $\mu\text{m}$ . Figure adapted from [1].

*Effect of aspect ratio on the structural color spectral response of colloidal discoid films, as adapted from results reported in [2].* We introduced shape anisotropy by synthesizing colloidal ellipsoids and characterized how the reflection peak intensity and spectral bandwidth of structural color could be engineered. The discoidal particles, which displayed homologous variation in shape and size, were self-assembled into thin films (thickness = 1.5  $\mu\text{m}$ ). We examined the effect of discoid aspect ratio and found that the structural color of the self-assembled films displayed a component due to diffuse backscattering and one due to multilayer reflection. As the discoids became more anisotropic, the reflection peak height became progressively smaller and the bandwidth broader (Figure 2).

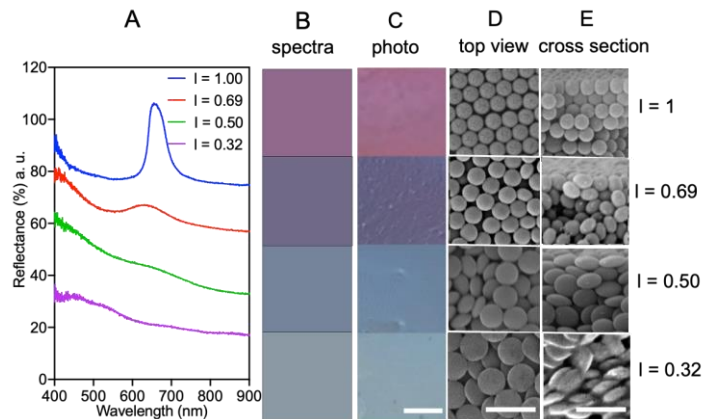


**Figure 2.** Effect of aspect ratio on structural color and microstructures, examined by reflection spectra, photographs, and SEM images. (A) Reflection spectra of the sphere crystal ( $l = 1$ ) and discoid films with an aspect ratio of 0.61, 0.42, or 0.27. The volume of particles with different aspect ratios is constant,  $0.012 \mu\text{m}^3$ , which corresponds to an initial sphere size of  $d = 286 \text{ nm}$ . (B) Colors derived from the measured reflection spectra in (A). (C) Images of the specimens under the D65 lamp illumination, scale bar is 1 mm. The top view (D) and cross section (E) SEM image of discoid films assembled from discoids with different aspect ratios. The scale bar is 1  $\mu\text{m}$ . Figure adapted from [2].

*Role of waveform in defect annealing, as adapted from results reported in [4].* We investigated the effects of reconfiguring external fields on the annealing of colloidal crystals (Figure 3). External field-assisted self-assembly is widely used to accelerate colloidal crystallization kinetics [3]. Yet, faster self-assembly kinetics can also bring about negative impacts on the quality of the crystal structures. These negative impacts can result from kinetic trapping of defects structures, vacancies, and grain boundaries. We showed that cyclically applied electric fields can produce high quality colloidal crystal monolayers by annealing local disorder (Figure 3a,b). We used confocal microscopy and small-angle light scattering (SALS) to characterize the short-range and long-range ordering of colloidal crystal monolayers produced from polystyrene latex particles of diameter  $4\ \mu\text{m}$  (Figure 3b,d). The off duration of the electric field was varied as a multiple of the melting time, while the on duration was held fixed. The optimal off time for annealing was discovered to be approximately one-half of the characteristic melting half lifetime for the equivalent system (Figure 3c). A local measure of the six-fold bond orientational order evolved more rapidly under the cyclic field than the kinetics of light diffraction, consistent with the idea that annealing of local disorder is a precondition for global annealing of the global microstructure (Figure 3e).

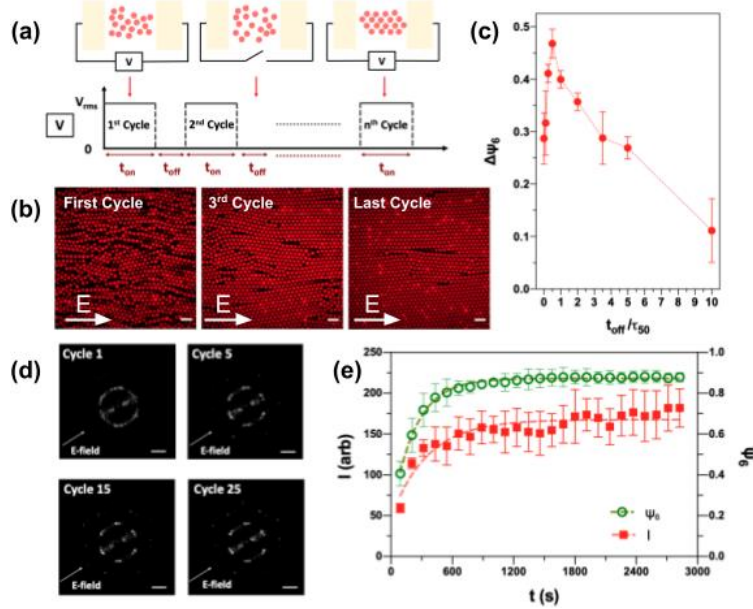


**Figure 3.** Time cycling of applied fields to improve crystal quality of self-assembled sphere crystals. (a) Cyclic toggling of applied field by modulating off-time. (b) CLSM characterization of evolution of crystal quality with cycling. The particles are  $4.0\ \mu\text{m}$  polystyrene spheres. The field strength is  $8.0\ \text{V}_{rms}$ ,  $5\text{MHz}$ . At optimal off times, the crystal ordering improves with annealing cycles. The direction of the electric field is shown in the figures. (c) Local ordering parameter calculated as the 6-fold bond orientational order,  $\psi_6$ , as a function of off-time. Optimal ordering is achieved when off time is equal to half of the crystal melting half-time under same field conditions. (d) Evolution of long-range order characterized by SALS diffraction pictographs. We observe sequential improvement in scattering peaks with annealing cycle consistent with the development of a single crystal lattice on the scale of the scattering volume. (e) Evolution of local order parameter and peak intensity of diffraction response with cycle time. The study shows that local ordering leads global annealing by about 50%. Figure adapted from [4].

## Future Plans

Our future plans will take us in three new directions. First, we will study the effect of electric fields applied to colloidal crystals to test how an aligning field generates an orientationally anisotropic distribution of defect annealing. Second, we will use multipolar-electrode devices to apply angularly oscillating electric fields to colloidal crystals composed of spheres, rods, or discs to couple an aligning field to rotational degrees of freedom for defect annealing. Third, active Janus particles, with non-equilibrium energies many times thermal energy, will be introduced into colloidal crystals and their interaction with defect structures evaluated.

## References

1. Liu, T., B. VanSaders, J.T. Keating, S.C. Glotzer, and M.J. Solomon, “Effect of Particles of Irregular Size on the Microstructure and Structural Color of Self-Assembled Colloidal Crystals,” submitted (2021).
2. Liu, T., T. Liu, F. Gao, S.C. Glotzer, and M.J. Solomon, “Structural Color Spectral Response of Dense Discoid Packings Generated by Evaporative Self-Assembly,” in preparation (2021).
3. Solomon, M.J., “Tools and Functions of Reconfigurable Colloidal Assembly,” *Langmuir* 34 11205-11219 (2018); DOI: 10.1021/acs.langmuir.7b03748.
4. Kao, P-K., B.J. VanSaders, S.C. Glotzer and M.J. Solomon, “Accelerated annealing of colloidal crystal monolayers by means of cyclically applied electric fields,” *Scientific Reports* **11** 11042 (2021). DOI: 10.1038/s41598-021-90310-7

### **Publications supported by BES in last two years**

1. Liu, T., B. VanSaders, J.T. Keating, S.C. Glotzer, and M.J. Solomon, “Effect of Particles of Irregular Size on the Microstructure and Structural Color of Self-Assembled Colloidal Crystals,” submitted (2021).
2. Kao, P-K., B.J. VanSaders, S.C. Glotzer and M.J. Solomon, “Accelerated annealing of colloidal crystal monolayers by means of cyclically applied electric fields,” *Scientific Reports* **11** 11042 (2021). DOI: 10.1038/s41598-021-90310-7
3. Liu, T., B. VanSaders, S.C. Glotzer, and M.J. Solomon, “Effect of Defective Microstructure and Film Thickness on the Reflective Structural Color of Self-Assembled Colloidal Crystals,” *ACS Applied Materials and Interfaces* **12** 8 9842-9850 (2020). DOI: 10.1021/acsami.9b22913.
4. Kao, P-K. B.J VanSaders, M.D. Durkin, S.C Glotzer and M.J. Solomon, “Anisotropy Effects on The Kinetics of Colloidal Crystallization and Melting: Comparison of Spheres and Ellipsoids,” *Soft Matter* **15**, 7479 – 7489 (2019). DOI: 10.1039/C9SM00887J

# Materials Exhibiting Biomimetic Carbon Fixation and Self Repair: Theory and Experiment

Michael S. Strano, Carbon P. Dubbs Professor of Chemical Engineering

Department of Chemical Engineering, Massachusetts Institute of Technology

## Program Scope

The United States alone generates 35.4 million tons of plastic, mostly petroleum derived, with 26.8 million tons ending up in landfills<sup>[1]</sup>. Along with this material waste, between 8 to 10% of the energy annually consumed to produce these materials is thrown away. The programmatic vision of this MIT project is to remake plastics and materials such that they could continuously absorb atmospheric carbon dioxide (CO<sub>2</sub>) and scavenge energy from the environment to renew and self-regenerate. The use of carbon dioxide and energy sources such as solar fluence model such materials after natural mechanisms operative in the trunk of a tree or leaf of a plant. Materials tend to fail though the propagation of microcracks and relatively small defects that accumulate over time. The amount of mass and energy needed to prevent such failure and avoid the landfill is small, meaning that growth rates of such Carbon Fixing Materials (CFMs) can be commensurate with living plants. This Department of Energy sponsored program has enabled our laboratory at MIT to study and develop mechanisms of self-assembly and self-repair similar to living plant systems to create human-synthesized analogs that benefit from these higher functions operating under non-biological conditions. In this presentation, we highlight our efforts towards engineering such CFMs. These are a novel class of biomimetic materials that exploit ambient solar energy harvesting and carbon dioxide conversion to interior monomers that regenerate and repair the material. Our work develops the chemical, mathematical and material science basis for realizing such CFMs. Overall, the establishment of CFMs will benefit many economic sectors such as transportation and construction while reducing waste streams worldwide.

## Recent Progress

We have utilized extracted plant chloroplasts as unique photocatalysts that react with atmospheric carbon dioxide using ambient solar energy to produce sugars such as glucose<sup>[2]</sup>. Within the material prototype, glucose oxidase converts this produce to the reactive gluconolactone which subsequently reacts with a primary amine-functionalized acrylamide monomer to form a continuously extending polymer matrix. The rheology and mechanical properties evolve over time, and the material grows measurably over a 24-hour period to produce a polymer matrix that can be augmented with nanoparticle inclusions such as graphene oxide to enhance its mechanical properties. This study establishes that *carbon fixing materials* are possible and possess desirable materials science properties.

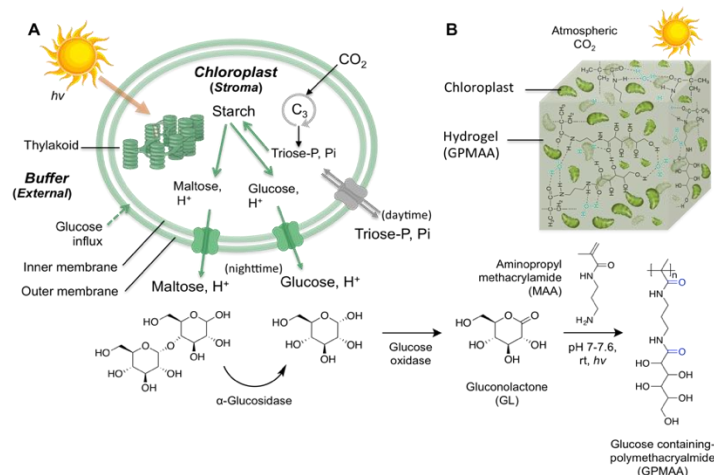


**Figure 1. Schematic illustration of System II.** (A) Chloroplasts transform solar energy and carbon dioxide into the chemical energy and export the newly fixed carbon in form of triose phosphate during the day. Alternatively, chloroplasts export maltose and glucose resulting from the breakdown of starch through the translocators at night. Exported glucose and glucose from enzymatic hydrolysis of maltose are converted to gluconolactone (GL) by glucose oxidase, subsequently react to primary amine functionalized methacrylamide (MAA) and polymerize to glucose-containing polymethacrylamide (GPMAA) in the medium. (B) GPMAA forms hydrogel as lightly cross-linked by hydrogen bonding in water. The hydrogel continuously grows, densifies and self-repairs as long as chloroplasts carry out carbon fixation and export glucose.

Further, we have also completed a reaction engineering analysis of carbon fixing materials to understand the maximum limits of growth from CO<sub>2</sub> absorption or conversion, conversion selectivity, and polymer growth, hence organizing the chemical kinetic literature<sup>[3]</sup>. By performing a Damköhler analysis, we derive criteria for the cross over from the regime of kinetic limitations (CO<sub>2</sub> conversion or polymerization) to mass transfer limited growth (CO<sub>2</sub> absorption)—defining the upper limits on growth rate of this new class of materials. This framework allows us to rapidly analyze any combination of absorbent, CO<sub>2</sub> reduction photocatalyst, and polymerization chemistry to understand optimal material growth rates as well as the inherent limitations within the potential *carbon fixing material* system.

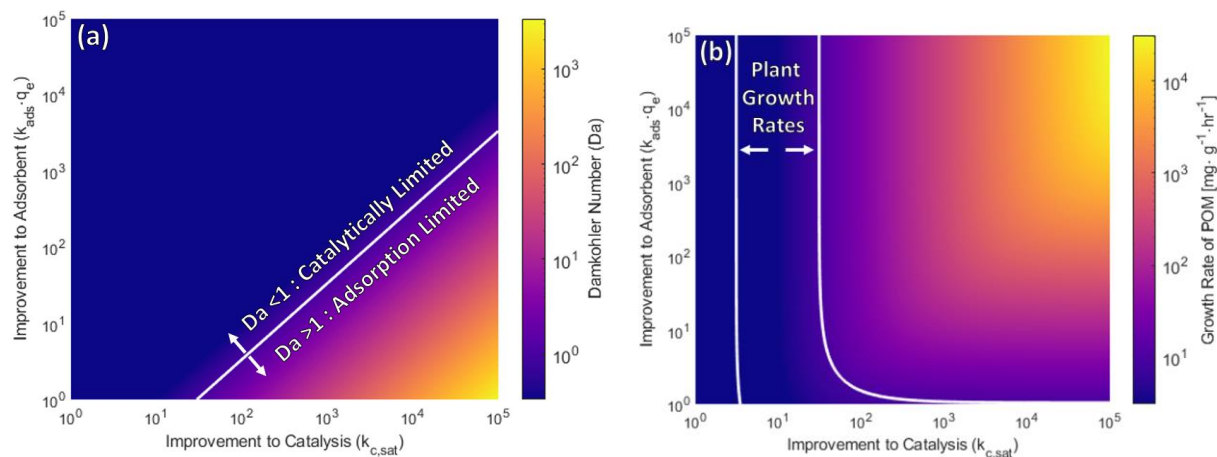


**Figure 2.** (a) Damköhler number of Carbon Fixing Material incorporating improved  $\text{CO}_2$  adsorbents and photocatalysts. Where Damköhler number is unity (white curve), represents when an equivalent improvement to either the photocatalyst ( $k_{c,sat}$ ) or adsorbent ( $k_{ads} \cdot q_e$ ) result in the same relative improvement to system growth rate. (b) Overall growth rate of Carbon Fixing Material incorporating improved  $\text{CO}_2$  adsorbents and photocatalysts. The white lines present the bounds of plant-like growth rate. Comparison is made to the relative growth rates of natural plant systems bracketed by the bounds as white curves at  $1$  and  $10 \text{ mg g}^{-1} \text{ hr}^{-1}$ . The lower left-hand corner of each section of this figure represents the values for the case study presented in this work, with no improvements to catalyst or adsorbent.

Through this framework, we have identified formaldehyde as an intermediate monomer from direct  $\text{CO}_2$  photocatalytic reduction under ambient conditions. Formaldehyde is capable of homopolymerization and copolymerization with co-monomers such as melamine or phenol to give a variety of thermoplastic and thermosetting material systems. Formaldehyde is however often relegated as an undesirable side product during the photocatalytic reduction of  $\text{CO}_2$ , where methane and methanol are generally desired as high energy density fuels and or chemical precursors. As such, it is the subject of scant investigation, especially under the reaction conditions appropriate for carbon fixing materials, low partial pressure  $\text{CO}_2$  and room temperature. As such, formaldehyde is often left unquantified—due in part to the difficulty of quantification (traditional gas-chromatography with flame ionization detection is insensitive) and the challenge of separating both gas and liquid phase products. To address the lack of knowledge about selective photocatalytic formaldehyde production, we have developed a high throughput catalytic screening and characterization infrastructure capable of complete analysis of C1 product analysis from photocatalytic carbon dioxide reduction, including both gaseous and liquid products.

We have made significant progress in making hybrid particulate photo-electro-catalytic platforms that leverage and combine ambient solar energy harvesting with energy derived from a newly discovered solvent-nanomaterial electrical coupling developed in our laboratory for CFMs.<sup>[4]</sup> These platforms can combine the semiconducting photocatalyst with a carbon Janus particle capable of electrochemical augmentation through a process of Asymmetric Chemical Doping (ACD). Here, we can augment the pure photocatalytic transformation using the solvent-derived electrical potential generated from ACD, establishing a hybrid process still untethered to external electrical inputs but potentially with much higher reactivity. Asymmetric Chemical Doping (ACD) utilizes a chemical potential gradient across a single-walled carbon nanotube network (SWNT),

established via solvent molecular doping (e.g., CH<sub>3</sub>CN or H<sub>2</sub>O), as means of electricity generation. In this process, the broken spatial symmetry in the Fermi levels of electrical carriers inside the SWNT network translates directly into a voltage potential. By coupling semiconductor photocatalyst with engineered SWNT particles capable of generating electron flow through the ACD process, we can overcome the hindered and low-rate electron transfer to CO<sub>2</sub>. With the photocatalyst-SWNT interface properly tuned, this hybrid system can create a high-rate electron transfer pathway to CO<sub>2</sub> molecules, thereby improving CO<sub>2</sub> reduction kinetics. Moreover, interfacing the photocatalysts with ACD-enabled SWNT particles creates additional active catalytic sites that allow us to alter or more precisely control the reaction pathways, and hence increase the selectivity of some products over the others.

## Future Plans

**Selective and High-Yield Photocatalytic Production of CO<sub>2</sub>-derived Monomers:** We are currently exploring a series of noble metal-free alkali-ion intercalated tungsten oxide, M<sub>0.33</sub>WO<sub>3</sub>, as an efficient CO<sub>2</sub> reduction photocatalyst effective directly from air at atmospheric pressure. Tungsten oxide is a well-known semiconductor material utilize for catalytic applications of this type. The Z-scheme strategy can be used for two materials that do not satisfy the redox potential requirements for an CO<sub>2</sub> photoreduction reaction individually, but can perform reduction or oxidation half reactions<sup>[5]</sup>. By using the Z-scheme strategy, photogenerated electrons in one material flows to the holes from the other material and overall catalyze the corresponding reduction and oxidation half reactions. We are leveraging several advances in 2-dimensional (2D) materials, particularly graphene and hBN, with variable bandgaps that differ from their bulk counterparts and hence the potential for tuning the efficiency of the CO<sub>2</sub> photoreduction activity. 2D materials can be easily surface decorated with nanoparticles to enable the desired reaction, and these surface modifications can be used to design efficient catalysts and select reaction products.

In parallel, we are also synthesizing and studying bio-inorganic hybrids for efficient CO<sub>2</sub> reduction and polymerization, combining the most promising aspects of these systems. As an example, electron transfer to CO<sub>2</sub> and formate, the primary bottleneck in inorganic photocatalytic reduction of CO<sub>2</sub>, can be improved by interfacing formate and formaldehyde dehydrogenase with inorganic semiconductor photocatalysts. This cascade of enzymatic reactions on an inorganic semiconductor will improve the formaldehyde production rate and yield.

**Plant-Based Composites and System with Hyper-Stable Isolated Chloroplasts using Nanobionics:** Isolated chloroplasts outside of plant cells have limited photoactive lifetimes of less than a day for photoactivity, and only a few hours for sugar export. In this sub-aim, we are fabricating materials where chloroplasts can be encapsulated in a hydrogel matrix as a 3-dimensional scaffold topography. We will explore a variety of polymer gel matrices building on the previous hydrogel GPMAA chemistry and construct nanoparticle embedded platforms to improve CO<sub>2</sub> fixation to polymers. We also intend to investigate various nanocarriers and nanoparticles to achieve enhanced chloroplast function. For example, previous nanobionic engineering from our lab resulted in three times higher photosynthetic activity and increased maximum electron transport rates in chloroplasts as well as hyperstable chloroplasts using nanoceria to scavenge reactive oxygen species generated inside chloroplasts<sup>[2]</sup>.

## References

- [1] Okan, M.; Aydin, H. M.; Barsbay, M. Current Approaches to Waste Polymer Utilization and Minimization: A Review. *J. Chem. Technol. Biotechnol.* **2019**, *94* (1), 8–21.
- [2] Kwak, S. Y.; Giraldo, J. P.; Lew, T. T. S.; Wong, M. H.; Liu, P.; Yang, Y. J.; Koman, V. B.; McGee, M. K.; Olsen, B. D.; Strano, M. S. Polymethacrylamide and Carbon Composites That Grow, Strengthen, and Self-Repair Using Ambient Carbon Dioxide Fixation. *Adv. Mater.* **2018**, *30* (46), 1–10.
- [3] D. Parviz, D.J. Lundberg, S.Y. Kwak, H. Kim, M. Strano, A Mathematical Analysis of Carbon Fixing Materials that Grow, Reinforce, and Self-Heal from Atmospheric Carbon Dioxide, *Green Chem.* **2021**
- [4] A. Liu, Y. Kunai, A. Cottrill, A. Kaplan, G. Zhang, H. Kim, R. Mollah, Y. Eatmon, M. Strano, Solvent-induced electrochemistry at an electrically asymmetric carbon Janus particle, *Nature Comm.* **2021**
- [5] Low, J.; Jiang, C.; Cheng, B.; Wageh, S.; Al-Ghamdi, A. A.; Yu, J. A Review of Direct Z-Scheme Photocatalysts. *Small Methods* **2017**, *1* (5), 1700080.

## Publications

- 1- A Mathematical Analysis of Carbon Fixing Materials that Grow, Reinforce, and Self-Heal from Atmospheric Carbon Dioxide, 10.1039/D1GC00965F
- 2- Liquids with Lower Wettability Can Exhibit Higher Friction on Hexagonal Boron Nitride: The Intriguing Role of Solid–Liquid Electrostatic Interactions, 10.1021/acs.nanolett.8b04335
- 3- Addressing the isomer cataloguing problem for nanopores in two-dimensional materials, 10.1038/s41563-018-0258-3
- 4- Solvent-induced electrochemistry at an electrically asymmetric carbon Janus particle, 10.1038/s41467-021023038-7

## Supramolecular Dynamics in Self-Assembling Materials

### Principal Investigator: Samuel I. Stupp, Northwestern University

Board of Trustees Professor of Materials Science & Engineering, Chemistry, Medicine, and Biomedical Engineering

Director, Center for Bio-Inspired Energy Sciences (CBES)

Director, Simpson Querrey Institute for BioNanotechnology

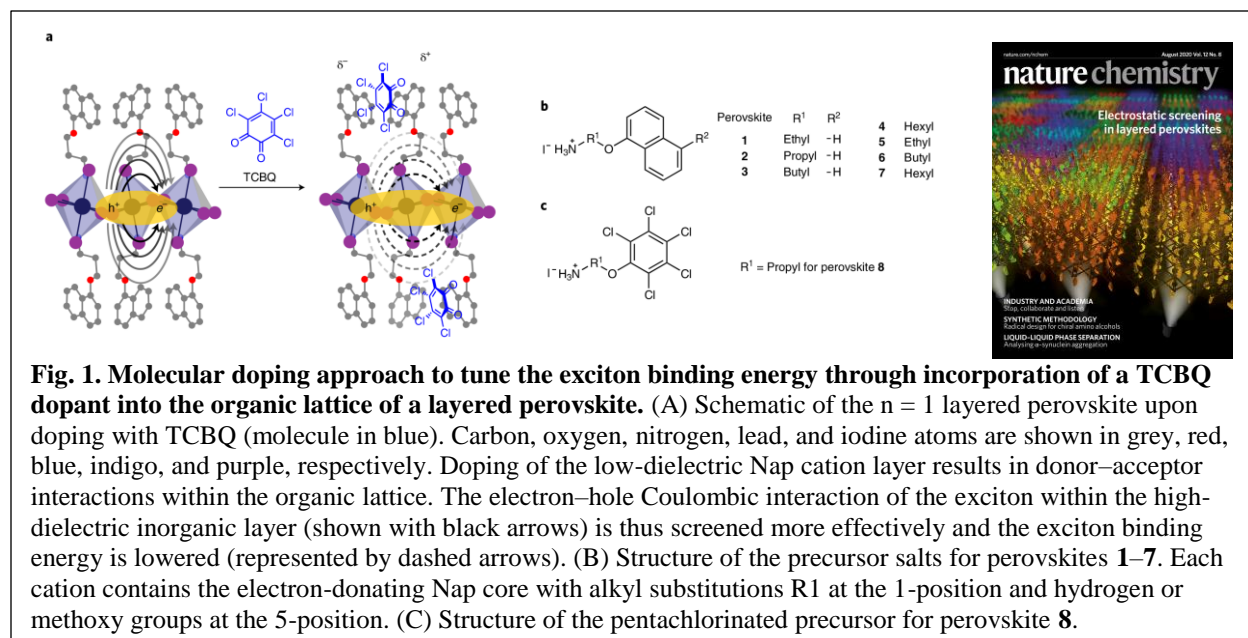
### Program Scope

Our previous research supported by the DOE Biomolecular Materials program uncovered for us the existence of complex exchange dynamics among biomolecular supramolecular assemblies based on peptides and oligonucleotides in which strong interactions can occur among components. The structural diversity that could be accessed through dynamic processes in these systems would not be possible when interactions among molecules are weak and systems exchange rapidly to reach equilibrium. That research also unexpectedly revealed that well-defined structures can emerge through dynamic exchange when two separate supramolecular assemblies contain components that interact strongly. We hypothesize that exchange dynamics among separate assemblies, each containing molecular components designed to interact strongly, is a possible pathway to discover new materials, particularly hierarchical superstructures similar to those found in biological systems. Thus, our objective is to explore the development of a strategy we describe here as “bonding-directed dynamics” as a tool to search for novel functions in supramolecular materials. The non-covalent strong bonds among molecular components could be broken and re-formed, thus implying that we could form the structures reversibly and change their functions reversibly while guiding their dynamic exchange. The targeted functions in our current program involve emergent mechanical properties in superstructures, charge transport, ferroelectricity, and catalytic activity. The interactions chosen to explore these dynamic phenomena in supramolecular materials include hydrogen bonding and electrostatic interactions among peptides, and charge transfer interactions.

### Recent Progress

#### *Donor-Acceptor Interactions in Two-Dimensional Hybrid Layered Perovskites*

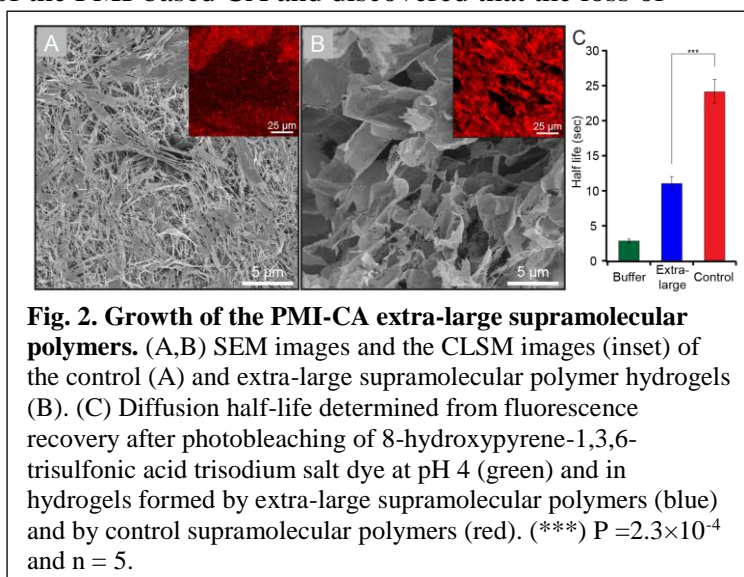
We recently published a paper in *Nature Chemistry* with the group of Prof. William Tisdale at MIT on the use of donor-acceptor interactions to tune the structural and excitonic properties of 2D perovskites (featured on the cover, shown below).<sup>1</sup> Donor-acceptor interactions are under investigation now in our program to study bonding-directed dynamics. In particular, the Biomolecular Materials program supported the synthesis of a series of seven functionalized naphthalenes as organic ammonium components (donors) for the synthesis of lead iodide perovskites (Fig. 1). By doping the systems with tetrachloro-1,2-benzoquinone (TCBQ) as an acceptor, we found that we could increase the electrostatic screening of the exciton and lower the binding energy. Interestingly, differences in the crystal packing of the organic component in the undoped perovskites determined the extent of incorporation of the acceptor and consequently the binding energy and the overall optoelectronic properties. It is possible that in future experiments



these systems could benefit from bonding-directed dynamics to create specific superstructures in the organic layers of hybrid perovskites as a handle for novel properties.

### *Growth of Extra-Large Chromophore Supramolecular Polymers for Enhanced Hydrogen Production*

In a paper very recently published in *Nano Letters*, we focused on the supramolecular polymerization pathways for perylene monoimide (PMI)-based chromophore amphiphiles (CAs).<sup>2</sup> Previous studies in our laboratory, initiated at the former Argonne-Northwestern EFRC on Solar Energy (ANSER) have established the photocatalytic proton reduction functions of these CA supramolecular assemblies, but the dynamic formation and growth pathways of these systems were unexplored. In working toward our proposed goal of uncovering the exchange dynamics of these assemblies for functional materials synthesis, we performed detailed *in-situ* investigations on thermal annealing of the PMI-based CA and discovered that the loss of crystallinity at elevated temperatures facilitate Ostwald ripening, which then recrystallizes into extra-large supramolecular polymers upon cooling while retaining the unimolecular thickness. The resulting material was found to be highly porogenic compared to the smaller supramolecular polymers, revealed by scanning electron microscopy (Fig. 2A), and led to greater diffusion as shown by fluorescence recovery after photobleaching studies (Fig. 2B).

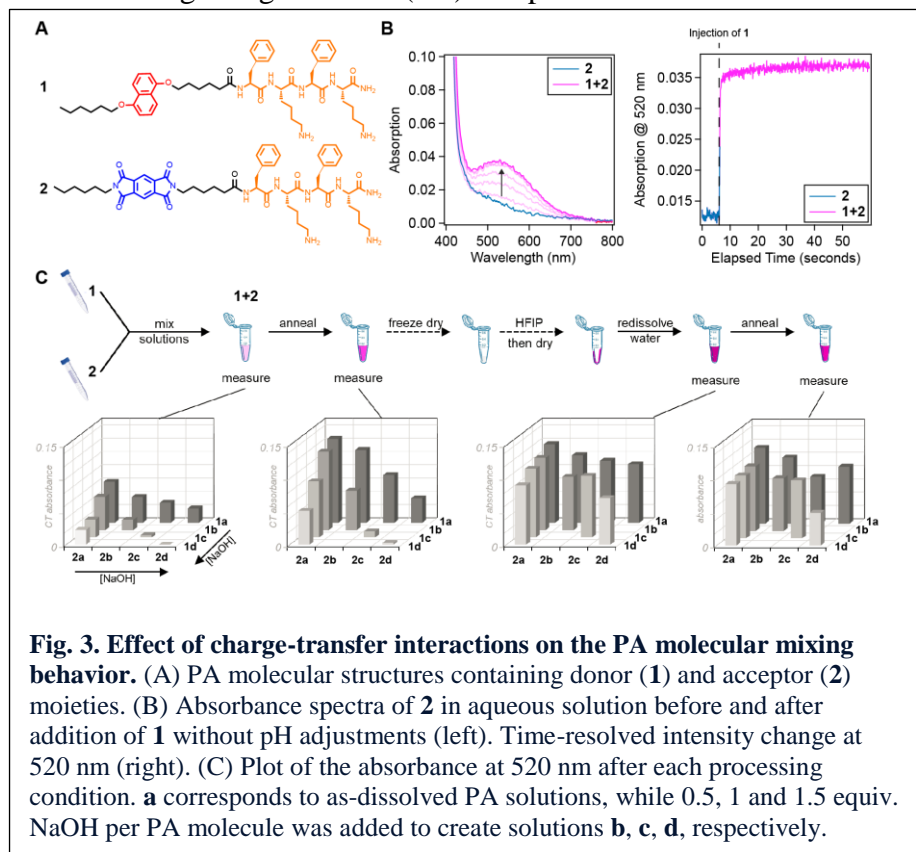


## Dynamic Supramolecular Self-Assembly

During this funding period, we have also explored the exchange kinetics of self-assembling peptide amphiphiles (PAs) under different solution conditions in the absence of attractive enthalpic interactions by conducting time-resolved isotope-edited Fourier-transform infrared (FTIR) spectroscopy experiments. Here we used a PA with the sequence palmitoyl-VV\*VAAEEEE-CONH<sub>2</sub> molecule, in which the carbonyl of the second valine residue was isotopically labeled with carbon-13. The native and labeled molecules were mixed in 1,1,1,3,3,3-hexafluoroisopropanol (HFIP) to completely dissolve the components at varying ratios. The HFIP solution was dissolved and the solid was redissolved in water and thermally annealed. Using FTIR spectroscopy, we observed a linear relationship between the absorption intensity of the peak positions for the <sup>13</sup>C=O stretch and the composition under the uniformly mixed conditions. The exchange kinetics were tracked by preparing solutions of the native and labeled molecules separately in water, then mixing the aqueous solutions in a 1:1 ratio and thermally annealing while aliquoting for FTIR analysis. We found that even at high pH, where increased electrostatic repulsion among carboxylate groups on glutamic acid side chains weakens the intermolecular  $\beta$ -sheet hydrogen bonding, the position of the <sup>13</sup>C=O stretch peak did not shift significantly over the course of several hours at 80°C. This result suggests that an additional cohesive force between the mixing pair of PAs is crucial for driving molecular rearrangement within the nanofibers.

We have also synthesized and performed preliminary exchange kinetics experiments with a series of peptide amphiphiles containing charge transfer (CT) complex moieties in the

hydrophobic core of the nanofibers (Fig. 3A) to understand how the enthalpic driving force of the CT interactions accelerate the molecular level mixing. Standard Fmoc solid-phase peptide synthesis and purification with preparative HPLC afforded both molecules with amine groups of the lysine protonated as the trifluoroacetate salt. We would therefore expect these PA molecules to be charged fully (+2 per molecule) upon dissolution in water.



Upon addition of the donor PA (1) solution to the acceptor PA (2) solution without pH adjustment, we immediately observed the appearance of an absorption peak corresponding to the formation of the CT complex (Fig. 3B), indicating the fast molecular level mixing of the two PAs. When the pH of the solution was increased to reduce the net positive charges on the PA headgroups and strengthen the cohesive hydrogen bonding within the PA nanofibers, the degree of molecular mixing upon simple solution addition gradually decreased, and this trend continued even with thermal annealing (Fig. 3C, left two panels). Only by first dissolving the mixture in HFIP did the CT complex absorption peak become visible in the highest pH samples (Fig. 3C, right two panels). Together with the isotope-edited FTIR method described above, this result shows that there are two steps associated with molecular exchange in supramolecular assemblies: one in which the molecules exchange between the supramolecular fibers and the other in which the molecules translate and rearrange within the supramolecular polymer. The interfiber exchange appears to be facilitated by the existence of micellar or other small, exchange-active species that allow for dissociation from and association to the supramolecular assemblies. The molecular exchange within the fiber is mediated by specific attractive interactions such as CT complexation.

## Future Plans

During the next reporting period, we will continue to explore the use of donor-acceptor interactions to create dynamic materials. In particular, we will further characterize the charge transfer system with the carbon-13 isotope-edited FTIR technique. We hypothesize that the introduction of two competing strong supramolecular attractive interactions such as peptide hydrogen bonding and CT interactions would lead to tunable exchange kinetics through subtle environmental parameter changes such as elevated temperatures or salt addition. We are also exploring how the intermolecular dynamics can be used to control the reversible formation of superstructures of the nanofibers and explore their mechanical behavior. Finally, we will also apply our new understanding of molecular dynamics in these systems to design supramolecular catalysts that mimic enzymatic active sites like chymotrypsin.

## References

1. Passarelli, J. V.; Mauck, C. M.; Winslow, S. W.; Perkinson, C. F.; Bard, J. C.; Sai, H.; Williams, K. W.; Narayanan, A.; Fairfield, D.J.; Hendricks, M. P.; Tisdale, W. A.; Stupp, S. I. "Tunable Exciton Binding Energy in Two-Dimensional Hybrid Layered Perovskites Through Organic-Layer Donor-Acceptor Interactions" *Nature Chemistry* **2020**, 12, 672.
2. Dannenhoffer, A. J.; Sai, H.; Harutyunyan, B.; Narayanan, A.; Powers-Riggs, N. E.; Edelbrock, A. N.; Passarelli, J. V.; Weigand, S. J.; Wasielewski, M. R.; Bedzyk, M. J.; Palmer, L. C.; Stupp, S. I. "Growth of Extra-Large Chromophore Supramolecular Polymers for Enhanced Hydrogen Production" *Nano Letters* **2021**, 21, 3745.

**Publications resulting from work supported by the DOE grant over the previous two years.**

Dannenhoffer, A.; Sai, H.; Huang, D.; Nagasing, B.; Harutyunyan, B.; Fairfield, D. J.; Aytun, T.; Chin, S. M.; Bedzyk, M. J.; Olvera de la Cruz, M.; Stupp, S. I. "Impact of Charge Switching Stimuli on Supramolecular Perylene Monoimide Assemblies" *Chemical Science* **2019**, 10(22), 5779-5786.

Fairfield, D.; Sai, H.; Narayanan, A.; Passarelli, J.; Chen, M.; Palasz, J.; Palmer, L.; Wasielewski, M.; Stupp, S. I. "Structure and Chemical Stability in Perovskite-Polymer Hybrid Photovoltaic Materials" *Journal of Materials Chemistry A* **2019**, 7(4), 1687-1699.

Clemons, T. D. and Stupp, S. I. "Design of Materials with Supramolecular Polymers" *Progress in Polymer Science* **2020**, 111, 101310.

Passarelli, J. V.; Mauck, C. M.; Winslow, S. W.; Perkinson, C. F.; Bard, J. C.; Sai, H.; Williams, K. W.; Narayanan, A.; Fairfield, D.J.; Hendricks, M. P.; Tisdale, W. A.; Stupp, S. I. "Tunable Exciton Binding Energy in Two-Dimensional Hybrid Layered Perovskites Through Organic-Layer Donor-Acceptor Interactions" *Nature Chemistry* **2020**, 12, 672-682.

Dumele, O.; Chen, J.; Passarelli, J. V.; Stupp, S. I. "Supramolecular Energy Materials" *Advanced Materials* **2020**, 32(17), 1907247.

Stupp, S. I.; Clemons, T. D.; Carrow, J K.; Sai, H.; Palmer, L. C. "Supramolecular and Hybrid Bonding Polymers" *Israel Journal of Chemistry* **2020**, 60(1-2), 124-131.

## Protein Self-Assembly by Rational Chemical Design

F. Akif Tezcan, University of California, San Diego

### A) Program Scope

Our research aims to develop design strategies to control protein self-assembly and to construct protein-based materials with emergent properties. To circumvent the challenge of designing extensive non-covalent interfaces for controlling protein self-assembly, we have endeavored to develop a chemical bonding toolkit (metal coordination, disulfide linkages, computationally prescribed non-covalent bonds, etc.) to mediate protein-protein interactions. This toolkit has been further supplemented by synthetic molecules, DNA and polymer frameworks to guide the structures and dynamics of protein assemblies. The initial focus of our DOE-funded program was to establish design strategies for obtaining desired structures such as discrete (*i.e.*, finite) or 0, 1, 2 and 3D (*i.e.*, extended) protein assemblies with crystalline order. While we still pursue such methodology development, our efforts now also focus on a) designing functional, dynamic, and reconfigurable protein architectures, b) constructing composite protein-inorganic-organic materials with new functional/physical properties, and c) developing an experimental/computational/theoretical framework to obtain structure-property relationships in these materials.

### B) Recent Progress

Adaptive 3D Protein Crystals with Integrated Polymer Networks: Natural protein assemblies like viruses, microtubules, and collagen superstructures have remarkable mechanical attributes yet to be matched by rational design. Ultimately, the functions of many protein assemblies and protein-based materials depend largely on their ability to interface with other biological or abiological components to form hierarchical systems. Such hierarchical assembly not only leads to emergent properties that arise from combining multiple components (*e.g.*, flexibility/responsiveness, simultaneous strength and toughness, self-healing) but also augments the individual properties (*e.g.*, catalysis, stability) of the components themselves. With these advantages in mind, we recently developed a new class of protein-based materials, termed polymer-integrated protein crystals (PIX), using the cage-like, 24meric protein human heavy chain ferritin (HuHF) as a building block (Zhang et al., *Nature*, 557, 86, 2018). HuHF was chosen due to its well-understood structural/biochemical properties and its octahedral symmetry which enables its metal-directed assembly into mesoporous lattices. We exploited the mesoporosity of the HuHF crystals to thoroughly infuse them with acrylate/acrylamide, which were then polymerized *in crystallo* to form a hydrogel network that intimately bonded to underlying HuHF lattice through non-covalent interactions. The resulting HuHF-PIX possessed several unprecedented properties

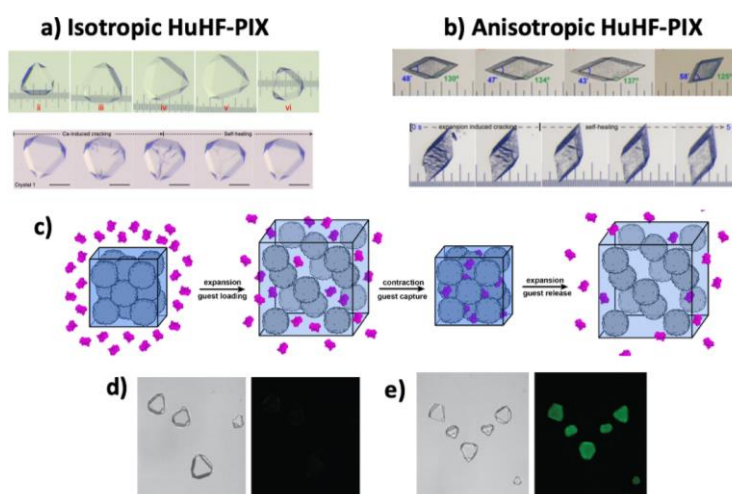


**Figure 1.** (a, b) Reversible expansion/contraction (top) and self-healing (bottom) behavior of isotropic/*fcc* (a) and anisotropic/rhombohedral (b) HuHF-PIX. (c) Cartoon illustration for the uptake/release of large macromolecular guest molecules in PIX. (d, e) Confocal micrographs (bright-field and fluorescence) of HuHF-PIX soaked in GFP solution (d) without expansion and (e) after expansion and contraction.

(Figures 1a and 1b): a) volumetric expansion by >500% while retaining crystalline periodicity, b) reversible contraction back to their original state to fully regain atomic-level periodicity, c) highly efficient self-healing behavior, and d) isotropic or anisotropic motion, dictated by the inherent symmetry of the HuHF lattices (Pub 6).

Given that HuHF-PIX can undergo large changes in unit cell dimensions without losing crystallinity (unlike typical 3D crystals), we envisioned that a) they could be leveraged for the controlled capture and release of large biomolecules (Figure 1c), and b) the polymer network and surfaces of the HuHF components of the lattice could provide a distinct chemical environment for controlling the physical and functional properties of guest biomolecules. The 2-nm wide channels of HuHF set an upper size limit for the molecular cargo that can passively penetrate the lattice. Indeed, when native HuHF crystals or unexpanded HuHF-PIX were incubated in solutions of GFP (2.4 x 4.2 nm), cytochrome *c* (cyt *c*, 2.5 x 2.5 nm) or lysozyme (lysozyme, 2.8 x 2.8 nm), we observed little to no penetration of these proteins into the lattice by confocal microscopy (Figure 1d). In contrast, when HuHF-PIX were expanded in low-ionic strength solutions containing these guest proteins and then contracted through salt addition, we observed a thorough encapsulation of these proteins into the HuHF-PIX (Figure 1e). These experiments demonstrated that PIX could uptake larger cargo than their original exclusion limits, enabled by their ability to reversibly expand and contract.

The cellular functions of natural proteins and protein assemblies, including those involved in storage and delivery, are predicated upon reversible interactions with their biological guests. Thus, we investigated whether the protein uptake by HuHF-PIX was reversible and could be controlled by external stimuli. Given our hypothesis that positively charged cyt *c* and lysozyme interact with the negatively charged HuHF-PIX matrix primarily through electrostatic interactions, we surmised that their uptake/release could be controlled by changes in ionic strength or pH. Indeed, upon increasing the solution ionic strength to  $\mu > 500$  mM or lowering the pH to  $< 4$ , r-lysozyme and cyt *c* were released from PIX in less than 1 min. The PIX could be reloaded within tens of seconds to a few minutes upon transfer into a low-ionic strength or pH  $> 6$  solution containing the guest proteins (Figure 2). We did not observe any deterioration of the crystalline PIX morphology over several uptake/release cycles, indicating the robustness of HuHF-PIX as a recyclable uptake and release system.

The interstitial spaces in HuHF-PIX provide an environment that is a) spatially constrained, yet somewhat flexible (due to the elasticity of PIX) and accessible to the external environment through the porosity of the lattice, and b) surrounded by the diverse chemical functionalities of the polymer chains and ferritin surfaces. The combination of these features distinguishes the guest@HuHF-PIX platforms from other systems such as cage-encapsulated or protein-lattice immobilized enzymes. Our preliminary studies showed that cyt *c*@PIX systems were highly catalytically active and protected from digestion by proteolytic enzymes, thus setting the stage for future investigations of enzyme@HuHF-PIX systems as dynamic crystalline platforms for biocatalysis and controlled delivery.

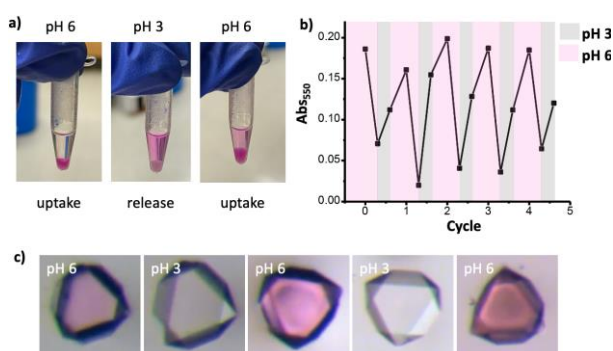


**Figure 2.** (a, b) pH-dependent, reversible uptake and release of rhodamine-labeled lysozyme by HuHF-PIX, as monitored by bulk or (c) single-crystal measurements.

**Functional, Porous Protein-Organic Frameworks:** The construction of protein-based assemblies with desired physical and mechanical properties hinges critically on the ability to tailor the interactions between protein building blocks. However, it is difficult to predict how intermolecular interactions at the Å-to-nm scale influence collective properties at the bulk scale and to manipulate these interactions accordingly. Thus, there is a need for modular design platforms that systematically alter interprotein interactions, providing access to libraries of ordered, yet dynamic structures for materials discovery. To this end, we had previously developed protein-metal-organic frameworks (protein-MOFs), in which HuHF molecules were engineered with metal coordination motifs in their  $C_3$  symmetric vertices such that they could assemble into 3D lattices upon binding ditopic linkers bearing hydroxamate functional groups (Sontz et al., *J. Am. Chem. Soc.* 137, 11598, 2015; Bailey et al., *J. Am. Chem. Soc.* 139, 8160, 2017). The structures and symmetries of the resulting protein-metal-organic frameworks (protein-MOFs) could then be controlled in a modular fashion by changing the length and geometry of the di-hydroxamate linkers as well as the coordination preferences of the metal ions anchored in the  $C_3$  symmetric vertices. In our systematic study of a library of >20 body-centered cubic and body-centered tetragonal HuHF-MOFs, we discovered that the thermodynamic stabilities of these crystalline materials could be dramatically altered simply through the isostructural replacement of the metal ions. Most notably, we discovered that a HuHF-MOF (Ni-fdh-<sup>H122f</sup>ferritin) underwent a highly cooperative, reversible, isotropic lattice contraction near room temperature (Pub 5). The abruptness of this transition and hysteretic behavior were consistent with a first-order phase transition, enabled by the flexible interactions between  $Ni^{2+}$  ions and the dihydroxamate linkers that held the protein-MOF lattice together. This example highlighted the benefits of modular design strategies in the discovery of novel material properties that are not predictable from first principles and thus lie beyond the current reach of *de novo* design. It also illustrated the emergent properties that arise from combining chemically/structurally disparate components.

While synthesizing ditopic hydroxamate linkers for constructing protein-MOFs, we realized that such linkers could in principle also be used to build non-proteinaceous MOFs. Despite the immense diversity of MOFs, they rarely feature linkers with metal-chelating (*i.e.*, multidentate) functionalities. With the proper design of a biphenyl-tetrahydroxamate linker TBTH, we were able to obtain first-in-class, Fe-MOFs based on metal-chelating groups, which are remarkably stable in aqueous solutions (pH 1-13) and can selectively sequester cationic substrates with high efficiencies (Figure 3) (Pub 2). Perhaps more importantly from a biomolecular self-assembly perspective, the metal-hydroxamate nodes in these porous materials are highly thermodynamically stable but kinetically labile, meaning that they can potentially be used for directed self-assembly on the surface of proteins (Figure 4a). This

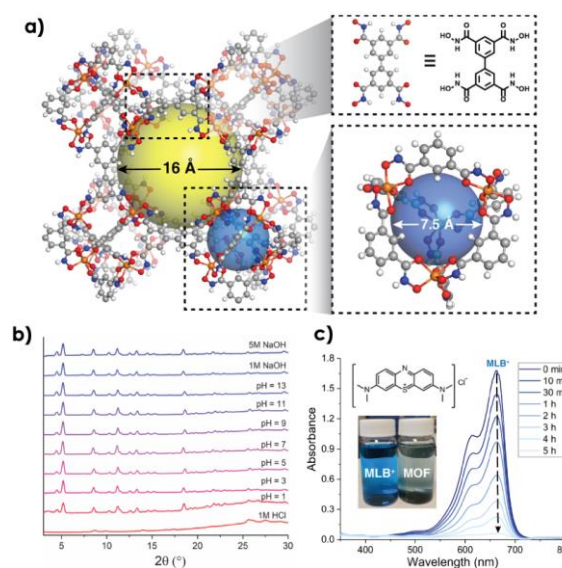


**Figure 3.** (a) The cubic Fe-MOF lattice (termed Fe-HAF-1), constructed from the chelating tetrahydroxamic acid ligand TBTH (upper right corner). Fe-HAF-1 is composed of interconnected tetrahedral clusters formed by Fe-TBTH coordination. (b) Fe-HAF-1 is highly stable in aqueous solution at pH 1 to 13 (as shown by powder-XRD measurements here), and (c) selectively uptakes cationic molecules.

“biomineralization” process, in turn, would create a porous, organic (or metal-organic) exoskeleton on protein nuclei, yielding proteinaceous biomaterials that could a) operate under harsh, non-biological conditions and b) display new or augmented functions due to the integration of protein and synthetic components. With these possibilities in mind, we

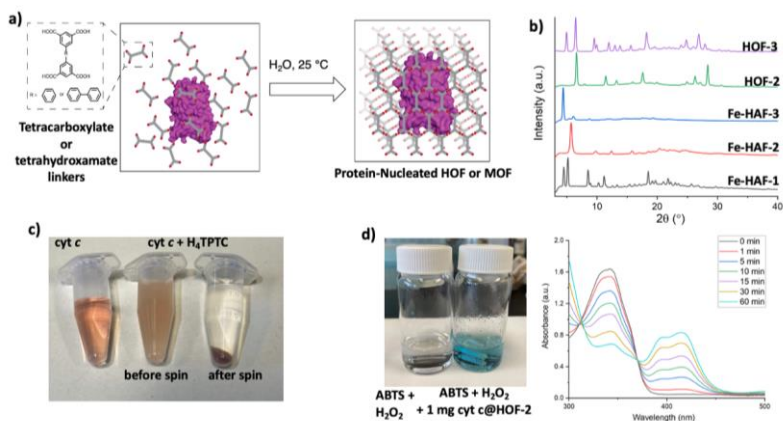


**Figure 4.** (a) Protein-Nucleated Self-Assembly of HOFs/MOFs. (b) Powder XRD patterns of various HOFs and MOFs assembled from our synthetic tetracarboxylate and tetrahydroxamate linkers. (c) Cyt *c*-nucleated formation of cyt *c*@HOF-2 crystals. (d) ABTS/H<sub>2</sub>O<sub>2</sub> oxidation catalyzed by cyt *c*@HOF-2.

have synthesized a library of three tetrahydroxamate and three related tetracarboxylate linkers. We demonstrated that these linkers formed porous 3D frameworks under solvothermal conditions, with the former three yielding crystalline MOFs in the presence of Fe<sup>3+</sup> and the latter three forming crystalline hydrogen-bonded organic frameworks (HOFs) (Figure 4b). Uniformly, these MOFs and HOFs are very stable in aqueous conditions, maintaining their stability at >200 °C and a pH range of 1-13. We ran initial tests with H<sub>4</sub>TPTC to examine whether it could form protein-nucleated HOFs. Gratifyingly, we found that the simple mixing of cyt *c* with H<sub>4</sub>TPTC in water at room temperature yielded a red crystalline powder within minutes (Figure 4c). These crystals displayed the same powder-XRD pattern as the corresponding HOF, indicating that framework structure was maintained. Importantly, based on mass analyses, we calculated the cyt *c* loading yield to be at least 50% (w/w), which is several-fold higher than that of any protein@MOF system reported in the literature. *Notably, in the absence of proteins, H<sub>4</sub>TPTC does not self-assemble into framework crystals under these conditions.* Thus, our results indicate that proteins can actively nucleate the formation of crystalline organic frameworks, in turn leading to high guest protein loadings. As desired, preliminary experiments showed that cyt *c*@HOF displayed high catalytic activities and stabilization of encapsulated proteins (Figure 4d). Our goal is now to extend these studies to other protein@HOF systems with the goal of a) creating new functional, composite biomaterials, and b) obtaining a molecular understanding of the protein-organic framework interface and the protein-templated nucleation/growth mechanism.

**C) Future Plans:** Our continuing goal is to fabricate increasingly more complex, functional protein materials that not only emulate but also extend what natural evolution has produced. Our immediate objectives are: 1) to understand and expand the scope of HuHF-PIX as platforms for controlled biomolecular encapsulation and release (by variations of the polymer and HuHF components and the characteristics/types of biomolecules) through combined experimental and computational studies, 2) to use HuHF-PIX or PIX constructed with other protein lattices to construct functional, multi-protein assemblies with coupled functions, 3) to understand the effects of the crystalline/polymeric environment of PIX on the functions and stabilities of encapsulated proteins, 4) to understand and expand the scope of protein@HOF and protein@MOF systems, 5) to understand and manipulate the nucleation and growth of HOF and MOF networks on protein surfaces, 6) to design and construct topologically woven protein assemblies.

## D) Publications

- 1) E. Golub, R. H. Subramanian, J. Esselborn, R. G. Alberstein, J. B. Bailey, J. A. Chiong, X. Yan, T. Booth, T. S. Baker, F. A. Tezcan, “Constructing Protein Polyhedra from Asymmetric Monomers via Chemically Orthogonal Interactions”, **Nature**, *578*, 172-176 (2020).
- 2) J. Chiong, J. Zhu, J. B. Bailey, M. Kalaj, R. H. Subramanian, W. Xu, S. M. Cohen, F. Akif Tezcan, “An Exceptionally Stable Metal–Organic Framework Constructed from Chelate-Based Metal–Organic Polyhedra”, **J. Am. Chem. Soc.**, *142*, 6907-6912 (2020).
- 3) S. Zhang, R. G. Alberstein, J. De Yoreo, F. A. Tezcan, “Assembly of a patchy protein into variable 2D lattices via tunable multiscale interactions”, **Nat. Commun.**, *11*, 3770 (2020).
- 4) K. C. Bentz, K. Gnanasekaran, J. B. Bailey, S. Ayala Jr., F. A. Tezcan, N. C. Gianneschi, S. M. Cohen, “Inside polyMOFs: Layered Structures in Polymer-Based Metal-Organic Frameworks”, **Chem. Sci.**, *11*, 10523-10528 (2020).
- 5) J. B. Bailey, F. A. Tezcan, “Tunable and Cooperative Thermomechanical Properties of Protein-Metal-Organic Frameworks”, **J. Am. Chem. Soc.**, *142*, 17265–17270 (2020).
- 6) K. Han, J. B. Bailey, L. Zhang, F. A. Tezcan, “Anisotropic Dynamics and Mechanics of Macromolecular Crystals Containing Lattice-Patterned Polymer Networks”, **J. Am. Chem. Soc.**, *142*, 19402-19410 (2020).
- 7) R. H. Subramanian, Y. Suzuki, L. Tallorin, S. Sahu, M. Thompson, N. C. Gianneschi, M. D. Burkart, F. A. Tezcan, “Enzyme-Directed Functionalization of Designed, Two-Dimensional Protein Lattices”, **Biochemistry**, *60*, 1050–1062 (2021).
- 8) R. H. Subramanian, J. Zhu, J. B. Bailey, J. A. Chiong, Y. Li, E. Golub, F. A. Tezcan, “Design of Metal-Mediated Protein Assemblies via Hydroxamic Acid Functionalities”, **Nat. Protoc.**, (2021) <https://doi.org/10.1038/s41596-021-00535-z>
- 9) J. Zhu, N. Avakyan, A. Kakkis, A. M. Hoffnagle, K. Han, Y. Li, Z. Zhang, T. Choi, Y. Na, C. J. Yu and F. A. Tezcan “Protein Assembly by Design” **Chem. Rev.**, (2021) *in press*.

# Designing adaptive information processing materials using non-equilibrium forcing

Suriyanarayanan Vaikuntanathan, Department of Chemistry, University of Chicago

## Program Scope

The main goal of this proposal is to develop theoretical design principles for the construction of bio-inspired adaptive materials. We are specifically focused on uncovering theoretical design principles that will enable bio-inspired materials to (a) respond to external forcing in an adaptive manner (b) record changes in external conditions in their internal structure and (c) respond accurately to spatio-temporal molecular cues and self-assemble or reorganize. Non-linear dimensional reduction techniques will be used (as required) to extract thermodynamic principles from complex non-equilibrium biophysical data. Each of these goals is inspired by functionality seen in biological materials - actin polymerization networks and actomyosin networks.

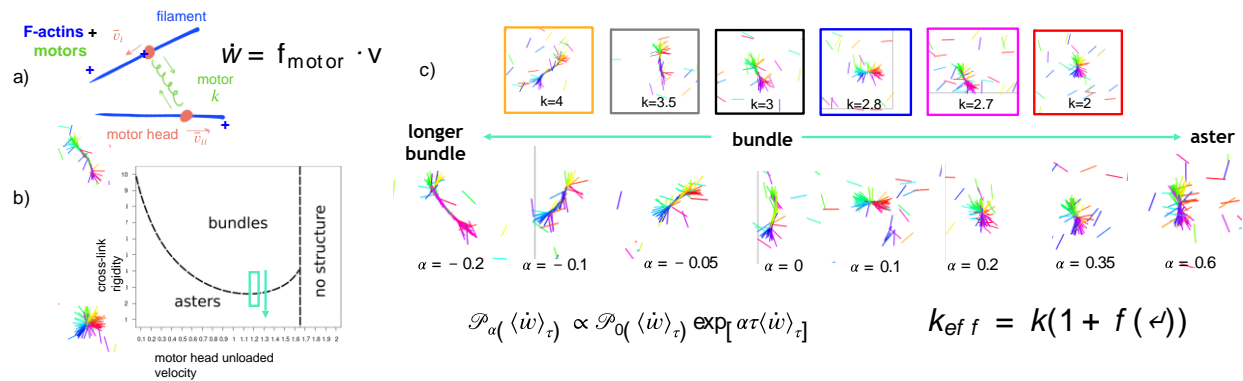


Fig 1: (a) A model cytoskeleton system with F-actin and molecular motors (b) Depending on the motor rigidity and speed, the system can be made to form aster like or bundle like structures in the steady state. (c) Our new non-equilibrium thermodynamic control theory suggests that the transition from bundles to aster in (b)-indicated by the green box- can be accessed even when the motor rigidity is held fixed by simply allowing the motor to access trajectories that dissipate more energy. In this way, the biomaterial can access different regimes (and consequently respond to different force stimuli) by tuning the rate at which the molecular motor consumes chemical fuel. Our new non-equilibrium control theory provides a basis to anticipate how the properties of this biomaterial can be reliably tuned at the cost of energy consumption.

## Recent Progress

Active biological systems such as the actin networks in cytoskeleton can respond efficiently and accurately to various external force stimuli. Understanding the non-equilibrium thermodynamic

basis of such adaptive response remains an important grand challenge. In our recent work, we have discovered a new and general non-equilibrium thermodynamic control principle for modulating the material properties of such biomaterials. We consider a biomaterial system made of actin filaments and molecular motor crosslinkers. This system can be made to exhibit many of the well known phases seen in actomyosin assemblies, including *aster* like configurations and *bundled* configurations. A transition from the *aster* to the *bundled* configuration can be readily obtained by tuning the rigidity or the stiffness of the molecular motor.

*Our new non-equilibrium control principle shows how the acto-myosin network can access the same transition by simply tuning the rate of energy consumption by molecular motors attached to actin* (Fig 1). The *aster* and *bundle* configurations of the biomaterial have different force generating properties. Depending on the external force stimuli, the biomaterial can tune its material properties simply by controlling an energy budget. Hence, our results can form the basis for the development of an adaptive biomaterial that is able to mount a very specific controlled response, by tuning the rate at which it consumes chemical fuel, in response to changing conditions.

Our theoretical and computational framework, based on the mathematical framework of large deviation theory and stochastic thermodynamics, can predict this interplay between energy dissipation and renormalized material properties. Our work can thus form the basis of a control theory for changing the properties of the actomyosin biomaterial at the cost of energy dissipation. This work is currently being written up and will be submitted for publication shortly.

This progress builds on very recent work where we used machine learning to show that signatures of dissipation are in fact encoded in the microscopic correlations of a non-equilibrium liquid. This work is described in detail in Ref (1) below. This progress is also complimentary to another recent advance (described in Ref (2) below) where we derived a generalization of the classical linear irreversible thermodynamics framework and the classical linear response framework to far from equilibrium bundling and polymerizing actin networks.

Overall, these set of results identifies (to the best of our knowledge) new and fundamental constraints imposed by thermodynamics on the non-equilibrium properties of biological materials.

## **Future Plans**

Future work will address will use Reinforcement learning to further explore efficient protocols that biomaterials can use to adapt to changing external conditions. The protocols extracted from reinforcement learning will be compared with the above-described thermodynamic control laws. In this way, combining machine learning and non-equilibrium thermodynamics, our goal will be to uncover physically realizable rules that can support adaptive behavior in non-equilibrium materials.

## References

- 1) L. Tociu, G. Rassolov, E. Fodor, S. Vaikuntanathan “Quantifying dissipation from structure in active matter”. arXiv preprint arXiv:2012.10441 (under revision Nat Comm) (2021)
- 2) Y. Qiu, M. Nguyen, G. Hockey, A. Dinner, S. Vaikuntanathan “A strong non-equilibrium bound for sorting of crosslinkers on growing biopolymers”. arXiv preprint arXiv:2012.11588 (under revision PNAS) (2021).

## Publications

- 1) L. Tociu, G. Rassolov, E. Fodor, S. Vaikuntanathan “Quantifying dissipation from structure in active matter”. arXiv preprint arXiv:2012.10441 (under revision Nat Comm) (2021)
- 2) Y. Qiu, M. Nguyen, G. Hockey, A. Dinner, S. Vaikuntanathan “A strong non-equilibrium bound for sorting of crosslinkers on growing biopolymers”. arXiv preprint arXiv:2012.11588 (under revision PNAS) (2021).

## Reciprocal Energy Exchange in Hierarchical DNA Origami-Nanoparticle Composites

Dr. Jessica Winter, The Ohio State University (PI)

Dr. Carlos Castro, The Ohio State University (co-PI)

Dr. Michael Poirier, The Ohio State University (co-PI)

Dr. Ezekiel Johnston-Halperin, The Ohio State University (co-PI)

### Program Scope

This research investigates reciprocal interactions between DNA origami (DO) and nanoparticle (NP) constituents in composite materials and their emergent behaviors in higher order assemblies, providing fundamental insights into energy efficiency, work delivery, and self-healing capabilities. Reciprocal interactions between NPs and DOs can take a variety of forms, from passive steric disruption of DNA binding to active energy input via external fields (i.e., plasmonic, magnetic) that alter double-stranded (dsDNA) stability. Few studies have addressed these concepts [58], and no studies have quantified mechanical work capacity. To achieve these goals, we will employ DO hinges studied previously and other dynamic devices with well-defined motion and entropic tunability (e.g., pistons [23], switches [59]) (**Figure 1**). These materials present multiple, programmable NP attachment sites and can be polymerized with many conformations to investigate emergent effects of scaling. We will also employ plasmonic gold nanoparticles (AuNPs), as we did previously, and magnetic NPs of varying size. Our research plan will be accomplished through the following objectives:

**Objective 1:** Evaluate DNA-NP composite conversion of energy inputs into mechanical work

**Objective 2:** Evaluate cooperative energy conversion in higher order DNA-NP arrays

**Objective 3:** Explore reciprocal control in DNA-NP composite self-healing mechanisms

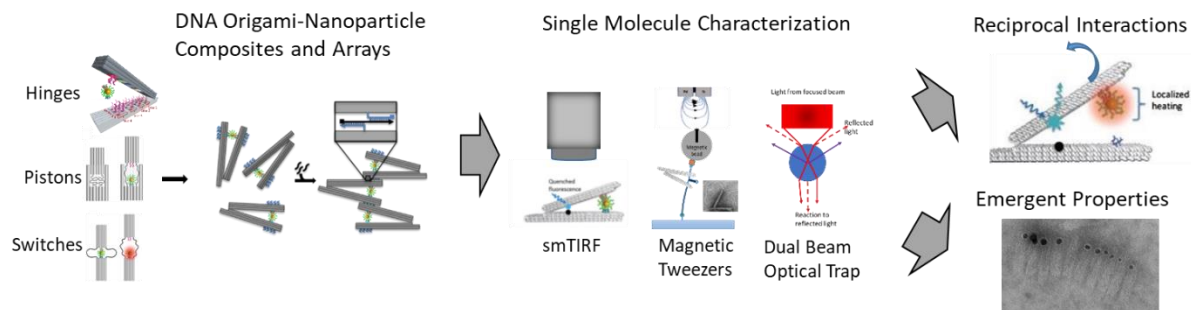


**Figure 1.** Individual NPs and DNA origami units are combined into composites that can be polymerized into arrays. These materials will be characterized with single molecule fluorescence and force microscopy to identify reciprocal and emergent behaviors, including transmission of work and self-healing properties.

### Recent Progress

We have focused recent efforts on studying DNA origami switch devices (Figure 1, bottom left) by characterizing their dynamic and mechanical properties as a function of structural

design parameters. The DNA switch devices consist of two barrel components that are connected together via 6 flexible single-stranded DNA (ssDNA linkers) organized around the perimeter of the two barrels. The 6 flexible linkers are 90 nucleotides long (nt), allowing flexible relative motion of the two barrels up to separation distances of approximately

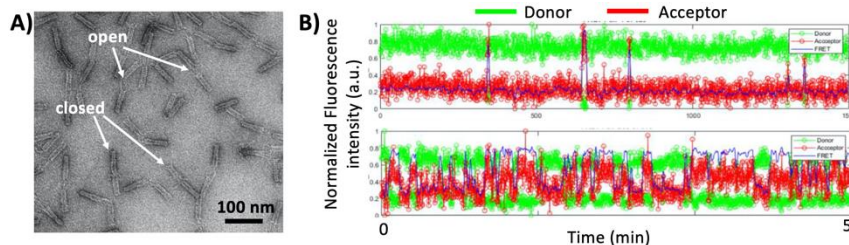


**Figure 2.** Dynamic properties of DNA origami switch nanodevice. A) TEM images of the switch device illustrating wide range of conformations. Two examples of open and closed devices are labeled. B) Representative single molecule FRET traces illustrate the dynamic conformational changes of the switch. The switch remains mostly open (high donor and low acceptor signal) when the linkers are double-stranded (top), whereas single-stranded linkers are more flexible and facilitate fast closing of the device.

50 nm when the devices are in an “open” conformation. On one of the ssDNA linker strands, we can incorporate a DNA strand (i.e., closing strand) that binds to the linker to pinch the two ends together and convert the switch structure into a “closed” conformation where the two barrels are held close together. On one end of the linker, the closing strand binds stably, whereas on the other end, the closing strand affinity can be tuned from a stable interaction that remains in the closed state to a weak interaction that primarily remains open and only transiently binds into the closed state. Figure 2A illustrates a transmission electron microscopy (TEM) image where examples both open and closed devices are shown.

We previously demonstrated this type of device can be used as a nanomechanical sensor where forces bias the distribution of opened or closed states [1]. In this prior work, we used a 10 nt interaction, which led to a device that was primarily open, and as we introduced high molecular weight polymer polyethylene glycol (PEG), the device was biased into a closed state due to a depletion force resulting from the PEG crowding agent. Recently we have established multiple approaches to control the dynamic and mechanical properties of the device. For example, Figure 2B shows single molecule Förster resonance energy transfer (FRET) studies of a device with a 10nt interaction in which the remaining 5 linkers are either double-stranded (Figure 2B, top) or single-stranded (Figure 2B, bottom). The double-stranded linkers are stiffer and inhibit the closing of the device, whereas the entropic elasticity of the single-stranded linkers causes them to coil up and facilitate closing of the device. This provides multiple design parameters (e.g., stability of closing interaction and the properties of the DNA linkers) to tune the dynamic properties of the nanodevice.

In addition to the dynamic properties of the device, we are currently studying the mechanical properties of devices with more stable closing interactions. We have developed a magnetic tweezers force spectroscopy assay to apply controlled forces to single DNA origami switch devices (Figure 3A). Forces are applied by tethering the nanodevice between a coverslip

and a micron-scale magnetic bead and then bringing a magnet into proximity of the of the sample to introduce a magnetic field gradient. Figures 3B-C shows representative data traces illustrating the extension of the device as a function of time under an increasing applied force (Figure 3B) as well as the force versus extension behavior (Figure 3C) for the same individual device. Both traces illustrate a step change in extension, which occurs when the force is sufficiently high to rupture the DNA interaction holding the device in the closed state (i.e., cause a conformational change to the open state). In this example, the switch device opened under an applied force of  $\sim 8$  pN. We have developed devices with rupture forces ranging from  $\sim 5$ -10 pN. In addition, we have observed reversible conformational changes, where devices close upon decreasing force suggesting a self-healing behavior (data not shown). Similar to our established capability to tune the dynamic properties of the device, we are now exploring the ability to tune mechanical transitions (i.e., forces required to open and close the device) by adjusting structural design parameters.

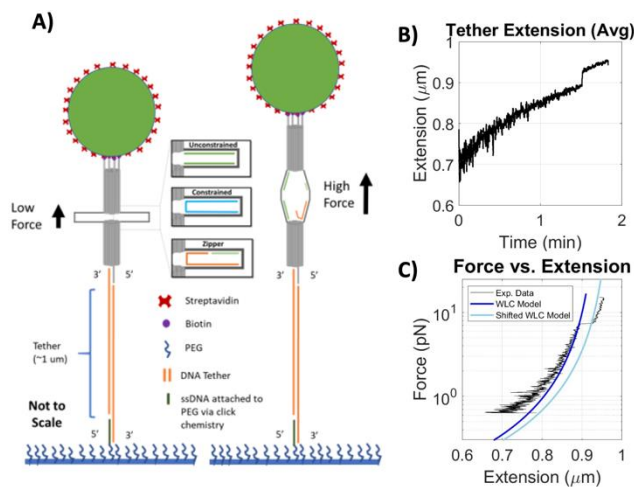


**Figure 3.** Mechanical properties of a DNA origami switch nanodevice. A) For force spectroscopy studies, a switch nanodevice is tethered between a PEG-coated coverslip and a micron-sized magnetic bead. B) When a force is applied to the magnetic bead, the tether and device construct extend. The sharp step change in extension indicates the conformational change from the closed to the open state. C) The force-extension behavior of the construct follows the typical wormlike chain behavior of the dsDNA tether. At  $\sim 8$  pN of force, the closing interaction ruptures and the device changes conformation into the open state.

### Future Plans

We have established a foundation for controlling and characterizing the dynamic and mechanical properties of dynamic DNA origami switch devices, which will be the basis of a publication we plan to prepare in the coming year. Moving forward we will build on this foundation to incorporate nanoparticles and test the effects of NPs on dynamic and mechanical properties. We will test cases for which the base-pairing interactions holding the device into a closed state form directly on the surface of the NP or just in the vicinity of the NP. We hypothesize that the presence of a bulky NP will influence the stability of the closing interaction and cause a shift towards the open state. We will also leverage our prior work on thermal actuation of DNA origami-NP composites to test the effects of temperature on dynamic and mechanical properties of DNA origami-NP composites. Finally, we plan to leverage the photothermal response of NPs to trigger laser-induced heating of gold NPs to study how photothermal NP properties are coupled to dynamic and mechanical properties switch devices.

We also plan to transition single molecule force spectroscopy experiments to be carried out on an optical trapping (Lumicks C-Trap) instrument recently acquired by Ohio State University. The key advantage of this instrument is it combines force measurements with high-speed fluorescence imaging and microfluidic control of the environment. Hence, we can directly detect the conformation of the device or the formation/dissociation of particular base-pairing interactions using fluorescence readouts, both of which we have previously demonstrated in the absence of externally applied forces [1-2]. With the microfluidic control, we can also rapidly cycle between different solution environments to test the effects of environmental conditions such as ion concentrations.

## References

1. Hudoba, M.W., Luo, Y., Zacharias, A., Poirier, M., Castro, C.E. *A Dynamic DNA origami device for measuring compressive depletion forces*. *ACS Nano*, 2017 11(7):6566-6573
2. Johnson, J.A., Dehankar, A., Winter, J., Castro, C.E. Reciprocal Control of Hierarchical DNA Origami-Nanoparticle Assemblies. *Nano Letters*, 2019. 19(12): 8469-8475

## Publications

1. Dehankar, A., T. Porter, J.A. Johnson, C.E. Castro, and J.O. Winter, *Compact quantum dot surface modification to enable emergent behaviors in quantum dot-DNA composites*. *The Journal of Chemical Physics*, 2019. **151**(14): p. 144706. [Partially supported by BES. DNA modification chemistry and FRET studies were funded by the NSF, whereas DNA origami studies were funded by the DOE.]
2. Johnson, J.A., A. Dehankar, A. Robbins, P. Kabtial, E. Jergens, K. Ho Lee, E. Johnston-Halperin, M. Poirier, C.E. Castro, and J.O. Winter, *The path towards functional nanoparticle-DNA origami composites*. *Materials Science and Engineering: R: Reports*, 2019. **138**: p. 153-209. [Supported by BES]
3. Johnson, J.A., Kolliopoulos, V., Castro, C.E. Co-self-assembly of multiple DNA origami nanostructures in a single pot. *Chemical Communications*, 2021. **57**:4795–4798 [Supported by BES]
4. Johnson, J.A., Dehankar, A., Winter, J., Castro, C.E. Reciprocal Control of Hierarchical DNA Origami-Nanoparticle Assemblies. *Nano Letters*, 2019. 19(12): 8469-8475 [Supported by BES]

## DNA-Tile Caged NPs toward Materials Agnostic Surface Modification

**Dr. Jessica Winter, The Ohio State University (PI)**

**Dr. Carlos Castro, The Ohio State University (co-PI)**

**Dr. Michael Poirier, The Ohio State University (co-PI)**

**Dr. Ezekiel Johnston-Halperin, The Ohio State University (co-PI)**

### Program Scope

This research investigates reciprocal interactions between DNA origami (DO) and nanoparticle (NP) constituents in composite materials and their emergent behaviors in higher order assemblies, providing fundamental insights into energy efficiency, work delivery, and self-healing capabilities. Reciprocal interactions between NPs and DOs can take a variety of forms, from passive steric disruption of DNA binding to active energy input via external fields (i.e., plasmonic, magnetic) that alter double-stranded (dsDNA) stability. Few studies have addressed these concepts [58], and no studies have quantified mechanical work capacity. To achieve these goals, we will employ DO hinges studied previously and other dynamic devices with well-defined motion and entropic tunability (e.g., pistons [23], switches [59]) (**Figure 1**). These materials present multiple, programmable NP attachment sites and can be polymerized with many conformations to investigate emergent effects of scaling. We will also employ plasmonic gold nanoparticles (AuNPs), as we did previously, and magnetic NPs of varying size. Our research plan will be accomplished through the following objectives:

**Objective 1:** Evaluate DNA-NP composite conversion of energy inputs into mechanical work

**Objective 2:** Evaluate cooperative energy conversion in higher order DNA-NP arrays

**Objective 3:** Explore reciprocal control in DNA-NP composite self-healing mechanisms

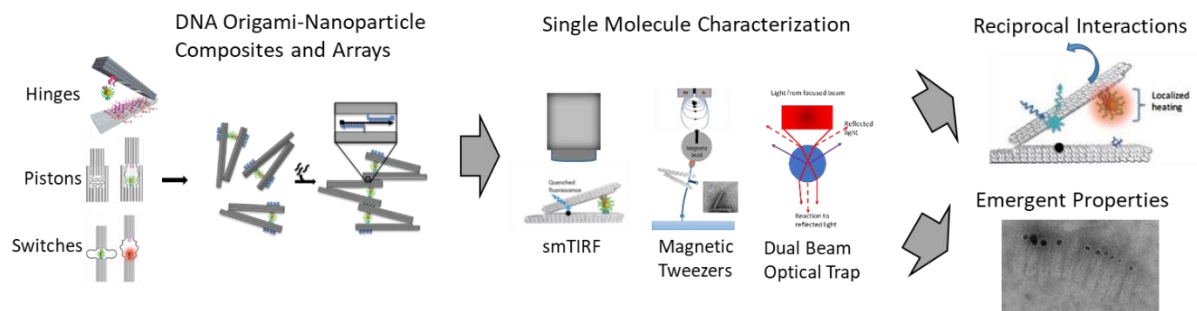


**Figure 1.** Individual NPs and DNA origami units are combined into composites that can be polymerized into arrays. These materials will be characterized with single molecule fluorescence and force microscopy to identify reciprocal and emergent behaviors, including transmission of work and self-healing properties.

### Recent Progress

All of these goals require that NPs be modified with DNA for integration with DNA nanostructures. Yet, this can be surprisingly challenging. DNA is negatively charged and can

result in colloidal instabilities resulting from electrostatic interactions [1]. DNA density is a critical variable [2]. If too little DNA is added, strands may be attracted to the NP surface, precluding useful binding. If too much DNA is added, steric hindrance may prevent complement strand access. Further, over modification can result in structure aggregation as multiple NPs and DO bind in an uncontrolled manner. It is crucial to control DNA number and density on NP surfaces. We recently reported methods to conjugate ~ 1 single stranded DNA (ssDNA) strand per NP through careful optimization of standard bioconjugation protocols and validated these methods via (NSF-funded) Förster Resonance Energy Transfer (FRET) and (DOE-funded) DO binding experiments (**Figure 2**) [1].

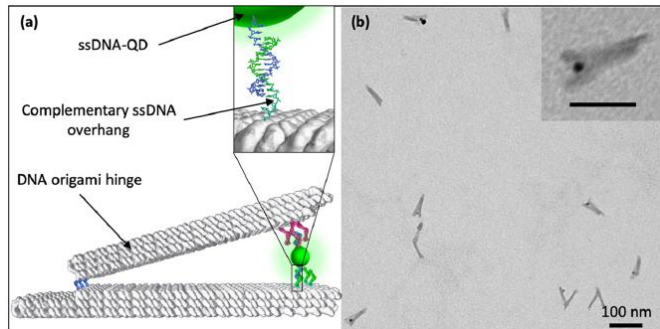


**Figure 2:** Quantum dot (QD) nanoparticles (NPs) were modified with a single ssDNA strand using Click chemistry. QDs were then bound to individual DNA origami (DO) hinges with little unwanted aggregation. These methods provide enabling technologies for the formation of complex DO-NP composite materials capable of harvesting, storing, and transforming energy.

However, these approaches require time consuming optimization for each new NP material and geometry. Thus, we have developed methods toward universal NP modification based on DNA tile nanostructures that form cages around NPs (**Figure 3**). DNA tiles offer several benefits versus traditional conjugation approaches in that (i) tiles can stabilize NPs in harsh environments by providing a protective barrier and (ii) tiles enable control over DNA presentation number, density, and geometry through programmability. Our initial work has focused on modifying polymer NPs with DNAs, as these are large (i.e., ~25 nm) and provide an easy template for DNA tile design. Triangular DNA nanostructure tiles, inspired by artificial cytoskeleton designs [3], were employed for caging. In these designs, three ssDNA strands form a 3-way junction from which ssDNA interlocking strands (purple) and targeting strands (green) emanate. Interlocking strands enable tiles to interlock into hexagonal shaped superstructures that are attracted to micelle surfaces through electrostatic interactions (**Figure 3A**). Negatively-charged tiles adsorb on the surface of positively-charged polystyrene-polyethylene oxide (PS-PEO) or 1,2-distearoyl-sn-glycero-3-phosphoethanolamine-N-[amino(polyethylene glycol)] (DSPE-PEG) micelles terminated with NH<sub>2</sub> groups.

DNA cage formation on micelle surfaces was confirmed using transmission electron microscopy (TEM), which indicated different structures for DNA only, micelle only, and DNA tile + micelle materials (**Figure 3B**). In addition, cage formation was verified by determining saturation on micelle surfaces using fluorescently-labeled tiles, with fluorescence increasing to a saturation point after which addition increases are not observed (**Figure 3C**). We also showed that DNA tiles bind micelle surfaces and do not form separate structures using tiles labeled with black hole quencher and fluorescent micelle surfaces (**Figure 3D**). Finally, DNA tile interlock

formation was ascertained using FRET reporter pairs on interlocking sequences. Fluorescence initially increases as tiles bind micelles, then decreases as interlocks are formed (**Figure 3E**). To confirm ssDNA functionality, we bound fluorescently-labeled complimentary strands to DNA-caged micelles, then erased those strands with non-labeled strands with greater complementarity (**Figure 3F**) (efficiency > 95%). DNA-caged NPs demonstrated greater stability than micelles without cages, as they were tolerant to Triton and Tween detergents that dissolved micelles without cages. We plan to submit a publication on this work in the coming year.

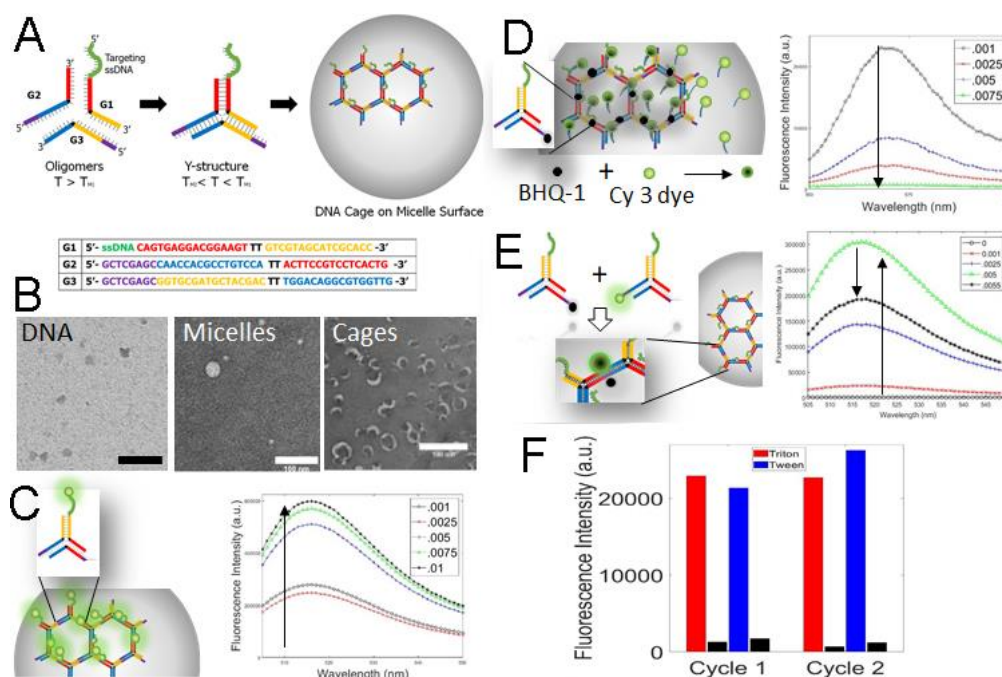


**Figure 3:** DNA-caged polymer NPs (A) Schematic. Interlocking ssDNAs (purple) form a cage around a ~20-50 nm polymer micelle. Targeting ssDNAs (green) are available for DO binding. (B) TEM images of DNA only, micelles only, and DNA-caged micelles. Scale bar = 100 nm. (C-F) Using fluorescent dyes and quenchers (Black hole quencher-1 (BHQ-1)), we have shown that: (C) FAM-6 cages bind micelles increasing their fluorescence to saturation, (D) BHQ-1 cages bind micelles with Cy-3 modified surfaces quenching its fluorescence, (E) Cy-3 and BHQ-1 DNA cages interlock. Signal increases with initial binding, and quenches as cages form interlocks, and (F) DNA cages are stable in detergents as shown by binding and release of fluorescent target DNA.

## Future Plans

We have now begun to extrapolate these methods to our target inorganic NPs with much smaller sizes. In particular, we are attempting cage formation on 15 nm AuNPs to be used in energy harvesting studies. We have preliminarily shown that DNA tiles bind AuNP surfaces using fluorescently-labelled tiles and form interlocks using FRET pairs (**Figure 4**). Fluorescence of purified AuNP samples increases with increasing tile addition (**Figure 4A**). We have also shown that DNA tiles form interlocks using FRET quenching studies (**Figure 4B**). These initial studies provide proof of concept of a powerful enabling technology for modifying NP surfaces with DNA. In future work, we will employ these technologies to generate complex DNA-NP

composite materials, such as DNA arrays shown in **Figure 1**. These methods will reduce stochastic variation and aggregation, facilitating our emergent property and reciprocal control studies.

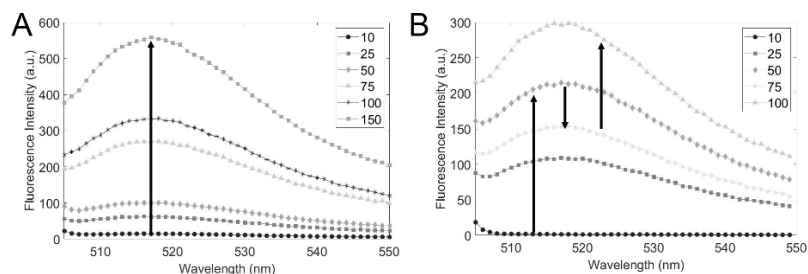


**Figure 4:** DNA-caged 15 nm AuNPs. (A) Saturation curve showing increasing fluorescence with cage adsorption. (B) Interlocking study showing initial increase in fluorescence with DNA cage adsorption, followed by a decline as interlocks form. With continuing increase in DNA fluorescence begins to increase again as steric hindrance prevents interlocking of adjacent tiles.

## References

1. Dehankar, A., T. Porter, J.A. Johnson, C.E. Castro, and J.O. Winter, Compact quantum dot surface modification to enable emergent behaviors in quantum dot-DNA composites. *The Journal of Chemical Physics*, 2019. 151(14): p. 144706.
2. Johnson, J.A., A. Dehankar, A. Robbins, P. Kabtiyal, E. Jergens, K. Ho Lee, E. Johnston-Halperin, M. Poirier, C.E. Castro, and J.O. Winter, The path towards functional nanoparticle-DNA origami composites. *Materials Science and Engineering: R: Reports*, 2019. 138: p. 153-209.
3. Kurokawa, C., K. Fujiwara, M. Morita, I. Kawamata, Y. Kawagishi, A. Sakai, Y. Murayama, S.M. Nomura, S. Murata, M. Takinoue, and M. Yanagisawa, DNA cytoskeleton for stabilizing artificial cells. *Proceedings of the National Academy of Sciences of the United States of America*, 2017. 114(28): p. 7228-7233.

## Publications (2019-2021)

1. Dehankar, A., T. Porter, J.A. Johnson, C.E. Castro, and J.O. Winter, Compact quantum dot surface modification to enable emergent behaviors in quantum dot-DNA composites. *The Journal of Chemical Physics*, 2019. **151**(14): p. 144706. [Partially supported by BES. NSF: DNA modification chemistry, FRET studies, DOE: DNA origami.]
2. Johnson, J.A., A. Dehankar, A. Robbins, P. Kabtiyal, E. Jergens, K. Ho Lee, E. Johnston-Halperin, M. Poirier, C.E. Castro, and J.O. Winter, The path towards functional nanoparticle-DNA origami composites. *Materials Science and Engineering: R: Reports*, 2019. **138**: p. 153-209. [Supported by BES]
3. Johnson, J.A., Kolliopoulos, V., Castro, C.E. Co-self-assembly of multiple DNA origami nanostructures in a single pot. *Chemical Communications*, 2021. 57:4795–4798 [Supported by BES]
4. Johnson, J.A., A. Dehankar, J.O. Winter, and C.E. Castro, Reciprocal Control of Hierarchical DNA Origami-Nanoparticle Assemblies. *Nano Letters*, 2019. 19(12): p. 8469–8475. [Supported by BES]

## **Biomimetic Light Harvesting Complexes Based on Self-Assembled Dye-DNA Nanostructures**

**Hao Yan, Arizona State University, Principal Investigator**

**Neal Woodbury, Arizona State University, (Co-Investigator)**

**Su Lin, Arizona State University, (Co-Investigator)**

### **Program Scope**

The main scope of this research is to use DNA nanostructures as a template for the self-assembly of dye aggregates in specific and programmable arrangements. The goal is to create a new class of photonic materials that mimic biological light-harvesting systems with robust and scalable components for photonic network development. We first conducted an in-depth characterization of self-assembled K21 aggregates on DNA duplexes and demonstrated that their formation and spectral properties are only weakly sequence-dependent and that almost no excitation energy loss occurs upon energy transfer through an aggregate of up to 30 nm. This holds great promise for the design and construction of excitonic systems with larger sizes and more complex geometries. We next focused on the development of more versatile modular constructs that enable photonic networks on extendable scales. Such materials, inspired by the design of natural photosynthetic light-harvesting systems, employ self-assembled DNA-helix-bundles as templates that are up to microns in length (**Figure 1a**), with programmability and chemical addressability for functionalization. We have (1) optimized the one-dimensional (1-D) excitonic architectures, performed experimental and computational characterization to reveal exciton dynamics along the K21 aggregates formed on DNA helix bundles, and used this “excitonic wire” for directional energy transfer over sub-micron distances, and (2) expanded the size and geometric design of the DNA templates to create programmable and scalable excitonic constructs serving as modular building blocks for fabrication of higher order excitonic architectures. This work provides both a fundamental understanding of self-assembled cyanine dye aggregates directed by DNA-helix-bundles, as well as a much more comprehensive toolset for the development of biomimetic photonic structures using DNA-dye aggregates as a programmable photonic material.

### **Recent Progress**

In an effort to the further development of bio-inspired photonic materials, we have investigated the excitonic features of K21 aggregates organized by using four-helix-bundle DNA nanostructures (4HB) as templates. Multiple spectroscopic approaches and Monte Carlo (MC) simulation were employed to understand the photonic properties in detail. The coherently coupled excitonic characteristics of DNA templated dye aggregates was evidenced by a red-shifted sharp absorption peak, a strongly enhanced emission band, and a prolonged fluorescence lifetime (**Figure 1b-d**). To further examine the exciton distribution and propagation along such sub-micron-scale dye

aggregate complexes, energy acceptors, Alexa Fluor 555 (AF) dye molecules, were attached to the construct. Energy transfer efficiencies between the aggregate and the AF molecules of more than 50% were observed regardless of the placement of the acceptor molecules along the DNA, indicating that the DNA-templated dye aggregates can serve as an “exciton wire” in which excitation can move freely visiting the vicinity of an acceptor multiple times before captured. Using Monte Carlo simulations based on a 1-D unbiased random walk model, we concluded that the energy transfer process involved fast exciton hopping between neighboring units with an effective rate of  $1/20 \text{ fs}^{-1}$  and a relatively slow trapping rate of  $1/16 \text{ ps}^{-1}$ . The parameter set derived from the Monte Carlo simulation can also successfully predict the energy transfer efficiency for constructs in which the number of AF acceptors have been varied from 4 to 40 and in which the length of template has been varied between 250 and 600 nm. Further, singlet exciton-exciton annihilation experiments were carried out to explore the coherent properties of DNA-templated K21 aggregates on 4HB. The experimental results suggest that annihilation predominantly occurs in the species that emits at 470 nm, the spectral feature associated with K21 J-like aggregates. Fitting the decay kinetic traces in the presence of annihilation with a diffusion model results in a diffusion constant of  $10 - 30 \text{ cm}^2 \cdot \text{s}^{-1}$  and a diffusion length of 370 – 630 nm along the longitudinal dimension of the dye aggregate complex. Again, consistent with rapid sub-micron exciton transfer within the 4HB-templated K21 aggregates.

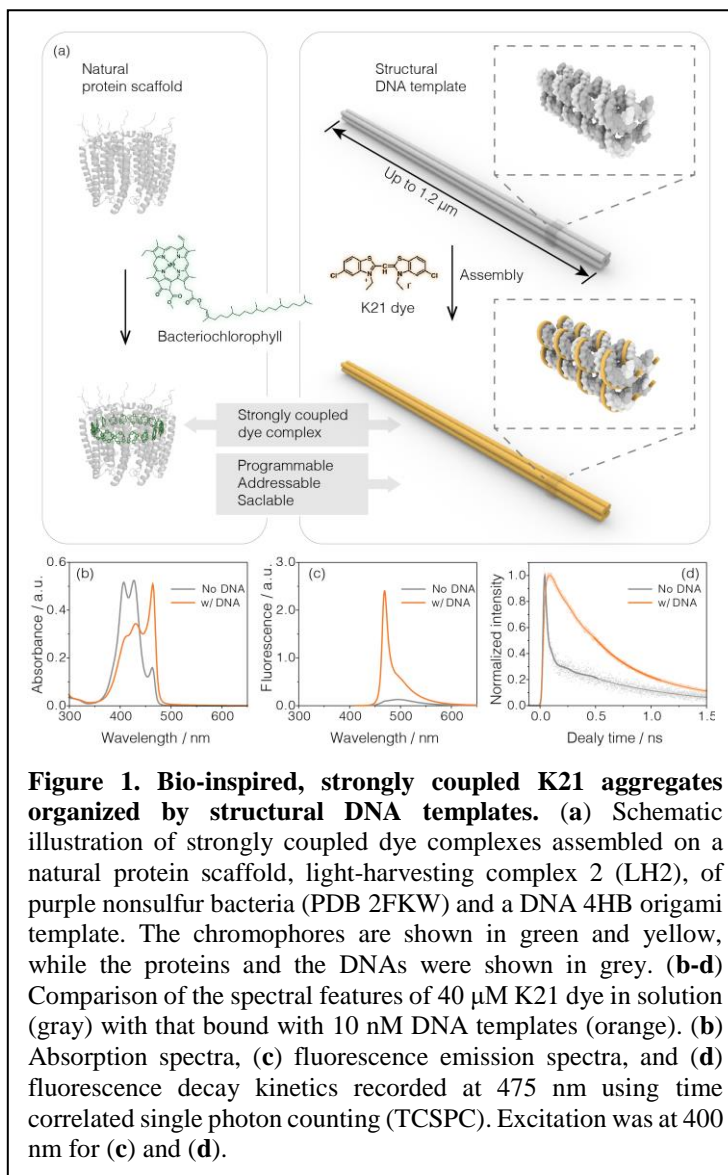


**Figure 1. Bio-inspired, strongly coupled K21 aggregates organized by structural DNA templates.** (a) Schematic illustration of strongly coupled dye complexes assembled on a natural protein scaffold, light-harvesting complex 2 (LH2), of purple nonsulfur bacteria (PDB 2FKW) and a DNA 4HB origami template. The chromophores are shown in green and yellow, while the proteins and the DNAs were shown in grey. (b-d) Comparison of the spectral features of 40 μM K21 dye in solution (gray) with that bound with 10 nM DNA templates (orange). (b) Absorption spectra, (c) fluorescence emission spectra, and (d) fluorescence decay kinetics recorded at 475 nm using time correlated single photon counting (TCSPC). Excitation was at 400 nm for (c) and (d).

The above characterized DNA-templated “excitonic wires” (4HB) were then used to mediate directional energy transfer over a submicron distance, extended to dimeric constructs with micron lengths, and utilized to construct excitonic systems with complex geometries, as described in more detail below.

The above characterized DNA-templated “excitonic wires” (4HB) were then used to mediate directional energy transfer over a submicron distance, extended to dimeric constructs with micron lengths, and utilized to construct excitonic systems with complex geometries, as described in more detail below.

1. Directional donor-to-acceptor energy transfer over sub-micron distances. Donor molecules (Alexa Fluor 350, **D**) and acceptor molecules (Alexa Fluor 555, **A**) have been attached onto the

two ends of a DNA template, separated by a distance of  $\sim 400$  nm, as shown in **Figure 2**. To increase the absorption cross section of the donor molecules to a point where they effectively compete with direct excitation of K21 aggregates, forty 3-way junction DNA tiles holding a total of 400 donor molecules were attached at one end of the 4HB. Twenty acceptor molecules were attached to the opposite end. The K21 aggregates templated on the 4HB serves as a bridge **B** to fill in the geometric and spectral gap between the **D** and **A**. The observed increase in **A**'s emission in the presence of **D**, suggested that excitation captured by donor molecules was transferred to acceptor molecules along the K21 bridge with an efficiency  $\sim 20\%$  over a half-micron distance.

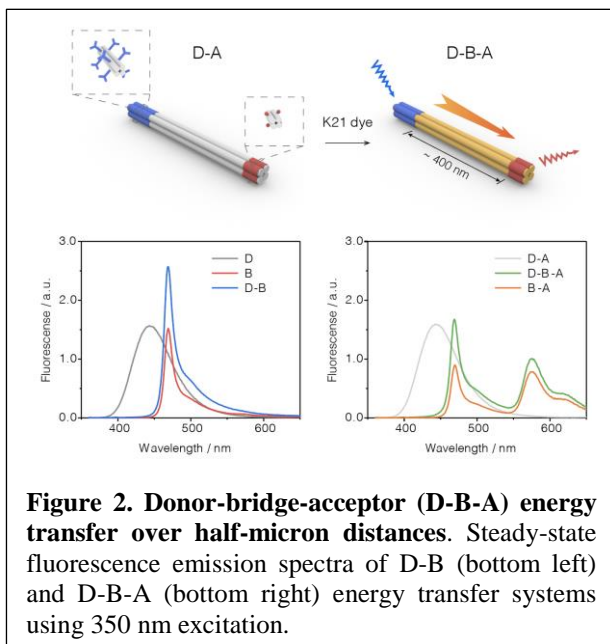


**Figure 2. Donor-bridge-acceptor (D-B-A) energy transfer over half-micron distances.** Steady-state fluorescence emission spectra of D-B (bottom left) and D-B-A (bottom right) energy transfer systems using 350 nm excitation.

2. Extended excitonic wires for micron-distance exciton transfer. The structural DNA template can be further extended to the dimeric form via sticky end hybridization forming micron-length “excitonic wires”. TIRF images of both monomeric and dimeric constructs showed elongated fluorescence spots. However, the length of the spot for dimeric wire is  $1.12 \pm 0.07 \mu\text{m}$ , about twice of the length of the monomeric wire ( $0.65 \pm 0.03 \mu\text{m}$ ). The result agrees well with the designed length of monomer ( $\sim 600$  nm) and dimer ( $\sim 1.2 \mu\text{m}$ ). To investigate excitation transfer across the connection junction of dimers, we have compared the energy transfer efficiency of the K21-aggregate to the AF donor for several constructs (**Figure 3**), including a monomeric wire with 40 AF555 molecules attached (4HB-AF-i), a 1:1 mixture of AF labeled and unlabeled monomers (Mix), and four different dimeric wire arrangements in which 40 AF555 molecules are attached with four modification patterns (i.e. at 4 different locations on the dimeric wires, 2 such constructs, 4HB-D-AF-I and 4HB-D-AF-II are shown in **Figure 3**). The K21-to-AF energy transfer of these samples show efficiencies as expected for the structure of the constructs. The predicted results from Monte Carlo simulations also show a trend similar to the experimental results. Both experimental and simulated results imply no obvious drop in energy transfer efficiency at the junctions of the DNA origami and give rise to efficient energy transfer on the micron-scale.

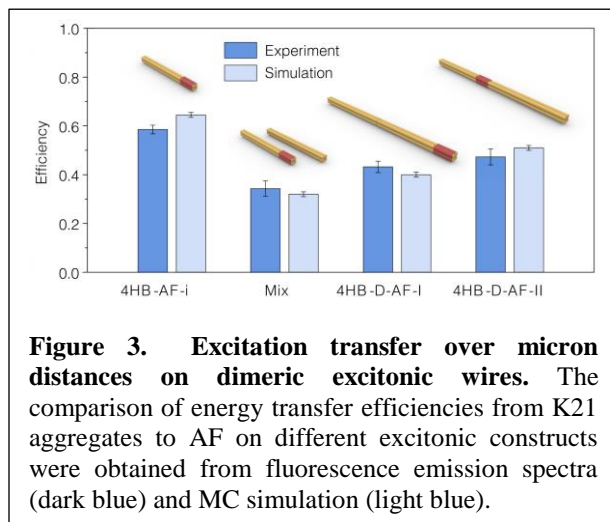


**Figure 3. Excitation transfer over micron distances on dimeric excitonic wires.** The comparison of energy transfer efficiencies from K21 aggregates to AF on different excitonic constructs were obtained from fluorescence emission spectra (dark blue) and MC simulation (light blue).

3. Modular building block for fabrication of higher order excitonic architectures. The design of structural DNA templates has been expanded from linear bundles to more complex geometries, including L-shapes, zigzag shapes, rings, and T-junction forms and verified by AFM imaging

(Figure 4). We studied the energy transfer capabilities of the dye aggregates assembled on those DNA templates after coupling energy acceptor molecules. The results indicate that similarly robust energy transfer takes place in each of those excitonic constructs even though they have different geometric designs. Those constructs were utilized as modular building blocks to fabricate higher order systems in an extendable fashion. As a proof-of-concept, a series of extended constructs, including L-dimers, L-trimers, and T-tetramers were assembled. The elongated DNA templates were verified by AFM

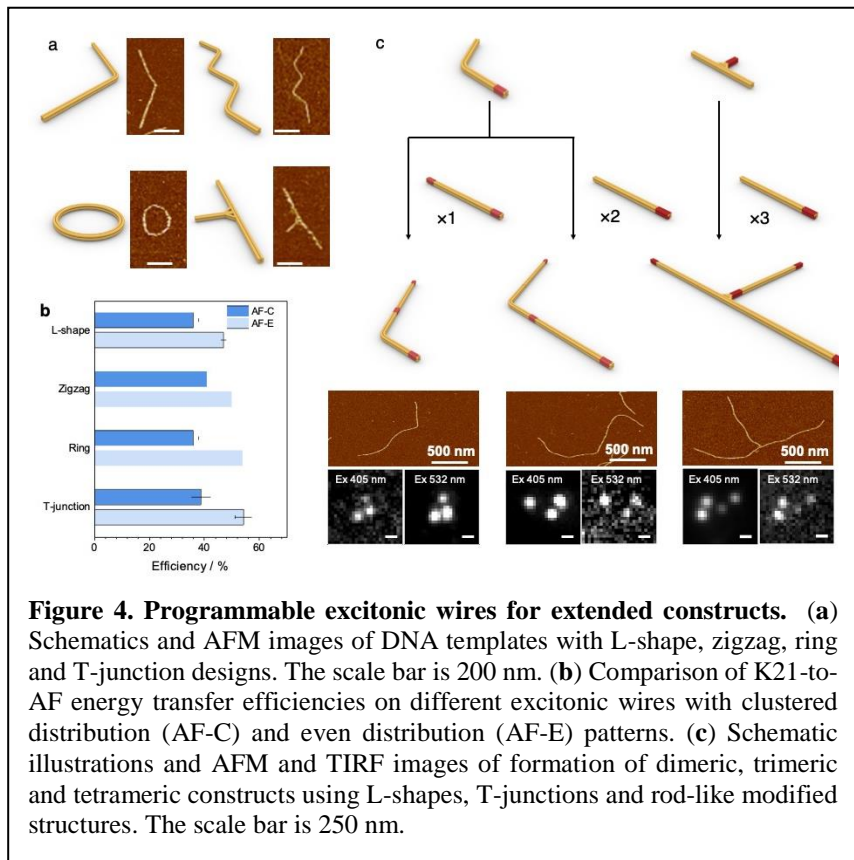


**Figure 4. Programmable excitonic wires for extended constructs.** (a) Schematics and AFM images of DNA templates with L-shape, zigzag, ring and T-junction designs. The scale bar is 200 nm. (b) Comparison of K21-to-AF energy transfer efficiencies on different excitonic wires with clustered distribution (AF-C) and even distribution (AF-E) patterns. (c) Schematic illustrations and AFM and TIRF images of formation of dimeric, trimeric and tetrameric constructs using L-shapes, T-junctions and rod-like modified structures. The scale bar is 250 nm.

imaging and serve as templates to organize K21 dye aggregates into excitonic complexes on the micron-scale. These complexes can be visualized via TIRF imaging after attaching acceptor molecules with specific spatial arrangements (Figure 4c). Our study demonstrated that those excitonic constructs show robust energy transfer capabilities and can be used as modular building blocks for constructing assemblies of higher order excitonic architectures.

## Future Plans

We will pursue the design and construction of bio-inspired 2-D and 3-D excitonic systems directed by self-assembled structural DNA templates. In particular, the future work will focus on:

- (1) exploring the large-scale 2-D excitonic networks organized by the DNA 2-D arrays based on DNA tile/origami assembly. In-depth investigation will be performed to excitonic features and energy transfer characterize the entire micron-scale excitonic network;
- (2) designing and constructing dynamic excitonic devices and stimuli-responsive excitonic networks directed by programmable DNA nanostructures. Those switchable excitonic systems will be triggered or tuned by DNA strand displacement, redox chemistry or light via rational sequence and structural designs; and
- (3) investigating the structural features of strongly coupled dye complexes using structural DNA crystals as templates. Such dye aggregates templated on 3-D DNA crystals will not only be used

to determine the molecular arrangement of pigment molecules on DNA via X-ray crystallography, but will also serve as a photonic antenna with highly dense chromophore arrangements.

## References

**Programmed coherent coupling in a synthetic DNA-based excitonic circuit** Etienne Boulais, Nicolas Sawaya, Rémi Veneziano, Alessio Andreoni, James Banal, Toru Kondo, Sarthak Mandal, Su Lin, Gabriela Schlau-Cohen, Neal Woodbury, Hao Yan, Alán Aspuru-Guzik, and Mark Bathe, *Nat. Mater.* 17:159-166 (2018).

**Molecular model of J-aggregated pseudoisocyanine fibers** William P. Bricker, James L. Banal, Matthew B. Stone, Mark Bathe, *J. Chem. Phys.* 149:24905 (2018)

## Publications

**Directed Energy Transfer through DNA-templated J- aggregates** Sarthak Mandal, Xu Zhou, Su Lin, Hao Yan, Neal Woodbury, *Bioconjugate Chem.* 141(49), 19336-19341 (2019).

**Efficient Long-range, Directional Energy Transfer through DNA-Templated Dye Aggregates** Xu Zhou, Sarthak Mandal, Shuoxing Jiang, Su Lin, Jianzhong Yang, Yan Liu, David G. Whitten, Neal W. Woodbury and Hao Yan, *J. Am. Chem. Soc.* 141 (21) :8473-8481 (2019).

**DNA-Templated Programmable Excitonic Wires for Long-Range Exciton Transport** Xu Zhou, Hao Liu, Franky Djutanta, Shuoxing Jiang, Xiaodong Qi, Lu Yu, Su Lin, Rizal F. Hariadi, Yan Liu, Neal W. Woodbury and Hao Yan, *manuscript in preparation*.

## Steering the Pathways of Hierarchical Self-assembly at Solid Surfaces

Tao Ye,<sup>1</sup> Yonggang Ke,<sup>2</sup> and Gaurav Arya<sup>3</sup>

<sup>1</sup> Chemistry and Biochemistry, University of California, Merced <sup>2</sup> Biomedical Engineering, Emory University and Georgia Institute of Technology <sup>3</sup> Mechanical Engineering and Materials Science, Duke University

### Program Scope

The prevailing paradigm of artificial self-assembly of biomolecular materials remains mixing and annealing molecules in a homogeneous solution,<sup>1,2</sup> which has limited successes in forming multiscale structures that are needed for energy relevant applications. Significantly less explored is the 2D self-assembly of these biomolecules at the solid-liquid interface.<sup>3-5</sup> Surface mediated self-assembly not only allows these structures to be readily integrated with materials to form devices but also can potentially be integrated with top-down approaches to exert control over matter across many spatial scales. However, existing efforts in 2D self-assembly of biomolecules have been limited to the formation of simple, symmetric structures that consist of a few unique components.<sup>3-5</sup>

This project seeks to systematically elucidate the roles of surface/interfacial interactions on self-assembly of biomolecular nanostructures and tailor these interactions to steer the self-assembly pathways of complex hierarchical structures. We will site-specifically nucleate the formation of surface-tethered DNA origami, prototypical designer biomolecular complexes (Figure 1) on dynamic surfaces and then allow these mesoscale structures to connect to form superstructures. We hypothesize that our new approach to controlling the conformational degrees of freedom of these mesoscale components can help bypass many of the kinetic traps that make multicomponent self-assembly fundamentally difficult and facilitate rapid, defect-free self-assembly. By combining single molecule biophysical techniques and multi-scale simulation, we will develop a systematic understanding how the interactions of the solid surface influence self-assembly at two hierarchical levels, the assembly of mesoscale supramolecular complexes and the interconnection of supramolecular complexes to form superstructures. The knowledge will be applied to rationally regulate the interactions to steer the self-assembly pathways to form complex hierarchical structures.

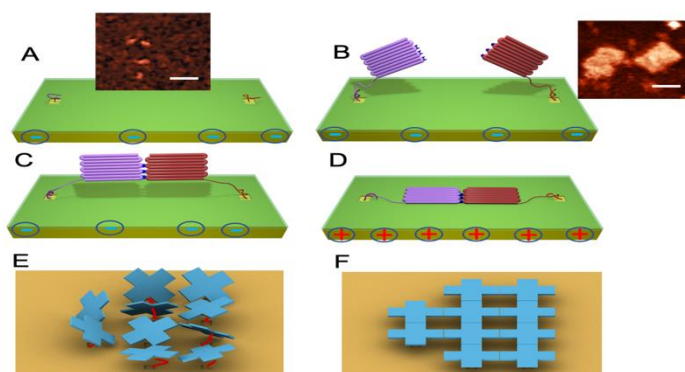


**Figure 1** Probing and controlling hierarchical self-assembly of complex structures on surfaces. (A) Seed strands will be patterned using single molecule patterning techniques.<sup>6</sup> (B) These seed strands will direct the folding of distinct DNA origami tiles at specific locations. (C) On a negatively charged surface, the tiles have the conformational freedom to approach each other and connect. (D) the structure can be immobilized onto the surface to allow high resolution AFM imaging. (E), (F) Surface-mediated hierarchical self-assembly of custom-designed shapes into 2D extended structures.

### Recent Progress

#### *(1) Probing the folding pathways of DNA origami.*

Despite the popularity of DNA origami, much remains unknown about the pathways of the self-

assembly process, which makes it difficult to rationally improve the yield. Here we are combining seeded self-assembly, ex situ and in situ imaging and multiscale simulation to understand the folding pathways of DNA origami in solution and at a surface.

First, we designed experiments to investigate how seed strands can be introduced in the assembly process to control the folding pathways and final yields (Figure 2). So far, we have experimentally studied two model DNA origamis: a 150nm four-helix-bundle (4HB) nanorod and a 400nm six-helix-bundle (6HB) nanorod. The nanorods were divided to multiple same-sized modules (e.g., 4HB was divided into 12 domains) at the design stage for programmably, systematically introducing seed strands at selected positions (Figure 2A). We developed optimal isothermal folding protocols for the assembly of DNA nanorods and investigated their folding kinetics and yields via analytic gel electrophoresis and transmission electron microscopy (Figure 2B). The data showed that the initial binding of a few seed strands can significantly alter the folding pathways and yields of both 4HB and 6HB nanorods. Our results provide new information about assembly pathways of DNA origami nanostructures and can be clearly explained in computational simulations. For example, when two seed strands within were placed the 4HB according to two different schemes (Figure 2A), we observed enhanced folding kinetics and yields for the scheme 2, which is believed to be the result of the folding pathways induced by the seed strands, as shown in simulation as well. We expect the new knowledge regarding the origami folding pathways will serve as the foundation for the investigation of origami assembly on solid surfaces.

In parallel, we are developing a new coarse-grained model that can simulate the DNA origami folding process on timescales sufficient to capture the self-assembly process (staple diffusion and binding and subsequent folding of scaffold). This model is able to capture the mechanical properties

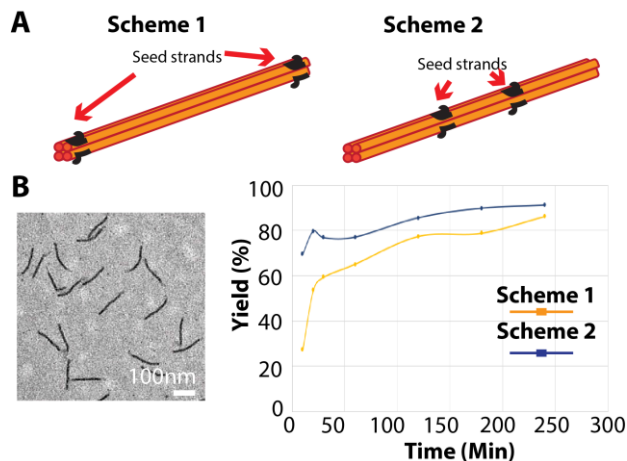


**Figure 2:** Overview and examples of investigating and controlling the folding pathways of DNA origami via seeded assembly. (A) Before the assembly of DNA origami, seed strands are added to selected positions in 4HBs to induce different folding paths. (B) Experimental data revealed that the different seeding schemes resulted in different folding kinetics and yields.

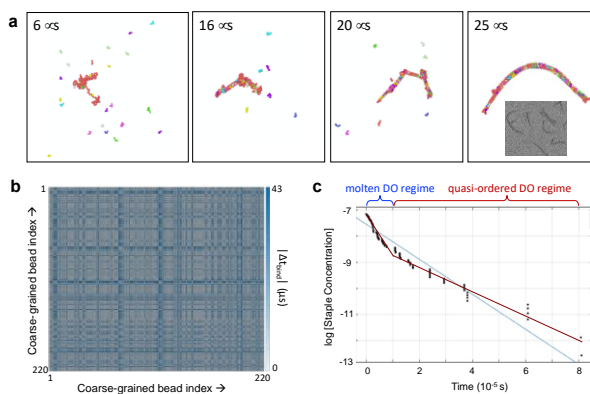


**Figure 3:** Coarse-grained modeling of the DO folding process. (a) Snapshots of a 4HB DO showing the evolution of the structure during its self-assembly. The inset shows the corresponding TEM image of the fully assembled DOs. (b) Map of absolute time difference between the binding times of all 8-bp long sites in the DNA origami. (c) Depletion of staple concentration due to binding in time showing two kinetic regimes of folding.

of both single- and double-stranded DNA through the use of “switching” functions in a low-resolution description of DNA unlike other models that require high-resolution descriptions to model both forms of DNA. Using a current version of our model, we simulated the assembly of the 4HB (**Figure 3a**). We were able to capture the initial conformations of the unbound DO scaffold and changes in the conformational dynamics of the scaffold as staples bind to the scaffold, the search by unbound staple sections for their complements on the scaffold, and the constraint of the scaffold on completion of staple binding to ultimately yield the completed DO structure which matches that seen in experiments. By comparing binding times of staples to their neighbors (**Figure 3b**) and concentration of unbound staples as a function of time (**Figure 3c**), we can begin to establish domain-specific cooperativity of the DO folding process and the existence of at two distinct regimes of folding kinetics. Further investigation into the mechanisms of DO folding should aid in shifting the DO design paradigm in the pursuit of optimal folding time and yield.

## (2) *Interconnection of surface tethered DNA origami tiles.*

Another proposed goal of the project is to investigate the self-assembly of surface-tethered DNA origami tiles into superstructures. During the first year, we have laid the groundwork by developing a mesoscopic model of DO tiles capable of binding to each other via stacking interactions between their blunt-ends and a new method to site-specifically pattern DNA strands onto the surface that can serve as seeds to direct the site-specific growth of surface tethered DNA origami structures.

In our mesoscopic model (**Figure 4a**), the DO tiles are treated as rigid bodies composed of coarse-grained beads, each representing  $\sim 10$  bp of dsDNA. Each blunt end is treated as a pair of five-bead flower-like structures, allowing us to capture the directionality of stacking interactions. The flexibility of the interconnected pairs of dsDNA carrying the blunt ends is treated using bending potentials with bending stiffness of dsDNA and the dsDNA tethers connecting the DO tiles to the surface are treated using a discretized worm-like chain model. The interaction potential for interactions between the flower structures is currently being rigorously derived using free energy calculations carried using metadynamics simulations to reproduce the binding thermodynamics of blunt-end stacking interactions measured experimentally. The development of this model will allow us to accurately study the self-assembly of DNA nanostructures at solid surfaces. By end-tethering DOs to surfaces, the influence of parameters such as the length and spacing between tethers, the affinity between nanostructures, the length and mechanical properties of the tethers, and the properties of the surface on the self-assembly process can be assessed (**Figure 4b**).

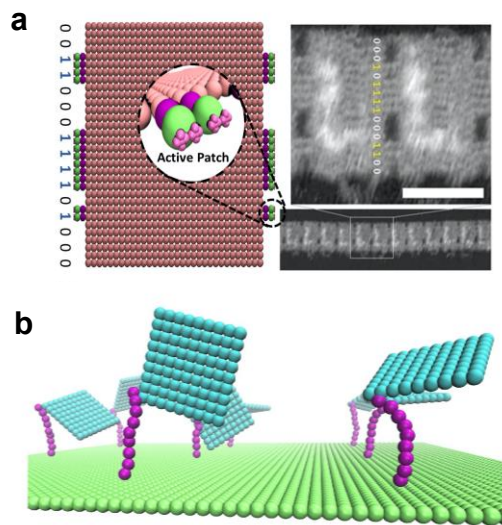


**Figure 4: Mesoscopic modeling of DO tile assembly.** (a) Schematic of our model of DO tiles showing active patches of blunt-ends that mediate assembly. (b) Proposed system of tethered tiles to be used for investigating their assembly.

While we have previously developed an AFM based single molecule patterning method,<sup>6</sup> it would be helpful to have a complementary method that can pattern these seed strands with a better

throughput. Here we developed a method that uses DNA origami as a nanoscale stamp that transfers thiolated DNA onto a self-assembled monolayer coated gold surface (Figure 5). By depositing DNA origami tiles bearing thiolated DNA strands, we allowed the thiol anchors to be in close contact with the gold surface and have the opportunity to be inserted into the SAM to form covalent gold-thiol bonds. Then the DNA origami frame was denatured to expose the spatial pattern. The surface passivation reduces nonspecific adsorption and allows high resolution, label-free characterization of the transferred spatial patterns. Spatial statistical analysis revealed the ink molecule transfer yield to be 70%, comparable to the highest yield achieved with existing DNA-origami-based nanoimprinting methods. Additional study is underway to further improve the transfer yield.

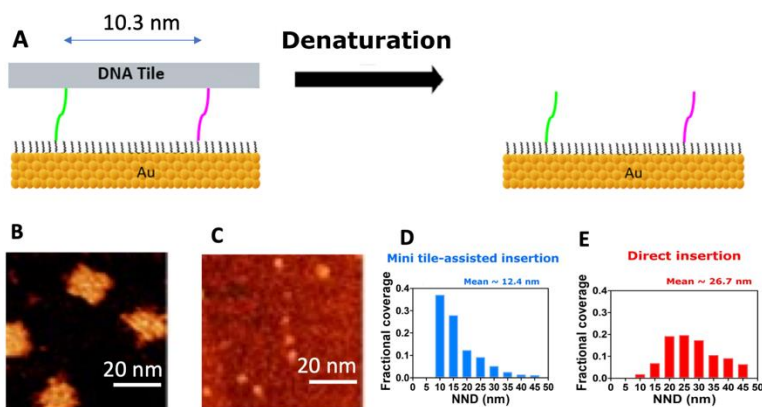


**Figure 5:** (A) Schematic of DNA origami-mediated surface patterning. A DNA tile carrying two thiolated staples with an extension protruding from the origami surface (green and purple) are deposited onto a Mercaptodecanoic acid self-assembled monolayer on a gold surface. The frame of the DNA mini-tile is then denatured and rinsed out to expose the surface-tethered staples. (B) AFM image of DNA origami tiles deposited. (C) AFM image the same surface after denaturing. Nearest-neighbor distance (NND) analysis of the inserted staples using DNA mini-tile-assisted nanoimprinting (D) and direct insertion (E).

## Future Plans

Building upon the progress we made in Year 1, we will focus on the following areas in Year 2.

- (1) In situ imaging of self-assembly of surface tethered DO. These results will be compared to those for DO self-assembly in solution. In tandem, multiscale simulations of surface seeded self-assembly will be carried out to elucidate the folding pathways.
- (2) Study the self-assembly of surface tethered DO tiles. into superstructures. We will seed the growth of DO tiles at specific locations and let them connect to form superstructures. Multiscale simulation as well in situ single molecule/structure imaging will be carried out to understand the pathways of hierarchical self-assembly.

## References

1. King, N. P.; Bale, J. B.; Sheffler, W.; McNamara, D. E.; Gonen, S.; Gonen, T.; Yeates, T. O.; Baker, D., Accurate design of co-assembling multi-component protein nanomaterials. *Nature* **2014**, *510* (7503), 103.
2. Hong, F.; Zhang, F.; Liu, Y.; Yan, H., DNA Origami: Scaffolds for Creating Higher Order Structures. *Chem. Rev.* **2017**, *117* (20), 12584-12640.
3. Suzuki, Y.; Endo, M.; Sugiyama, H., Lipid-Bilayer-Assisted Two-Dimensional Self-Assembly of DNA Origami Nanostructures. *Nat. Commun.* **2015**, *6* (8052), 1-9.
4. Woo, S.; Rothmund, P. W. K., Self-Assembly of Two-Dimensional DNA Origami Lattices Using Cation-Controlled Surface Diffusion. *Nat. Commun.* **2014**, *5* (4889), 1-9.
5. Pyles, H.; Zhang, S.; De Yoreo, J. J.; Baker, D., Controlling Protein Assembly on Inorganic Crystals Through Designed Protein Interfaces. *Nature* **2019**, *571* (7764), 251-256.
6. Josephs, E. A.; Ye, T., Nanoscale Positioning of Individual DNA Molecules by an Atomic Force Microscope. *J. Am. Chem. Soc.* **2010**, *132* (30), 10236-10238.

## **Publications**

Wang, D., Yu, L., Huang, C. M., Arya, G., Chang, S., & Ke, Y. (2021). Programmable Transformations of DNA Origami Made of Small Modular Dynamic Units. *Journal of the American Chemical Society*, 143(5), 2256-2263.

Gu, Q., Zhang, Y., Cao, H. H., Ye, S., & Ye, T. (2021). Transfer of Thiolated DNA Staples from DNA Origami Nanostructures to Self-Assembled Monolayer-Passivated Gold Surfaces: Implications for Interfacial Molecular Recognition. *ACS Applied Nano Materials*.

DOI:[10.1021/acsnm.1c01685](https://doi.org/10.1021/acsnm.1c01685)

***AUTHOR  
INDEX***



Abbott, Nicholas L.....	39
Aizenberg, J.....	43
Aronson, Igor S.....	48
Arya, Gaurav.....	216
Ashby, Paul D.....	25
Baer, Marcel D.....	3, 19
Baker, David.....	52
Balazs, Anna C.....	43, 56, 61
Bathe, Mark.....	167
Bedzyk, Michael J.....	140
Castro, Carlos.....	203, 207
Chaikin, Paul M.....	66, 76
Chen, Chun-Long.....	19
Chen, Qian.....	131
Choi, Jong Hyun.....	72
de Pablo, Juan.....	10, 39
De Yoreo, James J.....	19, 52
Delhommelle, Jerome.....	76
Dishari, Shudipto Konika.....	81
Dogic, Zvonimir.....	86
Emrick, Todd.....	90
Estroff, Lara A.....	94
Ewert, K.....	157
Franco, Elisa.....	100
Gang, Oleg.....	119
Geissler, Phillip.....	25
Glatz, Andreas.....	31
Glotzer, Sharon C.....	180
Good, Matthew C.....	109
Grason, Gregory M.....	162
Guan, Zhibin.....	105
Hammer, Daniel A.....	109
Hartley, C. Scott.....	114
Helms, Brett A.....	25
Hillier, Andrew.....	4
Johston-Halperin, Ezekiel.....	203, 207
Ke, Yonggang.....	216
Kloxin, Chris.....	148
Konkolewicz, Dominik.....	114
Kowalewski, Tomasz.....	56
Kumar, Sanat K.....	119
Lavrentovich, Oleg D.....	126
Lee, Daeyeon.....	109
Li, Y.....	157
Lin, Su.....	211
Liu, Andrea J.....	135
Luijten, Erik.....	131
Mallapragada, Surya.....	4
Matyjaszewski, Krzysztof.....	56
Nagel, Sidney R.....	135
Nealey, Paul.....	10
Nilsen-Hamilton, Marit.....	4
Noy, Aleksandr.....	19
Olvera de la Cruz, Monica.....	140
Palacci, Jérémie.....	146
Pine, David.....	66
Pochan, Darrin.....	148
Poirier, Michael.....	203, 207
Prozorov, Tanya.....	4
Rothmund, Paul W.K.....	152
Russell, Thomas P.....	25
Sacanna, Stefano.....	76
Safinya, C. R.....	157
Santore, Maria M.....	162
Saven, Jeffery G.....	148
Schlau-Cohen, Gabriela S.....	167
Schulman, Rebecca.....	100
Seeman, Nadrian C.....	66
Sen, Ayusman.....	48
Shirts, Michael R.....	172
Silberstein, Meredith N.....	176
Snezhko, Alexey.....	31
Sokolov, Andrey.....	31
Solomon, Michael J.....	180
Strano, Michael S.....	185
Stupp, Samuel I.....	190
Tezcan, F. Akif.....	195
Tirrell, Matthew.....	10
Travesset, Alex.....	4
Vaikuntanathan, Suriyanarayanan.....	200
Vaknin, David.....	4
van Burren, Anthony.....	19
Wang, Wenjie.....	4
Weck, Marcus.....	66
Wiesner, Ulrich.....	94
Willard, Adam.....	167
Winter, Jessica.....	203, 207
Woodbury, Neal.....	211
Yan, Hao.....	211
Ye, Tao.....	216
Zettl, Alex.....	25



***PARTICIPANT  
LIST***



<b>Name</b>	<b>Email</b>	<b>Organization</b>
Abbott, Nicholas	nla34@cornell.edu	Cornell University
Agarwal, Siddharth	sidagarwal@g.ucla.edu	University of California, Los Angeles
Aizenberg, Joanna	jaiz@seas.harvard.edu	Harvard University
Aronson, Igor	isa12@psu.edu	Pennsylvania State University
Arya, Gaurav	gaurav.arya@duke.edu	Duke University
Baer, Marcel	marcel.baer@pnnl.gov	Pacific Northwest National Laboratory
Baker, David	dabaker@uw.edu	University of Washington
Balazs, Anna	balazs@pitt.edu	University of Pittsburgh
Barpuzary, Dipankar	d.barpuzary@uci.edu	University of California, Irvine
Baza, Hend	hbaza@kent.edu	Kent State University
Bedzyk, Michael	bedzyk@northwestern.edu	Northwestern University
Cai, Hongyi	hc953@cornell.edu	Cornell University
Chaikin, Paul	chaikin@nyu.edu	New York University
Chapman, Dana	dvc25@cornell.edu	Cornell University
Chen, Chun-Long	chunlong.chen@pnnl.gov	Pacific Northwest National Laboratory
Chen, Qian	qchen20@illinois.edu	University of Illinois, Urbana-Champaign
Choi, Jong Hyun	jchoi@purdue.edu	Purdue University
Curk, Tine	curk@northwestern.edu	Northwestern University
de Pablo, Juan	depablo@uchicago.edu	The University of Chicago
De Yoreo, Jim	James.DeYoreo@pnnl.gov	Pacific Northwest National Laboratory
Delhommelle, Jerome	jerome.delhommelle@und.edu	University of North Dakota
DeLuca, Marcello	marcello.deluca@duke.edu	Duke University
Dishari, Shudipto	sdishari2@unl.edu	University of Nebraska, Lincoln
Dogic, Zvonimir	zdogic@ucsb.edu	University of California, Santa Barbara
Emrick, Todd	tsemrick@mail.pse.umass.edu	University of Massachusetts, Amherst
Ennist, Nathanr	ennist@uw.edu	University of Washington
Estroff, Lara	lae37@cornell.edu	Cornell University
Fecko, Chris	christopher.fecko@science.doe.gov	Department of Energy
Fiechtner, Gregory	gregory.fiechtner@science.doe.gov	Department of Energy
Fobe, Theodore	theodore.fobe@colorado.edu	University of Colorado, Boulder
Franco, Elisa	efranco@seas.ucla.edu	University of California, Los Angeles
Gang, Oleg	og2226@columbia.edu	Columbia University
Geissler, Phillip	PLGeissler@lbl.gov	Lawrence Berkeley National Laboratory
Glatz, Andreas	glatz@anl.gov	Argonne National Laboratory
Graf, Matthias	matthias.graf@science.doe.gov	Department of Energy
Grason, Gregory	grason@mail.pse.umass.edu	University of Massachusetts, Amherst
Guan, Zhibin	zguan@uci.edu	University of California, Irvine
Hammer, Daniel	hammer@seas.upenn.edu	University of Pennsylvania
Hartley, Scott	scott.hartley@miamioh.edu	Miami University
Hedderick, Konrad	krh89@cornell.edu	Cornell University
Helms, Brett	bahelms@lbl.gov	Lawrence Berkeley National Laboratory
Hsia, Yang	yhsia@uw.edu	Institute for Protein Design

Jergens, Elizabeth	jergens.8@osu.edu	The Ohio State University
Johnston-Halperin, Ezekiel	johnston-halperin.1@osu.edu	The Ohio State University
Ke, Yonggang	yonggang.ke@emory.edu	Emory University
Kewalramani, Sumit	s-kewalramani@northwestern.edu	Northwestern University
Kim, Ahyoung	ahyoung2@illinois.edu	University of Illinois, Urbana-Champaign
Kloxin, Chris	cjk@udel.edu	University of Delaware
Konkolewicz, Dominik	d.konkolewicz@miamiOH.edu	Miami University
Kumar, Sanat	sk2794@columbia.edu	Columbia Univ/Brookhaven National Lab
Lavrentovich, Oleg	olavrent@kent.edu	Kent State University
Lee, Daeyeon	daeyeon@seas.upenn.edu	University of Pennsylvania
Lin, Po-An	poan.lin@duke.edu	Duke University
Lin, Su	slin@asu.edu	Arizona State University
Liu, Andrea	ajliu@physics.upenn.edu	University of Pennsylvania
Lu, Qinyi	qlu22@emory.edu	Emory University
Luijten, Erik	luijten@northwestern.edu	Northwestern University
Lyu, Zhiheng	zlyu@illinois.edu	University of Illinois, Urbana-Champaign
Madden, Ian	Ianmadden2020@u.northwestern.edu	Northwestern University
Mallapragada, Surya	suryakm@iastate.edu	Ames Laboratory
Maracas, George	george.maracas@science.doe.gov	Department of Energy
Markowitz, Michael	mike.markowitz@science.doe.gov	Department of Energy
Nagel, Sidney	srnagel@uchicago.edu	The University of Chicago
Nealey, Paul	pnealey@anl.gov	Argonne National Laboratory
Nilsen-Hamilton, Marit	marit@iastate.edu	Iowa State University
Noy, Aleksandr	noy1@llnl.gov	Lawrence Livermore National Laboratory
Ohayon, Yoel	Yoel.ohayon@nyu.edu	New York University
Olvera de la Cruz, Monica	m-olvera@northwestern.edu	Northwestern University
Padmini, H Nilanthi	hpadmini@kent.edu	Kent State University
Palacci, Jérémie	palacci@ucsd.edu	UCSD/IST Austria
Palmer, Liam	liam-palmer@northwestern.edu	Northwestern University
Paul, Sanjoy	spaul11@kent.edu	Kent State University
Pine, David	pine@nyu.edu	New York University
Pochan, Darrin	pochan@udel.edu	University of Delaware
Poirier, Michael	poirier.18@osu.edu	The Ohio State University
Prozorov, Tanya	tprozoro@ameslab.gov	Ames Laboratory
Ranabhat, Kamal	kranabha@kent.edu	Kent State University
Ross, Tyler	tross@caltech.edu	California Institute of Technology
Rothmund, Paul	pwkr@dna.caltech.edu	California Institute of Technology
Russell, Thomas	tom.p.russell@gmail.com	Lawrence Berkeley National Laboratory
Sacanna, Stefano	s.sacanna@nuy.edu	New York University
Safinya, Cyrus	safinya@mrl.ucsb.edu	University of California, Santa Barbara
Sai, Hiroaki	hiroaki.sai@northwestern.edu	Northwestern University
Santore, Maria	santore@mail.pse.umass.edu	University of Massachusetts
Saven, Jeffery	saven@upenn.edu	University of Pennsylvania

Schlau-Cohen, Gabriela	gssc@mit.edu	Massachusetts Institute of Technology
Schulman, Rebecca	rschulm3@jhu.edu	Johns Hopkins
Schwartz, Andrew	andrew.schwartz@science.doe.gov	DOE-BES
Selmani, Serxho	sselmani@uci.edu	University of California, Irvine
Sen, Ayusman	asen@psu.edu	Pennsylvania State University
Sennett, Michael	michael.sennett@science.doe.gov	Department of Energy
Shirts, Michael	michael.shirts@colorado.edu	University of Colorado, Boulder
Shiyanovskii, Sergij	sshiyano@kent.edu	Kent State University
Silberstein, Meredith	meredith.silberstein@cornell.edu	Cornell University
Snezhko, Alexey	snezhko@anl.gov	Argonne National Laboratory
Snyder, Deborah	djsnyder@umass.edu	University of Massachusetts, Amherst
Sokolov, Andrey	sokolov@anl.gov	Argonne National Laboratory
Solomon, Michael	mjsolo@umich.edu	University of Michigan
Strano, Michael	srgoffice@mit.edu	Massachusetts Institute of Technology
Stupp, Samuel	s-stupp@northwestern.edu	Northwestern University
Tezcan, F. Akif	tezcan@ucsd.edu	University of California, San Diego
Thedford, R. Paxton	Rpt55@cornell.edu	Cornell University
Tirrell, Matthew	mtirrell@uchicago.edu	The University of Chicago
Vaikuntanathan, Suriyanarayanan	svaikunt@uchicago.edu	The University of Chicago
Valencia, Dulce Maria	dulce.manrique@northwestern.edu	Northwestern University
Vecchioni, Simon	sv1091@nyu.edu	New York University
Walker, Christopher	Christopher.Walker-1@colorado.edu	University of Colorado Boulder
Wang, Hao	hwang37@kent.edu	Kent State University
Wang, Zhongtong	zw582@cornell.edu	Cornell University
Watson, Garrett	garrettwatson2023@u.northwestern.edu	Northwestern University
Weck, Marcus	mw125@nyu.edu	New York University
Winter, Jessica	winter.63@osu.edu	The Ohio State University
Woodbury, Neal	nwoodbury@asu.edu	Arizona State University
Yan, Hao	hao.yan@asu.edu	Arizona State University
Yang, Zhefei	yangzhef@umass.edu	University of Massachusetts, Amherst
Yao, Lehan	lehan2@illinois.edu	University of Illinois, Urbana-Champaign
Ye, Tao	tye2@ucmerced.edu	University of California, Merced
Yu, Fei	fy84@cornell.edu	Cornell University
Zhang, Lucy	lzbloop@gmail.com	Duke University
Zhou, Xu	xzhou110@asu.edu	Arizona State University
Zhou, Yilong	yz393@duke.edu	Duke University